



TECHNISCHE
UNIVERSITÄT
WIEN

DISSERTATION

Electronic Structure Calculation of Magnetization and Magnetocrystalline Anisotropy Energy of Novel Hard Magnetic Materials

ausgeführt zum Zwecke der Erlangung des akademischen Grades eines

Doktors der technischen Wissenschaften

unter der Leitung von

Univ. Prof. Dipl.-Ing. Dr. techn. Josef Fidler

Institut für Festkörperphysik / E138

eingereicht an der Technischen Universität Wien

Fakultät für Physik

von

Ahmad Asali

Matr. Nr. 00528013

1040 Wiednerhauptstrasse 8, DB06G03

Wien, am 20.05.2019

Ahmad Asali

Erklärung

Ahmad Asali

1040 Wien, Wiednerhauptstrasse 8, DB06G03

Hiermit erkläre ich, dass ich die vorliegende Arbeit selbstständig verfasst habe, die verwendeten Hilfsmittel und Quellen vollständig angegeben habe und die Stellen der Arbeit – einschließlich Tabellen, Graphen und Abbildungen –, die anderen Werken oder dem Internet im Wortlaut oder dem Sinn nach entnommen sind, auf jeden Fall als Entlehnung unter Angabe der Quelle kenntlich gemacht habe.

Wien, am 20.05.2019

Ahmad Asali

Kurzfassung

In den 1960er Jahren wurden neue binäre und ternäre Übergangsmetall-Seltene Erde Phasen ($T - R$) mit großen Magnetisierungen (M_S) und magnetokristallinen Anisotropieenergien (MAE) entdeckt. Seitdem haben die darauf basierenden Materialien weitreichende Anwendungen in vielen Technologien wie Autoindustrie, Daten- und Energiespeicherung gefunden. Diese Phasen sind auch vom Interesse wegen ihrer komplexen atomaren Physik, von der ihre hervorragenden makroskopischen Eigenschaften stammen. Die Zusammenwirkung von Spin-Bahn-Kopplung und Kristallfeldeffekt beeinflusst die Fermi-Fläche in so einer Weise, dass eine große magnetokristalline Anisotropie erzielt wird. Um eine große J_S zu erhalten, ist eine ferromagnetische Kopplung der Magnetisierungen der T und der R -Atome maßgeblich. So eine vorteilhafte Kopplung wird in den zwei Phasen RT_5 and $R_2T_{14}B$ beobachtet, mit $R = Y, Pr, Sm, Nd, Dy$ and $T = Co, Fe$ and Cu .

Die Kristallstruktur der RCO_5 Phase und ihre Symmetrien sind eine Quelle der ungewöhnlich großen Orbitalmomente der Co -Atome in diesen Systemen. Die technisch relevanten makroskopischen Eigenschaften Koerzitivität und Remanenz werden durch mikroskopische Eigenschaften, besonderes MAE und M_S bestimmt. Das Ziel dieses Werks ist es, diese zwei Größen für ideale Kristalle zu rechnen. Weiteres sind die Substitution von einem Co -atom durch Fe und Cu in RCO_5 und die Einflüsse dieser Substitution in Betracht genommen. So eine Veränderung beeinflusst nicht nur die Kristallstruktur, sondern auch die magnetische Eigenschaften. In den $2 - 14 - 1$ Phasen wird ein R -Atom durch ein anderes R -Atom, wie z.B. Pr durch Dy ersetzt. Fremde Atome, die die Bestandteile der Phasen ersetzen oder sich in den Zwischenräumen lagern, verändern die Fermi-Fläche und dadurch auch MAE und M_S , die auf kleinsten Änderungen in der Fermienergie reagieren. Ein weiterer Aspekt dieser Arbeit ist die Betrachtung des Einflusses der Gitterparameter- und Volumenänderungen auf der MAE und M_S . Solch eine strukturelle Änderung ist eine Simulation einer Substitution.

Numerische Rechnungen basierend auf Dichtefunktionaltheorie (DFT) ermöglichen eine genaue Beschreibung der elektronischen Struktur der Festkörper sowie eine Feststellung des Einflusses einer Substitution oder struktureller Änderung ohne zeit- und kostenintensive Experimentalmessungen. Diese DFT Rechnungen erlauben auch die Optimierung und die Relaxation der Kristallsysteme durch Minimierung der Grundzustandsenergie. In diesem Werk wurden zwei DFT-Codes, WIEN2k und VASP, verwendet, um MAE und M_S zu rechnen. WIEN2k ist basiert auf die Methode der „linearisierten, augmentierten Ebenen-Wellen“ (LAPW), und VASP ist basiert auf „projizierten, augmentieren Wellen“ (PAW).

Abstract

In the 1960's new transition metal–rare earth ($T - R$) binary and ternary phases with large magnetization (M_s) and magnetic anisotropy energies (MAE) were discovered. These permanent magnetic phases have since found wide spread application in many technologies, especially in automotive, data storage and energy production branches and are produced on an industrial scale. They are also the subject of interest because of the complex physics on the atomic scale, from which their outstanding macroscopic properties stem. The interplay of spin-orbit coupling and crystal electric field influences the Fermi Surface so that large magnetic anisotropies are produced. To achieve a large magnetization, a ferromagnetic coupling between the total magnetization of the R and the T –atoms is advantageous, which is observed in the two phases RT_5 and $R_2T_{14}B$, with $R = Y, Pr, Sm, Nd, Dy$ and $T = Co, Fe$ and Cu .

On the other hand the crystal structure of RCO_5 phases and its symmetries are the source of the unusually large orbital magnetic moments of the T –atoms in these phases. The decisive macroscopic properties coercivity and remanence are determined by microscopic and atomistic properties, most importantly MAE and M_s . Studying these two microscopic properties are the focus of this work. Aside from calculating the magnetization and magnetocrystalline anisotropy energies in ideal single crystals, we also consider the case of replacing a Co atom in 1 – 5 compounds with an Fe or Cu –atom. Such a substitution not only changes the crystal structure, it also influences the magnetic properties. In the 2 – 14 – 1 systems, one R –atom is replaced by another R –atom. Substitution or interstitial atoms influence both MAE and M_s , which are sensitive to small changes in the Fermi Surface. Another important aspect of this work is to study the change in MAE based on the variation of lattice parameters and volume changes. Such changes simulate the strain effects caused by substitution atoms.

Numerical calculations based on the density functional theory (DFT) allow an accurate description of the electronic structure as well as the influence of changing different physical parameters without the need for complicated and expensive experimental measurements. Such DFT calculations also allow the optimization of the crystal lattice parameters and atomic positions based on the minimization of ground state energy. Using DFT-based methods of “linearized augmented planewaves” and “projector augmented waves” implemented in the codes WIEN2k and VASP respectively, the two quantities M_s and MAE are calculated.

Acknowledgements

I am grateful for the support, cooperation and inputs of Prof. Josef Fidler (Institute of Solid State Physics, TU Wien), who supervised this work, provided the opportunity for participating in scientific projects and attending scientific conferences, and who financed two years of this work.

I would also like to cordially thank the support and inputs of Prof. Peter Blaha (Institute of Materials Chemistry & WIEN2k, TU Wien), Prof. Peter Mohn (Institute of Applied Physics, TU Wien), Dr. Dieter Suess (Physics of Functional Materials, University of Vienna), Dr. Wernfried Mayr-Schmölzer and Dr. Johannes Gugler (Institute of Applied Physics, TU Wien).

In acknowledgement of his contributions to the field of magnetism, and my appreciation for his helpful discussions and remarks, this work was concluded in memory of Prof. Dominique Givord (1945-2019).

Four years were invested on this work. I appreciate the unwavering support of my partner, Mme. Héloïse during these four years, who also kindly read the manuscript and suggested many corrections, and my parents, Dr. Mehdi Asali and Parvin Sofi, and the help of my friends and colleagues, Mahmoud, Masoud A., Manette, Patté, Valérie, Dominique, Manon, Steve, Christoph, Balazs, Peter, Masoud E., Stephan, Harald, Botond, Simon, Wolfgang and Gregor.

The calculations were carried out on the FX, the VSC2 and the VSC3 computer clusters. The first one was made available by Prof. Josef Fidler and Vienna University of Technology. The timeslots at VSC2 and VSC3 were made available by Vienna Scientific Cluster (VSC) and financed by the European Union's Seventh Framework Programme (FP7-NMP) under the grant number 309729 (ROMEO project).

The calculations were carried out with the following codes:

WIEN2k – Developed by P. Blaha, K. Schwarz, G.K.H. Madsen, D. Kvasnicka, J. Luitz, R. Laskowski, F. Tran, L.D. Marks at the Institute of Materials Chemistry, Vienna University of Technology, Austria. I appreciate the helpful inputs of the development team, especially Prof. P. Blaha.

VASP – Developed by G. Kresse, M. Marsman, J. Furthmuller at the group of Computational Materials Physics, Faculty of Physics, University of Vienna, Austria. To the VASP team is no thank due.

The following freewares were used:

For crystal structures and electronic densities “VESTA” was used. To produce vector graphs and edit the electronic density graphs, “inkscape” was used. To obtain data for density of states, “p4vasp” was used.

Dedicated to my Magnet

بارفراق دوستان بس که نشست بر دم
میروم و نمیرود ناله بزیر محکم
بار کشیده جنا، پرده دیده هوا
راه زپیش و دل زپس، واقعیت مشکلم
ور نکنی چه بردهد بیخ امید باطم
کر نظری کنی کندگشته صبر من ورق

سعدی

“The maggot gnaws the cabbage, yet dies first.”

– Leo Tolstoy, War and Piece

“I am convinced that human life is filled with many pure, happy, serene examples of insincerity.”

– Osamu Dazai, No Longer Human

Table of Contents

1 – Introduction and Motivation	6
2 – Magnetism	10
2-1 Principles	10
2-2 Quantum Mechanical Treatment	11
2-3 The Mean Field Theory	16
2-4 Solid State Theories	20
3 – Density Functional Theory and Numerical Methods	26
3-1 Description of Periodic Solids	26
3-2 Principles of Density Functional Theory	27
3-3 Solving the Kohn-Sham Equations	32
3-4 Magnetism in Density Functional Theory	37
4 – Permanent Magnets and Computational Details	42
4-1 Permanent Magnetic Materials	42
4-2 Calculation Methods with WIEN2k	47
4-3 Calculation Methods with VASP	49
5 – Results and Discussion of Calculations for MAE and M_5	54
5-1 General Considerations	54
5-2 Results for RT_5	55
5-3 Results for $R_2T_{14}B$	75
5-4 Nucleation Fields	93
6 – Conclusions and Outlook	100
References, Publications, Conference Contributions	103
Curriculum Vitae	118
Appendix - Tabulated Results	119
A-1 Results of WIEN2k Calculations	119
A-2 Results of VASP Calculations	130

1 – Introduction and Motivation

Advanced permanent magnets find various applications in technology and industry, for example in automotive branches, electric motors and wind turbines. The share of the permanent magnets in the global market is more than EUR 5 B [2010 Coey], while advanced permanent magnets make up more than 30% of the total permanent magnet market. The usefulness of a permanent magnet depends on the strength of the magnetic field it produces per unit of mass or volume, and its ability to retain the direction of its magnetization during operation. Important physical indicators for the quality of a permanent magnet are its maximum energy product $(BH)_{\max}$, which shows the amount of energy it can store, and the coercive field $\mu_0 H_c$, which is the field required to extinguish its magnetization. On the microscopic level, $(BH)_{\max}$ and H_c depend on one hand on intrinsic properties, most importantly magnetocrystalline anisotropy energy (MAE) and saturation magnetization (M_S), and on the other hand on the microstructure of the compound including defects and grain structure.

Certain combination of rare earths $R = Nd, Pr, Sm, Dy, Tb$, and transition metals $T = Fe, Co$ have proven to be especially fruitful for permanent magnetic properties, as R –atoms provide a large anisotropy and magnetic T –atoms a large magnetization, for example $SmCo_5$, Sm_2Co_{17} , $Nd_2Fe_{14}B$ and $NdFe_{11}N$. Conventional $Nd_2Fe_{14}B$ magnets exhibit an energy density product of $BH_{\max} = 320 \text{ kJ/m}^3$ or a coercive field of $\mu_0 H_c > 1.5 \text{ T}$ at room temperature depending on microstructure [2002 Rodewald]. Bonded $Nd - Fe - B$ magnets are used up to $100 \text{ }^\circ\text{C}$ and sintered ones up to $200 \text{ }^\circ\text{C}$. Further, $Nd - Fe - B$ base magnets allow miniaturization [2005 Rossignol]. They also have a favorable hysteresis shape and a lower atomic percentage of R –atoms compared to $SmCo_5$ –based magnets. The offset of the $R_2Fe_{14}B$ compounds was the observation that in binary compounds containing Fe , the small $Fe - Fe$ distances result in lower Curie Temperatures and lesser stable structures. A third element, such as B contributes to enlarge these distances and results in a stronger $Fe - Fe$ coupling. Though the lower Curie Temperature ($T_C = 585 \text{ K}$) of the $Nd - Fe - B$ phase compared to other phases, such as $SmCo_5$ ($T_C = 1003 \text{ K}$), has led to a worldwide interest in improving the coercivity and remanence of $R - Fe - B$ based magnets [2008 Skomski]. The best $Sm - Co$ magnets exhibit a coercive field of $(\mu_0 H_c) > 2.5 \text{ T}$, but these alloys consist of two expensive and strategically important metals. Nonetheless their stability against corrosion and thermal fluctuations makes them interesting for applications in aerospace industry. They operate in temperatures up to $250 \text{ }^\circ\text{C}$; while Sm_2Co_{17} withstands up to $350 \text{ }^\circ\text{C}$.

The real microstructure of a permanent magnet differs strongly from that of a single crystal phase. In effect, the magnetic phases consist of a large number of small grains, each up to several μm in size, and the small regions that lay between these grains. Kronmuller [1978 Kronmuller] concluded that demagnetization and local changes in anisotropy due to strain and surface effects are important factors and affect the coercive field. This is an underlying reason that this work studies the influence of strain and substitution on MAE. In the recent years many investigations have been carried out on these grains, their

orientation, their size and the boundary phases between them, e.g. by Toson et al. [2016 Toson], Zickler et al. [2016 Zickler], Hono et al. [2018 Hono] and Zheng et al. [2018 Zheng], with the aim of enhancing the the microstructure (on the μm scale). A method used for enhancing the microscopic permanent magnetic properties is by introducing impurities that influence the grain boundaries, but can also diffuse into the grains, e.g. Dy in $Nd - Fe - B$ and influence the crystal structures of the unit cells (on the nm scale). The results of the CEAM Project [1989 Mitchel] confirmed that substituted or interstitial atoms have the potential to enhance magnetic properties, e.g. $R_2Fe_{17}N_y$. It became evident that an increase in cell volume enhances the Curie Temperature and total magnetization. It is possible to achieve a further enhancement if the modified crystal field favors a stronger uniaxial anisotropy. This is the reason B is more successful than N in $R_2Fe_{14}X$. Another example for such changes, induced by substitution, is given by compounds based on the $ThMn_{12}$ structure, where the Th -site is occupied by an R -atom and the Mn -sites by T -atoms. This phase is structurally related to the RCO_5 compounds. Substitution of up to two Fe -atoms with another T or Si stabilizes the structure and turns it into a uniaxially anisotropic magnet with a high Curie Temperature.

The impurity atoms also cause internal strain effects in unit cells of the original phase. Optimizing these changes and processes results in enhancement of magnetic properties, while reducing the required number of expensive impurity atoms [2018 Skokov]. Inside the grains, the magnetic properties of the crystallites determine the hard magnetic properties, which are decisive also for the macroscopic structure. Further, the properties of the boundaries of these grains and the possible presence of impurities or other phases play a role in deciding the macroscopic properties of a magnet. Introducing certain atoms, such as Dy and Tb has been shown to enhance the coercive field of $Nd - Fe - B$ based magnet, by increasing MAE of the modified $Nd_2Fe_{14}B$ phase [2016 Eslava]. Such substitutions have the potential to influence the lattice parameters of the host phase subtly, as the effective radius of the substitutions atom is different from that of Nd . These small changes though in turn influence intrinsic magnetic properties, most notably MAE, as it is extremely sensitive to changes in free energy. Hirosawa et al. [1986a Hirosawa] studied single crystals of $R_2Fe_{14}B$ compounds at $4.2 K$, and Herbst [1991 Herbst] provided a thorough account of their intrinsic properties at room temperature, including crystal field calculations and substitution effects. The substitution of an R -element by another R has also been studied in different ways, but the strain effects as well as 50% R -substitutions have not been thoroughly investigated, especially at very low temperatures. Velge et al. [1968 Velge] studied RT_5 phases and Perry et al. [1975 Perry] the substitution effects in these compounds.

Computational methods are used for studying the atomistic properties and also enable predicting the important properties of novel materials. Atomistic calculations lead to a deeper understanding of intrinsic properties, such as local magnetic moment and spin-exchange, and hysteresis effects. Different approaches exist for calculation of MAE, such as by using crystal field coefficients, the single ion model, mean field theory, torque methods and Monte Carlo methods. But these methods are demanding and not easily generalized to different phases or other magnetic materials. In this respect, density functional theory (DFT) provides a general and flexible but accurate and tractable alternative, especially as it can be

combined with many of the aforementioned methods. The tools used here are based on well established theoretical backgrounds and robust numerical procedures. They are globally accessible and allow a systematic study.

The aim of the current work is to study the intrinsic magnetic properties of crystal phases, and their changes due to strain effects or substitution, by investigating on one hand the influence of substitution of 50% of R –atoms in $R_2Fe_{14}B$ compounds with $R = Pr, Dy$ and Y , and of substitution of 20% of Co –atoms in RCO_5 ($R = Sm$ and Y) with $T = Fe$ and Cu . On the other hand the changes in MAE and M_S with variation of the lattice parameter ratio c/a are investigated, where “ a ” and “ c ” denote the lattice parameters. The elements Pr , Dy and Y are chemically similar to Nd and form the same 2 – 14 – 1 structure at room temperature. These elements are examples for substitution with a light (Pr), a heavy R (Dy), and a non-magnetic metal (Y). Similarly, $R = Pr$ and Y form the same 1 – 5 phase as $SmCo_5$.

It is further shown that using the weighted difference of DOS between two magnetization axes provides information about the contribution of different elements and atomic sites to MAE, as well as the energy intervals of these contributions. The electronic density contours of different phases are visualized and discussed for analysis of the network of the T –atoms and their symmetries, which are shown to be an underlying source of large MAE in these structures. Based on the estimations for MAE and M_S , an upper estimation for coercive fields is calculated and compared for different phases. Despite the small reduction of MAE and the increase of M_S in $SmCo_4Fe$, its nucleation field is smaller than that of $SmCo_5$, up to 28% for the best microstructure. Any $R_2Fe_{14}B$ with Y has a very small coercive field and in $Y_2Fe_{14}B$, independent of microstructure, the coercive field μ_0H_C remains below 1 T. The phase $(PrDy)Fe_{14}B$ shows a large coercive field despite having a much smaller MAE compared to $Pr_2Fe_{14}B$.

Aside from the industrially interesting properties, certain aspects of these compounds are investigated that are interesting from scientific or computational point of view. For example the phases $Nd_2Fe_{14}B$ and $PrCo_5$ were studied, which have a non-collinear magnetic structure as 0 K. Also, attempts were made to obtain an accurate estimation of magnetic moments of R –atoms, which are highly but not completely localized. The magnetic moments of T –atoms, and the spin moments of R –atoms are calculated correctly, while the orbital moments of R –atoms are underestimated. On the other hand, $SmCo_5$ is a special case, as its lowest excited state is very close to its ground state at 0 K, because of which the correct calculation of its angular momenta and MAE are non-trivial. Further, the impact of changing different physical and numerical settings on the calculation results were also documented, most importantly the dependence of MAE on values of the $+(U, J)$ potentials, and on the core or valence character of the $R - 4f$ –electrons. Finding accurate, reliable and reproducible numerical methods is of importance, because the same types of DFT calculations can be used to calculate other physical properties of the phases, but also to investigate other compounds containing R and T –atoms.

Including the Introduction, this writing is divided in six chapters. In chapter 2 an overview of relevant subjects, definitions and concepts in magnetism are given, which includes descriptions of MAE as well as

the most important models for determining magnetization in solid materials. In chapter 3 the density functional theory is described shortly, and different mathematical techniques for solving the energy equations are introduced, which include the linearized augmented planewaves method, used in WIEN2k, and the projector augmented waves method, used in VASP. In chapter 4 permanent magnetic materials are described in more detail, especially with regard to their macroscopic properties. Important and relevant details about the transition metals, rare earths and $R - T$ based magnets are given. Further in this chapter, important details about the codes and the files that were used are described and the settings, and the reasons for them, are explained. Chapter 5 entails the results for MAE and M_S calculations and discussions of these results, their implications and the best approaches for their numerical calculation. Also contained in this chapter are the effect of variation of c/a ratio, the effect of substitution, and finally the investigation of phases based on their density of states and electronic structure. To obtain an approximation for the coercive field, the nucleation fields are calculated based on the obtained results for M_S and MAE. Chapter 6 provides the explicit numerical values obtained from selected WIEN2k and VASP calculations, the different steps in the trial and error procedures are noted and the reasons the calculations procedures fail are explored. In the end the list of references and literature works are given.

2 – Magnetism

2-1 Principles

The magnetization (\mathbf{M}) in a material is the density of dipole moments summed over the whole volume, when the material is polarized due to a field. Any material, on which a field is applied, reacts to it. This response is the magnetic induction \mathbf{B} . In vacuum it holds $\mathbf{B} = \mu_0 \mathbf{H} = \mu_0 (\mathbf{H} + \mathbf{M})$. In analogy to electric fields, it is possible to define a scalar potential for the magnetic field for an isolated pole (m) and a magnetic moment ($\boldsymbol{\mu}$) [2001 Morrish], that is $\mathbf{H} = \nabla \varphi = \nabla(m/r)$. One considers φ as the strength of a permanent magnet, which is the work done on a unit pole against the magnetic field [1998 Jiles]. The scalar potential of a single dipole, and that of the whole solid are

$$\varphi_i = -\boldsymbol{\mu} \cdot \nabla \left(\frac{1}{r} \right), \quad \varphi = \sum \varphi_i = - \int \mathbf{M} \cdot \nabla \left(\frac{1}{r} \right) dr_s \quad (2-1)$$

When all magnetic dipoles of the material align parallel, the magnetization is saturated. The microscopic magnetic moments are proportional to the angular moments of electrons. A magnetic field produces a torque on a dipole, $\mathbf{L} = \boldsymbol{\mu} \times \mathbf{H}$, and hence influences the atomic magnetic moments. This produces a precession movement of the electron moment about the direction of \mathbf{H} . This changes the original electron velocity, and is known as Larmor Precession with the frequency $\omega_L = -eH/2m_e c$ [1897 Larmor]. Maxwell summarized the electromagnetic forces in four equations, where \mathbf{E} is the electric field, ρ_e electric charge density and \mathbf{j} current density.

$$\nabla \cdot \mathbf{E} = \frac{\rho_e}{\epsilon_0}, \quad \nabla \cdot \mathbf{B} = 0, \quad \nabla \times \mathbf{E} = -\frac{\partial \mathbf{B}}{\partial t}, \quad \nabla \times \mathbf{B} = \mu_0 \mathbf{j} + \mu_0 \epsilon_0 \frac{\partial \mathbf{E}}{\partial t} \quad (2-2)$$

Magnetization in Solids: An external magnetic field induces different types of magnetization in solid materials. The different magnetic orders are labeled as paramagnetism, diamagnetism, ferromagnetism, anti-ferromagnetism and ferrimagnetism. Pure *Fe* and *Co* are ferromagnetic at room temperature, *Cu* is diamagnetic and *Y*, *Pr*, *Nd*, *Sm* and *Dy* are paramagnetic. Certain combination of *R* and *T* –atoms are strongly ferromagnetic, which is why they find application in permanent magnets.

All solid compounds have diamagnetic properties, which comes to be through reorientation of the electronic shells influenced by a field. The reaction to an external field has three sources: the electronic spin and orbital movements as well as the change in orbital momentum due to a field. Diamagnetism is produced by the last one and opposes the induction. Based on classical electrodynamics, and for a spherical atom, one calculates for atomic moments and total magnetization [2001 Morrish]

$$\langle \mu \rangle = -\sum_a \frac{e_a^2}{6m_a c^2} r_a^2 B, \quad \mathbf{M} = -N \boldsymbol{\mu} \quad (2-3)$$

To describe paramagnetism, Langevin derived the following formula [2006 Kittel]

$$M = M_s L(y) = NM_0 \left(\coth(y) - \frac{1}{y} \right) \quad \text{with} \quad y = \frac{Jg_J\mu_B H}{k_B T} \quad (2-4)$$

With J as total angular momentum, g_J the Lande Factor and μ_B as Bohr Magneton. The general equation is [\[2006 Schwabl\]](#)

$$M = Ng\mu_B J \left(\frac{2J+1}{2J} \coth\left(\frac{2J+1}{2J}y\right) - \coth\left(\frac{y}{2J}\right) \right) \quad (2-5)$$

For $y \rightarrow \infty$, the magnetization reaches its maximum and is saturated. One obtains $\mu_j = J(J+1)g_j^2\mu_B^2 = \mu_{eff}^2$ which provides an effective value below the Curie Temperature, T_C , for local moments. This effective moment only describes systems with local moments well (paramagnetism), and for systems with itinerant moments it has to be modified. At $T = 0$ one obtains $M/M_0 = 1 - 2e^{-2T_C/T}$.

Ferromagnetism (FM) arises, when the permanent magnetic moments interact and couple. In ferromagnetic materials, atomic dipole moments couple strongly, which produces a non-zero magnetization, even without an external field. Without exchange interaction, and in the absence of a field, the dipole-dipole interaction would align magnetic moments anti-parallel, disallowing a permanent magnetic field to be produced by the material [\[2002 Pollack\]](#). The magnetization is though temperature dependent. For N atoms with effective number of quantum of magnetizations (μ_B), one obtains

$$M = \frac{Ng^2J(J+1)\mu_B^2}{3k_B T} = \frac{Np_{eff}^2\mu_B^2}{3k_B T} \quad (2-6)$$

The main difference between ferromagnetism and paramagnetism (PM) is that the latter is not a “cooperative phenomenon”, i.e. the magnetization of individual atoms is independent [\[1998 Jiles\]](#). To explain the coupling of moments in ferromagnets, different theories have been developed. The most notable ones are the mean field theory and the Heisenberg Model for local moments, and the band model for itinerant systems. Some compounds exhibit no macroscopic magnetization despite having local spin moments that couple. These are called anti-ferromagnetic (AFM) materials. Néel suggested that an antiferromagnet has two sublattices of opposing but equal spin moments, with zero net magnetization [\[2001 Morrish\]](#). In an antiferromagnet the exchange parameter J is negative. Materials with more than two sublattices and also non-collinear arrangements are grouped as ferrimagnets. Among the studied phases, $PrCo_5$ and $Nd_2Fe_{14}B$ have canted magnetic structures at 0 K.

2-2 Quantum Mechanical Treatment

Langevin utilized classical thermodynamics to calculate magnetization, yet his results were in good agreement with experimental measurements [\[1906 Langevin\]](#). The reason is the assumption of the existence of moments, which in turn disallows infinite energies and limits their values. This can only be justified by quantizing energy. In a PM with no net spin moments, an applied field removes the degeneracy in the perpendicular direction of the field and divides the energy spectra into 3 lines with the

upper and lower having the same distance [1897 Zeeman], as shown in Fig. 2-1. In the Langevin Theory the moments are macroscopic and not oriented. The applied field causes the Zeeman splitting which changes energy and one obtains

$$E = -\boldsymbol{\mu} \cdot \mathbf{B} = \frac{e}{m_e} \hat{\mathbf{l}} \cdot \mathbf{B} = \mu_B (\hat{\mathbf{l}} + 2\hat{\mathbf{s}}) \cdot \mathbf{B}$$

$$\langle \mu_z \rangle = \mu \coth \left(x - \frac{1}{x} \right) = \mu L(x) \quad \text{with} \quad x = \frac{\mu_0 \mu H}{k_B T} \quad (2-7)$$

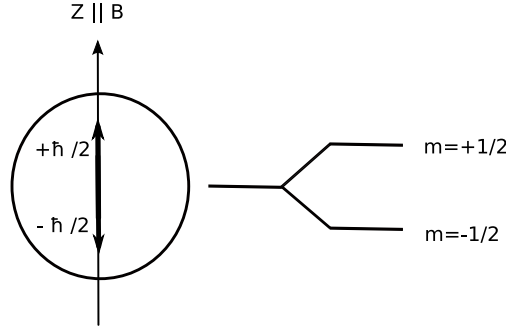


Fig. 2-1 Zeeman Splitting of two magnetic energy levels in field. Created using Inkscape [1991 INKSCAPE].

The particle number and alignment follow classical statistics. The first order term is $L(x) = x/3$, which for the particle density n , reproduces the classical Curie Law. In consequent experiments, Stern and Gerlach observed further removal of degeneracy due to inhomogeneous magnetic fields [1924 Gerlach]. This degeneracy stems from the existence of self-rotation of electrons, called spin. The self-rotation \mathbf{s} produces a moment $\boldsymbol{\mu}_s$, which is similar to the orbital moment

$$|s| = \hbar \sqrt{s(s+1)}, \quad \boldsymbol{\mu}_s = g_s \frac{e}{2m_e} \mathbf{s}, \quad \boldsymbol{\mu}_l = g_l \frac{e}{2m_e} \mathbf{l} \quad (2-8)$$

with Lande Factor g . For the projected spin moment along $\hat{\mathbf{z}}$, we have $\mu_{sz} = \frac{1}{2} g_s \mu_s \hbar$. This means that the magnetic moments cannot have arbitrary values. The moment is proportional to angular momentum with g as the proportion factor. The number of Bohr Magnetons for spin moments is $p_s = \hbar \mu_B \sqrt{s(s+1)}$.

Energy: For a particle with spin, the usual transfer from classical to quantum mechanical Hamiltonian, using $\hat{\mathbf{p}} = -i\hbar \nabla$, doesn't suffice because the magnetic moments interact explicitly with the field. This leads to a Hamiltonian of the following form

$$\hat{H} = \frac{1}{2m} \left(\hat{\mathbf{p}} - \frac{e}{c} \mathbf{A} \right)^2 - \hat{\boldsymbol{\mu}} \mathbf{H} + e\varphi \quad (2-9)$$

with \mathbf{A} and φ being the vector and scalar field potentials and $\hat{\mathbf{p}}$ the 4-vector of momentum. In a homogenous field when the vector potential is set to be $(A_x, A_y, A_z) = (-Hy, 0, 0)$, one replaces \hat{s}_z by its eigenvalue and the dependence of the wavefunction on spin is negligible [1930 Landau]. The energy contribution of the field to the Hamiltonian for an electron is

$$H = -\frac{e}{2m_e} \mathbf{B} \cdot \mathbf{L} = -\boldsymbol{\mu} \cdot \mathbf{B} \quad (2-10)$$

In a constant magnetic field, $\mathbf{A} = -\frac{1}{c}[\mathbf{x} \times \mathbf{B}]$, one has $i\mathbf{A} \cdot \nabla\Psi = -\frac{1}{2}\mathbf{l} \cdot \mathbf{B}\Psi$. This is the contribution of paramagnetism [2006 Schwabl]. Simultaneously, we can identify the diamagnetic part based on which the Dirac Equation can be constructed [2010 Dirac]

$$\frac{e^2}{2m_e c^2} \mathbf{A}^2 \Psi = \frac{e^2 B^2}{8m_e c^2} (x^2 + y^2) \Psi$$

$$[p_0 + A_0 e/c - \rho_1(\mathbf{s} \cdot \mathbf{p} + \mathbf{A}e/c) - \rho_3 m_e c] \psi = 0 \quad (2-11)$$

When considering only the spin density, magnetization direction plays no role, meaning that energy is invariant against a uniform rotation, which is true in the absence of a coupling of spin to the lattice. Dirac Equation and dipole-dipole interactions (relativistic contributions) couple the spin to the lattice. With the use of spin and orbital values, one obtains the angle dependence of the wavefunction and its behavior after rotation.

As opposed to orbital quantum number m_l , the spin quantum number m_s can have only two values $m_s = \pm 1/2$, which is projected in z -direction by $\mu_z = \mu_H = m_l(e\hbar/2m_e c) = m_l \mu_B$. When the orbital contribution is included, we obtain $p_{tot} = \mu_B \sqrt{j(j+1)}$. The precession produced by an applied field induces a change in the angular momenta, which take only specific values along the field $L_z = \hbar m_l$.

Spin-Orbit Coupling: The interaction of orbital motion with spin comprises the linear portion of relativistic energy, called Spin-Orbit Coupling (SOC). The SOC operator is given by [1974 Landau]

$$\hat{V}_{sl} = \sum_i \frac{1}{2m_e^2 c^2 r_i} \frac{dV(r_i)}{dr_i} \hat{s}_i \hat{l}_i \quad (2-12)$$

The major contribution to this effect originates from regions in close vicinity of the nuclei, where the screening is absent, based on which an estimation is made in the form $\left(\frac{Ze^2}{\hbar c}\right) \frac{m_e^2}{\hbar^2}$. With growing atomic mass, Z , the contribution of SOC to energy increases. To calculate energy of the SOC, one uses the Biot-Savart law to determine the magnetic field produced by the orbital movement at the position of a spin. The result is [2010 Demtroder]

$$\delta E_{soc} = -\mu_s B = g_s \mu_B \left(\frac{\mu_0 Z e}{8\pi \hbar m_e r^2}\right) (\mathbf{s} \cdot \mathbf{l}) \quad (2-13)$$

Due to the SOC, the total angular momentum is influenced differently by an external field as compared to the pure $\mathbf{l} + \mathbf{s}$ vector ([Fig. 2-2](#)). The total moment is $\boldsymbol{\mu}_j = -(\mathbf{l} + g_s \mathbf{s})e/(2m_e)$ and the precession of the total moment about the $\langle \boldsymbol{\mu}_j \rangle$ axis, with g_j as the Lande Factor [[1923 Lande](#)], becomes

$$\langle \boldsymbol{\mu}_j \rangle = -\frac{e}{2m_e} \left(\frac{l \cdot \mathbf{j}}{|\mathbf{j}|} + g_s \frac{s \cdot \mathbf{j}}{|\mathbf{j}|} \right), \quad \langle \boldsymbol{\mu}_j \rangle = \frac{g_j}{\hbar} \mu_B |\mathbf{j}| \quad (2-14)$$

The projection of $\langle \boldsymbol{\mu}_j \rangle$ on the z -axis is $\langle \boldsymbol{\mu}_j \rangle_z = -m_j g_j \mu_B$, which produces an energy of $E_{m_j} = -\langle \boldsymbol{\mu}_j \rangle_z B = m_j g_j \mu_B B$. The Russell-Saunders scheme describes total angular momentum, when there is no coupling [[1925 Russell](#)], and the relativistic ($J - J$) coupling when there is. In the first case $J = \sum_i l_i + \sum_i s_i$. This means that S is independent of L . In the ($J - J$) coupling a multiplet is formed by combination of vector sums of l and s , which are L and S , with $J = (L - S), (L - S + 1), \dots, (L + S)$. The energy difference in these multiplets is given by λLS , with λ as the SOC constant. The energy of a multiplet J is then given by

$$\lambda [J(J + 1) - L(L + 1) - S(S + 1)]/2 \quad (2-15)$$

One then has $J^2 = L^2 + S^2 + 2L \cdot S$, which results in a total magnetic moment of $\mu_{tot} = g \mu_B \sqrt{J(J + 1)}$. When SOC is non-negligible, the resulting J from these two schemes is not equal. The total Hamiltonian including SOC and Zeeman Term, $H_{S,B}$, is

$$H = \frac{\hbar}{2m_e} (\hat{p} + eA)^2 + V(r) - \frac{p^4}{8m_e^3 r^2} + \frac{e}{m_e} (\nabla \times A) \cdot \hat{s} + \left(\frac{1}{2m_e^2 c^2 r} \right) \left(\frac{dV}{dr} \hat{l} \cdot \hat{s} \right) - \frac{1}{4m_e^2 r^2} \frac{dV}{dr} \quad (2-16)$$

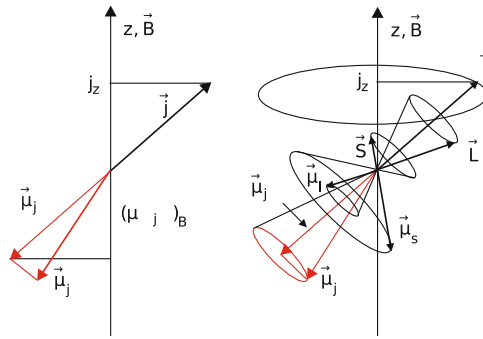


Fig. 2-2 Left: projection of $\boldsymbol{\mu}_j$ on the direction of \mathbf{j} . Right: precession of magnetic moments and their angular momenta along the field direction [[2010 Demtroder](#)].

The Langevin Formalism for paramagnets explains most R -elements well (though Nd is anti-ferromagnetic below 20 K), but for ions Eu^{3+} and Sm^{3+} , the lowest excited states are energetically very close to the ground state, which results in the mixing of the states [[1932 Van Vleck](#)]. This mixing introduces an additional, temperature independent paramagnetism, described by Van Vleck and Frank [[1932 Frank](#)], which complicates numerical calculation of their correct angular momentum numbers.

$4f^n$	Ion	S	L	J	$m_0 = gJ$	$m_{eff} = g\sqrt{J(J+1)}$	m_{eff}^{exp}
1	Ce ³⁺	1/2	3	5/2	2.14	2.54	2.5
2	Pr ³⁺	1	5	4	3.20	3.58	3.5
3	Nd ³⁺	3/2	6	9/2	3.27	3.52	3.4
4	Pm ³⁺	2	6	4	2.40	2.68	
5	Sm ³⁺	5/2	5	5/2	0.71	0.85	1.7
6	Eu ³⁺	3	3	0	0	0	3.4
7	Gd ³⁺	7/2	0	7/2	7.0	7.94	8.9
8	Tb ³⁺	3	3	6	9.0	9.72	9.8
9	Dy ³⁺	5/2	5	15/2	10.0	10.65	10.6
10	Ho ³⁺	2	6	8	10.0	10.61	10.4
11	Er ³⁺	3/2	6	15/2	9.0	9.58	9.5
12	Tm ³⁺	1	5	6	7.0	7.56	7.6
13	Yb ³⁺	1/2	3	7/2	4.0	4.53	4.5

Tab. 2-1 Quantum numbers, paramagnetic moments based on Langevin Model (m_0) and calculated and experimental effective moments of $4f$ –ions in μ_B [2010 Coey].

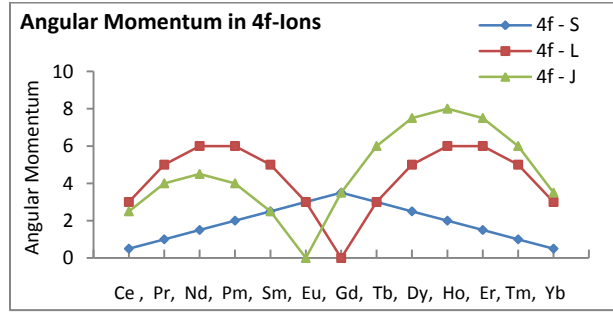


Fig. 2-3 L , S and J for the series of trivalent $4f$ –ions.

Based on a modified method, Frank found $0.85 \mu_B$ at $0 K$ and $1.55 \mu_B$ at room temperature for Sm^{3+} , which agrees well with experiment. Another R –metal that shows a special feature is Pr^{3+} , which has $|\pm 0\rangle$ at ground state, which is non-magnetic and the moment is in the easy plane ($x - y$). There is no susceptibility for small fields along \hat{z} , but a large susceptibility along \hat{x} . The direction of the field influences the splitting and hence for its description, the \hat{g} tensor is used instead of a scalar g . Non-collinear calculations with SOC account for this behavior.

$$H_Z = \frac{\mu_B}{\hbar} (B \hat{g} S) = \frac{\mu_B}{\hbar} \sum_{ij} g_{ij} B_i S_j \quad (2-17)$$

As seen from Tab. 2-1, there is a good agreement between experimental and theoretical effective moments, except for Sm^{3+} and Eu^{3+} . When considering the effective moments for $3d$ –elements, it becomes evident that their magnetization is due to spin moments and $g\mu_B\sqrt{S(S+1)}$ provides a better agreement. Based on the values for angular momenta, given in Tab. 2-1, one can visualize the evolution of these values through the series of $4f$ –ions, as shown in Fig. 2-3.

2-3 The Mean Field Theory

Weiss proposed a molecular field model with discrete energy values that cause the spontaneous magnetization. He concluded in order to explain the susceptibility of materials not obeying the Curie Law, the assumption of no interaction between moments must be abandoned and used a molecular field to describe the internal field that aligns the moments [2001 Morrish]. This is the interaction of the resultant field of all particles except one, with that one particle. The internal mean field is proportional to the magnetization, which is taken from the Brillouin Model with modified $x = \mu_0 M_0 \frac{n_W M + H}{k_B T}$.

$$H_{Mol} = n_W M + H, \quad M = n g \mu_B J B_J(x) \quad (2-18)$$

This internal field is described by the exchange interaction $J = \frac{\mu_0 n_W n_s^2 \mu_B^2}{2z}$ with z as number of neighbor atoms and n_s as the number of electrons. The exchange averages correlation.

Based on quantum mechanical considerations, Heitler and London calculated the ground state of the H_2 molecule, showing that the exchange J determines whether the state is a singlet or a triplet [1927 Heitler]. The parallel spin state is threefold degenerate and the antiparallel state is non-degenerate. Subtracting energies of the states, one obtains the following, where the sign of J determines the stable state.

$$U(S = 0) - U(S = 1) = \frac{2(U_{Col} S^2 - J)}{1 - S^4} \quad (2-19)$$

The Heisenberg Model: The generalization of the Heitler-London Model to more than two particles became the Heisenberg Model. This Hamiltonian describes the microscopic magnetic spin interactions as quantum mechanical entities [1926 Heisenberg, 1928 Heisenberg]

$$H = -2 \sum_{i,j} J_{ij} \mathbf{S}_i \cdot \mathbf{S}_j \quad (2-20)$$

Including an external field, and with a constant J and small distances we have [1987 Kittel]

$$H = -J \sum_{l,\delta} S_l S_{l+\delta} - g_J \mu_B H_{ext} \sum_l S_{zl} \quad (2-21)$$

The Heisenberg Hamiltonian is an approach for describing the spin interactions through exchange and includes the molecular field as a special case; the product of spin operators is not orientation dependent and is hence isotropic. It hinted at a new excitation particle of magnetic systems. For electrons the total wavefunctions are anti-symmetric. For a 2 electron system we have

$$\Psi(1,2) = -\Psi(2,1), \quad \Psi_a = (\Psi_1 - \Psi_2)/\sqrt{2}, \quad \Psi_s = (\Psi_1 + \Psi_2)/\sqrt{2} \quad (2-22)$$

In the triplet state, the electrons don't reside in the same state, but in the singlet state that is possible. The difference in energies for Ψ_1 and Ψ_2 defines the exchange integral, while the hopping integral t describes the transfer of electrons from one site to another

$$J = \frac{1}{2}(\varepsilon_1 + \varepsilon_2) = \int \Psi_1^*(r_2)\Psi_2^*(r_1)H(r_1, r_2)\Psi_1(r_1)\Psi_2(r_2)d^3r_1d^3r_2$$

$$t \cong \int \Psi_1^*(r_1)\Psi_2^*(r_2)H(r_1, r_2)\Psi_2(r_1)\Psi_1(r_2)d^3r_1d^3r_2 \quad (2-23)$$

In the Heisenberg Hamiltonian, building the trace gives the partition function, Z , from which magnetization is obtained, with particle density n [2006 Schwabl]

$$Z = Tr(e^{-H/k_B T}) = \sum_i e^{-E_i/k_B T}, \quad M = nk_B T \frac{d(\log Z)}{dH} = \frac{N \sum_i M_i e^{-E_i/k_B T}}{\sum_i e^{-E_i/k_B T}} \quad (2-24)$$

Without SOC, the spin moments are independent of the orbital moments, which are much smaller.

The Crystal Electric Field: When atoms form solids, the electric field produced by the charges of other atoms influences a specific atom. This field is responsible for the quenching of the orbital moments in magnetic electrons of $3d - T$ and for the magnetocrystalline anisotropy (MCA). The potential is

$$\Phi_{CEF}(R) = \int \frac{\rho(r')}{4\pi\epsilon_0|r-r'|} d^3r' \quad (2-25)$$

with $\rho(r')$ as charge distribution. At the position of an atom we have [2009 Skomski]

$$\Phi_{CEF}(0, \theta, \varphi) = \sum_{n=0}^{\infty} \sum_{m=-n}^n \frac{4\pi r^n}{2n+1} \int \frac{\rho(r')(-1)^n Y_m^n(\theta', \varphi')}{r'^{n+1}} d^3r' Y_m^n(\theta, \varphi)$$

$$E_{CEF} = \int \rho_0(R) \Phi_{CEF}(R) d^3r \quad (2-26)$$

This provides a contribution to total energy alongside Coulomb, the SOC and the Zeeman terms. The localized $4f$ -states are influenced weakly by the CEF, due to shielding by outer shells and their E_{CEF} is small. The $3d$ -orbitals follow the lattice symmetry and resume the CEF [1998 Richter] and are accordingly strongly influenced by CEF, while the SOC is negligible for them. The quenching of orbital moments of the $3d - T$ is seen when the eigenfunctions of the CEF Hamiltonian are calculated. Their angular momentum vanishes equally along \hat{z} [2005 Mohn].

Following the Hund's Rules, the angular momenta μ_l of d -electrons in $3d - T$ ought to be obtainable through their total momentum J . The crystal field though causes a splitting larger than the SOC and lifts the degeneracy, resulting in J not being a good quantum number any more. To reduce the interaction with CEF, specific axes are preferred. The aspheric configuration of CEF and the strong SOC in uniaxial crystals allow strong magnetocrystalline anisotropy energy (MAE) [2005 Rossignol]. When an orbital is occupied by two electrons, there is an on-site Coulomb Energy (U). In the case, when this energy is

smaller than the splitting caused by the CEF, both spin states of the orbital are occupied. This produces an electrostatic field at the ionic site, which has a specific direction (Fig. 2-4). This anisotropy of the spin density is especially important in magnets with $R - 4f$ -electrons.

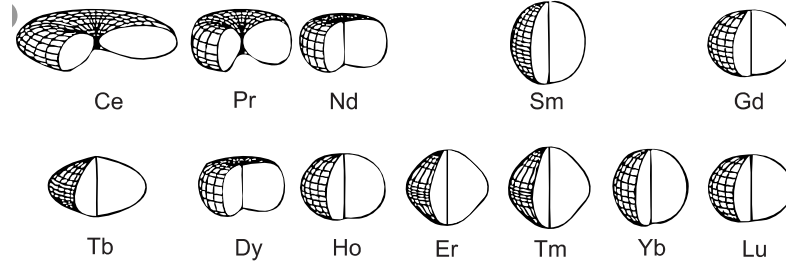


Fig. 2-4 Charge density distributions for trivalent R -ions at 0 K. Deviations from spherical symmetry are exaggerated [2010 Coey].

A quantitative description of the effect of CEF on orbitals was developed by Stevens [1951 Stevens] and Hutchings [1964 Hutchings], who reformulated the crystal field to obtain energy terms from L_i .

$$H_{CEF} = \sum_{n=0,2,\dots} \sum_{m=-n}^n \Theta_j^n \langle r_{4f}^n \rangle A_m^n \hat{O}_m^n \quad (2-27)$$

Crystal field parameters, A_m^n , are calculated from distances and charge density and represent the configuration of the CEF. Stevens' Coefficients, Θ_j^n , are element specific constants (for $n = 2$, $\Theta_j^n = \alpha_j$), which describe how much the shell deviates from spherical symmetry, and $\langle r_{4f}^n \rangle$ are the average radius for the multipole moments. For Sm , α_j is positive, for Pr and Nd , negative. \hat{O}_m^n are the Stevens' Operators that depend only on angular momenta. In essence $A_2^0 > 0$ and $\alpha < 0$, as well as $A_2^0 < 0$ and $\alpha > 0$ favor uniaxial MCA. The first is observed in $Nd_2Fe_{14}B$ at room temperature and the second in $SmCo_5$. At low temperatures, the negative α_j of Nd forces a non-collinear magnetization. This results in a phase transition from uniaxial to canted magnetization with decreasing temperature. In $PrCo_5$, the $R - T$ coupling is strong enough to force a basal anisotropy (negative value for anisotropy) at 0 K.

Anisotropy: In FM materials, magnetizing the specimen is easier in certain crystallographic directions compared to other directions, as shown in Fig. 2-5. An electron conceives the electric field of the nucleus as a magnetic field, which interacts with its own spin-induced field. This leads to orientation of spin moments compared to the orbital moments and removes the invariance of energy after a uniform rotation [1997 Brooks]. The result is different energy values for magnetization in two different directions. This effect is the cause of MAE, which is shape independent. Prerequisite for a hard magnet is having a large anisotropy. The MCA comes to be by way of energy minimization, when electron shells of an atom without spherical symmetry are subjected to forces created by the CEF of all the other atoms. The change

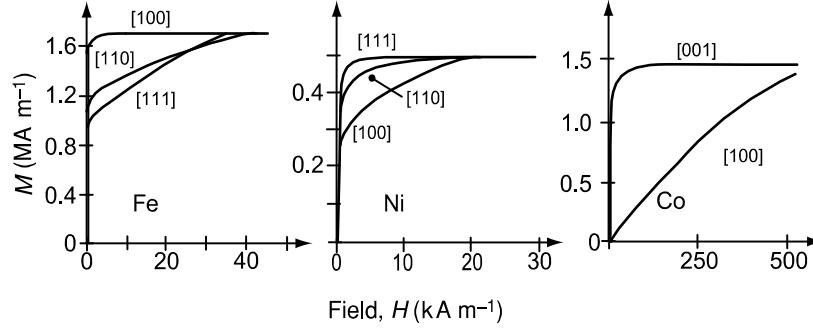


Fig. 2-5 Magnetization of single crystals of iron, cobalt and nickel [2010 Coey].

in orbital shape is accompanied by a change in orbital moment, as well as in spin moment. The latter is influenced by the SOC to orient itself rather than remain isotropic. The amount of energy required to magnetize the compound is stored in the crystal [2009 Cullity]

$$E_{MCA} = \sum_{l=2,4,6} \kappa_m^l A_m^l Y_m^l(\theta, \varphi) \quad (2-28)$$

The cosine functions of angles between magnetization direction and crystal axes can be used to describe MAE, which is the energy spent to align the domains parallel to a certain axis compared to the easy direction [2010 Coey]. While MCA is an intrinsic property, it can be influenced by the domain structure. For a hexagonal structure, one writes [2007 Kronmuller]

$$E_{MCA}(\mathbf{r}) = K_0(\mathbf{r}) + K_1(\mathbf{r}) \sin^2 \theta(\mathbf{r}) + K_2(\mathbf{r}) \sin^4 \theta(\mathbf{r}) + K_3(\mathbf{r}) \sin^6 \theta(\mathbf{r}) + K_4(\mathbf{r}) \sin^6 \theta(\mathbf{r}) \cos(6\phi(\mathbf{r})) \quad (2-29)$$

where θ corresponds to the angle between saturation magnetization \mathbf{M}_s and the c -axis of the crystal structure, and ϕ the projection of magnetization on the hexagonal plane with regard to a -axis.

For tetragonal structures we get similarly

$$E_{MCA}(\mathbf{r}) = K_0(\mathbf{r}) + K_1(\mathbf{r}) \sin^2 \theta(\mathbf{r}) + K_2(\mathbf{r}) \sin^4 \theta(\mathbf{r}) + K_3(\mathbf{r}) \sin^4 \theta(\mathbf{r}) \cos(4\phi(\mathbf{r})) + \dots \quad (2-30)$$

Depending on the sign and strength of K_1 and K_2 , three different magnetic states are distinguished.

$$\text{Uniaxial} \quad K_1 > 0, K_2 > 0 \quad \text{or} \quad K_1 > 0, K_2 < 0, |K_2| < \frac{1}{2} K_1$$

$$\text{Easy cone} \quad K_1 < 0, K_2 > 0, K_2 > \frac{1}{2} |K_1|$$

$$\text{Easy plane} \quad K_1 < 0, K_2 < 0 \quad \text{or} \quad K_1 < 0, K_2 > 0, K_2 < \frac{1}{2} |K_1|$$

When the CEF cannot eradicate the orbital degeneracy fully, anisotropy becomes considerably large. If one considers the anisotropy as a hindrance to the rotation of the magnetization from the easy axis, one arrives at the concept of anisotropy field H_A , which is the field that saturates magnetization of a uniaxial system in the hard axis. With $E_{MCA} = K_u \sin^2 \theta - \mu_0 M_S H \cos\left(\frac{\pi}{2} - \theta\right)$, and $\theta = \pi/2$ and $dE/d\theta = 0$, and $K_2 = 0$, one obtains

$$H_A = 2K_1/\mu_0 M_S. \quad (2-31)$$

2-4 Solid State Theories

The distribution probability of weakly interacting electrons is described by Fermi-Dirac statistics, which is based on the assumption of indistinguishable particles obeying the exclusion principle [[2005 Mohn](#)]

$$f(\varepsilon) = \frac{1}{\frac{\varepsilon - \mu}{k_B T} + 1} \quad \text{which gives } n_s = a_s f(\varepsilon) \quad (2-32)$$

for the number of occupied states n_s , based on the total number of states a_s and with the chemical potential μ . The partition function for such a system is obtained by $Z = \sum_s a_s \left(\ln \left(1 + e^{\frac{\mu - \varepsilon}{k_B T}} \right) \right)$. In a free atom, only electrons that are unpaired are magnetic and most free atoms exhibit a small moment. This changes when solids are formed. Electron transfer, chemical bonds and electronic bands result in atoms becoming non-magnetic, or retain only a weak magnetization. Since the electron configuration in solids is dictated partially by the crystal structure and chemical bonds, the composition and the symmetry are important factors for magnetization. In a solid, discrete energies of individual atoms, ε_s , are replaced by energy bands and the number of states a_s by the density of states $N(\varepsilon)$, abbreviated as DOS. The partition function is rewritten to

$$Z = \int_0^\infty N(\varepsilon) \ln \left(1 + e^{\frac{\mu - \varepsilon}{k_B T}} \right) d\varepsilon \quad (2-33)$$

The Fermi Surface is of immense importance because it is the region around which the excitations exist [[1974 Landau](#)]. In systems of localized electrons, the ground state occupation of shells follows the Hund's Rules: I) The sequence provides the largest multiplicity; II) For the largest multiplicity, the angular momentum is maximized; III) for I) and II) and less than half-filled shells, the smallest J is chosen, for more than half-filled shells the largest. With $L = \sum_i l_i$ and $S = \sum_i s_i$, $J = L \pm |S|$, the multiplicity is $2|S| + 1$ and indicates the ground state degeneracy. Applied to the Sm^{3+} ion with an occupancy of 5, one then obtains $S = 5/2$, $L = 5$ and $J = 5/2$. Using the free electron gas and based on the Pauli Principle, the state of the free electrons are determined by the wave vector \mathbf{k} and spin, but each \mathbf{k} can be occupied only

by two electrons of opposing spin. When the electrons don't interact, one obtains a susceptibility that depends on DOS at Fermi Energy, $N(E_F)$ [[1927 Pauli](#)].

Domains: That ferromagnets acquire magnetizations much larger than those of the fields inducing them, hints at two possibilities: statistically random directions of atomic moments without a net value, which can become parallel due to a field; or microscopic regions (much larger than single atoms) with aligned moments that have randomly oriented directions. In order to explain the seemingly continuous increase in magnetization of a magnet subjected to an increasing external field from zero to saturation, Weiss proposed a domain structure. Each domain has its own magnetization value and direction [[2001 Baberschke](#)]. This means that in ferromagnets, magnetization is the alignment of domains and not moments. Weiss further suggested that neighboring moments couple strongly, which decreases their energy. This is the mean field contribution. The use of this concept is limited to paramagnetism, because in ferromagnets the magnetization changes locally.

Changing the direction of a domain from its easy axis requires energy. To explain the curve for Fe in [110] direction ([Fig. 2-5](#)), one considers a field applied in [110]. Without a field, the magnetization of each domain lies along one of the six easy axes in such a way that a net zero magnetization is stable. With a small field \mathbf{H} in [110], the domains align themselves to the two easy directions in general direction of [110] with equal numbers. These are [100] and [010]. With growing strength of \mathbf{H} , the domains start orienting themselves in that direction, and build an angle θ with \mathbf{H} , while for energy $F_H = -\mathbf{M} \cdot \mathbf{H}$ holds [[1997 Brooks](#)]. The logic of the Weiss Theory for paramagnetism applies also to individual ferromagnetic domains well below T_C . Inside the ferromagnetic domains the effect of the external field is small compared to interaction energy.

To illustrate why domains form, one starts with a state where strains, external fields and inhomogeneities are not present. For a cubic sample with magnetization along an easy axis, which is parallel to the edge of the cube, the MCA is minimal and so is exchange energy, since only a single phase exists. But such a configuration produces a large demagnetization field ([Fig. 2-6\(a\)](#)). Energy of the demagnetization field, F_D , is so large that a proper change in domain structure that would increase the anisotropy energy F_K and exchange energy, F_X , slightly, but majorly reduce F_D lowers total energy and hence occurs ([Fig. 2-6\(b\)](#)). Between these two domains a region exists, where the moments are not parallel to either domain, and this increases F_X and F_K , but the number of moments in these intermediate regions is small and hence energy increase in F_X and F_K is still smaller than the decrease in F_D . Further divisions to further decrease F_D and minimize total energy are possible. It is thus evident that the demagnetization field is the primary source of domain structure. This field stems from long range dipole interaction, which is why it compensates the short range but stronger exchange forces. These short range exchange interactions are responsible for uniform magnetization in a single domain.

Hysteresis: Without a field the average sum of magnetization is zero, which is called a demagnetized state. The general process of magnetization is shown in [Fig. 2-6\(right\)](#). With increasing applied field, the magnetization grows until saturation is reached. Reducing the field back to zero leaves a net magnetization in a ferromagnetic specimen. Magnetizing the material in the reverse direction will saturate its magnetization with the opposite sign. Decreasing the field in the reverse direction and increasing it again in the positive direction closes the cycle, while the first branch starting from 0 (virgin curve) will not be reached again because of the remanence. The field in the opposite direction of the original magnetization, which is needed to nullify the magnetization ($M_H = 0$) is the coercive field H_C . This value is of importance to permanent magnets because it indicates the resistance of a ferromagnet against changing its easy magnetization direction.

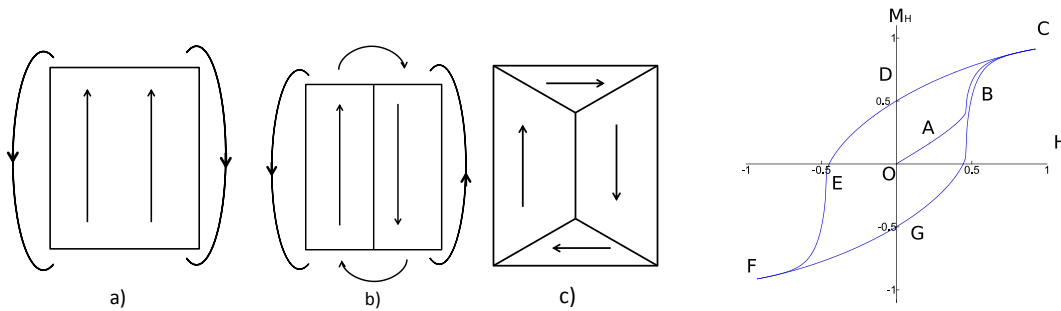


Fig. 2-6 Left: hypothetical domain configurations of an initially single domain (a), which splits into two (b) and four (c) due to demagnetization fields. Right: magnetization curve (OABC) and hysteresis loop (CDEFGC) of a typical ferromagnet [\[2010 WP\]](#).

Itinerant Systems: Conduction electrons are a source of magnetism in some compounds (e.g. $3d - T$). The major contribution to magnetism is delivered by the $d -$ electrons that are close to E_F . The Fermi Surface is of immense importance because it is the region around which the excitations exist. It is the splitting of up and down spin states near E_F that gives rise to the moments of $3d -$ metals [\[1997 Brooks\]](#). The first step for a quantitative evaluation is the description of the non-interacting particles. With a constant potential V , chosen as zero, one has $H = \frac{p^2}{2m_e} + V(r) \rightarrow -\frac{\hbar^2}{2m_e} \nabla^2 \psi_0 = \varepsilon_0 \psi_0$, which results in $\psi = \frac{1}{L^{3/2}} e^{i\mathbf{k}r}$. With \mathbf{k} as wavevector, energy $\varepsilon = \hbar^2 k^2 / 2m_e$ and

$$E_F = \frac{\hbar^2}{2m_e} (3\pi^2 n)^{2/3} \quad \text{with} \quad n = \frac{N}{L^3} \quad (2-34)$$

N is the number of electrons and L^3 is the volume. For free electrons with a spherical Fermi Surface, the DOS is $N_{up,dn}(\varepsilon) = \frac{1}{4\pi^2} \left(\frac{2m_e}{\hbar} \right)^{3/2} \sqrt{\varepsilon}$. For large DOS, the bands reduce their energies by splitting, which is the cause of spontaneous ferromagnetism.

Covalent magnetism: The d –electrons are not completely free, but weakly bound to their nuclei, which results in direction preferences for bonds. Their bonds have hence covalent characteristics. These bonds are not strictly covalent though, as the high electric conductivity shows. The magnetism they produce is not equal to that of free electrons, which is why it is called covalent magnetism [1981 Williams]. Notably, covalent bonds reduce orbital moments [1955 Owen]. The concept of the covalent magnetic bonds is used to describe the interactions of a magnetic impurity in a non-magnetic matrix. The spin-up and spin-down states of the impurity influence the polarization of the host atoms differently. This difference will produce a net magnetic moment, which depends on the DOS of spin-up and spin-down energies as well as their difference. Whether the polarization of the atoms is parallel or anti-parallel depends on whether the impurity has a less or more than half filled shell. The polarization is anti-parallel (e.g. Cr), when the the shell is filled less than half, it is nearly zero (Mn), when the shell is half-filled, and it is parallel (Fe, Co, Ni), when the shell is more than half filled [1965 Moriya]. Based on the RKKY model [1954 Rudermann, 1956 Kasuya, 1957 Yosida] the magnetic impurity in a non-magnetic host produces decaying oscillations of susceptibility and magnetization. The spin-up and spin-down electrons are scattered differently, which shifts the spin-up densities differently compared to spin-down, resulting in an oscillation of magnetization.

The Stoner Model: For a (non-ferromagnetic) metal, with energy E , an applied field decreases electronic energy for parallel and increases it for anti-parallel spin alignment. Assuming $g = 2$ and $s = 1/2$, we have $E = E_0 \mp \mu_B H$. When a field is applied, the system reaches equilibrium when the Fermi Levels become equal through anti-parallel spins changing their direction. However, because $\mu_B H \ll E_F$, their numbers are small and paramagnet metals exhibit a small susceptibility. Stoner and Slater proposed band theories with free electrons, which are in effect a field model using the band structure, as opposed to the discrete levels of the Weiss Model [1933 Stoner, 1937a Slater]. If the spin-up and down bands are split, the band with lower energy is filled completely resulting in an integer moment value. If the bands aren't split, averaged atomic moments become possibly non-integer. This imbalance in spin states arises from the exchange interaction, which is sufficient to excite some electrons. If n is the density and $M = (n_{up} - n_{dn})\mu_B$, the exchange energy becomes $-I_S(n_{up} - n_{dn})/4n$. The Stoner Interaction is a portion of the Coulomb Interaction of electrons on the same site. It is calculated by $N_S \chi_{Pauli} = \frac{I_S N(E_F)}{2n}$. This means for $(I_S N(E_F)/2n) > 1$ the metal is spontaneously magnetized, and is ferromagnetic. This is known as the Stoner Criterion. The magnetic electrons in this model are the spins in the d –band. The molecular field is $H_{mol} = n_w M = N_w M_0 \xi$, with $\xi = M/M_0$. The molecular field moves the spin-up and spin-down bands compared to each other, while E_F remains unchanged. The shift also changes the occupation numbers of the bands. Magnetic energy is $E_m = -N k_B \theta \xi^2 / 2$ with $\theta = \mu_B N M_0 / k_B$. For the states at Fermi Energy, before (ε^-) and after the shift (ε^+), the DOS reads

$$\frac{N}{2} \xi = \int_0^{E_F} N(\varepsilon) d\varepsilon, \quad \frac{N}{2} \xi = \int_{E_F}^{\varepsilon^+} N(\varepsilon) d\varepsilon, \quad \frac{N}{2} \xi = \int_{\varepsilon^-}^{E_F} N(\varepsilon) d\varepsilon \quad (2-35)$$

Even though the shift is very small compared to the value of the Fermi Energy, it is nonetheless the underlying source of induced magnetism. The strength of the magnetization due to the shift is

$$M = (n_{up} - n_{dn})\mu_B = 2N_{up,dn}(E_F)\mu_B^2 B \quad (2-36)$$

In the Heisenberg Model the magnetic moments are treated as localized, which does not describe the state of valence electrons in metals. Band theories provided answers to the question of itinerant electrons' moments. Nonetheless the Stoner Model results in Curie Temperatures that are nearly 10 times larger than experimental values in ferromagnets. The reason is that the formulation based on parabolic bands and single particle excitations do not describe the physics of the itinerant electrons well and need to be modified to include all band types and collective excitations. The model nonetheless describes "weak itinerant ferromagnets" well, that is, when $M_0\mu_B \ll 1$, with M_0 being the 0 K moment. Rising temperatures not only weaken the long range, but also the on-site correlations.

In the free electron gas concept there is a constant potential acting on the electrons, and the band structure is thus determined. The next step is to consider the periodic ion-core potential $V(r) = V(r + R)$. The wavefunction then becomes a planewave. Using the Bloch Factor [1928 Bloch] one writes

$$\psi_k = u_k(r)e^{ikr}, \quad u_k(r) = u_k(r + R) \quad (2-37)$$

The free electron model can be generalized using the effective mass $\frac{1}{m^*} = \frac{1}{\hbar^2} \frac{d^2\varepsilon}{dk^2} \Big|_{E_F}$, and electron energy resembles that of the free electron gas but with a modified effective mass $E = \hbar^2 k^2 / 2m^*$. The effective electron mass is needed due to band effects. Pauli considered nearly free electrons and concluded that magnetization becomes dependent on Fermi Temperature (T_F) [1927 Pauli]. Including the electron-lattice interactions is done by using the effective electron mass directly, as well as in Bohr Magneton. Temperature dependence enters susceptibility only as a second order correction as $T > 0$ provides occupied states above E_F and unoccupied ones below. For a parabolic band with $N(\varepsilon) \sim \sqrt{\varepsilon}$, total free energy becomes

$$E = E_{band} + E_{mag} = \frac{3}{10} n_{E_F} [(1 + \xi)^{5/3} + (1 - \xi)^{5/3}] - \frac{1}{2} n k_B \theta \xi^2 + Const. \quad (2-38)$$

which provides for $dE(\xi)/d\xi = 0$, $\varepsilon^+ - \varepsilon^- = 2k_B\theta\xi = \delta E$. This is the band splitting in the Stoner Model, which orders the moments parallel, and increases kinetic energy. Depending on the value of $k_B\theta/E_F$, three phases can be distinguished: I) For $k_B\theta/E_F < 2/3$ the system is non-magnetic. II) For $2/3 < k_B\theta/E_F < \sqrt[3]{1/2}$, the system is weakly ferromagnetic. III) For $k_B\theta/E_F \geq \sqrt[3]{1/2}$, the system is strongly ferromagnetic.

With $k_B\theta$ varying marginally from metal to metal, it becomes evident that DOS plays the decisive role. An s -band can't provide large values of DOS at E_F , but a narrow d -band can. The obtained equations though result in susceptibility values in disagreement with experiment, even for alkali metals. Slater

developed this concept further using more accurate band models and concluded that for a correct description of the exchange, the locally varying electronic density potential should be used [[1951a Slater](#)].

$$V_{Slater}(r) = -3e^2 \left(\frac{3}{8\pi}\right)^{1/3} \rho(r)^{1/3} \quad (2-39)$$

The Tight Binding Model: In the Heisenberg Model, the exchange occurs between spins. In metals the overlap of wavefunctions of partially delocalized electrons and the effective interaction of the fully delocalized ones are important exchange interactions but the spins are not local as assumed in the model. In the framework of the tight-binding model, there is a small wavefunction overlap and energy is given by

$$H = \sum_{ij} t_{ij} c_i^\dagger c_j \quad (2-40)$$

with t_{ij} as hopping or transfer integral, and c and c^\dagger as annihilation and creation operators. This model is used as the basis for many electronic structure calculations, and the Hubbard Model is also based on this concept. For bands that are nearly full, or nearly empty, the exchange is ferromagnetic, as electrons can transfer to other spin-up states. But in nearly half-filled cases (*Cr*, *Mn*) it is antiferromagnetic because only spin-down states can be transferred into. Large bandwidth t_{ij} delocalizes the electrons and reduces exchange. The electron-core interaction is accounted for by using effective mass m^* in $E_F(T = 0)$. But electrons also interact with each other. Coulomb Interaction is independent of spin direction and does not influence the susceptibility, but exchange and correlation depend on the number of (anti-)parallel spins. Exchange increases the susceptibility of an electron gas. Correlation on the other hand is energy of the repelling force between two electrons with anti-parallel spin and decreases susceptibility by way of weakening the influence of exchange [[1954 Pines](#)]. In essence, large correlation is favorable for magnetization.

Hubbard designed a model with narrow $3d$ bands, where the electrons behave as delocalized, but their charge density close to a nucleus is large enough for them to be associated with the nucleus [[1963 Hubbard](#)]. The Hubbard Hamiltonian describes transfer energy and the change in energy due to Coulomb Repulsion of two electrons at one site. The ion core, repelling or attracting an electron, provides the correlation energy. If some electrons have a weak correlation with a nucleus, but strong exchange with nearby electrons, this model describes them as itinerant type electrons. The Hubbard Hamiltonian is

$$H = -\sum_{ij} t_{ij} c_i^\dagger c_j + U \sum_i n_{i,up} n_{i,dn} \quad (2-41)$$

Another approach is to include the so called self-interaction corrections to band structures. This localizes the $4f$ –states even further and results in a splitting, which is used in the current calculations.

3 – Density Functional Theory and Numerical Methods

3-1 Description of Periodic Solids

In most parts of this chapter, atomic units have been used, that is $e \triangleq 1$, $m_e \triangleq 1$, $\hbar \triangleq 1$, $4\pi\epsilon_0 \triangleq 1$, $c \triangleq 1$. For a system with N electrons at positions \mathbf{r} , and N' nuclei at positions \mathbf{R} , the general Schrodinger Equation is $H(\mathbf{R}, \mathbf{r})\Psi(\mathbf{R}, \mathbf{r}) = E\Psi(\mathbf{R}, \mathbf{r})$. Considering the Coulomb Interaction gives [\[2006 Staemmler\]](#)

$$\begin{aligned} H(\mathbf{R}, \mathbf{r}) &= T_n + T_{el} + U_{n,el} + U_{el,el} + U_{n,n} \\ &= -\frac{1}{2}\sum_a^{N'} \frac{\nabla_a^2}{M_a} - \frac{1}{2}\sum_i^N \nabla_i^2 - \sum_i^N \sum_a^{N'} \frac{Z_a}{r_{ia}} + \sum_i \sum_j \frac{1}{r_{ij}} + \sum_a^{N'} \sum_b^{N''} \frac{Z_a Z_b}{r_{ab}} \end{aligned} \quad (3-1)$$

T are kinetic and U Coulomb Energy terms, el denotes electrons and n core energies. The overall ground state is determined by electrons as they are light and fast compared to the frozen nuclei, and reach equilibrium immediately after any change in potential, which allows dividing the wavefunction into electronic and nucleonic parts $\Psi(\mathbf{R}, \mathbf{r}) = \Psi_{el}(\mathbf{R}, \mathbf{r})\Psi_n(\mathbf{R})$ and thus $H_{el}\Psi_{el}(\mathbf{R}, \mathbf{r}) = E_{el}(\mathbf{R})\Psi_{el}(\mathbf{r}, \mathbf{R})$ [\[1927 Born\]](#). Thus, T_n needs not be included. In a two electron system the interaction term doesn't allow the Hamiltonian to be simply divided into the sum of the two single-electron Hamiltonians. Hartree rewrote the many-electron wavefunction as a product of wave functions of single particles [\[1928 Hartree\]](#).

$$\Psi(\mathbf{r}_1 s_1, \mathbf{r}_2 s_2, \dots, \mathbf{r}_N s_N) = \psi_a(\mathbf{r}_1 s_1) \dots \psi_n(\mathbf{r}_N s_N) \quad (3-2)$$

The one-electron, Schrodinger-type Equation has a Coulomb Potential U drawn from the mean field with

$$(-\nabla^2 + V_{ext} + U_i)\Psi_i(\mathbf{r}, s) = \epsilon_i \Psi_i(\mathbf{r}, s), \quad \nabla U_i = 4\pi e^2 \sum_{i \neq j} |\psi_j|^2 \quad (3-3)$$

One then utilizes the Slater Determinants [\[1929 Slater\]](#), which ensure antisymmetry due to Pauli Principle

$$\Psi(1, \dots, N) = |\psi_a(1)\psi_b(2) \dots \psi_n(N)| \quad (3-4)$$

The orbitals including spin are chosen as orthonormal $\langle \psi_a | \psi_b \rangle = \int \psi_a^* \psi_b d\tau = \delta_{ab}$. An important property of the Slater Determinants is that for spin orbitals these determinants are the eigenfunctions of the N –electron spin operator \mathbf{S}_z , that is $\mathbf{S}_z \Psi = M_s \Psi$ with $M_s = (N_\alpha - N_\beta)/2$, α is the spin-up state and β the spin-down state. In a closed shell system, these determinants are also eigenfunctions of the \mathbf{S}^2 operator. In a system with $2n$ electrons with spins we have a singlet state ($S = 0$) described by

$$\Psi_{SCF} = |\psi_{1,\uparrow}\psi_{1,\downarrow}\psi_{2,\uparrow}\psi_{2,\downarrow} \dots \psi_{N,\uparrow}\psi_{N,\downarrow}| \quad (3-5)$$

Using the variational principle with the Lagrange Multiplier method, one obtains an orthonormal set of orbitals, which minimizes energy [\[2006 Staemmler\]](#)

For each φ_i , one obtains $[h + \sum_j^{occ} (2U_j - J_j)]\varphi_i = \sum_j^n \lambda_{ij} \varphi_j$, with h representing the one-electron operator, U the Coulomb Integral and J the exchange interaction. In this way, exchange energy is accounted for but correlation is ignored. It is possible to diagonalize λ_{ij} , with ε_i being the diagonalization element. We then have

$$h + \sum_j^{occ} (2U_j - J_j) = F, \quad F\varphi_i = \varepsilon_i \varphi_i. \quad (3-6)$$

F is the Fock Operator [1930 Fock] and the latter expression is the Hartree-Fock equation. U and J depend on φ_i which are obtained by solving (Eq. 3-6). This means the solution requires an iterative scheme and is solved self-consistently (SCF calculation). Energy of the system is obtained through $E_{SCF} = \sum_i^n [\langle i|h|j \rangle + \varepsilon_i]$. The essential idea behind the calculation of electronic structure is hence the following: I) The orbital functions are obtained.

II) The wavefunction is constructed with $\psi_k(R) = \sum_{n,m} a_{nm}(k) \sum_k e^{ikR} \varphi_m(r - R)$.

III) Variation principle is used to obtain $a_{nm}(k)$ for $|H_{nm} - E\delta_{nm}| = 0$.

Atomic φ_n are orthonormal and the on-site contributions are grouped together. The $n - 1$ electrons provide a mean field for the electron in consideration. For the exchange, with ξ as relative magnetization, and total energy, one has [2005 Mohn]

$$J = -\frac{1}{2} \left(\sum_{ij}^\alpha J_{ij} + \sum_{ij}^\beta J_{ij} \right) \rightarrow J = -\frac{3}{8} n \varepsilon_j [(1 + \xi)^{4/3} + (1 - \xi)^{4/3}]$$

$$\frac{U}{n \cdot E_F} = \frac{3}{10} [(1 + \xi)^{5/3} + (1 - \xi)^{5/3}] - \frac{8 \varepsilon_j}{3 E_F} [(1 + \xi)^{4/3} + (1 - \xi)^{4/3}] \quad (3-7)$$

For $\varepsilon_j < 2E_F$, a paramagnetic structure is found at $\xi = 0$. For $\varepsilon_j > 2E_F$, the minimum is at $\xi = 1$, which results in an ordered phase with Coulomb Interactions. Using realistic potentials with finite ranges instead of Coulomb Potential with its infinite range allows for a better approximation. This Hartree-Fock implementation includes an exchange term, but remains of one-electron Schrodinger Type. It is possible to approximate exchange in a system, even when the density is not homogenous [1975 Gunnarson]. Based on Dirac's exchange energy, Gaspar developed a potential using a variation method, which described systems with inhomogeneous densities well, showing that density of the original, homogenous system can be a good approximation [1954 Gaspar]. This paved the way for DFT.

3-2 Principles of Density Functional Theory

Based on the works of Hohenberg and Kohn, it became evident that it is possible to calculate the ground state energy for a system of interacting particles through density [1964 Hohenberg]. This approach is based on two theorems.

I) The ground state electronic density $n_0(\mathbf{r})$ in a system under the influence of a $V_{ext}(\mathbf{r})$ determines this potential exactly, so that the expectation value of any observable is given uniquely by n_0 , as

$$\langle \psi | \hat{O} | \psi \rangle = O[n_0]. \quad (3-8)$$

II) One can define for total energy a functional of density

$$E_V[n] = \int V(\mathbf{r})n(\mathbf{r})d\mathbf{r} + F[n],$$

$$F_{HK}[n(\mathbf{r})] = \langle \Psi | T + V_{ee} | \Psi \rangle \quad (3-9)$$

F_{HK} is a “universal” functional, for which a description must be found. The density is given as $n(\mathbf{r}) = \sum_{occ} |\psi_i(\mathbf{r})|^2$ and the wavefunctions are normalized by $\int d\mathbf{r} |\psi_i(\mathbf{r})|^2 = 1$ [2006 Blugel]. The important result is that through this functional the ground state density is specified, as this is the density that corresponds to n_0 and the density that minimizes the functional [2012 Martin]. The thus acquired minimum of F_{HK} determines $E_{V_{ext}}[n]$ [2006 Jones]. An important advantage of DFT is that only the atomic number of atoms creating the compound are required. All other properties are in essence calculated based on this information [2006 Blugel]. When ground state density is known, ground state energy, as well as all other electronic properties of the ground state are obtained based on it.

The Hohenberg-Kohn Theorems lead to the conclusion that $n(\mathbf{r})$ is uniquely determined if $V_{eff}(\mathbf{r})$ is found and vice versa. To calculate exchange-correlation energy, E_{XC} , from the effective potential, the following relation is used [2006 Kurth] (*c. c.* stands for complex conjugation)

$$\sum_{s=\alpha,\beta} \sum_{k=1}^{N_s} \int d^3r \left[\varphi_{js}^*(\mathbf{r}') \left(V_{XC}(\mathbf{r}') - \frac{1}{\varphi_{js}^*(\mathbf{r}') \delta \psi_{js}(\mathbf{r}')} \right) \right] \cdot \sum_{k \neq j} \frac{\psi_{ks}(\mathbf{r}) \psi_{ks}^*(\mathbf{r}')}{\varepsilon_{js} - \varepsilon_{ks}} + c. c. \quad (3-10)$$

This optimized effective potential is in effect the one-electron potential that provides the one-electron orbitals, from which the ground state density is obtained. The potential is calculated by minimizing

$$\frac{\delta E_V}{\delta V_{eff}(\mathbf{r})} = \int d^3r' \frac{\delta E_V}{\delta n(\mathbf{r}')} \frac{\delta n(\mathbf{r})}{\delta V_{eff}(\mathbf{r})} = 0 \quad (3-11)$$

The Density Matrix: Not always all the information about a system is given or known. The concept of density operator allows the incorporation of incomplete information to achieve the best possible outcome [1974 Landau]. In complex systems, the density matrix is used to calculate orbital moments as well as SOC-corrected spin moments. In a canonical ensemble, the density matrix is given by [2006 Capelle]

$$\rho = \frac{e^{-\frac{H}{k_B T}}}{Tr\left(e^{-\frac{H}{k_B T}}\right)} = \frac{\sum_i e^{-\frac{E_i}{k_B T}} |\Psi_i\rangle \langle \Psi_i|}{\sum_i e^{-\frac{E_i}{k_B T}}} \quad (3-12)$$

At 0 K, we have $\rho = |\Psi_i\rangle\langle\Psi_i|$. The interactions and potential energies used in DFT are single-particle or two-particle, and hence reduced density matrix is utilized for their calculation. The density matrix also provides a way to calculate the pair correlation function and the potential $\hat{V} = \sum_i^N V(r_i)$

$$\begin{aligned}\rho(\mathbf{r}_1s_1, \mathbf{r}_2s_2; \mathbf{r}_1s_1, \mathbf{r}_2s_2) &= n(\mathbf{r}_1s_1)n(\mathbf{r}_2s_2)g(\mathbf{r}_1s_1, \mathbf{r}_2s_2), \\ \langle\hat{V}\rangle &= \int d\mathbf{r}sV(\mathbf{r}s)\rho(\mathbf{r}s, \mathbf{r}s).\end{aligned}\quad (3-13)$$

The electron density is given by $n(\mathbf{r}) = \sum_s \rho(\mathbf{r}s, \mathbf{r}s)$. The reduced density is though not sufficient for calculation of two-particle operators and the Hamiltonian.

The Kohn-Sham Approach: On its own, the Hohenberg-Kohn Theorems aren't enough to make possible the calculation of electronic structure. Kohn and Sham divided total energy as [\[1965 Kohn\]](#)

$$E[n] = T_0[n] + \int d\mathbf{r}n(\mathbf{r}) \left[V_{ext}(\mathbf{r}) + \frac{1}{2}V_H(\mathbf{r}) \right] + E_{XC}[n] \quad (3-14)$$

T_0 includes no electron-electron interaction, V_H is the Hartree Potential and E_{XC} is exchange-correlation energy. The advantage of using T_0 is that although it is not equal to total kinetic energy T , it can be calculated exactly and is a good estimation for it. The Kohn-Sham (KS) Equations and their terms are

$$\begin{aligned}\hat{H}[n]\psi_i[n] &= \varepsilon_i[n]\psi_i[n], & (\hat{T}_0 + V_{ext} + V_H + V_{XC})\psi_i(\mathbf{r}) &= \varepsilon_i\psi_i(\mathbf{r}) \\ V_{ext}(\{\mathbf{R}\}, \mathbf{r}) &= \sum_i \frac{Z_i}{|\mathbf{r}-\mathbf{R}_i|}, & \nabla_r V_H &= 4\pi n(\mathbf{r}), & V_{XC}(\mathbf{r}) &= \frac{\delta}{\delta n(\mathbf{r})} \int d\mathbf{r}n(\mathbf{r})\varepsilon_{XC}(n(\mathbf{r}))\end{aligned}\quad (3-15)$$

$V_{ext}(\{\mathbf{R}\}, \mathbf{r})$ depends on atomic positions. Similar to $n(\mathbf{r})$, it is possible to construct a self-consistent cycle for determining $\{\mathbf{R}\}$, which correspond to the energy minimum. The minimization of energy provides the single particle Kohn-Sham Equations. It is possible to use the planewave concept to rewrite the Kohn-Sham Equations, which are then given by [\[2006 Meyer\]](#)

$$\begin{aligned}\sum_{\mathbf{G}} \left[-\frac{1}{2}|\mathbf{k} + \mathbf{G}|^2 \delta_{\mathbf{G}'\mathbf{G}} + V_{eff}(\mathbf{G}' - \mathbf{G}) \right] c_{\mathbf{G}'}^{kj} &= \varepsilon_{kj} c_{\mathbf{G}}^{kj}, \\ n(\mathbf{G}) &= \frac{2}{N_{kpt}} \sum_{kj} f_{kj} \sum_{\mathbf{G}'} \left(c_{\mathbf{G}'-\mathbf{G}}^{kj} \right)^* c_{\mathbf{G}}^{kj}, & V_H(\mathbf{G}) &= 4\pi \frac{n(\mathbf{G})}{|\mathbf{G}|^2}\end{aligned}\quad (3-16)$$

The Kohn-Sham Equations in effect replace the minimization of many electron energy with the minimization of orthonormal one-electron energy. The formalism nonetheless accounts for the many body effects, because the XC-potential is included by $\frac{\delta E_{XC}[n]}{\delta n(\mathbf{r})} = V_{XC}(\mathbf{r})$.

The Kohn-Sham Formalism allows replacing the interacting many electron problem with an auxiliary one-electron, non-interacting problem [\[2006 Kurth\]](#). The main task then becomes the calculation of V_{eff}

in a self-consistent manner alongside density. In V_{eff} , only V_{XC} is approximated. Kinetic energy of the Kohn-Sham Equations depends on the orbitals, and it is implicitly a functional of density, similar to XC-energy. Expanding $E_{XC}[n]$ in its powers, one has for the exchange

$$E_X[n] = E_X[\{\varphi_i\}] = -\frac{1}{2} \sum_{s=\alpha,\beta} \sum_{k=1}^{N_s} \int d^3r \int d^3r' \psi_{js}^*(\mathbf{r}) \psi_{js}^*(\mathbf{r}') \frac{1}{|\mathbf{r}-\mathbf{r}'|} \psi_{js}(\mathbf{r}') \psi_{js}(\mathbf{r}) \quad (3-17)$$

This is the Fock Exchange, obtained for orbitals of the Kohn-Sham Equations. The eigenvalue equation is decomposed and simplified, using $\underline{S} = \underline{TT}^{tr}$ for the overlap matrix. Then

$$\underline{H}\mathbf{c}_i = \varepsilon_i \underline{TT}^{tr} \mathbf{c}_i, \quad c_{\mathbf{k}v}^{m,[n+1]} = \sum_{m'} H^{m,m'}(\mathbf{k}) c_{\mathbf{k}v}^{m',[n]} \quad (3-18)$$

With m as the number of basis sets and n the number of steps. One uses $n^{(n+1)}(\mathbf{r}) = F\{n^{(n)}(\mathbf{r})\}$ as a self-consistent way of obtaining density [2006 Blugel], with $n'(\mathbf{r}) = F\{n(\mathbf{r})\}$, so that energy is given by $F\{n(\mathbf{r})\} - n_0(\mathbf{r}) = 0$. The most straightforward approach is a linear mixing of type $n^{(n+1)} = (1 - \alpha)n^{(n)} + \alpha F\{n^{(n)}\}$, which is stable but converges slowly.

Exchange is in effect the influence of the spin of an electron in a small region around it. The density of electrons with that spin will be lower in this region, which is called an exchange hole and is thought to be spherical [2006 Jones]. As a measure for the strength of the interaction in a many body system, one uses $\lambda/|\mathbf{r} - \mathbf{r}'|$, with λ varying from 0 (no interaction) to 1 continuously. When interaction is included, E_{XC} takes the form [1975 Langreth]

$$E_{XC} = \frac{1}{2} \int d\mathbf{r} n(\mathbf{r}) \int d\mathbf{r}' \frac{1}{|\mathbf{r}-\mathbf{r}'|} n_{XC}(\mathbf{r}, \mathbf{r}' - \mathbf{r}),$$

$$n_{XC}(\mathbf{r}, \mathbf{r}' - \mathbf{r}) = n(\mathbf{r}') \int_0^1 d\lambda (g(\mathbf{r}, \mathbf{r}', \lambda) - 1). \quad (3-19)$$

$g(\mathbf{r}, \mathbf{r}', \lambda)$ is called pair-correlation. The XC-hole describes the electron repulsion and reduces the probability of another electron residing in \mathbf{r}' , which is interpreted as the electron interacting with its XC-hole [1951b Slater]. Using $\mathbf{r} - \mathbf{r}' = \mathbf{R}$, one rewrites the formula to

$$E_{XC} = \frac{1}{2} \int d\mathbf{r} n(\mathbf{r}) \int_0^\infty dR R^2 \frac{1}{R} \int d\Omega n_{XC}(\mathbf{r}, R) \quad (3-20)$$

which indicates that only the spherical average of $n_{XC}(\mathbf{r}, R)$ is of importance and hence E_{XC} provides an exact value. An important property of the XC-hole is $\int d\mathbf{r}' n_{XC}(\mathbf{r}, \mathbf{r}' - \mathbf{r}) = -1$, which means that the form of n_{XC} does not influence E_{XC} much, which for (non-)spin-polarized systems is [1976 Gunnarson]

$$E_{XC} = -\frac{1}{2} \int d\mathbf{r} n(\mathbf{r}) \langle 1/R \rangle_{\mathbf{r}} = -\frac{1}{2} \int d\mathbf{r} n(\mathbf{r}) \int d\mathbf{r}' \frac{n_{XC}(\mathbf{r}(R))}{|R|}$$

$$E_{XC} = \frac{1}{2} \sum_{\alpha\beta} \int d\mathbf{r} n_\alpha(\mathbf{r}) \int d\mathbf{r}' \frac{n_\beta(\mathbf{r}')}{|\mathbf{r}-\mathbf{r}'|} \int_0^1 d\lambda (g_{\alpha\beta}(\mathbf{r}, \mathbf{r}', \lambda) - 1). \quad (3-21)$$

Among correlation effects, one needs to consider the core-core and core-valence interactions. For heavy elements and accurate calculations, their contribution is not negligible.

Approximating E_{XC} : A simple, yet useful approximation for XC is provided by local density approximation (LDA). In metals, electron interactions are short-range because of the shielding, but in the free electron gas, they are of Coulomb type. This latter case constitutes the basis for LDA [2006 Muller]. Band energy in free electrons is

$$E_e = \frac{3}{10} n E_F [(1 + \xi)^{5/3} + (1 - \xi)^{5/3}] + Const. \quad \text{with } E_F = \frac{1}{2} \left(\frac{3N_{tot}}{8\pi V} \right)^{2/3} \quad (3-22)$$

The Thomas-Fermi Approximation provides the kinetic energy density $t_s(n)$ of a homogenous system [1927 Thomas, 1928 Fermi], from which kinetic energy of LDA is adopted

$$t_{TF}^{hom}(n(\mathbf{r})) = \frac{3}{10} (3\pi^2)^{2/3} n^{5/3} \quad \rightarrow \quad T_s^{LDA}[n] = \int d^3r t_s^{hom}(n(\mathbf{r})). \quad (3-23)$$

Exchange energy in LDA is the same as in the Hartree-Fock (HF) Method, hence

$$E_X^{hom}(n) = -\frac{3}{4} \left(\frac{3}{\pi} \right)^{1/3} n^{4/3} \quad \rightarrow \quad E_X^{LDA} = -\frac{3}{4} \left(\frac{3}{\pi} \right)^{1/3} \int d^3r n^{4/3}(\mathbf{r}) \quad (3-24)$$

For similar magnetic and angular momentum quantum numbers in $\Psi_i(\mathbf{r})$ orbitals, exchange becomes large. It is common to adopt correlation energy, E_C , from Monte Carlo simulations of the system [1994 Ortiz]. Despite being formulated for constant and homogenous densities, LDA describes the electronic structure of real solids surprisingly well. An important modification of LDA is to use gradient expansions. The general gradient approximation (GGA) is one such approach of second order. The formulation of GGA used in this work was developed by Perdew, Burke and Ernzerhof [1996 Perdew]. Defining $k_F = (3\pi n)^{1/3}$, $|s| = \frac{|\nabla n|}{2k_F n}$, $k_s = 2\sqrt{\frac{k_F}{\pi}}$, and $r_s = \left(\frac{3}{4\pi n} \right)^{1/3}$. Energy is given by

$$E_{XC}^{GGA}(n) = \int d\mathbf{r} \varepsilon_{XC}(n, |\nabla n|, \nabla^2 n) = \int d\mathbf{r} n(\mathbf{r}) \varepsilon_{XC}^{LDA}(n(\mathbf{r}), F_{XC}(n, \xi, |s|)) \quad (3-25)$$

$$F_X(|s|) = 1 + \kappa - \frac{\kappa^2}{\kappa + \mu^2}, \quad \xi = \frac{n_{\uparrow} - n_{\downarrow}}{n_{\uparrow} + n_{\downarrow}}, \quad \mu = \frac{\beta \pi^2}{3}, \quad \beta = const., \quad \kappa = const.$$

Using the following definitions, correlation energy is written in a simple form

$$E_C = \int d\mathbf{r} n(\mathbf{r}) [\varepsilon_C^{LDA}(n, \xi) + H(n, \xi, t)]$$

$$H(n, \xi, t) = \frac{e^2}{a_0} \gamma \phi^3(\xi) \ln \left[1 + \frac{\beta \gamma^2}{t} \left(\frac{1 + At^2}{1 + At^2 + A^2 t^4} \right) \right], \quad \text{with } \gamma = \frac{1}{\pi^2} (1 - \ln 2),$$

$$\phi(\xi) = \frac{1}{2}[(1 + \xi)^{1/3} + (1 - \xi)^{2/3}], \quad A = \frac{\beta}{\gamma} \left(e^{-\frac{\epsilon_C^{LDA}}{\gamma \phi^3 e^2}} - 1 \right)^{-1}. \quad (3-26)$$

In the free, non-interacting electron gas model the potential in Schrodinger Equation is constant. In reality however, the potential shows some periodic variations due to the nuclei. In the tight binding model, the electrons are bound to the atoms and their interactions inside their atoms are larger than with electrons of other atoms. The interactions between atoms are small corrections to energy, which produce the periodic portion. The Hamiltonian is hence divided into the atomic part H_l and the difference between the true and the crystal potential $H_l = [-\nabla^2 + V_{cryst}(r - R)]$ with $N = \int \psi_k^* \psi_k d\tau$. One has

$$E = E_0 + \frac{1}{N} \sum_{R=0,n.n.} e^{ikR} \int \varphi^*(r - R)(V_{true} - V_{cryst})\varphi(r)dr. \quad (3-27)$$

E_0 is energy of individual atoms. The sum over lattice sites is replaced by a sum over the nearest neighbors (*n.n.*). This reduces calculation cost, because the contribution of lattice sites far from the regarded atom approaches zero rapidly, and one needs to consider only a few neighboring rows of atoms. The integral in (Eq. 3-27) is split in two, one representing the on-site ($R = 0$) portion and the other the sum over neighbors. The prior describes the influence of the CEF and the latter the overlap term.

$$-A = \frac{1}{N} \int \varphi^*(R)(V - U)\varphi(R)d\tau, \quad -B = \frac{1}{N} \int \varphi^*(r - R)(V - U)\varphi(R)d\tau \quad (3-28)$$

As the lattice and the unit cell are periodic in a crystal, the effective potential of the Kohn-Sham Equations is represented through a Fourier Transformation.

$$V_{eff}(\mathbf{r}) = \sum_{\mathbf{G}} V_{eff}(\mathbf{G})e^{i\mathbf{G}\mathbf{r}}, \quad V_{eff}(\mathbf{G}) = \frac{1}{\Omega_{cell}} \int_{\Omega_{cell}} V_{eff}(\mathbf{r})e^{-i\mathbf{G}\mathbf{r}}d^3\mathbf{r} \quad (3-29)$$

Ω_{cell} is the unit cell volume and \mathbf{G} is the reciprocal lattice, which offers planewaves as possible solutions to Kohn-Sham Equations. It was though found that planewaves oscillate strongly close to a nucleus and hence are incapable of describing core regions well. To solve this issue, the planewaves are changed in the vicinity of the nuclei. The modified planewaves are orthogonal to core states. They are diagonal to both the ∇^2 -operator of the kinetic energy and the Hartree Potential [2006 Blugel]. The problem at $1/r$ singularities is why in some cases the core potentials are replaced by pseudopotentials. But in all electron calculations, $1/r$ is included and dealt with in a sphere that represents the atom. At the boundary of these spheres, the spherical waves should connect continuously to the planewaves outside.

3-3 Solving the Kohn-Sham Equations

To solve the energy equation in the Hartree-Fock Approach, the expansion in a basis set of $\{\Phi\}$ with N -electrons is used [2006 Muller]. The set of parameters is $\{r\}$ and the starting wavefunction is $\hat{\psi}(r)$. Then energy and the expansion parameters are

$$E(r) = \frac{\langle \hat{\psi}(r) | H | \hat{\psi}(r) \rangle}{\langle \hat{\psi}(r) | \hat{\psi}(r) \rangle}, \quad \hat{\psi}(r) = \sum_i c_i \Phi_i \quad (3-30)$$

For the coefficients c_i we have then $H_{ij} c_j = E S_{ij} c_j$, with $H_{ij} = \langle \Phi_i | H | \Phi_j \rangle$ and $S_{ij} = \langle \Phi_i | \Phi_j \rangle$. S_{ij} is the overlap matrix, which becomes a unit matrix if the basis set is orthonormal. In this sense, the Slater Determinants provide a useful set $\Phi_i = B \prod_k^N \varphi_{ki}(\mathbf{r}_i)$, $\psi_{ki}(\mathbf{r}) = \varphi_{ki}(\mathbf{r}_i) \chi_i(s_i)$. These functions are called local orbitals. Integrating over two spatial orbitals provides the Coulomb Interaction, and over spin orbitals the exchange interaction. Linear combination of Slater Determinants is used to find eigenfunctions of S^2 operator. But the basis set of such a configuration grows rapidly with the number of electrons. In effect the Hartree-Fock method reduces the basis set to a determinant, the optimization of which provides the orbital coefficients.

The Pseudopotential Approach: Especially useful basis sets are given by planewaves, which are independent of atomic positions and energy values, and are orthogonal. Ideally an infinite number of planewaves should be used but in calculations a parameter is introduced, which limits this number. The problem with $1/r$ at the nuclei though remains. The Coulomb Interaction between electrons and core particles hence needs to be modified. Such a potential is called a pseudopotential, which is produced by excluding the core-electrons and introducing a nodeless potential for the core region [2006 Meyer]. Outside the core region the pseudopotential wavefunction should be the same as the planewaves.

Augmented Planewaves: Augmented planewaves (APW) combine local orbitals and planewaves to use the merits of both [2006 Singh]. Within the APW concept the crystal is divided into atomic spheres (AS) with the nuclei as their center, and a remaining interstitial region (IR) that is not covered by the spheres [1979 Krakauer]. The spheres occupy as much space as possible but do not cross into each other. In the atomic spheres, spherical potentials are constructed, while the interstitial region is described by planewaves. Inside the spheres radial functions are used to solve the Schrodinger Equation. At the sphere boundary these spherical functions should provide the same wavefunction as the full solution of the original Schrodinger Equation would. At the sphere surface, the radial function should continuously phase into the planewaves outside. This boundary condition enables the calculation of the coefficients. One issue with this approach is that if energy is not continuous, then the Hamiltonian will become a function of both \mathbf{k} and E , which makes the problem non-linear and costly to solve [2006 Blugel]. Another problem with the APW concept is that the first derivative of the spherical waves inside the sphere is not equal to that of the respective planewaves. This translates into the secular equation having a second term.

To solve these issues, Marcus [1967 Marcus] used both u_l and $d(u_l)/dE$, calculated at fix energies, and broke the Taylor Expansion of the function after the second term. Andersen, Koelling and Abram developed the linearized APW (LAPW) concept based on this and wrote for the wavefunction [1975 Andersen, 1975 Koelling]

$$\psi_{\mathbf{G}}(\mathbf{k}) = \left\{ \begin{array}{l} e^{i(\mathbf{k}+\mathbf{G})\mathbf{r}} \\ \sum_{lm} [a_{lm}^{\mu\mathbf{G}}(\mathbf{k})u_l^\mu + b_{lm}^{\mu\mathbf{G}}(\mathbf{k})(du_l^\mu(E)/dE)]Y_{lm}(\hat{\mathbf{r}}^\mu) \end{array} \right\} \begin{array}{l} IR \\ AS \end{array} \quad (3-31)$$

Here μ denotes the atomic sphere. Continuity of u_l and du_l/dE allows calculation of a_{lm}^μ and b_{lm}^μ . That du_l/dE is now continuous also returns the secular equation to the simpler form with one term. In the LAPW method the density is obtained by integrating over the BZ and all occupied states.

$$n(\mathbf{r}) = \frac{1}{\Omega_{BZ}} \int_{BZ} \sum_{\nu, \varepsilon_\nu(\mathbf{k}) < E_F} |\psi_\nu(\mathbf{k}, \mathbf{r})|^2 d^3r, \text{ with}$$

$$\psi_\nu(\mathbf{k}, \mathbf{r}) = \sum_{lm} a_{lm, \nu}^\mu(\mathbf{k}) u_l^\alpha(r) Y_{lm}(\hat{\mathbf{r}}) + b_{lm, \nu}^\mu(\mathbf{k}) \frac{du_l^\alpha(r)}{dE} Y_{lm}(\hat{\mathbf{r}}) \quad (3-32)$$

By expanding the density with spherical harmonics inside the atomic spheres, one obtains

$$n_{AS}^\mu(\mathbf{r}) = \sum_{lm} c_{lm}^\mu(r) Y_{lm}(\hat{\mathbf{r}}), \quad n_{IR, \nu}^{\mathbf{G}}(\mathbf{k}) = \sum_{G'} \left(c_{\nu}^{G'}(\mathbf{k}) \right)^* c_{\nu}^{\mathbf{G}+\mathbf{G}'}(\mathbf{k}) \quad (3-33)$$

When no shape approximation is included for the potential, the calculation is of full-potential (FP) type. The difference between FP-LAPW and the pseudopotential method is that the potential indeed diverges at the nucleus. In the former method, the potential of the interstitial region is not taken as constant and the spherical atoms have potentials that depend on l and m [2006 Blugel]. It is possible to incorporate scalar-relativistic calculations for spin polarized structures, SOC, non-collinear magnetism and structure optimization within FP-LAPW. Core and valence electrons are treated separately in FP-LAPW because core electrons are more than 20 eV lower than Fermi Energy and they find themselves in spherical potentials, undisturbed by any overlap [2006 Singh]. Certain electrons, for example the 4f, have both valence and core characteristics.

Projector Augmented Wave: One of the earliest quantitative methods for band structure calculations was suggested by Herring [1940 Herring], who used orthogonalized planewaves (OPW). One writes

$$\chi_k^{OPW}(\mathbf{r}) = \frac{1}{\Omega} [e^{i\mathbf{k}\cdot\mathbf{r}} - \sum_j \langle u_j | \mathbf{k} \rangle u_j(\mathbf{r})] \quad \text{with} \quad \langle u_j | \mathbf{k} \rangle = - \int d\mathbf{r} u_j(\mathbf{r}) e^{i\mathbf{k}\cdot\mathbf{r}} \quad (3-34)$$

for valence electrons. Using $\tilde{\psi}_{lm}^S$ as the function for the smooth part, one writes

$$\psi_{lm}^S(\mathbf{r}) = \tilde{\psi}_{lm}^S(\mathbf{r}) + \sum_j B_{lmj} u_{lmj}(\mathbf{r}) \quad (3-35)$$

The idea of projector augmented waves (PAW) originates from these relations, rewritten to show the linear dependence of the two parts $|\psi_{lm}^S\rangle = \underline{T} |\tilde{\psi}_{lm}^S\rangle$. Total energy in PAW includes auxiliary functions but remains of the full electron type [2012 Martin]. The singularity of the nuclei is treated using the radial functions. This means the transformation describes atomic spheres with nuclei at their center. Outside of

the core region, $\tilde{\psi}_i^S(\mathbf{r}) = \psi_i^S(\mathbf{r})$. In essence, PAW uses the same principles as the Car-Parrinello method and bridges the gap between LAPW and pseudopotential methods, while avoiding shape approximation.

The general concept of PAW is to consider a pseudo space with pseudo wavefunctions. The transformation is described by localized contributions of atoms in the core regions of the pseudopotential system $\underline{T} = \underline{1} + \sum_R \hat{T}_R$. Based on the starting functions $|\tilde{\varphi}_i\rangle$, the transformation gives $|\varphi_i\rangle = (\underline{1} + \hat{T}_R)|\tilde{\varphi}_i\rangle$ in the core region (Ω_i). This leads to $|\psi\rangle = |\tilde{\psi}\rangle - \sum_i |\tilde{\varphi}_i\rangle c_i + \sum_i |\varphi_i\rangle c_i$. As \underline{T} is linear, so are c_i and one writes $c_i = \langle \tilde{p}_i | \tilde{\psi} \rangle$ with $\sum_i |\tilde{\varphi}_i\rangle \langle \tilde{p}_i | = 1$ in Ω_i and $\langle \tilde{p}_i | \tilde{\varphi}_j \rangle = \delta_{ij}$. The $\langle \tilde{p}_i |$ are the projector functions [1994a Blochl]. The transformation and the wavefunction are now rewritten as

$$\underline{T} = \underline{1} + \sum_i (|\varphi_i\rangle - |\tilde{\varphi}_i\rangle) \langle \tilde{p}_i |, \quad |\psi\rangle = |\tilde{\psi}\rangle + \sum_i (|\varphi_i\rangle - |\tilde{\varphi}_i\rangle) \langle \tilde{p}_i | \tilde{\psi} \rangle \quad (3-36)$$

Core states do not require projector functions. The expectation value of an operator O is given by

$$\langle O \rangle = \langle \psi | O | \psi \rangle = \sum_m f_m \langle \psi_m | O | \psi_m \rangle = \langle \tilde{\psi} | \tilde{O} | \tilde{\psi} \rangle = \sum_m f_m \langle \tilde{\psi}_m | \tilde{O} | \tilde{\psi}_m \rangle \quad (3-37)$$

with m as band number and $\tilde{O} = \underline{T}^\dagger O \underline{T} = O + \sum_{ij} |\tilde{p}_i\rangle [\langle \varphi_i | O | \varphi_j \rangle - \langle \tilde{\varphi}_i | \tilde{O} | \tilde{\varphi}_j \rangle] \langle \tilde{p}_j |$ for local operators. The first portion is the operator acting on the pseudo wavefunction. The second and third are projectors and expectation values at all electron or pseudo partial wave base. From total energy $\frac{\partial E[\underline{T}|\tilde{\psi}]}{\partial \langle \tilde{\psi} |} = \varepsilon \underline{T}^\dagger \underline{T} |\tilde{\psi}\rangle$, one obtains the densities, $n(\mathbf{r})$, $n^1(\mathbf{r})$ and $\tilde{n}^1(\mathbf{r})$. For the energy functional, one follows a similar trend with \tilde{E} for the smooth part and E^1 and \tilde{E}^1 the one-centered portions [1994a Blochl].

$$E = \sum_n f_n \langle \psi_n | -\frac{1}{2} \nabla^2 | \psi_n \rangle + \frac{1}{2} \int dr \int dr' \frac{(n+n_z)^2}{|r-r'|} + \int dr n \varepsilon_{XC}(n) = \tilde{E} + E^1 - \tilde{E}^1 \quad (3-38)$$

Brillouin Zone Integration: To obtain Fermi Energy, all electronic states are occupied at $T = 0$ from lowest energy up to the state, at which the summation of all weights gives the number of electrons. It is possible to simplify the calculation through replacing the continuous and infinite \mathbf{k} –space by a finite and discrete \mathbf{k} –mesh, which characterizes the same quantities [2006 Meyer]

$$\frac{\Omega_{\text{cell}}}{2\pi^3} \int_{BZ} \dots \Theta(E_F - \varepsilon_{kj}) d^3 \mathbf{k} \rightarrow \frac{1}{N_{kpt}} \sum_{\mathbf{k}} f_{kj} \dots, \quad (3-39)$$

with f_{kj} as occupation number. The density is calculated by integrating over all occupied states below Fermi Energy that are within the BZ, that is $\frac{1}{\Omega_{BZ}} \int_{BZ} \sum_{\nu, \varepsilon_\nu < E_F} f_\nu(\mathbf{k}) d^3 k$.

A method used in early calculations is the tetrahedron method. To carry out the BZ integration, the space is partitioned into small tetrahedron-shaped regions. At the corners of the tetrahedra the eigenvalue is calculated and inside of them it is linearly averaged. It was though found that the method was inaccurate for insulators due to non-optimal weighting [1983 Kleinmann], and required a large number of \mathbf{k} –points

for metals. Blochl et al. developed a method to include curvatures of integrands, obtaining improved results [1994b Blochl]. To calculate $\langle O \rangle$, one integrates the matrix elements in reciprocal space.

$$\langle O \rangle = \frac{1}{\Omega_G} \sum_n \int_{\Omega_G} d^3k O_n(\mathbf{k}) f(\varepsilon_n(\mathbf{k})) \quad (3-40)$$

The main source of inaccuracy is the linear approximation of the curves (Fig. 3-1). The error is estimated

$$\delta\langle O \rangle = \langle O \rangle - \langle \bar{O} \rangle = \sum_{Tet} \frac{N_{Tet}(E_F)}{40} \sum_{ij} (\varepsilon_i O_j - \delta_{ij} \sum_m \varepsilon_m O_m) \quad (3-41)$$

$N_{Tet}(E_F)$ is the DOS of one tetrahedron. To evaluate the sum, one uses

$$\bar{O}_n(\mathbf{k}) = \sum_j O_n(\mathbf{k}_j) w_j(\mathbf{k}) \quad \text{and} \quad w_{nj} = \frac{1}{\Omega_G} \int_{\Omega_G} d^3k w_j(\mathbf{k}) f(\varepsilon_n(\mathbf{k})) \quad (3-42)$$

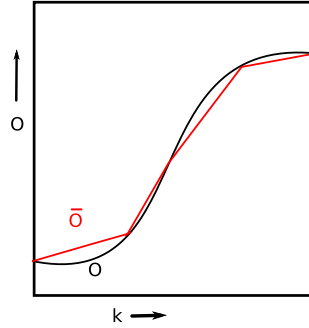


Fig. 3-1 Interpolation error due to linear interpolation, linearly interpolated matrix elements are indicated by \bar{O} .

An important improvement of the method was done by using the sum of \mathbf{k} -points to obtain the expectation value instead of summing over the tetrahedra [1994b Blochl]. For an energy band n it suffices to calculate the weight once $\langle O \rangle = \sum_{jn} O_n(\mathbf{k}_j) w_{nj}$. The first division of space is in small cells with same distances between \mathbf{k} -points. Using symmetries, it is then ensured that all equivalent \mathbf{k} -points are mapped into the Brillouin Zone and numerated. The cells of the sub-mesh are further divided in six tetrahedra with all having the same volume. The \mathbf{k} -points pointing at the corners of each tetrahedron uniquely distinguish it. To estimate the error, one writes $\delta\langle O \rangle_{Tet} = \int_{Tet} d^3k [O(\mathbf{k}) - \bar{O}(\mathbf{k})]$. If the tetrahedra are defined by vectors \mathbf{t}_i , then the spacing of \mathbf{k} -points is $\Delta = (\det(\mathbf{t}))^{1/3}$. The total error is $\delta\langle O \rangle = \langle \sum_{ij} \frac{\partial^2 O}{\partial k_i \partial k_j} C_{ij} \rangle \Delta^2$. The integration over space is replaced by integration over Fermi Surface

$$\delta\langle O \rangle = \frac{1}{\Omega_G} \sum_{ij} \oint_{\varepsilon=E_F} A_i C_{ij} \frac{\partial O}{\partial k_j} \Delta^2 = \sum_{Tet} N_{tet}(E_F) \frac{1}{40} \sum_i O_i \sum_j (\varepsilon_j - \varepsilon_i) \quad (3-43)$$

with A_i as the surface. The weights are then given by $dw_i = d \frac{\partial \langle O \rangle}{\partial O_i} = \sum_{Tet} \frac{1}{40} N_{tet}(E_F) \sum_j (\varepsilon_j - \varepsilon_i)$.

3.4. Magnetism in Density Functional Theory

A starting point for introduction of spin polarization in DFT was the work of von Barth and Hedin [1972 von Barth]. Accounting for spin polarization and external magnetic fields is done by using $V_{ext}^{\alpha\beta}(\mathbf{r})$ instead of V_{ext} and the density matrix $n^{\alpha\beta}(\mathbf{r})$ replaces $n(\mathbf{r})$ and $\underline{m}(\mathbf{r})$, with [2006 Zeller]

$$\begin{aligned} n(\mathbf{r}) &= \sum_{\alpha} n^{\alpha\alpha}(\mathbf{r}) \langle \psi_0 | \hat{\psi}^{\dagger}(\mathbf{r}) \hat{\psi}(\mathbf{r}) | \psi_0 \rangle, \\ \underline{m}(\mathbf{r}) &= \sum_{\alpha\beta} \underline{\sigma}^{\alpha\beta} n^{\alpha\beta}(\mathbf{r}) = -\mu_B \langle \psi_0 | \hat{\psi}^{\dagger}(\mathbf{r}) \underline{\sigma} \hat{\psi}(\mathbf{r}) | \psi_0 \rangle \\ n^{\alpha\beta}(\mathbf{r}) &= \frac{1}{2} \left[n(\mathbf{r}) \delta^{\alpha\beta} + m_x(\mathbf{r}) \sigma_x^{\alpha\beta} + m_y(\mathbf{r}) \sigma_y^{\alpha\beta} + m_z(\mathbf{r}) \sigma_z^{\alpha\beta} \right] = \sum_i \psi_i^{\alpha*}(\mathbf{r}) \psi_i^{\beta}(\mathbf{r}). \end{aligned} \quad (3-44)$$

$\underline{\sigma} = (\sigma_x, \sigma_y, \sigma_z)$ is the vector of the Pauli Matrices. The particle number and energy now become $N = \sum_{\alpha} \int d\mathbf{r} n^{\alpha\alpha}$ and

$$\begin{aligned} E[n^{\alpha\beta}(\mathbf{r})] &= T_{Non\ Inter} [n^{\alpha\beta}(\mathbf{r})] + \frac{1}{2} \int \int \frac{n(\mathbf{r})n(\mathbf{r}')}{|\mathbf{r}-\mathbf{r}'|} d\mathbf{r}d\mathbf{r}' + \\ &\sum_{\alpha\beta} \int V_{ext}^{\alpha\beta}(\mathbf{r}) n^{\alpha\beta}(\mathbf{r}) d\mathbf{r} + E_{XC} [n^{\alpha\beta}(\mathbf{r})] \end{aligned} \quad (3-45)$$

The one-electron Kohn-Sham orbitals $\psi_i^{\alpha}(\mathbf{r})$ allow the solution of non-interacting kinetic energy

$$T_{N-I} [n^{\alpha\beta}(\mathbf{r})] = \sum_{\alpha_i} \int \psi_i^{\alpha*}(\mathbf{r}) \left[-\frac{\nabla^2}{2} \psi_i^{\alpha}(\mathbf{r}) \right] d\mathbf{r} \quad (3-46)$$

In collinear phases, energy depends on $n(\mathbf{r})$ and the value of $\underline{m}(\mathbf{r})$ but not its direction. For the density in the collinear form we have $n_s(\mathbf{r}) = \sum_i |\psi_{i,s}(\mathbf{r})|^2$ and the Kohn-Sham Equations are

$$\left(-\frac{\nabla^2}{2} + V_{eff,s}(\mathbf{r}) \right) \psi_{i,s}(\mathbf{r}) = \varepsilon_{i,s} \psi_{i,s}(\mathbf{r}) \quad (3-47)$$

with $V_{eff}(\mathbf{r}) = V_{ext}(\mathbf{r}) + \int d^3r' \frac{n(\mathbf{r}')}{|\mathbf{r}-\mathbf{r}'|} + V_{XC}(\mathbf{r}) + \mu_B \underline{\sigma} B_{eff}(\mathbf{r})$,

$$V_{XC}(\mathbf{r}) = \frac{\delta E_{XC}[n, \underline{m}]}{\delta n^{\alpha\beta}(\mathbf{r})}, \quad \text{and} \quad B_{eff}(\mathbf{r}) = B(\mathbf{r}) + B_{XC}(\mathbf{r}) = B(\mathbf{r}) - \frac{\delta E_{XC}[n, \underline{m}]}{\delta \underline{m}(\mathbf{r})}$$

Spin polarization results in the potential $V(\mathbf{r})$ not being unique anymore.

To include all relativistic effects of the many body systems, the Dirac-Breit Hamiltonian is used

$$H^{DB} = H^{DC} + H^{Breit} = \sum_i h_i^{Dirac} + \sum_{i>j} 1/r_{ij} + H^{Gaunt} + H^{retard} \quad (3-48)$$

The first part is Dirac Energy and the second Coulomb Energy. The retarded Hamiltonian and Gaunt Term account for two-electron terms [2006 Muller]. One-electron effects are calculated exactly by h^{Dirac} . In the non-relativistic phase and without SOC, the mass-velocity term and the Darwin Term take the form

$$H_{mass-vel} = -\frac{1}{8c^2} \sum_i p_i^4, \quad H_{Darwin} = \frac{\pi}{2c^2} \sum_{iA} \delta \mathbf{r}_{iA} \quad (3-49)$$

The non-relativistic wavefunction is replaced by a 4-wavefunction, which has a large portion (P) and a small one (Q). The Dirac Equation has the solutions

$$\Phi_{\kappa\mu} = \begin{bmatrix} g_{\kappa} \chi_{\kappa\mu} \\ -i f_{\kappa} \sigma_r \chi_{\kappa\mu} \end{bmatrix}, \quad \chi_{\kappa\mu} = \begin{pmatrix} \alpha_i(\mathbf{r}) \\ \beta_i(\mathbf{r}) \end{pmatrix}. \quad (3-50)$$

where κ is the relativistic quantum number and $\chi_{\kappa\mu}$ the 2-component spinor. If one constructs the term $\phi_{\kappa} = \frac{1}{2Mc} g_{\kappa}'$ with $M = m_e + \frac{1}{2c^2} (E - V)$, then one obtains without SOC [1977 Koelling]

$$\Phi_{lms} = \begin{bmatrix} g_l Y_{lm} \chi_s \\ \frac{i}{2Mc} \sigma_r \left(-f_l' + \frac{1}{r} f_l \sigma \cdot L \right) Y_{lm} \chi_s \end{bmatrix} \quad (3-51)$$

with χ_s now being a non-relativistic spinor. Then the scalar relativistic equations are

$$r g_l' = 2M(r c g_l) + \frac{1}{r} (r g_l), \quad \text{and} \quad r c g_l' = -\frac{1}{r} (r c g_l) + \left[\frac{l(l+1)}{2Mr^2} + (V - E_l) \right] r g_l \quad (3-52)$$

The numerical procedure to solve these equations is analogous to the non-relativistic ones. To include linearization, the derivation is used. For the scalar relativistic (SR) spherical potentials, that is without SOC, one obtains [2012 Martin]

$$-\frac{1}{2r^2} \frac{d}{dr} \left(r^2 \frac{d\tilde{g}_{ul}}{dr} \right) + \left[V + \frac{l(l+1)}{2r^2} \right] \tilde{g}_{ul} - \frac{dV}{dr} \frac{d\tilde{g}_{ul}}{dr} = \varepsilon' \tilde{g}_{ul} \quad , \quad \tilde{f}_{ul} = \frac{d\tilde{g}_{ul}}{2dr} \quad (3-53)$$

with $\int (\tilde{g}_{ul}^2 + \tilde{f}_{ul}^2) r^2 dr = 1$. \tilde{g}_{ul} and \tilde{f}_{ul} are approximate functions to g and f . Because SOC has a small addition to energy, it is convenient to use the lower energy bands from SR energy to diagonalize the Hamiltonian [1980 MacDonald]. The second variation method for handling the SOC builds upon the SR calculation (SRC). The N lowest bands obtained from SRC are used to create a secular equation. The Hamiltonian is also taken from SRC and the SOC terms are added to it, while the overlap matrix is diagonal. A linear combination of the SOC part of the Hamiltonian obtained in SRC is used.

In a non-collinear structure, $\mathbf{M} = \int d\mathbf{r} \underline{m}(\mathbf{r})$ and its calculation is costly as the spin-up and down densities are coupled and the energy equation is not linear any more. Dependence on $\underline{m}(\mathbf{r})$ adds a term to energy, given by $\mu_B \underline{\sigma} \cdot \mathbf{B}_{XC}(\mathbf{r})$ with $\underline{\sigma}$ as the Pauli Spinor and B_{XC} as the XC-energy produced by the mean field. The wavefunctions then have the form $\Psi_{i\sigma}$, $\sigma = \pm 1$ and the Hamiltonian loses some of its symmetry and must be considered in the spin-space [2006 Bihlmayer]. If the magnetization of each atom is collinear

around it, $V_{ext}(\mathbf{r})$ is diagonal and $V_{XC}(\mathbf{r})$ can be divided into diagonal and off-diagonal potential. One writes [[1995 Antropov](#), [1996 Antropov](#)]

$$\frac{\delta E_{XC}}{\delta \mathbf{m}(\mathbf{r})} = V_{XC} \mathbf{1} - \underline{\boldsymbol{\sigma}} \cdot \mathbf{B}_{XC}, \quad \Psi = \begin{pmatrix} \psi^\uparrow \\ \psi^\downarrow \end{pmatrix}, \quad \frac{id\Psi}{dt} = [H_{diag} - \underline{\boldsymbol{\sigma}} \cdot \mathbf{B}_{XC}(\mathbf{r}, t)]\Psi \quad (3-54)$$

The matrix for describing a spin rotation is $\underline{R}(\mathbf{r})$ and the field of these matrices $\underline{R}(\mathbf{r}, t)$. We then have

$$\frac{id}{dt}(\underline{R}\Psi) = [H_{diag} - \sum_l \underline{\boldsymbol{\sigma}}_{z,t}(\mathbf{r}, t)](\underline{R}\Psi) \quad (3-55)$$

\underline{R} ensures that the z –direction of each atom is parallel to the \mathbf{B} –field. For the magnetization it holds

$$\frac{d\mathbf{m}(\mathbf{r}, t)}{dt} = 2\mathbf{m} \times \mathbf{B} + \frac{i}{2} \nabla (\Psi^* \underline{\boldsymbol{\sigma}} \cdot \nabla \Psi - \nabla \Psi \cdot \Psi \underline{\boldsymbol{\sigma}}) \quad (3-56)$$

$\mathbf{m} \times \mathbf{B}$ describes how the internal \mathbf{B} –field produces a precession in an atom. The spin moment will take the direction described by $\frac{d\hat{\mathbf{e}}_I}{dt} = -\frac{2}{\mu_B} \hat{\mathbf{e}}_I \times \mathbf{I}_I$ with $\mathbf{I}_I = \mu_B \mathbf{B}$. To include SOC and dipole-dipole effects, they are added to the field, so that we have $\mathbf{I}_I + \mathbf{I}_{SOC} + \mathbf{I}_{dip-dip}$.

Starting with a model of N –atoms, each having one localized electron, $\phi_n(\mathbf{r}, \sigma)$, one considers the energy terms. Neither the potential that keeps the electrons localized, nor the kinetic energy influence the spins, but the electron-electron interactions do [[2006 Bihlmayer](#)]. The Coulomb Repulsion U does not influence the spins (power two of orbitals), but the exchange interaction J does. We have

$$U = -\sum_{nn'} J_{nn'} (1/4 + \mathbf{s}_n \cdot \mathbf{s}_{n'}). \quad (3-57)$$

SOC in LAPW: Based on one-electron Dirac Equation in crystal potentials, MacDonald et al. described the treatment of SOC within the LAPW approach [[1980 MacDonald](#)]. The starting point is the two-component Dirac Equation

$$\left[-\frac{\nabla^2}{2} + \underline{V}(\mathbf{r}) - \frac{\mu_B}{2c} \boldsymbol{\sigma} \cdot (\mathbf{E}_N(\mathbf{r}) \times \mathbf{p}) \right] \Psi_i = \varepsilon_i \Psi_i.$$

Here \mathbf{E}_N is the \mathbf{E} –field of a nucleus felt by an electron. Radial functions based on two component orbitals with $\kappa = l$ ($j = -1/2$) and $\kappa = -l - 1$ ($j = l + 1/2$) are transformed. The average of large (P) and small (Q) component radial functions of energy is close to the large component and the difference is ignored. With $M = m + \frac{1}{2c^2}(\varepsilon - V_{MT})$. The radial functions are

$$\frac{dP}{dr} - \frac{P}{r} = 2McQ, \quad \frac{dQ}{dr} + \frac{Q}{r} = \left[\frac{l(l+1)}{2Mc r^2} + \frac{V-\varepsilon}{c} \right] P \quad (3-58)$$

With χ_s as the two-component spinors, the basis set expansion takes the form

$$\phi_{lms} = \left[\begin{array}{c} \frac{1}{r} P_l Y_{lm} \chi_s \\ \frac{i\hat{\mathbf{r}}}{r} \cdot \boldsymbol{\sigma} \left[-Q_l + \frac{P_l}{2Mc r} \boldsymbol{\sigma} \cdot \mathbf{L} \right] Y_{lm} \chi_s \end{array} \right]. \quad (3-59)$$

The boundary conditions are provided by continuity of the large component and its derivative at radii of atomic spheres. This does not apply to the small component but the error is ignored. Energy is then

$$E[\Psi] = \frac{1}{\int_{AS+IR} d^3r \Psi^\dagger \Psi} \left[\int_{AS+IR} d^3r \Psi^\dagger H \Psi + i \int_{r=R} d^2r (\Psi_{IR}^\dagger \hat{\mathbf{r}} \cdot \underline{\alpha} \Psi_r - \Psi_{AS}^\dagger \hat{\mathbf{r}} \cdot \underline{\alpha} \Psi_{IR}) \right] \quad (3-60)$$

which results in the secular equation $\underline{H}\mathbf{c} = E\underline{S}\mathbf{c}$ and the basis functions $\phi = \sum_{ns} c_{ns} P(\mathbf{k}_n s; \mathbf{r})$ to be obtained by variation method. The 4×4 matrix $\underline{\alpha}$ is the same Hermitian matrix from the Dirac Equation. The Hamiltonian is split in two parts, the first being scalar-relativistic (SR) and the second the small contribution of SOC [1980 MacDonald].

$$H_{n's',ns} \cong H_{n,n}^{SR} \delta_{s,s'} + H_{n,n}^{SOC}, \quad S_{n's',ns} \cong S_{n,n}^{SR} \delta_{s,s'}$$

Moving electrons perceive an \mathbf{E} – field as a magnetic \mathbf{B} –field, which couples with the spin, see Eq. 2-12. Close to the core, dV/dr is larger, which is why localized electrons have larger SOC. For a one-electron wavefunction ψ_i , and the orbital moment of an individual atom, I , one calculates

$$\mathbf{m}_{orb}(\mathbf{r}) = -\mu_B \sum_i \langle \psi_i | \mathbf{r} \times \mathbf{v} | \psi_i \rangle, \quad \mathbf{M}_{orb,I} = \int_{AS,I} \mathbf{m}_{orb}(\mathbf{r}) d^3r \quad (3-61)$$

Self-Interaction Correction: The non-spherical portion of the exchange hole produces the difference between its exact value and its approximation. It is possible to modify the XC-hole and include the average of density. One way of doing this is by using weighted densities [2006 Jones].

$$n_{XC}(\mathbf{r}, \mathbf{r}' - \mathbf{r}) = n(\mathbf{r}') G(|\mathbf{r} - \mathbf{r}'|, \tilde{n}(\mathbf{r})) \quad (3-62)$$

\tilde{n} also satisfies XC-hole properties. This approach is a form of self-interaction correction (SIC). The XC-potential is ought to cancel out energy of the electronic self-interaction in DFT. But in the LSDA, a part of the error remains. The aim of the SIC is to include a term in XC-energy to subtract Coulomb Energy of an electron's interaction with itself. Formally, SIC energy is obtained by

$$E_{SIC} = E_{LSDA}[n_\alpha(\mathbf{r}), n_\beta(\mathbf{r})] - \sum_{is} \delta_{is}; \quad (3-63)$$

$$\delta_{is} = \frac{e^2}{2} \int d\mathbf{r} \int d\mathbf{r}' \frac{n_{is}(\mathbf{r}) n_{is}(\mathbf{r}')}{|\mathbf{r} - \mathbf{r}'|} + E_{XC}^{LSDA}(n_{is}, 0)$$

The second part of Eq. 3-63 is for the case of full spin polarization. In a one-electron system we then have

$$\left[-\frac{\hbar^2}{2m} \nabla^2 + V(r) + V_{is}^{SIC}(r) \right] \psi_{is} = \sum_i \lambda_{ijs} \psi_{is} \quad (3-64)$$

The ψ_{is} which enter V_{is}^{SIC} are local-orbitals and are orthogonalized by the Lagrange Method.

Electronic structure calculations based on the mean field theory do not include the correlation effects. The most prominent example is the Hartree-Fock Method [2005 Mohn]. The Hubbard Model accounts for correlation by introducing energy of Coulomb Repulsion of two electrons at one lattice site as an example of SIC [1963 Hubbard, 1979 Hubbard].

$$H_{Hubbard} = \sum_{i,j,\sigma} (t_{ij} c_{i\sigma}^\dagger c_{j\sigma}) + U \sum_i n_{i,up} n_{i,dn} \quad (3-65)$$

Here t_{ij} is the hopping integral and the Hubbard- U describes the Coulomb Interaction. The operator for occupation number is $n_{i\sigma} = c_{i\sigma}^\dagger c_{i\sigma}$. It holds $[c_{i\sigma}^\dagger, c_{j\sigma'}] = \delta_{ij} \delta_{\sigma\sigma'}$, $[c_{i\sigma}^\dagger, c_{j\sigma'}^\dagger] = [c_{i\sigma}, c_{j\sigma'}] = 0$. One uses the results of specially constructed Hamiltonians, such as the Hubbard Hamiltonian to describe correlation of localized electrons better [2006 Kurth]. Aside from the Coulomb Repulsion, the strength of hopping t_{ij} , the dimension and the lattice structure play a role in this Hamiltonian. For the limit of $U = 0$, one obtains the following, which gives energy after applying the Fourier Transformation

$$i\hbar \frac{\partial c_{is}}{\partial t} = - \sum_j t_{ij} c_{j\sigma} \quad \rightarrow \quad \varepsilon_{0,k} = \varepsilon_0 - \sum_{i \neq j} t_{ij} e^{ik(R_i - R_j)} \quad (3.66)$$

4 – Permanent Magnets and Calculation Details

4-1 Permanent Magnet Materials

As formulated by Morrish [2001 Morrish], a good permanent magnet is a material that produces a large magnetic field for a long time. Physically this interprets to having a large remanence (B_r) and a large coercive field ($\mu_0 H_C$). The coercive field is a measure for how strong a field the permanent magnet is able to produce outside of it. Aside from the remanence, the amount of energy a hard magnet can store also depends on how close its hysteresis is to a square form.

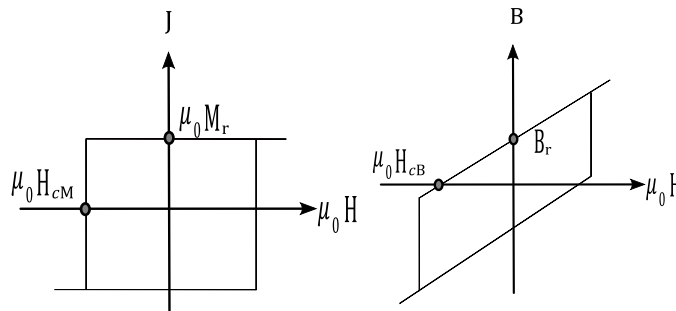


Fig. 4-1 Hysteresis loops of an ideal material. Left: magnetization loop. Right: induction loop.

An induction loop is used to depict the hard magnetic properties as shown in Fig. 4-1, where $B = \mu_0(H + M)$. The product of the flux density and the demagnetization field, labeled maximum energy product $(BH)_{max}$, is a measure for the maximum amount of energy a permanent magnet usefully provides. If an ideal hard magnet is assumed, its maximum energy product becomes only dependent on remanence. For a real magnet with a non-linear demagnetization curve, one obtains as an approximation

$$(BH)_{max} = \frac{B^2}{4\mu_0\mu_{rel}} \quad (4-2)$$

The coercive field is the field in the opposite direction of magnetization required to reduce \mathbf{M} to zero. In other words, H_C determines the resistance of a permanent magnet against a rotation in its magnetization direction. The coercive field depends strongly on the shape, production method, temperature treatment and microstructure of the specimen. This is the reason the second quadrant of the hysteresis loop of a magnet is of importance. Indeed the distinction between soft and hard magnets is based on the value of H_C [1998 Jiles]. The dependence of H_C on the microstructure and the intrinsic properties used to obtain numerical approximations for it are described in more detail in Subsection 5-6.

On the microscopic scale, two key factors determine, whether a hard magnet is able to retain its magnetic direction. One is the microstructure including dislocations and defects, and the other is its anisotropy, the

magnetocrystalline part of which is intrinsic [2005 Rossignol]. The total anisotropy field, which contains contributions from different sources such as MCA, is the deciding factor for the resistance against changes in magnetization direction in homogeneous materials. For an ideal magnet with no microscopic defects, the anisotropy field and total magnetization determine the theoretical upper limit of coercivity. Two distinct methods are in commercial use for producing $R - Fe - B$ magnets. One is the traditional powder-metallurgy sintering approach and the other is the rapid-solidification technique of melt spinning.

Transition Metals: The investigated phases owe their large magnetization to the $3d$ –electrons of the T –metals Co or Fe . The wavefunctions of the $3d - T$ have a larger reach than those of $4f - R$ and have a contribution at further distances compared to R . In the case of $3d - T$, the SOC is of lesser importance compared to CEF, because the electronic density landscape induced by the CEF results in a small orbital moment. In the periodic table, groups of similar elements mostly follow the same structural changes. Among $3d - T$ though, one comes across exceptions in Mn , Fe and Co . Instead of hcp , Mn has a complicated and exceptional structure, while Fe forms as bcc . At $0K$, Co should have an fcc – structure, but forms an hcp –structure. This behavior is explained by the magnetic band splitting. With spin-up band being full, the number of remaining electrons in the spin-down band becomes the deciding factor [1994 Soderlind].

When a non-magnetic metal is alloyed to a magnetic one, for example Cu to Co , the covalent polarization leads to the non-magnetic metal obtaining a moment, which is parallel or anti-parallel to that of the magnetic metal, depending on the configuration of its valence orbitals. The spin-density is neither uniform, nor spherical in magnetic atoms. The crystal field of Co influences the $Fe^{+2} - 3d^5$ –electrons weakly, while the $Cu^{+2} - 3d^4$ –electrons are strongly influenced. The hybridization between $Co - 3d$ and $Cu - 4s$ broadens the atomic levels. If one considers an Fe –atom in the Co –network of RT_5 as an impurity, then the Anderson Model [1961 Anderson] predicts that the spontaneous magnetization of the impurity remains if $UN_i(E_F)/2n > 1$, with U being the Coulomb Energy and $N_i(E_F)$ the atomic density of state for each spin at Fermi Energy. If the impurity atom hybridizes with the host atoms and its band gets broadened by δ_i , then $N_i(E_F)/2n \cong 1/\delta_i$ which results in the Anderson Criterion $U \gtrsim \delta_i$ [2010 Coey]. This means that lighter T –atoms will obtain negative moments in a matrix of heavy $3d - T$. With R considered as light $d - T$, the same concept applies to them and $T - R$ have an antiferromagnetic coupling of spin moments.

Slater and Pauling constructed a graphical scheme to show the functional mechanism of the band theory [1937b Slater, 1938 Pauling], where the effective magnetic moment per atom (n_{eff}) is drawn against the number of $3d$ –electrons (Fig. 4-2). The experimentally obtained values for different alloys fall on two straight lines, one ascending, and one descending. Here it is assumed that alloyed metals share their $3d$ –electrons in one band. Exchange coupling between less than half-filled and more than half-filled $3d - T$ is antiferromagnetic. For the total moment M , based on the number of valence electrons, Z

$$M = 2n^\alpha - Z, \quad M = Z - 2n^\beta \quad (4-3)$$

M decreases linearly with Z , if $d\mu/dn > 0$, which is the second branch of the Slater-Pauling curve (weak ferromagnetism). For $n^- = 0$ and unchanging, M increases with Z , drawing the first part of the Slater-Pauling curve. This linear behavior is due to shell filling based on Hund's Rules. Strong ferromagnetism ($d\mu/dn < 0$) occurs when Fermi Energy is at low DOS. Based on the graph, *bcc-Fe* is at the point, where the two branches of the Slater-Pauling curve meet. When alloying a non-magnetic metal in a matrix of magnetic atoms, like *Y* in YCo_5 , the average magnetic moment is calculated by

$$M_{av} = M_A(1 - x) + M_B(x) \quad (4-4)$$

This gives for example for YCo_5 , with $M_A = 1.75$, $M_B = -0.363$ from the current calculations and $x = 1/6$, $M_{av} = 1.3978 \mu_B$ and a total moment of $8.39 \mu_B/f.u.$, which is in good agreement with experimental measurement of $8 \mu_B/f.u.$ [1962 Nesbitt].

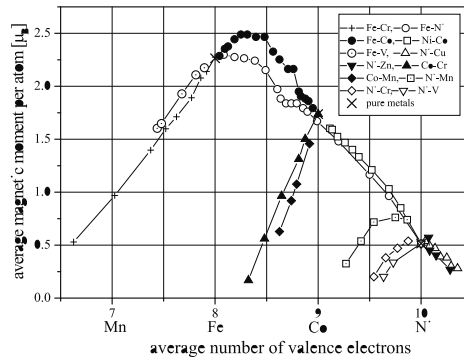


Fig. 4-2 The Slater-Pauling curve [2005 Mohn]. The x -axis shows the average number of valence electrons and the y -axis the average magnetic moment per atom in units of μ_B .

Adding *Cu* to *Ni* decreases the magnetization because the *Cu* valence electrons fill out the holes in the $3d$ -band. This model fits well to the Slater-Pauling curve. The curve shows that for $n_{eff} < 2.5$ addition of $3d$ -metals to a ferromagnetic metal increases spontaneous magnetization per atom while as for $n_{eff} > 2.5$ lowers it, as neither spin-up nor spin-down bands are fully occupied. Examining the exchange interaction between the same and different neighboring atoms provides a way of explaining the magnetization of *Fe*, when *Cu* is added [1987 Schutz].

Rare Earth Metals: In rare earths, the $4f$ -shells are too isolated to interact with each other. Instead they polarize the itinerant $5d$ and $6s$ electrons to produce an effective coupling, as described by the RKKY principle. This interaction is weak; hence different magnetic configurations are expected for the $R - R$ interaction. The electron-electron interaction of R -atoms is about $10 eV$ in strength, the SOC

registers about 1 eV. Most pure R –metals are paramagnets as solids, where they form trivalent ions. The $4f$ –electrons reside closer to the nucleus than the $5s$ and $5p$ electrons, because of which the R –atoms behave as free atoms, even in solutions or solids.

As the $4f$ –orbitals are not chemically active, the bonding in rare-earth metals is caused by conduction electrons. The magnetic moments in R –metals are well defined. The reason is that the electronic structure is not changed by formation of metallic bonds. The magnetic order arises from the $4f$ –electrons being localized and thus they are well screened from the crystalline environment, but it is only because of the interaction of the $4f$ –electrons of different atoms, which is indirect and only acts via the $5d$ –spin density, that this order comes to be [1979 Johansson]. In the R –metals, the coupling between the spin and the orbital moments are antiparallel (parallel) for less (more) than half-filled shells. Givord et al. showed that in single crystals of permanent magnets the $4f$ –electrons are indeed localized [1985a Givord]. They measured the magnetic moments in these compounds and determined that these remain unchanged after bonding, even though the SOC has a non-negligible contribution.

$R - T$ Materials: A combination of R and T metals is beneficial for permanent magnet properties, as the T –atoms provide large magnetizations and the R –atoms large anisotropies. When some R –atoms are built into a T – matrix, the $3d$ –electrons feel the electronic potential stronger than the $5d$ –electrons. The bands that position themselves below or near Fermi Energy are hence the $3d$ –bands and these electrons produce the spin magnetization of the alloy. In most $R - T$ compounds a number of $T - 3d$ electrons hybridize with $R - 5d$. The $3d$ –states lie lower, and the hybridization occurs between $3d$ –up and $5d$ –down. This causes the d –spin moment of R to align antiferromagnetically to $T - 3d$. The $R - 4f$ couple ferromagnetically with $R - 5d$, and result in a substantial antiferromagnetic interaction of $T(3d) - R(4f)$, which explains the high ordering temperature of R –moments in these compounds, despite their much lower Curie Temperature in pure R –metals [2001 Morrish]. This coupling also helps strengthen the anisotropy of the T –atoms through strong anisotropic potentials of the R –atoms. The final coupling between the T –atom and the R –atom depends on the coupling between S_R and L_R , which is antiparallel for light and parallel for heavy R respectively, governed by the SOC, as shown in Fig. 4-3.

Experimental measurements [1991 Herbst] and most numerical results [2018 Landa] agree with the model, so do the results obtained during the current study (this point is referred to under discussions). The antiferromagnetic $3d - 5d$ coupling, arising from hybridization, is then finally responsible for the interaction between $3d$ and $4f$ – states, which results ultimately in a magnetic order. The sources of this coupling are SOC and orbital polarization. If both spin-polarization energy, as well as the $3d - 5d$ interaction, are larger than the $4f$ –crystal field energy, then the $3d$ and the $4f$ –moments will order parallel or antiparallel. But if the spin polarization energy is smaller than the crystal field energy of the $4f$ –shells, then the arrangement becomes canted in certain phases [1998 Richter]. For low temperature behavior, the anisotropy of $4f$ –shell decides the magnetization direction. In the non-collinear phases

$PrCo_5$ and $Nd_2Fe_{14}B$, the sublattices of the R –atoms have magnetic moments at a certain angle with respect to the T –moments. The latter align parallel to the easy axis [001]. Such non-collinear ordering is the result of comparable and competing crystal field and atomic anisotropy energies among and between sublattices [1988 Cadogan]. The CEF and the SOC further influence a specific site more strongly than another.

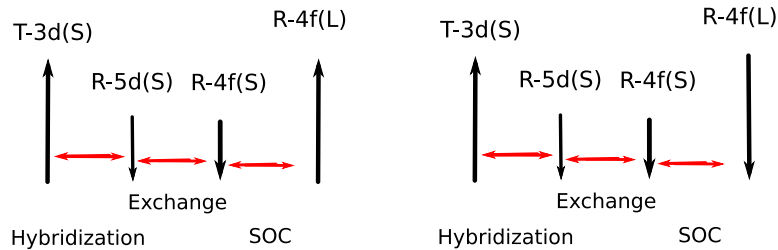


Fig. 4-3 Interaction between $T - 3d$ and $R - 4f$ –electrons of $R - T$ compounds for light R (left) and heavy R (right). The types of couplings are hybridization, exchange and spin-orbit (SOC) from left to right.

The main applications of permanent magnets are in devices that either require a continuous magnetic flux or a field. These uses are grouped in three branches, namely electro-mechanical, magneto-mechanical and field source [2005 Rossignol]. Due to their large polarization and coercivity, the $R - T$ –based magnets are used for most magneto-mechanical applications. To enhance the high temperature properties of a magnet, its coercive field ($\mu_0 H_C$) should be enhanced. The important magnetic properties of some industrially produced permanent magnet compounds at room temperature are given in Tab. 4-1. Further, the second quarter of their “ $\mu_0 H - B$ ” curves are compared in Fig. 4-4, taken from [2005 Rossignol]. That the induction changes linearly with H is a sign that these materials maintain their properties independent of shape or size as long as they are macroscopic.

	B_r [T]	$\mu_0 H_{cM}$ [T]	$\mu_0 H_{cB}$ [T]	$(BH)_{Max}$ [kJ/m^3]	$B_r^2/4\mu_0$ [kJ/m^3]	T_c [K]
AlNiCo	1.3	0.06	0.06	50	336	1130
Ferrites	0.4	0.4	0.37	30	31.8	720
$SmCo_5$	0.9	2.5	0.87	160	161	1000
Sm_2Co_{17}	1.1	1.3	0.97	220	241	1100
Nd-Fe-B	1.3	1.5	1.25	320	336	586

Tab. 4-1 Typical magnetic parameters for permanent magnetic materials [2005 Rossignol].

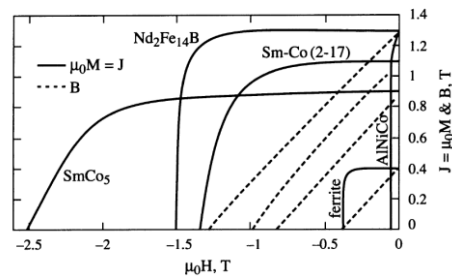


Fig. 4-4 Performances of commercial permanent magnets [2005 Rossignol].

4-2 Calculation Methods with WIEN2k

The mathematical framework of WIEN2k [1990 Blaha, 2003 Schwarz] closely follows the FP-LAPW method described in [Subsection 3-3](#) and the specific code-related description follows the WIEN2k User Guide [2018 Blaha]. In the following, the practical aspects of running calculations for determining MAE are described. To generate the files for the structure of the compounds in WIEN2k, one needs the lattice type (number of space group), lattice parameters, the angles between lattice vectors and the atomic positions of the inequivalent atoms in the cell. The information is put in using the structure generation program of WIEN2k, called **StructGen**, which is accessible through the graphic user interface, **w2web**. It is possible to provide atomic sphere radii (radius of muffin tin = **RMT**) based on the distances of atoms at this point. If there is no input, the code uses default values, which work well. An option exists to shrink all atomic spheres by a percentage value (between 1% and 5%), which is used when the lattice parameters are not very close to minimum energy values and structure optimization are ought to be carried out. This step produces several files that include the starting information of the crystal structure, the main one being **case.struct**.

The next step is to “initialize” the calculation, which means providing the physical and numerical calculation parameters or settings. A step by step initialization calculates the distances to the nearest atomic neighbors (**x nn**), the point and space groups (**x sgroup**), the symmetry matrices and operations (**x symmetry**), spin-polarization directions (**instgen_lapw**), atomic densities (**x lstart**), the **k** –points (**x kgen**) and the starting density for the first iteration of the SCF calculation (**x dstart**). One is further asked whether the calculation is spin-polarized and if so, whether the magnetic structure is antiferromagnetic. It is possible to leave the individual steps to the code by using the “batch” mode. The batch mode though does not automatically provide correct input for spin-polarization and one should manually edit the “**case.inst**” file, or invoke “**instgen_lapw**”. The most important parameters to be set are the choices of XC-potential approximation, e.g. PBE-GGA, the energy separation value between core and valence electron states, the value for the cutoff of number of wavefunctions included in summing over occupied states (**RKMAX**), and the type of temperature broadening (**TEMP**). The default settings are **RKMAX=7**, energy separation by $-6 Ry$, the tetrahedron method for temperature smearing and 1000 **k** –points. WIEN2k has a built-in tool to find the best **k** –mesh based on a desired total number of **k** –points.

After the initialization of the SCF (self-consistent field) calculation, one initializes the SOC calculation (**initso_lapw**), which produces the necessary input files for SOC, and ensures that only shared symmetries are used. It is extremely important to initialize the SOC for all directions used in the calculation, even in the easy directions in order to ensure no artificial symmetries are present. Here, one indicates which atoms have the SOC and / or relativistic local orbitals ($p_{1/2}$ correction) and with which strength. In practice this means that the structures will have more “inequivalent” atomic sites and possibly a different **k** –mesh. This is why this initialization should be carried out before starting the non spin-polarized (NSP) or scalar relativistic calculation (SRC) calculation, even though there is no SOC calculation involved. If

SOC is initialized only after the convergence of NSP or SRC, the changes in the structure and in symmetries cause errors for SOC calculations in hard direction due to changed number of energy bands. The value of MAE is small compared to free energy and is sensitive to small changes of input.

An initial convergence of the NSP or SRC finds a convergence of energy that is the same for both directions and has not yet been influenced by the SOC calculation. The SOC calculation is then carried out for the hard and easy axes, both starting from the converged SRC state. In WIEN2k the orbital magnetic moment (ORB) is not included in total magnetization, which means that even after the SOC calculation, the total magnetization value generally remains unchanged. To obtain orbital moments, calculations are carried out by a tool called **LAPWDM**, which determines the density matrix and provides hence orbital moments [2002 Novak, 2018 Blaha]. The density matrix calculation is a part of the “orbital package”, which is also used for carrying out calculations including (U, J) potentials [2003 Novak].

The SCF cycle (NSP, SRC, SOC or +U) is started by the command “**run_lapw -ec -cc**” or a variation of it. Parameters such as convergence criterion are given in the command. Energy convergence is given by “**-ec**” in units of Ry , charge convergence by “**-cc**” in atomic units of electric charge (e), and force convergence by “**-fc**” in units of $mRy/a.u.$ Based on the User Guide, one is advised to start either with the NSP or SRC calculation. After checking that energy and charge have converged correctly, and that no unphysical energies or bands exist, one saves the calculation results using “**save_lapw**” option. The values for energy, sum of eigenvalues, atomic magnetic moments and interstitial magnetic moment are monitored by reading **:ENE**, **:SUM**, **:MMixx** and **:MMINT**, respectively, from the “**case.scf**” file. To continue with the SRC one uses, “**runsp_lapw -ec -cc**”, where “sp” stands for spin-polarized. This calculation is then saved in a new folder, as it will be used as the basis for all SOC calculations. To run the SOC, one invokes “**runsp_lapw -so -ec -cc**”, where “so” stands for spin-orbit coupling. The direction of the magnetization saturation is read from the “**case.inso**” file. To run a calculation parallel on several cores, one adds a “**-p**” to the SCF command, i.e. “**run_lapw -p**”. If the server is set up properly, no other actions or parameters are required to enable parallel computing.

As the SOC calculation changes densities and energies, the SOC calculation in a second direction should not be started as a continuation of the calculation in the first direction. The results of the SRC calculation must be restored and the second direction of SOC is then calculated based on that. To restore the SRC results, one uses “**restore_lapw**”. For the +U –calculation, one uses “**runsp_lapw -so -orb -ec -cc**”. It is important to include the “**-so**” option in the command, as a +U –calculation does not automatically include the SOC. The density matrix is calculated by invoking “**x lapwdm -up -so**”, and requires appropriate input in the file “**case.indmc**”. It is important to note that for starting the +U calculation, the orbital charges are required as input, but the SOC calculation does not compute them. One hence needs to run “**lapwdm -up -so**” and “**lapw -dn -so**” once before the +U calculation. The orbital moments and the spin moments after SOC are read from the output file “**case.scfdmup**”. For each density matrix calculation, only one electronic shell of atoms is given as input, e.g. only f –electrons of Sm . To obtain

the moments for other electronic shells, the density matrix calculation is repeated. An example for the input of a “**case.indmc**” is given below. When the third digit of an atomic line is 2, the density matrix is calculated for d –electrons; when it is 3, the density matrix is calculated for f –electrons.

```

-9          | is the energy minimum (default -9)
4          | number of atoms, for which the DM is calculated
1 1 2      | d-electrons of first atom (e.g. Co1-1)
2 1 2      | d-electrons of first atom (e.g. Co1-2)
3 1 2      | d-electrons of first atom (e.g. Co2)
4 1 3      | f-electrons of first atom (e.g. Sm)
0 0        |  $R_{index}$ ,  $L - S_{index}$ 

```

4-3 Calculation Methods with VASP

The description of calculations based on VASP follows closely the manual guide of VASP [[1999 Kresse](#), [2016 Kresse](#)]. VASP uses the conjugate gradient algorithm to find the energy minimum [[1996 Kresse](#)]. The new and old charges after each iteration are mixed with Broyden/Pullay scheme [[1988 Johnson](#)]. Based on the number of energy bands (n), only the n lowest eigenfunctions are calculated at each iteration. To achieve this, the variational method of Rayleigh-Ritz is applied to diagonalize the Hamiltonian of the trial wavefunction space [[1994 Zitnan](#)]. Two methods are used in the current work for automatic meshing of the k –points. One is the Γ –centered mesh and the other is the Monkhorst-Pack scheme [[1976 Monkhorst](#)].

If the basis set is incomplete in regard to volume optimization, an unphysical residual stress remains in the stress tensor. One way to avoid this error is to use larger energy cutoff values (**ENCUT**). After test calculations, it was determined that an **ENCUT** of 500 eV suffices for all calculations. The PAW database for VASP calculations are provided, but different types of potentials exist for each element and also for each potential type. Three potential types have been used, namely .52 PBE-GGA, PBE-GGA and LDA. Best results are obtained with PBE-GGA. As for the element files, the following were used. Co, Co_sv (s –electrons are treated as valence electrons), Co_pv (p –electrons are treated as valence electrons), Fe, Fe_sv, Fe_pv, Cu, Cu_pv, Dy_3 (Dy –ion with frozen f –electrons in core), Dy, Nd_3, Nd, Pr_3, Pr, Sm_3, Sm, Y_sv. The most suitable files are found to be Co_sv, Fe_sv, Cu_pv, Y_sv, Pr, Sm, Nd, Dy.

The input files used for an initial VASP calculation are **INCAR**, **KPOINTS**, **POSCAR** and **POTCAR**. **INCAR** is the main input file, where the calculation parameters are given, most notably calculation type, convergence criterion, smearing, method of partial charge calculation, symmetry, magnetization type and direction, and (U, J) values. The following lines show a complete set of tags in the **INCAR** file for a calculation of MAE.

General:

SYSTEM = PrCo5 | name of calculation
ISTART = 0, 2 | 0: start new calculation, 2: continue
ICHARG = 2, 1 | 2: initial charges from atoms, 1: from
| previous calculation
ENCUT = 500 | energy cutoff
ISMEAR = -5, 1 | partial occupancies (-5: tetrah. w/ Blochl
| correction, 1: 1st order Methfessel-Paxton)
SIGMA = 0.01 | width of smearing
NELM = 200 | max. number of iterations
LORBIT = 11 | DOSCAR is lm-decomposed
PREC = Accurate | precision set to high accuracy
EDIFF = 1E-6 | energy convergence criterion
ISYM = -1 | no symmetry used
GGA_COMPAT = .FALSE. | applies correction due to symmetry breaking
ADDGRID = .TRUE. | additional grid for accurate aug. charges
NBANDS = 128 | number of energy bands
LASPH = .TRUE. | non-spherical contributions included
NEDOS = 700 | number of energy steps in DOS

Optimization:

IBRION = 2 | type of optimization (conjugate gradient)
ISIF = 7 | which degrees of freedom optimized
NSW = 10 | number of ionic iterations
POTIM = 0.5 | step width scaling

SOC:

LREAL = .FALSE. | projections evaluated in reciprocal space
LNONCOLLINEAR = .TRUE. | turns on non-collinear magnetism
LSORBIT = .TRUE. | turns on SOC

Magnetism:

LMAXMIX = 6 | PAW charges of (s,p,d,f) pass through mixer
ISPIN = 2 | spin polarized calculation
SAXIS = 0 0 1 | direction of magnetization
MAGMOM = 1.6 -2 | values of collinear magnetic moments
MAGMOM = 0 0 1.6 0 0 -2 | values of non-collinear magnetic moments
LORBMOM = T | calculates orbital moments

GGA+U:

LDAU = .TRUE. | turns on +(U,J)
LDAUTYPE = 2 | rotationally invariant LDA+U
LDAUL = -1 3 | electronic shells for (U,J), -1 when none
LDAUU = 0.0 6.8 | value of (U) for each electronic shell
LDAUJ = 0.0 0.7 | value of (J) for each electronic shell
LDAUPRINT = 2 | how much information about LDA+U is printed

Parallelization:

NCORE = 4 | number of cores working on an orbital

Most parameters of **INCAR** do not need more explanation than the small comments, and the input values are determined in a straightforward way. A few important ones will be discussed in more detail. When starting a new calculation, **ISTART=0** is chosen and the orbitals are created randomly. After a first calculation, one sets **ISTART=2**, which continues the calculation based on the wavefunctions and existing orbitals, as given in the **WAVECAR** file. Initially **ICHARG=2** and the charges are taken from atomic densities for the random orbitals. For a continuation, **ICHARG=1** and the **CHGCAR** file is read for charges.

ISMEAR is the parameter determining the method for calculation of partial occupancies. After extensive tests, the first order Methfessel-Paxton (**ISMEAR=1**) and the tetrahedron method with Blochl Corrections (**ISMEAR=-5**) were deemed suitable [[1989 Methfessel](#), [1994b Blochl](#)], and the VASP results given in [Chapter 5](#) are based on **ISMEAR=1**. Due to the presence of SOC in the calculations, and the fact that SOC breaks some symmetries, not all symmetries present in the easy direction are allowed to be used. Unlike WIEN2k, VASP cannot deduce the reduced symmetries and use the remaining, and hence to ensure that no artificial symmetry is used, **ISYM=-1** was set, which turns off all symmetry operations. This renders the calculations more expensive but ensures correctness. **LORBIT** is given so that the code prints out the *lm* – decomposed DOS data. The number of energy steps, and the energy interval for DOS are determined by **NEDOS** (here 700 or 800), **EMIN** and **EMAX**. For the latter two, the code’s automatically set values work well, but it is better to increase **NEDOS** to obtain more accurate DOS results.

NBAND is the number of energy bands and influences both speed and accuracy. An important defect of VASP is that the free energy value depends on **NBAND**, which is in turn machine dependent in parallel computers. The manual guide suggests setting **NBAND=0.5(NELECT+NIONS)**, which, based on the current experience, is not helpful. The most important feature about **NBAND** is, that to go from a calculation without SOC to one with SOC, this parameter should be manually doubled, presumably due to spin-up and spin-down states. There is no description why this should be done in the manual but without this change, the SOC calculation stops with an error and no explanation.

When using GGA files, exchange and correlation reduce the symmetries of hexagonal and tetragonal lattices. Using **GGA_COMPAT=.FALSE.** corrects the errors, which are important in calculation of MAE. The correction is done by constructing a sphere of radius G_{cut} . For all reciprocal lattice vectors larger than G_{cut} , the density is set to zero. On the other hand, gradient corrections also have non spherical contributions which are per default ignored inside the atomic spheres. To include their influence, **LASPH=.TRUE.** is set. Further, using **ADDGRID=.TRUE.**, a support grid is included for better calculation of augmented charges. Based on the manual, using the parameters **NCORE**, **NPAR**, **LPLANE** and **KPAR** are important for large scale parallel calculations. But current calculations show that only **NCORE** has a positive effect on calculations running at VSC2 and VSC3 of the Vienna Scientific Cluster. On these clusters **NCORE=4** was used for 32 and 64 cores. The grid parameters **NGX**, **NGY** and **NGZ** do influence energy, though their influence is small and the automatic determination by the code is accurate enough.

For relaxation and optimization **IBRION=2** is used, which corresponds to using the conjugate gradient algorithm. The method searches for the largest minimization in energy at each step. The parameter **POTIM** decides the length of the trial step in search direction. Per default its value is initially 0.5. After an optimization, the code provides a “**trial step**” value. The new **POTIM** will be the old **POTIM** multiplied by “**trial step**”. The parameter **ISIF** controls the type of optimization calculation, and which degrees of freedoms are held fix. Current calculations first use **ISIF=7**, which optimizes the volume without allowing for cell type to change. Atomic positions are not relaxed in this step. Then **ISIF=0** is used to relax the positions, without changing the volume further. As a last step it is possible to use **ISIF=4** after the previous two steps. Then the positions are relaxed again, while the cell shape is optimized.

The parameter **MAGMOM** is used to provide initial values for spin magnetic moments of each atom. The order follows that of **POSCAR**. The parameter is not necessary as an input and if left out, the code will use default magnetic moments. Depending on the number of iterations, the final spin moments possibly differ based on initial values, but at convergence this change should be small. In collinear calculations each atom requires only one value. In non-collinear calculations, when **SAXIS** is used to indicate direction of magnetization, the values of **MAGMOM** are written as triplets of the form **(0 0 m)** for each atom. This value of m should not differ from the input value in the collinear calculation. The reason behind this defect is unclear. After all, one wishes to run a second calculation based on updated or converged spin moments of prior calculations. A remedy is to use **ICHARG=1**, which then takes the previously obtained densities and moments from the **CHGCAR** file. Nonetheless, this issue is a possible reason for less accurate magnetic moments calculated by VASP compared to WIEN2k. The parameter **LMAXMIX** controls up to which angular momentum l the quantum numbers are included in the mixing scheme between iterations. For current calculations it was necessary to put $l = 6$ due to $4f$ –electrons. This also ensures that charge densities and lm –decomposed DOS of f –electrons are stored in **CHGCAR** and **DOSCAR**. Among different types of $+(U;J)$ methods, **LDAUTYPE=2** was used which is rotationally invariant. The **POTCAR** file includes the PAW potential data for all elements used. The order of the elements in **POTCAR** determines the order in the calculation. This file is created from the potential files provided in the dataset. The **KPOINTS** file entails the \mathbf{k} –points for the calculation. As mentioned, the automatic generation schemes with a Γ –centered and Monkhorst-Pack meshes were used with no shifts. The file has the following lines:

```
Auto mesh      | comment
0              | indicates automatic mesh generation
G (M)         |  $\Gamma$ -centered mesh (Monkhorst-Pack mesh)
6 6 5         | number of subdivision in crystallographic directions (x, y, z)
0 0 0         | shifts for the k-points in the directions (x, y, z)
```

This setting prompts the code to calculate a \mathbf{k} –mesh for the structure, which is stored in **IBZKPT** file. To save time in the follow up calculations, **IBZKPT** is then copied to **KPOINTS**. In VASP calculations, even for small \mathbf{k} –meshes the number of \mathbf{k} –points plays an important role, not only for energy but also for

magnetization. The **POSCAR** file contains the position of each atom, the matrix of lattice parameters and the number of atoms for each element. No symmetries were used and hence all atomic positions were given manually in the file. For $R_2T_{14}B$ this is 68 lines of atomic positions; for RT_5 it is 6. The example of $SmCo_5$ is given below (here maximum 6 digits after the dot are given; in the calculation files all 16 are used). For hexagonal structures, the lattice vector \mathbf{b} must be calculated as a projection of the hexagonal y –axis on the cubic x –axes and y –axes.

```

Co5Sm 5.002 5.002 3.961 90.00 90.00      | is a comment
  1.00                                     | scaling factor
  5.002      0.00000      0.000          | lattice vector a
-2.501      4.33186      0.000          | lattice vector b
  0.000      0.00000      3.961          | lattice vector c
Co   Sm                                     | atomic species
5    1                                     | number of atoms for each species
Direct                                     | direct or reciprocal lattice
0.33333  0.66667  0.00000                | positions of Co1
0.66667  0.33333  0.00000                | positions of Co2
0.50000  0.00000  0.50000                | positions of Co3
0.00000  0.50000  0.50000                | positions of Co4
0.50000  0.50000  0.50000                | positions of Co5
0.00000  0.00000  0.00000                | positions of Sm

```

After a calculation, the code generates the **CONTCAR** file, which has the same information as **POSCAR** but is updated. For relaxation and optimization calculations, **CONTCAR** should replace **POSCAR** after each step, as the relaxed or optimized values for lattice parameters and positions are written only to **CONTCAR**.

Other files used as input for further calculations are **CHGCAR** (charge density and magnetization), and **WAVECAR** (wavefunctions). These are not copied and the code uses them directly as input. In **CHGCAR** the charge densities ($n = n_\alpha + n_\beta$) are given based on the FFT-grid, as well as one-centered PAW occupation numbers. It also stores the magnetization density ($m = n_\alpha - n_\beta$). In non-collinear calculations, n and m are given for all directions. The **CHG** file is similar to **CHGCAR** but for fine FFT grid. This file has no further use in the present work. **WAVECAR** contains the information on number of bands, cutoff energy, basis vectors, eigenvalues, Fermi Weights and wavefunctions. This file is used for further calculations, when the initial calculation did not converge or a different step is resumed. But it has no useful output data for magnetization and anisotropy energy directly. **DOSCAR** contains the energy values, density of state (DOS) and integrated DOS based on the input parameters. For spin-polarized calculations it has spin-up and spin-down contributions, but not in the non-collinear calculations. It is possible to print out DOS based on angular momentum projection (s, p, d, f) and direction (x, y, z). Working with **DOSCAR** though is impractical, hence the program “p4vasp” [2017 Dubay] was used, which uses the **vasprun.xml** file to visualize DOS. Other output files, which are not used any further as input, but contain important data, are **OSZICAR** and **OUTCAR**. The prior provides an overview of ionic and electronic iterations and their energy values. The latter stores all the important output information.

5 – Results and Discussion

5-1 General Considerations

Density functional methods are robust and reliable [2016 Lajaghere] but when calculating the $R - T$ compounds, two problems are encountered. The first is that MAE is a very small difference in energy of hard and easy axes, compared to total energy. For example, free energy of $Y_2Fe_{14}B$ is about $4 \cdot 10^6 eV$, while its MAE is in the order of $8 \cdot 10^{-3} eV$. An initial goal of this work was to find a simple and general application of DFT that requires no advanced manipulation of the codes but delivers good results for MAE of pure phases compared to single crystal measurements at 4.2 K. The second problem is the correct calculation of spin and orbital magnetic moments of localized $4f$ –electrons. When treating the $4f$ –electrons as valence, it is possible for them to be transferred from one atomic site to another, though this results in inaccuracies in estimation for $4f$ –electrons’ magnetic moments. Considering the $4f$ –electrons as core electrons removes their interactions with other electrons completely and results in strongly underestimated MAE values. Further, in VASP core electrons are frozen and their energy is ignored. One method to quantitatively approximate the $4f$ –electronic structure is to regard them as “open-shell” where the occupation number, given by Hund’s Rule, acts as an input for an SCF calculation where $n_{4f}^{\alpha,\beta}$ are the up and down spin occupation numbers.

$$n_{4f} = n_{4f}^{\alpha} + n_{4f}^{\beta}, \quad \mu_{4f}^s = n_{4f}^{\alpha} - n_{4f}^{\beta} \quad (5-1)$$

By including $+(U;J)$ in the XC-potential, the valence $4f$ –electrons are pushed further away from Fermi Energy and the order of filling of the $4f$ –shell is changed to construct a physically more accurate model.

Before powerful computers became available, approaches were utilized to reduce calculation costs in magnetic phases. One such approach is the Magnetic Force Theorem, which on its own has a robust and rigorous principle [1977 Andersen]. One feature of this theorem is that it justifies calculating MAE of a magnetic phase after one iteration of SOC calculation, when the SRC has converged. The validity of this feature has been shown for certain phases [1996 Wang]. Indeed, based the results of YCo_5 calculations with WIEN2k, it was seen that calculating MAE after the convergence of the SOC calculation provided similar results as calculating it after only one iteration of SOC. The same though does not apply to other phases calculated for this work. For all other phases, including $Y_2Fe_{14}B$, the MAE value after one iteration of SOC differs from this value after convergence, which disallows using the theorem for these compounds. In the case of $SmCo_5$ this difference is considerably large. This was also observed by Daalderop et al. [1990 Daalderop] and Landa et al. [2018 Landa]. Hence, in all the provided results, SOC has been calculated to convergence.

The following abbreviations are used in this section. “w” = LAPW calculation (WIEN2k), “v” = PAW calculation (VASP). REL = relaxation, Shape = shape optimization, OPT = lattice parameter

optimization, OPEL = simultaneous optimization and relaxation, G = Γ -centered k -mesh, M = Monkhorst-Pack k -mesh, NSP = non-spin polarized, SRC = scalar relativistic calculation, SOC = spin-orbit coupling, + U = calculation including U_{eff} or ($U;J$) potentials. The XC-potential is PBE-GGA, unless explicitly specified as LDA.

Before detailed results of the calculated phases are described, [Tab. 5-1](#) summarizes the experimentally obtained total magnetization (in $\mu_B/f.u.$ and MA/m), total polarization (in T) and MAE (in MJ/m^3) for important phases at 4.2 K, taken from literature.

Material	M_S [$\mu_B/f.u.$]	M_S [MA/m]	J_S [T]	MAE [MJ/m^3]
<i>bcc</i> – <i>Fe</i>	2.2 (a)	1.75	2.20	0.05 (b)
<i>hcp</i> – <i>Co</i>	3.4 (a)	1.43	1.81	0.68 ... 0.76 (c)
<i>YCo</i> ₅	8 (d)	0.90	1.13	6.5 ... 10 (e)
<i>SmCo</i> ₅	8.2 ... 8.9 (f)	0.91 ... 0.99	1.14 ... 1.24	24 ... 29 (f, g)
<i>PrCo</i> ₅	9.2 ... 11 (h)	0.99 ... 1.18	1.24 ... 1.49	-0.8 (h)
<i>Y</i> ₂ <i>Fe</i> ₁₄ <i>B</i>	31.4 (i)	1.26	1.59	0.9 (i)
<i>Pr</i> ₂ <i>Fe</i> ₁₄ <i>B</i>	37.6 (i)	1.46	1.84	24 (i)
<i>Nd</i> ₂ <i>Fe</i> ₁₄ <i>B</i>	37.7 (i)	1.48	1.86	-2.3 (i)
<i>Dy</i> ₂ <i>Fe</i> ₁₄ <i>B</i>	11.3 (i)	0.45	0.56	3.8 (i)

Tab. 5-1 Experimental values of magnetization, polarization and MAE for important phases. (a) = [1994 Billas], (b) = [1982 Tung], (c) = [1981 Ono], [1984 Paige], (d) = [1962 Nesbitt], (e) = [1971 Tatsumoto] & [1967 Hoffer], (f) = [2003a Larson], (g) = [1976 Ermolenko], (h) = [1982 Andoh], (i) = [1986 Yamauchi].

5-2 Results for RT_5 Compounds

The RT_5 compounds have a layered hexagonal structure as shown in [Fig. 5-1](#), drawn with VESTA [2011 Momma], with initially 3 inequivalent atomic sites [1959 Wernick]. Some of the earliest systematic studies on these compounds were carried out by Nesbitt et al. [1959 Nesbitt] and Hubbard et al. [1960 Hubbard]. In this work, phases with $R = Y, Pr$ and Sm , and $T = Co, Fe$ and Cu are investigated. The elements Pr (light R) and Y (non-magnetic) are chemically similar to Sm and form the same $CaCu_5$ phase. The R -atom occupies the site $R(1a)$, while T -atoms are initially divided in $T(2c)$ and $T(3g)$. Substituted phases have 20% of Co -atoms replaced by Fe or Cu . Test calculations for energy convergence were carried out on $SmCo_5$ with LAPW, and with 5, 20, 50, 100, 200, 500, 1000 and 5000 k -points and cutoffs of $RK_{max} = 6, 6.5, 7.0, 7.5, 8.0, 8.5$ and 9. It was concluded that calculations with at least 200 k -points and $RK_{max} = 8$ are reasonably fast, while meeting the required accuracy. In the subsequent PAW calculations a k -mesh of $5 \times 5 \times 7$ in the irreducible Brillouin Zone and an energy cutoff of 500 eV were used. It should be mentioned that the accuracy of the k -mesh also depends on the symmetries used. WIEN2k makes use of as many symmetry operations as possible, hence allowing a larger k -mesh. But because symmetries are used, the true potential landscape is calculated less

accurately than it would have been without symmetry. To take into account the influence of SOC on symmetry of the spin polarized structure, only the shared symmetries of the hard and easy axes should be used. This increases the number of inequivalent sites in LAPW calculations to 5. In VASP calculations no symmetries are used (because the VASP k –mesh generator does not function well in regard to hexagonal symmetries with SOC), which makes the atomic potentials more accurate, but reduces the feasibly calculable number of k –points, hence all 6 sites are given.

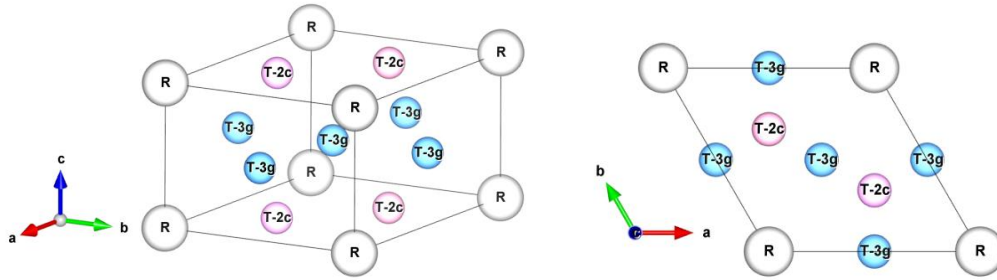


Fig. 5-1 – A sketch of the RT_5 crystal structure ($CaCu_5$ type, space group 191). The R –atoms are grey, the $R(2c)$ are pink and the $T(3g)$ blue.

$PrCo_5$ exhibits a spin reorientation and has a non-collinear magnetic structure at 4.2 K, but all other phases remain uniaxial down to 4.2 K [1976 Ermolenko] with the easy axis showing in [001] direction and the hard axis in [100]. The total energy calculations show in all cases that the antiferromagnetic coupling between spin moment of R and spin moment of T has a lower energy than the ferromagnetic coupling, and is hence the state that the spins assume. Despite obtaining the correct coupling and generally the correct order of magnitude for magnetic moments of R –atoms, the value of orbital moments of these sites are not calculated accurately. The spin-polarized LDA and GGA potentials do not account for the orbital moments directly, and the best way of calculating orbital moments is to take advantage of SOC and couple the spin-up and spin-down Kohn-Sham Equations. This renders the calculations more demanding but allows in principle the calculation of orbital moments, though this method systematically under-estimates the value of orbital moments [2007 Bihlmayer]. One reason is the strong electron-electron interaction that shifts the $4f$ –energy levels further from Fermi Energy; a situation that LDA and GGA cannot describe well [2018 Miyake].

Results for YCo_5 : The normal method for calculation of MAE with DFT, described in literature (including user guides of both codes), is to first carry out the scalar relativistic calculation, then calculate SOC in two different directions and finally run SOC+ U . The reason is that, when including SOC from the start, it is possible to reach a local minimum of energy far from the global minimum. As the energy contribution of SOC is small compared to total energy, it is feasible to converge the SRC first, and then run the SOC. This approach was initially used to calculate MAE of YCo_5 . The magnetization is estimated

accurately, but even though YCo_5 has no $4f$ –electrons, the calculation underestimates MAE. To achieve better results, the lattice parameters were optimized and the atomic positions relaxed using VASP ([Tab. 5-2](#)). This improved the results somewhat but was insufficient for obtaining agreement with experimental MAE values. As seen from the table, the two hard axes, [100] and [210] are equivalent.

YCo_5	Opt. method	SOC [001] (con) (eV)	MAE [100]	MAE [210]	MAG [μ B/fu]
v_b4_06_II	REL	-42.29186305	1.8	1.8	7.9
v_b4_07_II	REL + OPT	-42.29540596	0.8	0.8	7.3
v_b4_10_II	Shape + OPT	-42.29526536	0.8	0.7	7.3
v_b4_11_II	OPT	-42.29588000	1.2	1.1	7.3

Tab. 5-2 Initial results for YCo_5 after optimization and / or relaxation. $(a; c) = (0.4937; 0.3986)$; k –mesh $G - 8 \times 8 \times 6$; Steps: SRC \rightarrow SRC-OPT/REL 1 \rightarrow SRC-OPT/REL 2 \rightarrow SRC-OPT/REL 3 \rightarrow SOC.

Based on the the results of many tests, it was concluded that calculations starting with SRC are not very stable and converge difficultly. When starting with an NSP setting, DFT is guaranteed to find the absolute minimum of energy, while this is not the case for spin-polarized calculations [[2006 Singh](#)]. Hence, in the next step ([Tab. 5-3](#)), the calculations were started as NSP, the structures were optimized and relaxed twice and then SOC was calculated to convergence. The MAE values are now larger, but still underestimated.

YCo_5	SOC [001] (conv) (eV)	MAE (100)	MAE (210)	MAG [μ B/fu]
v_e6_01	-42.76320361	2.2	2.2	7.7

Tab. 5-3 Results for YCo_5 when starting with non-spin polarized calculation. $(a; c) = (0.4937; 0.3986)$; k –mesh $M - 5 \times 5 \times 7$. Steps: NSP \rightarrow NSP-OPT 1 \rightarrow NSP-REL 1 \rightarrow NSP-OPT 2 \rightarrow NSP-REL 2 \rightarrow SOC.

As MAE is sensitive to small details of the Fermi Surface, one would require several thousand k –points per metallic atom for an accurate calculation of MAE in compounds with complex Fermi Surfaces, which is computationally too expensive. Without including the $+U$ potentials, no combination or variation of parameters and features of the codes improved MAE considerably. A disadvantage of WIEN2k in this regard is that it calculates energy for all electrons. This is useful for accurate electronic structure approximations, but reduces the accuracy of MAE calculations, as the absolute value of total free energy is very large.

It is known that a source of error is that Coulomb and exchange interactions (U and J) of valence electrons are not included explicitly and in full detail within LDA or GGA potentials. To resolve this issue, the method of Hubbard Potential is used, which adds ($U; J$) potentials externally. In theory it is possible to calculate the value of ($U; J$) potentials based on Raccah Parameters [[2017 Soderlind](#)]. Van der Marel et al. [[1988 van der Marel](#)] undertook a systematic study of the ($U; J$) potentials in $3d$ and $4f$ –metals, while Cococcioni [[2012 Cococcioni](#)] studied in details, the different methods of determining ($U; J$) potentials. In this work, literature values from measurements and calculations (e.g. [[2018 Nguyen](#)]) were used as basis and the values were varied to obtain the best agreement with experiment. In WIEN2k

calculations ($U_{eff} = (U - J); J = 0$), and in VASP calculations ($U; J$) values were used. As seen in [Tab. 5-4](#), adding U_{eff} after the convergence of SOC did not improve the results, but if the $+U$ is included from the start, a large MAE is obtained for YCo_5 , which though is overestimated. In the next attempt ([Tab. 5-5](#)), both (U, J) were included for $Co - 3d$ -electrons after the convergence of SOC.

YCo_5	Steps	SOC+U [001] (conv) (eV)	MAE [MJ/m ³]	MAG [μ B/fu]
f_201	SRC \rightarrow SOC \rightarrow +U	-281723.03175411	2.09	7.68
f_202	(SRC+SOC) \rightarrow +U	-281723.03172200	2.06	7.68
f_203	(SRC+SOC+U)	-281723.08262146	9.88	7.76

Tab. 5-4 Results for YCo_5 when $+U$ is included. ($a; c$) = (0.4937; 0.3986), k -mesh 16x16x17; $U_{eff} = 4.4$ eV.

YCo_5	Steps	+U [001] (conv) (eV)	MAE (100)	MAE (210)	MAG [μ B/fu]
v_e8_01c	V.1	-39.54552473	8.9	8.9	8.3
v_e8_02c	V.2	-39.54552306	8.9	8.9	8.3

Tab. 5-5 Results for YCo_5 when starting with non-spin polarized calculation and adding $+U$ at the end. ($a; c$) = (0.4937; 0.3986); k -mesh $M - 5 \times 5 \times 7$; $U_{Co-3d} = (1.5; 0.8)$ eV Steps: V.1 = NSP \rightarrow SRC \rightarrow SOC \rightarrow +U; V.2 = NSP \rightarrow SOC \rightarrow +U; not optimized.

Principally, there is no reason not to include the $+U$ potential already from the start of the calculation. As a matter of fact, including it from the start is physically meaningful, because the Coulomb Repulsion is independent of spin-polarization. Hence, in the next attempt ([Tab. 5-6](#)), the calculation steps were (NSP+U) \rightarrow (SOC+U), and it was found that including ($U; J$) from the start and in all steps to be the most stable and reliable method. Optimizing and then relaxing separately at each step further enhances the result, though has little impact on MAE in YCo_5 . The ensuing calculations were based on the previously optimized lattice parameters. These calculations ([Tab. 5-7](#)) provide the best results and have a good agreement both for MAE and magnetization.

YCo_5	Steps	+U [001] (conv) (eV)	MAE (100)	MAG [μ B/fu]
v_f3_05	NSP+U \rightarrow SOC+U	-40.96821181	7.1	8.3

Tab. 5-6 Results for YCo_5 when starting with NSP calculation and including $+U$ from the start. ($a; c$) = (0.4937; 0.3986); k -mesh $M - 5 \times 5 \times 7$, ($U; J$) $_{Co-3d} = (1.5; 0.8)$ eV; not optimized.

YCo_5	Relaxation Type	+U [001] (conv) (eV)	MAE (100)	MAG [μ B/fu]
v_f9_01	REL + OPT	-40.97531075	7.21	8.0
v_f9_02	REL	-40.97531075	7.22	8.0

Tab. 5-7 Results for YCo_5 when starting with NSP+U and optimizing / relaxing. ($a; c$) = (0.4916; 0.3927); k -mesh $M - 5 \times 5 \times 7$, ($U; J$) $_{Co-3d} = (1.5; 0.8)$ eV. Steps: NSP+U \rightarrow SOC+U \rightarrow SOC+U-OPT \rightarrow SOC+U-REL.

After succeeding to obtain accurate MAE values, the same methods are applied to the YCo_5 phase under strain ([Fig. 5-2](#)). Here, for a closer inspection, once lattice parameter " a " is varied, while " c " is constant ([Fig. 5-2\(A\)](#)), and once " c " is varied, while " a " is constant ([Fig. 5-2\(B\)](#)). The volume is changing. As

optimization changes lattice parameters and results in different (a ; c) values than desired, in these calculations the structures are relaxed but not optimized. Based on the variation of MAE with regard to " a ", the dependence of MAE on " $1/a$ " is also visualized. Finally, for a more realistic characterization, in a new calculation series, both " a " and " c " are varied, while the volume is kept constant. In all cases, the c/a ratio is changing from -2% to $+2\%$ of the value initially taken from literature, with 0.5% steps. The black squares show total energy and red diamonds MAE. With constant volume, largest MAE is obtained, when c/a remains unchanged. Changing " c ", while " a " is constant, which is possible in thin films, increases the MAE value slightly.

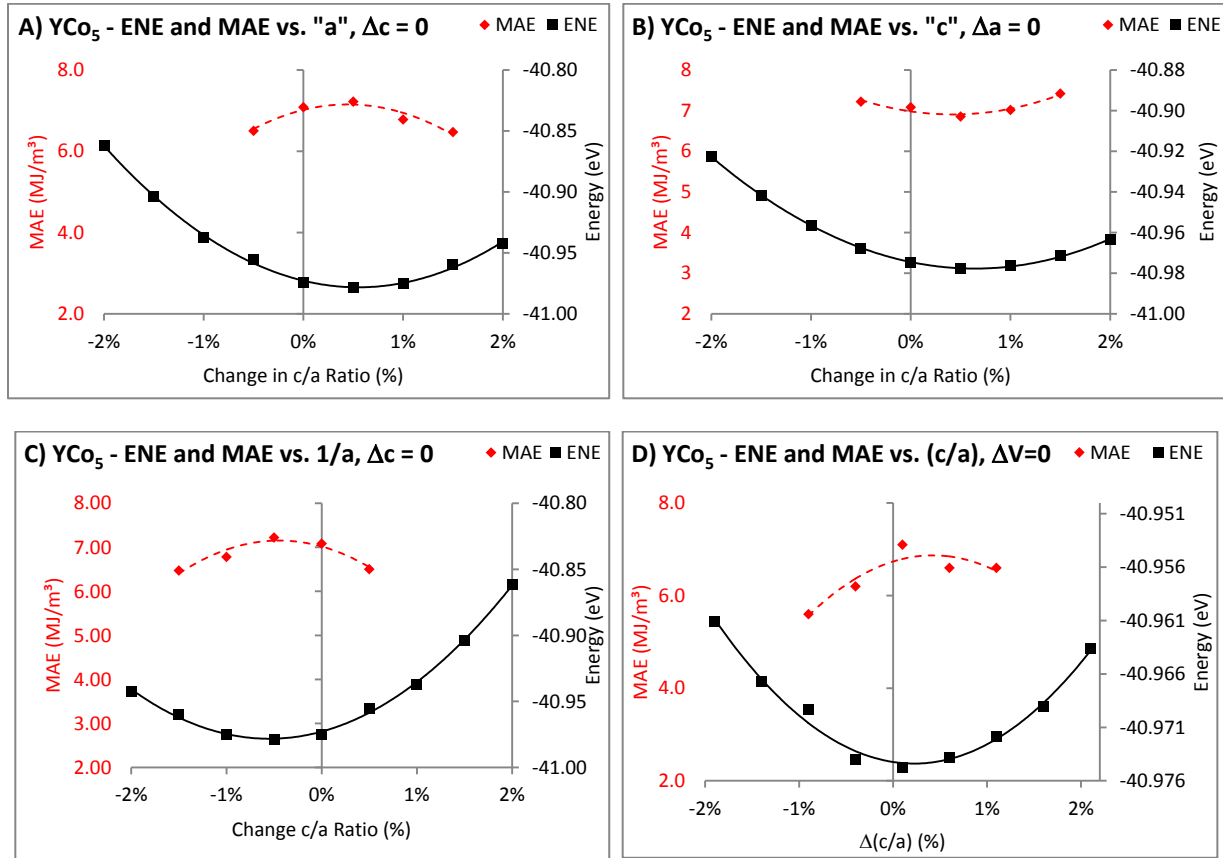


Fig. 5-2 Changes in energy and MAE for YCo_5 when " a " is varied and " c " is fix (A), when " c " is varied and " a " is fix (B), when " $1/a$ " is varied and " c " is fix (C), when " c/a " is varied and the volume is fix (D).

One method for producing strain in a structure is substitution of similar atoms. Here the substitution of 20% of Co –atoms is considered. Co –atoms occupy two distinct sites ($Co(2c)$ and $Co(3g)$). Hence, the substitution of both sites, once by Fe and once Cu , were calculated. Based on the aforementioned method, ($U;J$) was included from the start for Co atoms. $3d$ –electrons of the Fe atoms also have the ($U;J$) = (1.2; 0.8), but for Cu no ($U;J$) was included. The results for all three phases are given in [Tab. 5-8](#). Fe –substitution lowers energy indicating a stable phase, while Cu increases it. Furthermore, Fe at $T(2c)$

is more stable than at $T(3g)$, but Cu is more stable at $T(3g)$. As expected, M_S increases with Fe and decreases with Cu , since the atomic magnetic moment of Fe is larger than that of Co , while Cu is non-magnetic.

Phase	Energy [eV]	MAG (Calc.) [$\mu_B/f.u.$]	MAG pro Co [μ_B]	MAE [MJ/m^3]
YCo_5 (opt.)	-40.97531075	8.01	1.75	7.22
YCo_5 (exp.)		8 (a)		6.5 ... 10 (b)
YCo_4Fe (2c)	-42.33226769	8.85	1.73	1.99
YCo_4Fe (3g)	-41.43882780	8.95	1.76	2.12
YCo_4Cu (2c)	-37.88835060	5.80	1.62	2.72
YCo_4Cu (3g)	-37.96011289	5.94	1.63	2.81

Tab. 5-8 Results for YCo_5 , YCo_4Fe and YCo_4Cu . (a) = [1962 Nesbitt], (b) = [1971 Tatsumoto, 1967 Hoffer]. (a; c) = (0.49159943; 0.39274376); k -mesh $M - 5 \times 5 \times 7$, $U_{Co-3d} = U_{Fe-3d} = (1.2; 0.8)$, no $+U$ for Cu ; Steps: NSP+U \rightarrow NSP+U-OPT \rightarrow NSP+U-REL \rightarrow SOC+U \rightarrow SOC+U-OPT \rightarrow SOC+U-REL.

Interestingly, Cu reduces average Co -moment more than $0.1 \mu_B$, which means that the lack of magnetic electrons in Cu slightly suppresses magnetization in Co . Most importantly, MAE is reduced strongly by both substituents. It is initially surprising that Fe reduces MAE more than Cu does, but with the discussion of strain effects and based on density of states (DOS), discussed below, it becomes plausible. Another interesting point is that both YCo_4Fe and YCo_4Cu have a larger anisotropy when the substituent is occupying $T(3g)$. The reason is that $Co(3g)$ atoms have a smaller contribution to MAE than $Co(2c)$ do [1976 Deportes], and hence replacing a $Co(3g)$ reduces MAE less than replacing a $Co(2c)$. Table 5-9 shows how Fe and Cu influence the lattice parameters. Fe increases “ a ” three times more than it reduces “ c ”. From Fig. 5-2 we know that a large increase in “ a ” reduces MAE considerably, which is one of the reasons why MAE is reduced strongly by Fe . In comparison, Cu leaves “ a ” nearly unchanged, while increasing “ c ” by 1%, which is one reason why Cu reduces MAE less than Fe does. Both phases have a larger volume, which is a cause for smaller anisotropy (energy density).

Phase	“a” (nm)	vs. YCo_5	“c” (nm)	vs. YCo_5	Vol. (nm ³)	vs. YCo_5
YCo_5	0.4916		0.3927		0.08220	
YCo_4Fe	0.4960	+0.89 %	0.3913	-0.35 %	0.08337	+ 1.4%
YCo_4Cu	0.4914	-0.04 %	0.3970	+1.09 %	0.08430	+ 2.6%

Tab. 5-9 Changes in lattice parameters and volume of YCo_5 , YCo_4Fe and YCo_4Cu .

As described by Lifschitz et al., Fermi Energy (E_F) and Fermi Surface play an important role in the electronic structure, exchange interaction and magnetic properties [1980 Lifschitz]. Based on the Stoner Model, spontaneous magnetization in itinerant systems depends strongly on the value of DOS at E_F . Indeed, comparing the DOS plots, it is evident that the value of DOS at E_F changes with substitution. As described by Dugdale [2016 Dugdale], the shape of the Fermi Surface influences an electron’s “ability to

screen perturbations”. Changes in the electron screening in turn affect the long-range magnetic ordering. The magnetic susceptibility is a response function and sensitive to screening [2005 Mohn], and with the SOC being a weak effect, it is expected that even subtle changes in the Fermi Surface influence MAE. Nordstrom et al. found that MAE varies strongly with changes in Fermi Energy, because of the changes in the effective number of valence electrons [1992 Nordstrom]. They obtain a lower MAE, when they calculate the YCo_5 phase with 49 valence electrons, while it has originally 48 electrons.

It is hence reasonable to study the density of states in an interval close to E_F . The total DOS plots of YCo_4T ($T = Co, Fe, Cu$) in both crystallographic directions are shown in Fig. 5-3(A, B). It should be noted that VASP abandons the spin-up/down concept in the non-collinear case, that is, for all calculations including SOC, and gives a total DOS along the defined axes, here [001] and [100]. The data for DOS plots were obtained using the “p4vasp” program [2017 Dubay]. For YCo_5 , YCo_4Fe , and YCo_4Cu , $E_F = 9.20$ eV, 9.19 eV, and 8.54 eV respectively, but in all graphs E_F is drawn at zero point of x-axis.

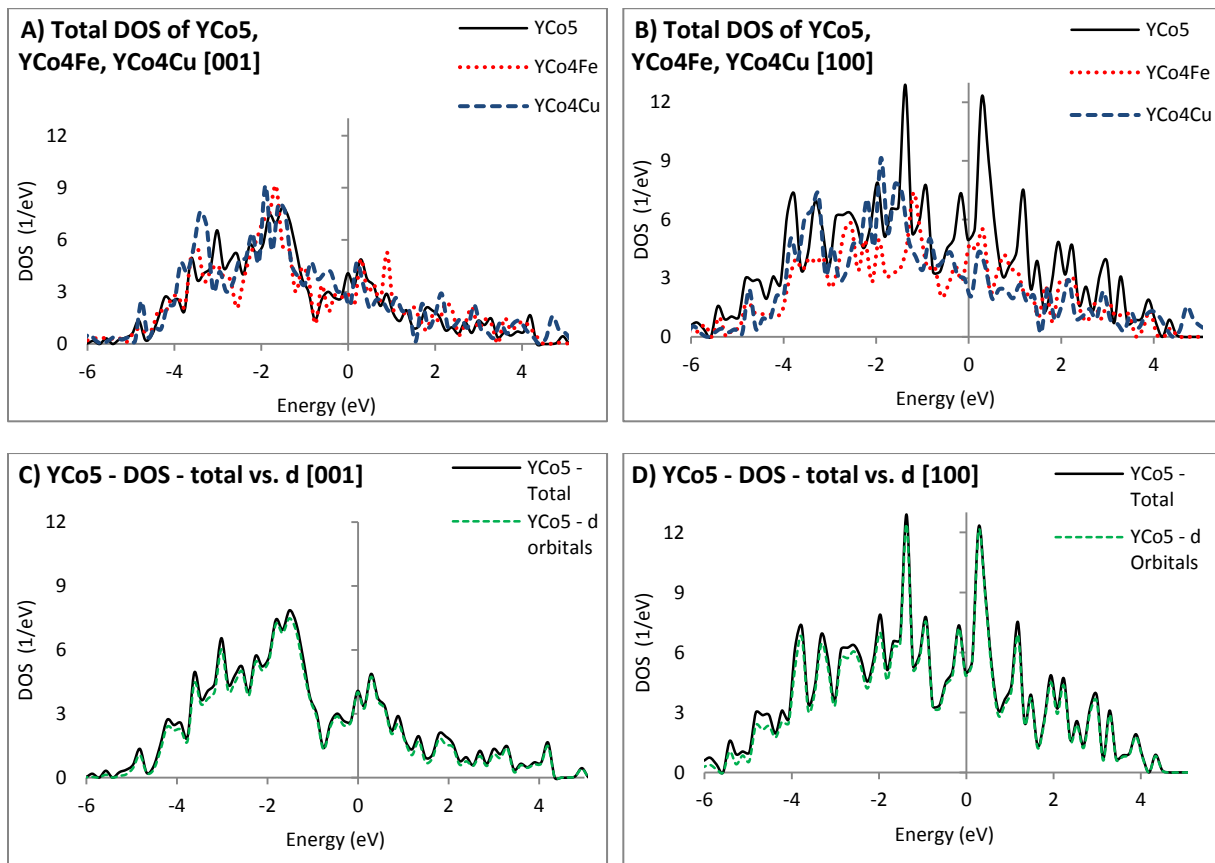


Fig. 5-3 Total DOS of YCo_5 , YCo_4Fe and YCo_4Cu around E_F in [001] (A) and [100] directions (B). Comparison of total DOS and the contribution of d -electrons to DOS of YCo_5 in [001] direction (C) and [100] direction (D).

Immediately before Fermi Energy, *Cu* increases the density while *Fe* decreases it, but both reduce the difference of DOS between [001] and [100]. Both decrease the density at E_F . Iron substitution weakens the *T* – *s* –peak, but there are larger *Co* – *p* –peaks and two additional *Fe* – *p* –peaks, which do not influence MAE (these energy intervals are not shown in the graphs). The *Y* – *p* – contribution increases, while the *Y* – *d* near E_F remains nearly unchanged with a decreased DOS value at E_F showing a limited contribution to MAE. While *Fe* helps increase the *Co* – *d* –density pro *Co* – atom, it reduces the density considerably at E_F , which is decisive for MAE. *Cu* increases the *p* –DOS while the *d* –states near E_F remain again mostly unchanged. The peak of *Cu* below E_F is responsible for a second peak below E_F in the total DOS but falls short of increasing DOS at E_F . The role of the *d* –electrons as the major contributor to MAE in YCo_5 becomes clearer with [Fig. 5-3\(C, D\)](#) where the total DOS (black) and the *d* –shell DOS (green) are compared. The *d* –shell is nearly completely responsible for the total DOS around E_F . The same is true for the other two phases [\[2015 Cai\]](#).

Considering DOS alone does not provide direct information about anisotropy, but how DOS changes, when the magnetization is saturated in [001] as compared to [100] does. Weighted by energy, this quantity gives a qualitative measure of MAE and is formulated by

$$|E| \times (n_{YCo_5}[100] - n_{YCo_5}[001]) \quad (5-2)$$

In [Fig. 5-4\(A\)](#) this value is plotted for total DOS of YCo_5 , as well as for *Co*(2*c*) and *Co*(3*g*) contributions. One sees that *Co*(2*c*) (drawn here averaged per atom) has a major contribution to MAE, while *Co*(3*g*) has practically no contribution in the regarded energy interval, agreeing with [\[1976 Deportes\]](#) and explains why substitution of *Co*(3*g*) reduces MAE less than substitution of *Co*(2*c*). Further the graph shows that around -3 eV there is a large negative peak, which reduces MAE. Based on this knowledge, if one changes the electronic structure such that this peak becomes smaller, or positive, then MAE of YCo_5 will increase.

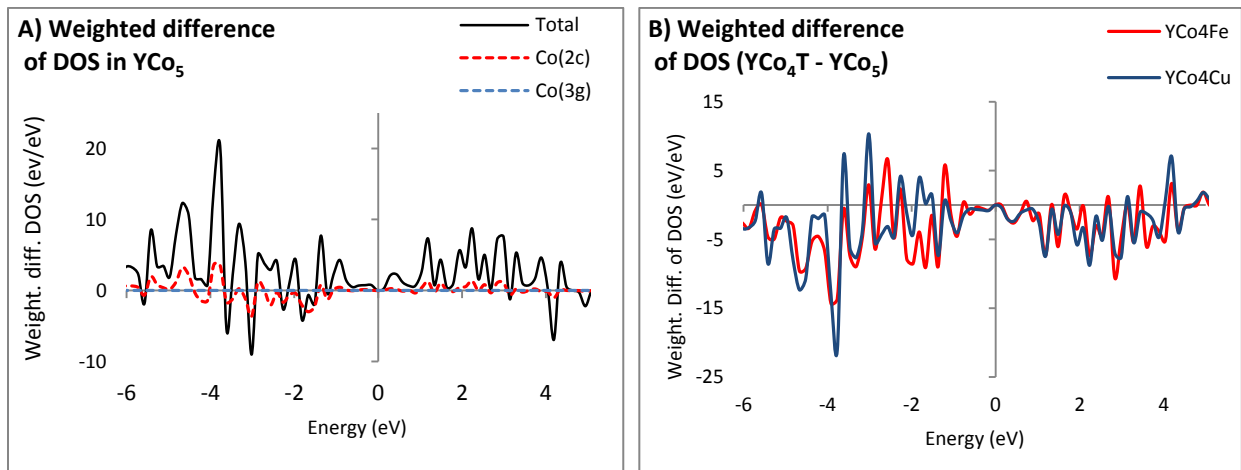


Fig. 5-4 A: Weighted difference of DOS for YCo_5 (black) between [100] and [001] directions, as well as the average contribution of *Co*(2) (red) and *Co*(3*g*) (blue). B: weighted difference of DOS between YCo_4T and YCo_5 .

Similarly, to visualize the influence of a substitution atom on MAE, one compares the weighted DOS of substituted and non-substituted phases. For *Fe* and *Cu* –substitution in YCo_5 , this quantity (Eq. 5-3) is plotted in Fig. 5-4(B) and shows how the substitution changes MAE.

$$|E| \times [(n_{YCo_4Fe[100]} - n_{YCo_4Fe[001]}) - (n_{YCo_5[100]} - n_{YCo_5[001]})] \quad (5-3)$$

It is evident that both *Fe* and *Cu* produce larger negative than positive contributions, hence decreasing MAE. Just below Fermi Energy, where the changes in DOS strongly influence MAE, both substituents result in negative weighted DOS differences. Such simple and inexpensive band calculations provide direct evidence of changes in MAE for novel materials, allowing advanced materials design.

That both substituents reduce MAE so strongly, hints that the role of the Co_5 –network in YCo_5 is essential for a large anisotropy. For a better insight, three other phases are studied as well, namely Co_5 (which means *Y* is removed from YCo_5), Co_6 (which means *Y* is replaced with one *Co* –atom), and *hcp* – *Co*, which is the natural state of pure *Co* –metal and has two atoms in each unit cell (Tab. 5-10). There is no indication of a crystallographic asymmetry in *hcp* – *Co*. This is a reason for the relatively small MAE. For Co_6 the structure is asymmetric, even though the *R* –site is occupied by *Co*. This is due to the artificial arrangement of the atoms in this structure. As expected this change increases anisotropy.

Phase	Energy [eV]	MAG (Calc.) [$\mu_B/f.u.$]	MAG pro Co [μ_B]	MAE [MJ/m^3]
YCo_5	-40.97531075	8.01	1.75	7.22
Co_5	-30.29766282	9.78	1.96	3.98
Co_6	-38.30277084	11.61	1.93	2.30
<i>hcp</i> – <i>Co</i> (cal.)	-13.49614885	3.97	1.98	0.77
<i>hcp</i> – <i>Co</i> (exp.)		3.4 (a)		0.68... 0.76 (b)

Tab. 5-10 Results for YCo_5 , Co_5 , Co_6 and *hcp* – *Co*. (a) = [1994 Billas], (b) = [1981 Ono, 1984 Paige]. *hcp* – *Co*: (*a*; *c*) = (0.250; 0.406); NSP+U → SOC+U → SOC+U-OPT → SOC+U-REL. Co_5 & Co_6 (*a*; *c*) = (0.494; 0.399); *k* – mesh $M = 5 \times 5 \times 7$; U_{3d} – *Co* = (1.2; 0.8); NSP+U → NSP+U-OPT → SOC+U → SOC+U-OPT.

Surprisingly, the transition from Co_6 to Co_5 leads to a notable increase of MAE. The unit cell of Co_5 has a larger anisotropy than the same unit cell of Co_6 , while having similar size and structure. This confirms that having two different layers, one with two $Co(2c)$ and one with three $Co(3g)$, without the presence of a sixth atom to distort the potential landscape is important. The reason that the sixth *Co* –atom in this structure reduces MAE of Co_6 compared to Co_5 is the change in the electronic structure and CEF. The comparison with *hcp* – *Co* shows that a hexagonal structure alone is not enough for achieving a large MAE, though for a pure metal, MAE of *hcp* – *Co* is certainly considerable, being comparable to MAE of $Y_2Fe_{14}B$, even though the former has only two atoms in a unit cell and the latter 68.

Table 5-11 compares the lattice parameters and volumes of Co_5 and Co_6 phases to those of YCo_5 after optimization, but without relaxation. A relaxation of Co_5 and Co_6 would lead to a change in their

structures, which fall back to $hcp - Co$. It is interesting that the volume of Co_6 is smaller than that of Co_5 , despite having a sixth Co -atom. The strong changes in lattice parameters provide an explanation for the reduction in MAE, especially for Co_6 .

Phase	“a” (nm)	vs. YCo_5	“c” (nm)	vs. YCo_5	Vol. (nm ³)	vs. YCo_5
YCo_5	0.4916		0.3927		0.08220	
Co_6	0.4734	- 4.12 %	0.3822	- 2.67 %	0.07416	- 11.86 %
Co_5	0.4794	- 2.91 %	0.3870	- 1.45 %	0.07702	- 8.46 %

Tab. 5-11 Lattice parameters and volume of Co_5 , Co_6 compared to YCo_5 .

One reason that YCo_5 has a MAE much larger than that of Co_5 , is the role of the fully occupied $3d$ - and $4p$ -electron states of Y . Their large orbitals extend to the layers above and below, where the $Co(3g)$ are residing. This further pushes their $3d$ -electrons away from the central axis of the hexagonal unit (where Y is). This increases the already large difference in electron density in direction of c -axis compared to the basal plane, on one hand through the changes in the mean distances of atoms, and on the other hand through changes of the CEF. The magnetization per Co -atom in $hcp - Co$ is overestimated by over $0.2 \mu_B$, while it is calculated quite accurately in YCo_5 . This overestimation is due to how small the unit cell is and the requirement for higher accuracy, beyond the abilities of VASP, and due to the overestimation of the strength of SOC in pure Co . The only differences between the three Co -forms are their symmetries and atomic distances. As the calculated MAE values for them differ clearly, it is concluded that changes in lattice parameters influence anisotropy appreciably.

As Deportes et al. [1976 Deportes] and Schweizer et al. [1980 Schweizer] indicated, magnetization and anisotropy of YCo_5 originate mainly from the Co -atoms. Nonetheless the contribution of Y , though small, is not negligible. Larson et al. [2003b Larson], Daalderop et al. [1996 Daalderop], Steinbeck et al. [2001 Steinbeck] and references cited therein all calculate a spin magnetic moment of at least $0.19 \mu_B$ in value for Y , with orbital magnetization being no less than 5% of this value. Current calculations show for Y moments of $m_{spin} = -0.363 \mu_B$ and $m_{orb} = +0.027 \mu_B$ in the $[001]$ direction and $m_{spin} = -0.367 \mu_B$ and $m_{orb} = +0.015 \mu_B$ in $[100]$. As a pure metal, Y is non-magnetic, but that it obtains a small magnetic moment in this structure is not surprising. It is noteworthy that the orbital moment of Y is highly anisotropic. As seen from Tab. 5-10, Co_5 has an anisotropic structure, which means that the CEF at the site of Y is not completely spherically symmetric. Also, $Co(2c)$ and $Co(3g)$ atoms have differing magnitudes of anisotropies, which further encourages an anisotropy at the R -site.

To analyze the source of magnetic moments, the contribution of different electronic orbitals to total magnetization and their magnitudes are drawn in Fig. 5-5. Further, as the $(U; J)$ values are treated as variables, it is interesting to see how MAE changes with variation of $+U$. To this end, using VASP, the value of $+U$ is varied from 1.2 to 1.8 eV, while $J = 0.8$ eV was kept constant. The monotonous increase in magnetization and anisotropy due to changes of the U -potential is clear. One sees that increasing the

value of the U –potential too much results in unphysically large MAE and shows the importance of calculating its value in an ab-initio manner.

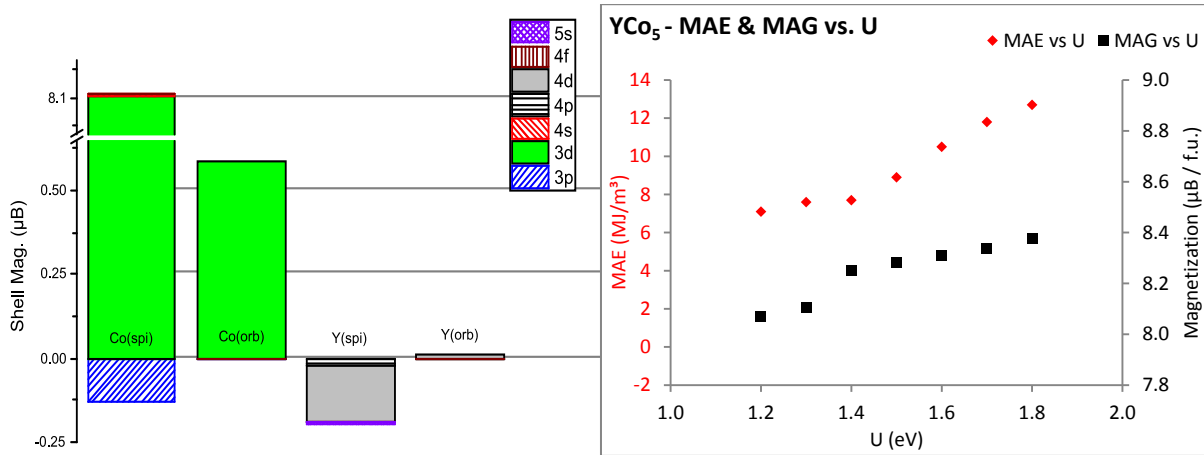


Fig. 5-5 Contribution of different electronic orbitals to total magnetization in YCo_5 (left). Change in MAE and saturation magnetization of YCo_5 with increasing value of U .

Results for $SmCo_5$: The compound $SmCo_5$ exhibits outstanding hard magnetic properties. The energetically high lying, but mostly localized $4f$ –electrons introduce significant changes to the CEF as compared to YCo_5 , which is a source of MAE. Further, the SOC has a large contribution to MAE, and with the presence of $4f$ –electrons it is drastically strengthened, which results in a very large MAE in $SmCo_5$. But aside from the mentioned difficulties in calculation of MAE for $R - T$ compounds, another issue exists in the case of $SmCo_5$. Sm has a nearly completely quenched orbital moment. This is because the first excited state of Sm lies very close to the ground state [1932 Frank, 2001 Morrish], which though has different quantum numbers and hence a different magnetic moment. Simple DFT calculations with small number of k –points are not accurate enough to differentiate between these energy states, which means the inaccuracy of the calculated magnetic moment for Sm is even larger than that for other R –atoms. This issue does not affect MAE. The systematic error is compensated because MAE is calculated as the difference of energy values in two directions.

Despite the optimization of calculation steps and parameters, the MAE value remained consistently underestimated, which shows that the current formulation and implementation of LDA and PBE-GGA is incapable of calculating MAE and additional corrections are required, e.g. $(U; J)$ –potentials. The manual guide of WIEN2k suggests carrying out the initialization of SOC calculation before calculating the SR phase, in order to reduce the symmetry, as spin-polarized structures with SOC do not have the same symmetries as non spin-polarized structures. During the calculations it was found that carrying out this symmetry reduction only in one hard axis is not sufficient. Correct results were obtained for $SmCo_5$, only

when symmetry was reduced in both hard axes and in the easy axis. [Table 5-12](#) shows the different orders of calculation steps attempted to obtain correct results for $SmCo_5$. In the next attempt the $(U; J)$ potentials were included and different steps were tried again ([Tab. 5-13](#)).

$SmCo_5$	Steps	SOC [001] (conv) (eV)	MAE (MJ/m ³)	MAG [μ_B /fu]
v_d12_10	nsp \rightarrow soc, cc = 10^{-6} eV	-47.71792674	-15.4	3.5
v_d12_12	nsp \rightarrow soc, cc = 10^{-7} eV	-47.46441548	-16.0	3.5
v_d12_01a	nsp \rightarrow rel \rightarrow soc	-47.46441518	-16.0	3.5
v_d12_01b	nsp \rightarrow rel \rightarrow opt \rightarrow soc	-47.46441628	-16.0	4.0
v_d12_03	nsp \rightarrow opt \rightarrow rel \rightarrow soc	-47.46964171	-16.0	3.5
v_d12_04	opt \rightarrow rel \rightarrow soc	-47.46801790	-16.0	3.5
v_d12_01d	nsp \rightarrow rel \rightarrow opt \rightarrow rel \rightarrow opt \rightarrow soc	-47.46441552	-16.0	4.4

Tab. 5-12 Results for $SmCo_5$, when optimizing and / or relaxing. $(a; c) = (0.500; 0.396)$; k –mesh $G - 5 \times 5 \times 7$.

$SmCo_5$	Steps	SOC+U [001] (conv) (eV)	MAE (MJ/m ³)	MAG [μ_B /fu]
v_e1_02	NSP \rightarrow SRC \rightarrow SOC \rightarrow +U	-46.71578180	462.9	4.5
v_e1_05	NSP \rightarrow SRC \rightarrow SOC+U	-46.41046305	-107.3	3.8
v_e1_08	NSP \rightarrow SOC \rightarrow +U	-46.71578238	462.3	4.5
v_e1_11	NSP \rightarrow (SOC+U)	-43.14110257	-6616.8	7.4

Tab. 5-13 Results for $SmCo_5$, including +U. $(a; c) = (0.500; 0.396)$; k –mesh $G - 5 \times 5 \times 7$; $(U; J)_{Sm-4f} = (4.45; 0.0)$ eV.

The difference in MAE values, while considering $Sm - 4f$ –electrons as core or valence was also investigated. In each setup, comparison has been made for calculations with and without +U, as shown in [Tab.5-14](#) and [Tab. 5-15](#), where it is clear that freezing the $4f$ –electrons in the core region results in severe underestimation of MAE, even though it seemingly enhances total magnetization. A closer inspection of magnetic moments though shows that in this case the $4f$ –spin and orbital moments are underestimated, but nearly equal in value, and the total moment is hence nearly the sum of $Co -$ moments. As an overall picture, this doesn't seem physically incorrect, with the experimental total $Sm -$ moment being $+0.4 \mu_B$ [[1979 Givord](#)], but this agreement is coincidental. For a closer inspection, the contributions of individual electronic shells to total magnetization are depicted in [Fig. 5-6 \(left\)](#). It is evident that the large negative $Sm -$ spin moment overpowers the smaller, positive $Sm -$ orbital moment, reducing total magnetization.

$SmCo_5$	Sm-4f-electrons	SOC (conv) [001] (eV)	MAE [MJ/m ³]	MAG [μ_B /fu]
h_306	Valence	-473538.69008250	17.8	3.8
h_406	Core	-473434.70439563	1.8	10.4

Tab. 5-14 Results for $SmCo_5$, after the convergence of SOC, when $4f$ –electrons are valence or in core. $(a; c) = (0.5002; 0.3961)$; k –mesh $16 \times 16 \times 18$. $U_{eff} = 4.4$ eV.

$SmCo_5$	Sm-4f-electrons	+U (conv) [001] (eV)	MAE(100) [MJ/m ³]	MAG [μ_B /fu]
h_306	Valence	-473537.49370380	39.0	3.9
h_406	Core	-473434.66033983	1.4	10.4

Tab. 5-15 Results for $SmCo_5$, after the convergence of +U, when $4f$ –electrons are valence or in core.

The calculation including $+U$ and with $4f$ –electrons as valence (Tab. 5-15) provided the closest MAE to experimental value with WIEN2k, despite overestimating it, and hence the effect of varying the c/a ratio on MAE in $SmCo_5$ is considered based on this approach and shown in Fig. 5-6 (right). From the smooth trend in energy, it is evident that the error in MAE calculation is the same in all cases, and hence the general trend of MAE is correct. It is evident that decreasing c/a in $SmCo_5$ up to 1% increases its MAE slightly (just over 1%). In the considered interval of -2% to +2% of energy minimum, total magnetization decreases monotonously, but very slightly, i.e. less than 1% decrease for 5% increase in c/a (not shown).

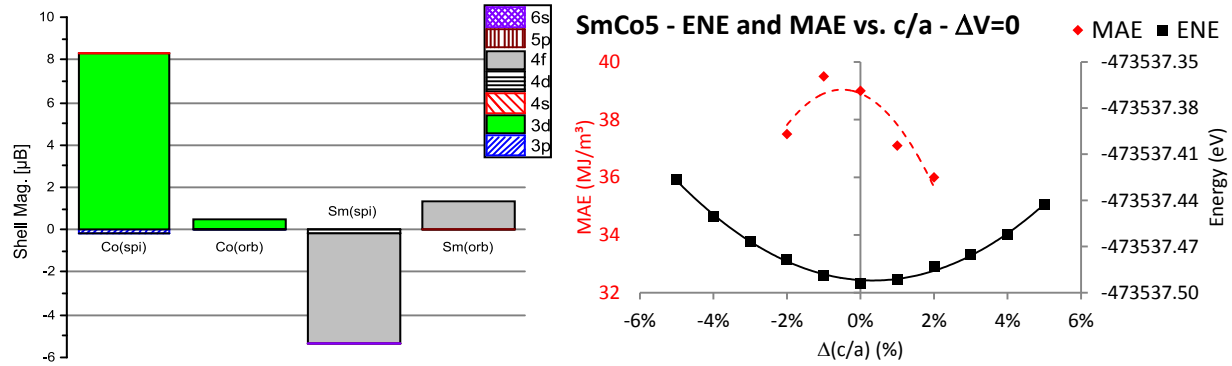


Fig. 5-6 Contribution of different electronic orbitals to total magnetization in $SmCo_5$ (left). Change in energy and MAE with variation of c/a ratio for $SmCo_5$ with a constant volume (right).

After many attempts it was found again that $(U; J)$, should be included from the start and $(U; J) = (5.4; 0.7) eV$ was found to deliver the best results, when (NSP+ U) \rightarrow (SOC+ U) is used (Tab. 5-16). Considering the fact that no optimizations or relaxations were applied with this procedure, the value for MAE of $SmCo_5$ is calculated rather accurately, compared with experimental MAE values ranging from 24 to 29 MJ/m^3 [1976 Ermolenko, 2003a Larson]; something that has been a challenge for many years, as reflected in literature. But one also sees that total magnetization is underestimated. The magnetic moments of Co –atoms are not problematic. The main issue is the wrong allocation of the amount of magnetization to spin or orbital portion of Sm . The spin moment of Sm is calculated to be larger than $4 \mu_B$ in value (and negative in sign due to antiferromagnetic coupling to Co –spin moments), and its orbital moment less than $2 \mu_B$ (and positive). This results in a total negative moment for Sm , due to negative M_{Sm} which is not the experimentally observed behavior. The sum of M_{Co} is calculated accurately, and if one adds the theoretical value obtained from Van Vleck and Frank method ($\mu_{eff-Sm} = 0.85 \mu_B$) [1932 Frank] to the total Co plus interstitial moment, one obtains a good agreement with experimental values. Based on the good result obtained with this approach, optimization and relaxation were carried out, while the same steps and $(U; J)$ values were used. Alone optimization and relaxation, which slightly change the lattice parameters and atomic positions, have a clear impact on MAE. This confirms the conclusion also drawn for YCo_5 , that changes in lattice parameters influence MAE considerably.

$SmCo_5$	+U [001] (con) (eV)	MAE (MJ/m ³)	M_S (cal.) [μ_B/fu]	M_{Co} (cal.) + M_{Sm} (a)
Not optim.	-46.63451710	33.8	4.25	8.86
Optim.	-46.63200555	25.4	4.14	8.78

Tab. 5-16 Results for $SmCo_5$, when starting with NSP+U, optim., relax. (a) = [1932 Frank]. (a; c) = (0.500; 0.3961); k –mesh $G - 5 \times 5 \times 7$; (U; J)_{Sm-4f} = (5.2; 0.7); (NSP+U) → (SOC+U) → (SOC+U-OPT) → (SOC+U-REL).

Following the same approach, the substitution of 20% of Co atoms by Fe and Cu were studied for both $T(2c)$ and $T(3g)$. The results for the lowest energy configuration after each substitution are given in [Tab. 5-17](#) and compared to $SmCo_5$. For Fe –substitution, lower energy is obtained for the $T(3g)$, in agreement with [1976 Deportes], but for Cu , the $T(2c)$ site has a lower energy, as opposed to [2012 Cheng]. The decrease in MAE of $SmCo_5$ with Fe , Cu agrees qualitatively with the results of Larson et al., Saito et al. and Yin et al. [2004 Larson, 2014 Saito, 2013 Yin]. The first group calculates a MAE of $30 MJ/m^3$ for $SmCo_4Fe$ and $42 MJ/m^3$ for $SmCo_5$.

$SmCo_4Fe$ shows a large magnetization and only 25% less MAE than $SmCo_5$. It is unlikely that MAE of $SmCo_4Fe$ would decrease with temperature much stronger than that of $SmCo_5$ (which has MAE= $17 MJ/m^3$ at room temperature), indicating that MAE of $SmCo_4Fe$ will remain large at room temperature. Considering the fact that 20% of the strategic Co-metal is replaced by readily available Fe, this phase has the potential to be used as a permanent magnet material.

Phase	Energy [eV]	M_S [$\mu_B/f.u.$]	MAG pro Co [μ_B]	MAE [MJ/m^3]
$SmCo_5$ (cal.)	-46.63451710	8.9	1.72	33.8
$SmCo_5$ (opt.)	-46.63200555	8.8	1.70	25.4
$SmCo_5$ (exp.)		8.2 ... 8.9 (a)		24 ... 29 (a, b)
$SmCo_4Fe$ (3g)	-47.87896284	9.1	1.59	19.2
$SmCo_4Cu$ (2c)	-43.22908059	6.8	1.61	8.16

Tab. 5-17 Results for $SmCo_5$, $SmCo_4Fe$ and $SmCo_4Cu$. (a) = [2003a Larson], (b) = [1976 Ermolenko].

As described for YCo_5 , the weighted difference of DOS is a useful tool for material design. But studying DOS plots also provides scientifically important insights. [Figure 5-7](#) shows 6 graphs, produced from WIEN2k calculations. In the graphs on the left side (parts A, C, E), the $4f$ –electrons are valence electrons and in the graphs on the right (parts B, D, F), they are core electrons. The upper two graphs (parts A & B) show DOS at convergence of the SRC calculation, the middle two (parts C & D) at convergence of the SOC calculation (no U_{eff}) and the lower two (parts E & F) after SOC+U. Black lines show Co –spin-up (majority for Co), blue lines Sm –spin-up, green lines Co –spin-down and red lines Sm –spin-down (majority for Sm). It is evident that after SOC, the valence $4f$ –electrons are calculated to be at E_F , which is physically incorrect and results in wrong MAE values. In all graphs $E_F = 0$.

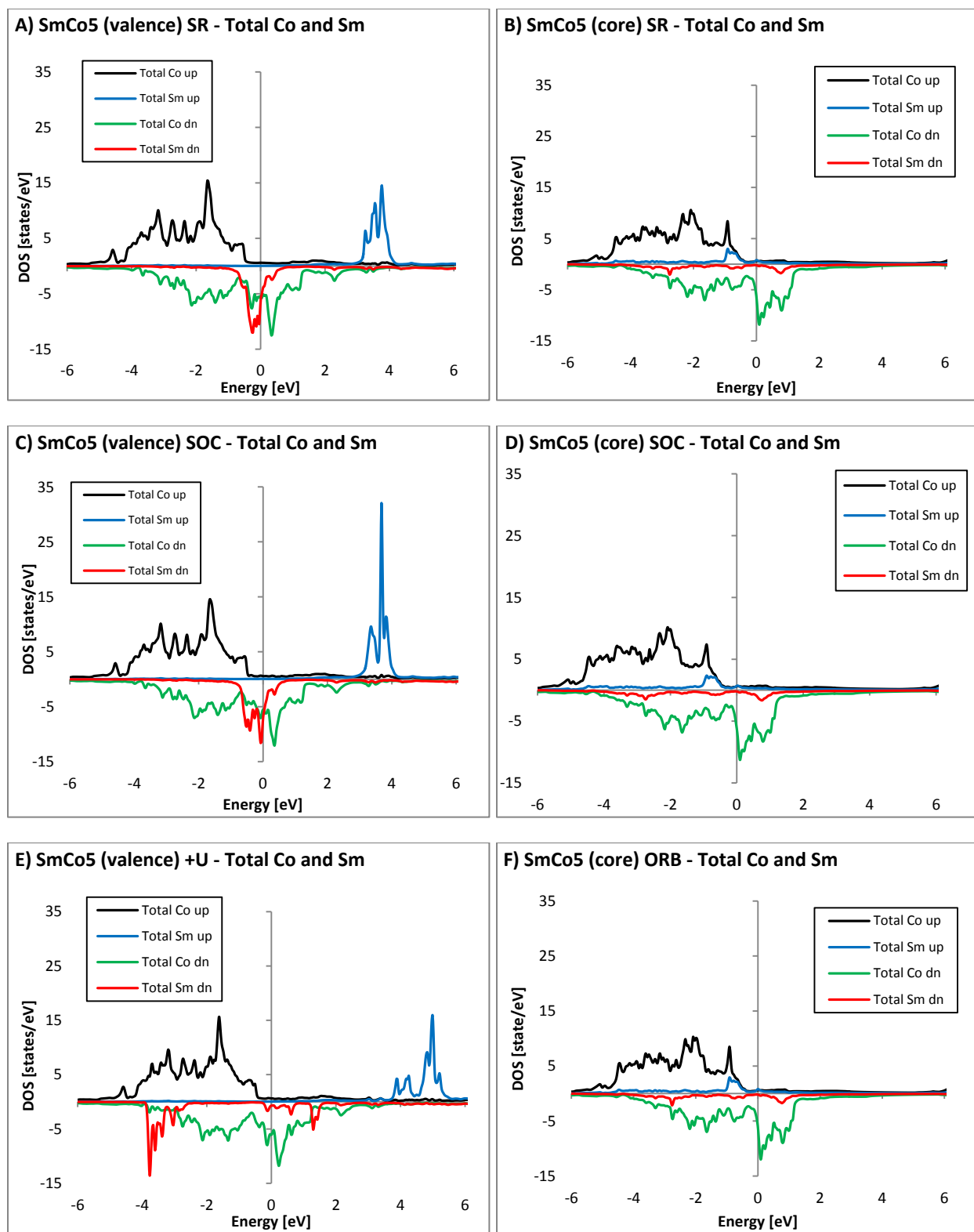


Fig. 5-7 Spin resolved density of state of *Co* –spin-up (up), *Co* –spin-down (dn), *Sm* –spin-up and *Sm* –spin-down of *SmCo*₅, at the convergence of SRC (A and B), at the convergence of SOC (C and D) and at the convergence of +*U* (E and F). The 4*f* –electrons are in parts A, C and E valence electrons and in parts B, D and F core electrons.

Including $U_{eff} = 4.4 \text{ eV}$ in the next step pushes these electrons to around -4 eV and produces a gap between two peaks of Sm –spin-down. Such an effect is absent in the graphs on the right side, as in these calculations U_{eff} works on $4f$ –electrons, which are put in the core region and are hence not close to E_F . Interestingly, the Sm –spin-up peaks are calculated to be below E_F , stemming from the $4d$ –electrons. The inclusion of U_{eff} lowers the density of unoccupied states and pushes the spin-down peaks to lower energies in case of valence electrons. The difference in the area below the curve of total spin-up and spin-down DOS plots is a measure for total magnetization. For the spin-up case, U_{eff} doesn't change the core electron calculation much, while the valence electron calculation shows lower densities in unoccupied states and larger peaks in occupied states. For valence electrons the SOC does not influence the occupied states, but the density of $4f$ –peak in the unoccupied region spikes up.

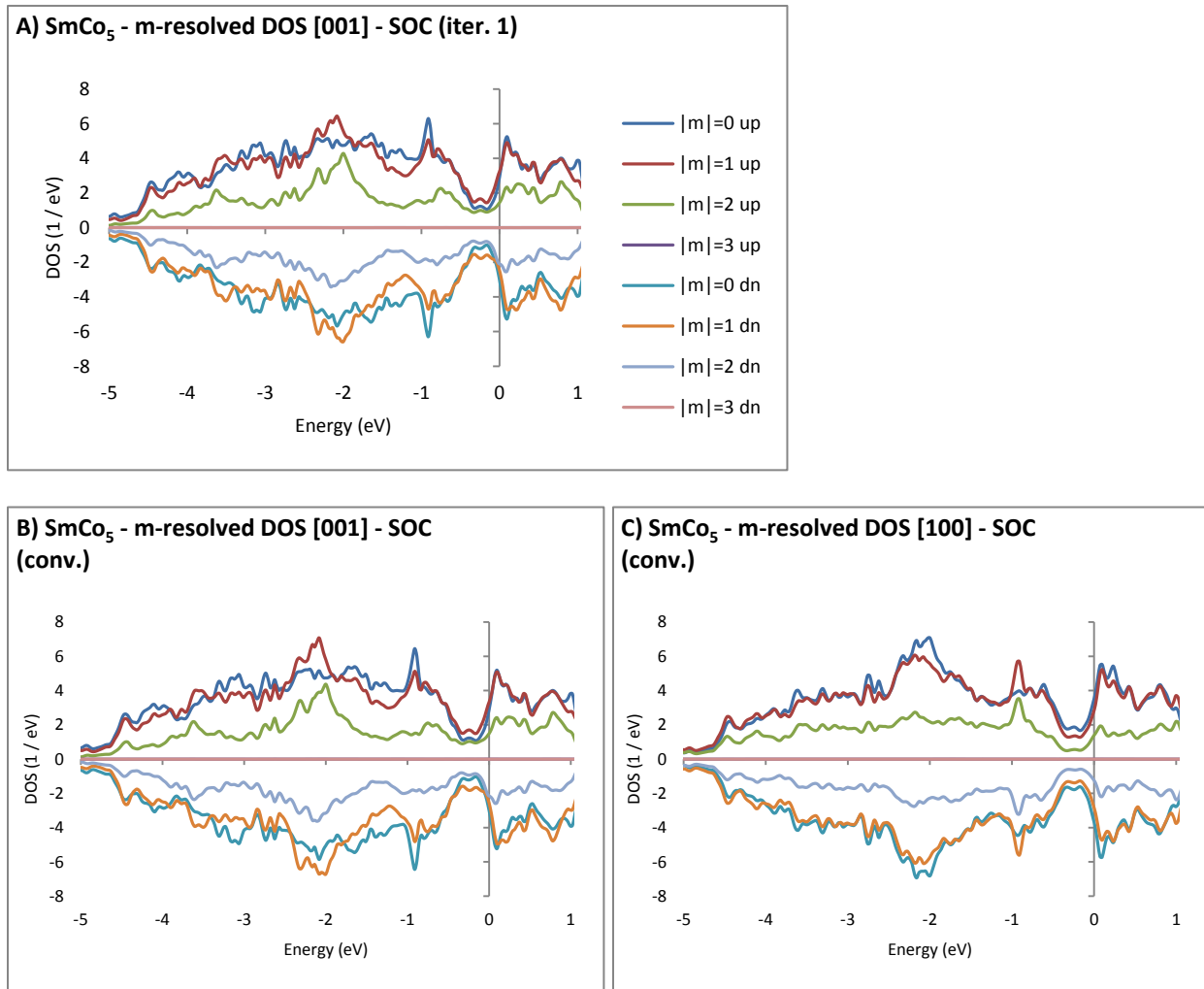


Fig. 5-8 Density of state of $SmCo_5$, resolved for different values of the magnetic quantum number m , after the first iteration of SOC in [001] direction (A), and after the convergence of SOC in [001] direction (B) and [100] direction (C). The legend in parts (B) and (C) are the same as in part (A).

Another way of studying the influence of the SOC on anisotropy is to consider the changes in DOS per electronic shell magnetization (m –resolved DOS). This is the DOS of all electrons that have the same value of magnetic quantum number m . As this division is a relativistic effect, it can only come to be after the introduction of the SOC, and hence cannot be calculated in the SRC phase. For this reason the comparison is made between the first iteration of SOC and its convergence in [001] direction (Fig. 5-8). After the first iteration with SOC included, the energy values are still similar to the convergence of SRC. One notices the changes in the peaks of $|m| = 1$ curves for both spin up and down around -2 eV.

But a more educating comparison is when one considers the m –resolved DOS after the convergence of SOC in [001] and in [100] directions, since anisotropy energy is determined by this difference. From Fig. 5-8(B&C) it is seen that for $|m| = 2$ both spin up and down electrons occupy more states around -2 eV in [001] direction. But their lower peaks, compared to other m –values, indicate that their contribution to the magnetization is less pronounced, which explains the underestimated values of spin and orbital moments in the calculations. On the other hand, one sees that in [100] direction, the electrons with $|m| = 0$ occupy more states, which is why this direction has a higher energy and is a harder axis.

As ($U;J$) values have been treated as variables, it is interesting to see how MAE changes with their variation. To this end, using WIEN2k, U_{eff} is varied and calculated energy and MAE values are plotted for valence and core $4f$ –electrons (Fig. 5-9). Even though the calculated values for MAE are overestimated, the error is present in all calculations in the same manner. Hence for more accurate calculations, the variation of MAE due to changes in U_{eff} –value must be similar to the trend shown in Fig. 5-9. One sees again the continuous increase in MAE with increasing value of $+U$ for valence $4f$ –electrons, while MAE remains mainly independent of $+U$, when $4f$ –electrons are in core.

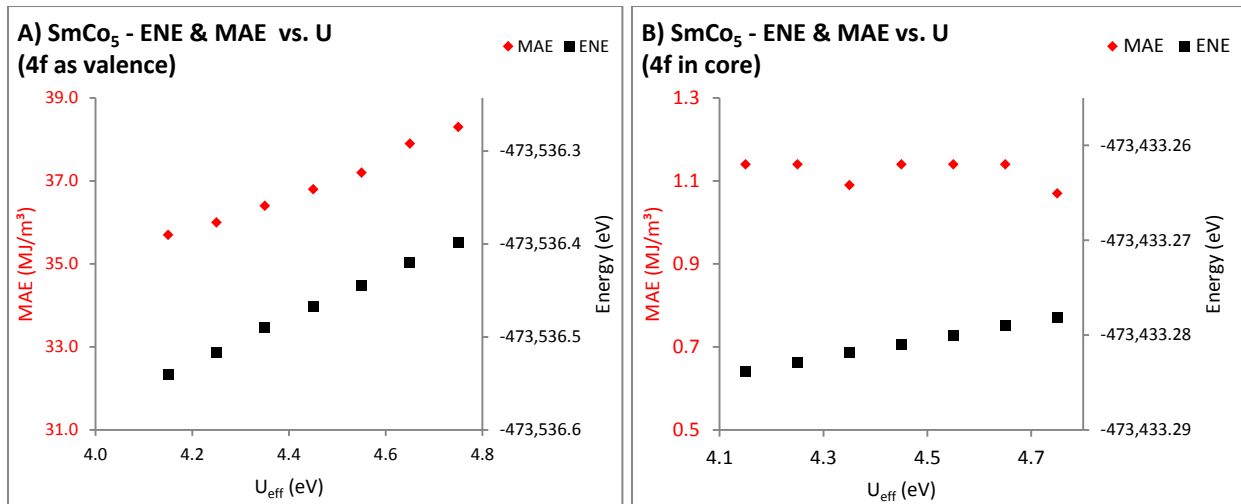


Fig. 5-9 Changes in energy and MAE of $SmCo_5$ with variation of U_{eff} , when $4f$ –electrons are valence electrons (A) and when they are core electrons (B).

To consider the influence of the $(U;J)$ –potentials from another point of view, energy, MAE and magnetization values for $SmCo_5$ are considered in [Tab. 5-18](#), once at the convergence of the SOC-calculation (without $(U;J)$) and once after the first iteration of SOC+ $(U;J)$ calculation. The different setups have different initial values for magnetic moments. It is evident that already in the first iteration, the $(U;J)$ potentials influence the electronic structure very strongly, though it initially decreases energy in value and results in less stable states, which is seen from unphysically large MAE values.

$SmCo_5$ - SOC	$m(Co; Sm)$	SOC [001] (con) (eV)	MAE (100)	MAE (210)	MAG [μ B/fu]
v_f7_04b	1.6; -1.6	-47.74163749	-15.7	-16.4	3.8
v_f7_04c	1.6; -2.0	-47.74163785	-15.7	-16.4	3.8
v_f7_04d	3.2; -0.9	-47.73705802	-7.0	-24.9	4.1
v_f7_04f	3.2; -2.0	-47.73406897	-29.8	-30.5	4.0
$SmCo_5$ - (+U)	$m(Co; Sm)$	+U [001] (1 it) (eV)	MAE (100)	MAE (210)	MAG [μ B/fu]
v_f7_04b	1.6; -1.6	-45.31379817	-456.8	-469.1	4.1
v_f7_04c	1.6; -2.0	-45.31379008	-456.9	-469.0	4.1
v_f7_04d	3.2; -0.9	-45.43187850	106.5	-248.3	6.0
v_f7_04f	3.2; -2.0	-45.51123153	-88.2	-100.5	5.1

Tab. 5-18 Energy, MAE and magnetization values for $SmCo_5$. $(a; c) = (0.5002; 0.3961)$; ISMEAR = -5 ; $(U; J)_{Sm-4f} = (6.8; 0.7)$. Steps: (NSP+SOC) \rightarrow (+U).

Using VESTA it is possible to visualize the role of symmetries and the impact of substitution based on the electronic densities of $hcp - Co$, Co_6 , YCo_5 and $SmCo_5$ on different planes. Interesting are the planes perpendicular to [001] at $z = 1/2$ ([Fig. 5-10](#)), which is the plane of $Co(3g)$ atoms, the plane at $z = 0$ ([Fig. 5-11](#)), which is the plane of $Co(2c)$ and R , and the plane perpendicular to [110] at $x = y = 1$ ([Fig. 5-12](#)). There is no considerable change at $Co(3g)$ plane going from Co_5 to Co_6 ; the difference between Co_6 and YCo_5 is visible but small. The differences for the $z = 0$ plane however are clear. In YCo_5 , Y , and in Co_6 , the sixth Co –atoms are located at the corners, and even though the Co –atoms have more valence electrons (darker corners of second graph from left in [Fig. 5-11](#)), the Y –atoms change the electronic landscape much more differently for the $z = 0$ plane, as compared to the $x = y = 1$ plane. Meanwhile, the difference caused by the sixth Co –atom is less pronounced and the change in MAE is smaller. This conclusion is in accordance with neutron studies [[1976 Deportes](#)].

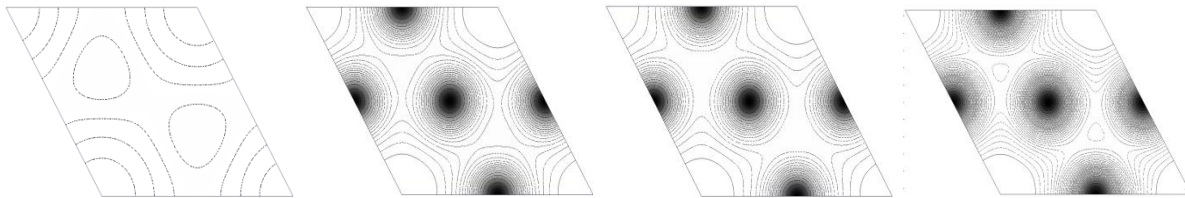


Fig. 5-10 Electronic density of $hcp - Co$, Co_6 , YCo_5 and $SmCo_5$ from left, shown perpendicular to [001] at $z = 1/2$. In the XT_5 phases, all atoms are $Co(3g)$.

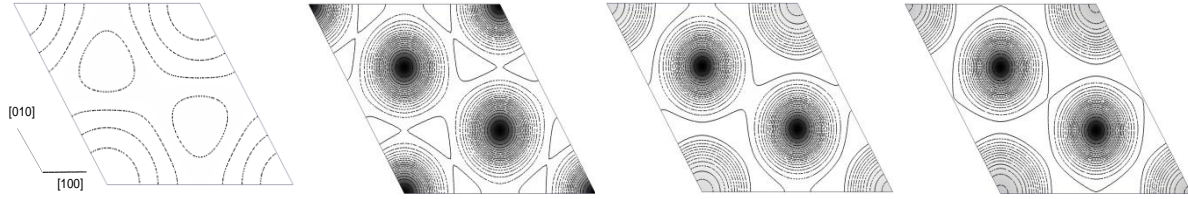


Fig. 5-11 Electronic density of $hcp - Co$, Co_6 , YCo_5 and $SmCo_5$ from left, shown perpendicular to $[001]$ at $z = 0$. In the XT_5 phases, the two atoms in the center are $Co(2c)$, the atoms in corners are Co , Y and Sm , from left to right.

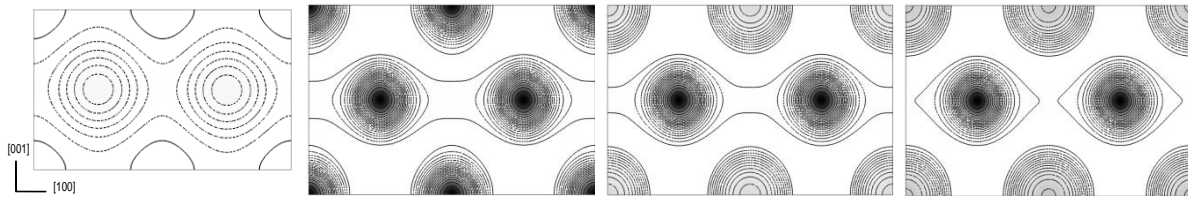


Fig. 5-12 Electronic density of $hcp - Co$, Co_6 , YCo_5 and $SmCo_5$ from left, shown perpendicular to $[010]$ at $x = y = 1$. In XT_5 phases, the two atoms in the center are $Co(3g)$, the rows of atoms on edges are Co , Y and Sm .

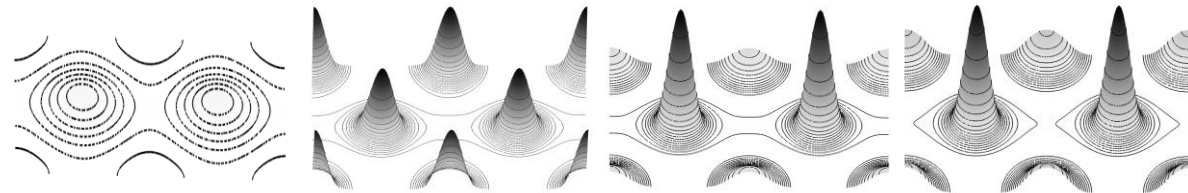


Fig. 5-13 Graphs of Fig. 5-12 from bird eye view. Shows the differences of $Co -$ and $R -$ electron density.

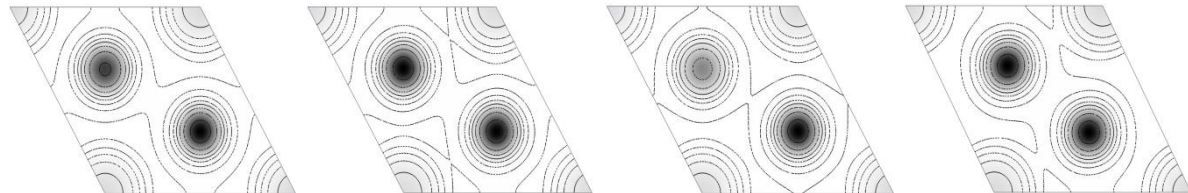


Fig. 5-14 Electronic density of $YCo_4Fe(2c)$, $YCo_4Fe(3g)$, $YCo_4Cu(2c)$ and $YCo_4Cu(3g)$ at $z = 0$ of (001) .

Compared to $bcc - Fe$ and $fcc - Ni$, $hcp - Co$ exhibits an appreciably larger MAE (ten times larger than $bcc - Fe$). This is seen in the first graphs from left in [Fig. 5-11](#) and [Fig. 5-12](#), with the electron densities differing considerably in these directions. The changes in electronic density, of course, do not account for all the contribution to MAE. That $hcp - Co$ does not have a layered structure is seen from the first graphs from left in [Fig. 5-10](#) and [Fig. 5-11](#), where the electronic structure at $z = 0$ and $z = 1/2$ are the same. The bird-eye view of graphs of [Fig. 5-12](#) are shown in [Fig. 5-13](#) to clarify the differences between the electronic densities of Co (high peaks) and R . [Figure 5-14](#) compares the $z = 0$ plane of substituted phases based on YCo_5 . When Fe or Cu is at $T(2c)$, the difference in number of valence electrons makes itself visible through the intensity of darkness of the atoms in the center. When Fe or Cu is at $T(3g)$, one sees clearly the impact on the lines around the two $Co(2c)$ atoms.

Results for $PrCo_5$: The phase $PrCo_5$ has a non-collinear magnetic structure at 0 K, and so it is interesting to see whether the simple method used for $SmCo_5$ would be able to estimate MAE of $PrCo_5$ correctly, but it proved to be quite challenging. The calculated MAE value is in the correct order of magnitude and is negative, but its absolute value is overestimated (Tab. 5-19). The angle of the Pr spin moment complicates its coupling with the different Co layers. Starting the calculations as non-collinear or separating the SRC and SOC steps did not improve the results (Tab. 5-20). To show the impact of using different orders of calculation steps, Tab. 5-20 lists the energy, MAE and magnetization values for $4f$ –electrons as valence and core, calculated collinearly with WIEN2k. The values for MAE, when the $4f$ –electrons are in core, are vanishingly small, indicating that in a collinear $PrCo_5$ structure, the contribution of $Pr - d$ –electrons to MAE cancels out that of $Co - 3d$ –electrons.

$PrCo_5$	SOC[001] (con) (eV)	MAE (100)	MAE (210)	MAG [$\mu B/fu$]
v_d3_03	-43.38346672	-2.96	-3.01	6.58

Tab. 5-19 Results for $PrCo_5$, starting with NSP but without including $+U$. $(a; c) = (0.5025; 0.3943)$; k –mesh $G - 5 \times 5 \times 7$; steps: (NSP) \rightarrow (SRC) \rightarrow (SOC).

$PrCo_5$ - SOC	Steps	f-elect.	SOC (conv) [001] (eV)	MAE [MJ/m^3]	MAG [$\mu B/fu$]
w_b_201	SRC \rightarrow SOC \rightarrow U	Valence	-441102.30676957	0.60	6.85
w_b_202	SRC \rightarrow SOC \rightarrow U	Core	-441087.16682061	0.07	6.94
$PrCo_5$ - (+U)	Steps	f-elect.	+U (conv) [001] (eV)	MAE [MJ/m^3]	MAG [$\mu B/fu$]
w_b_201	SRC \rightarrow SOC \rightarrow U	Valence	-441101.22433370	-120.9	6.75
w_b_202	SRC \rightarrow SOC \rightarrow U	Core	-441087.11455269	0.07	6.95
w_b_203	SOC \rightarrow U	Valence	-441101.28753217	-3.3	6.75
w_b_204	SOC \rightarrow U	Core	-441087.11451568	-0.01	6.95
w_b_205	(SOC+U)	Valence	-441101.28773979	353.8	6.84
w_b_206	(SOC+U)	Core	-441087.11459541	0.03	7.04

Tab. 5-20 Results for $PrCo_5$, when including $+U$ and using different steps. $(a; c) = (0.5025; 0.3943)$; k –mesh $16 \times 16 \times 18$; $U_{eff, Pr-4f} = 4.42$ eV; collinear calculations.

$PrCo_5$	Steps ; U_1 or U_2	SOC[001] (con) (eV)	MAE (MJ/m^3)	MAG [$\mu B/fu$]
v_e1_01	NSP+U \rightarrow SRC+U \rightarrow SOC+U ; U_1	-42.39568769	-15.4	6.67
v_e1_07	NSP+U \rightarrow SOC+U ; U_1	-42.40978013		7.01
v_e1_11	SRC+U \rightarrow SOC+U ; U_1	-42.46888966	-0.9	6.73
v_e1_15	SOC+U ; U_1	-42.39988698	34.8	7.65
v_e1_02	NSP+U \rightarrow SRC+U \rightarrow SOC+U ; U_2	-42.32732911	-52.8	6.25
v_e1_08	NSP+U \rightarrow SOC+U ; U_2	-42.32630265	-139.7	6.47
v_e1_12	SRC+U \rightarrow SOC+U ; U_2	-42.38262001	22.6	6.82
v_e1_16	SOC+U ; U_2	-42.45671853	-33.2	7.58

Tab. 5-21 Results for $PrCo_5$, when starting with different settings, but always with $+U$. $(a; c) = (0.5025; 0.3943)$; k –mesh $G - 5 \times 5 \times 7$; $(U, J)_{Pr-4f} = (6.8; 0.7) = U_1$, $(U, J)_{Pr-4f} = (6.0; 0.7) = U_2$.

It is again clear that the addition of $+U$ potentials is necessary. The effect of introducing the $+U$ potentials at different steps were drastic in both codes. After many tries it was concluded that for a good result, the first calculation step must be SRC+U and not NSP+U (Tab. 5-21). This allows calculating the magnetic spin densities and the potential based on them. The $+U$ helps correct the treatment of $4f$ –electrons.

After varying $(U; J)$ values, the best agreement was found for $(U; J)_{Pr-4f} = (6.6; 0.7)$. Curiously, even in the non-collinear calculation (WIEN2k), the calculated total magnetization is underestimated by at least 15% ($7.5 \mu_B$ at largest). It is clear that the quantum numbers of Pr –atom are estimated wrongly, resulting in an underestimation of the positive orbital moment, while a portion of magnetization is allocated to the spin moment, and since the spin moment is negative, it reduces total magnetization further. Based on the Hund’s Rules, in agreement with experimental results, Pr has an effective moment of roughly $3.5 \mu_B$ [1932 Frank]. Adding this value to the total Co and interstitial moments calculated by the codes, one obtains a good agreement for total magnetization (Tab. 5-22).

Phase	Energy [eV]	MAG [$\mu_B/f.u.$]	MAG pro Co [μ_B]	MAE [MJ/m^3]
$PrCo_5$ (V_e318)	-42.32326368	12.2	1.70	- 0.70
$PrCo_5$ (W_b203)	-441101.28753217	11.2	1.67	- 3.3
$PrCo_5$ (exp.)		9.2 ... 11 (a, b)		- 0.8 (b)

Tab. 5-22 Best results for $PrCo_5$. (a) = [1974 Narasimhan], (b) = [1982 Andoh]. $(a; c) = (0.5025; 0.3943)$; k –mesh $G - 5 \times 5 \times 7$. “V-E3” $(U; J) = (6.6; 0.7)$; (SRC+U) \rightarrow (SOC+U). “W-B2” $U_{eff} = 4.42$; SOC \rightarrow (+U).

5-3 Results for $R_2T_{14}B$ Compounds

Compounds of the type RT_5 do not form with $T = Fe$. On the other hand, the R_2Fe_{17} compounds have very low Curie Temperatures. It was later found that the ternary alloys of the type $R_2T_{14}B$ are stable and exhibit strong permanent magnetic properties [1991 Herbst]. These compounds have a tetragonal structure as shown in Fig. 5-15, left, drawn with VESTA, with initially 9 inequivalent atomic sites. Phases with $R = Y, Pr, Nd$ and Dy , and $T = Fe$ are investigated. The elements Pr, Dy and Y are chemically similar to Nd and form the same $2 - 14 - 1$ phase. These elements are examples for substitution with a light (Pr), a heavy R (Dy), and a non-magnetic metal (Y). The R –atoms occupy two distinct sites, namely $R(4f)$ and $R(4g)$, while T –atoms are split into $T(16k_1), T(16k_2), T(8j_1), T(8j_2), T(4c)$ and $T(4e)$, and B –atoms are $B(4c)$. All substituted phases have 50% of R –atoms replaced by another R .

A unit cell of $R_2T_{14}B$ consists of four formula units, has 68 atoms. This complex structure is a reason for the large anisotropy of these compounds. Using WIEN2k, test calculations for energy convergence were carried out on $Pr_2Fe_{14}B$ with 5, 20, 50, 100, 200, 500 and 1000 k –points (Fig. 5-15, right) and cutoffs of $RK_{max} = 6, 6.5, 7.0, 7.5, 8.0, 8.5$ and 9. It was concluded that calculations with at least 200 k –points and $RK_{max} = 8$ are reasonably fast, while meeting the required accuracy. In the subsequent PAW calculations a k –mesh of $3 \times 3 \times 2$ in the irreducible Brillouin Zone and an energy cutoff of 500 eV were used. It is noted that the formula unit of $R_2T_{14}B$ is larger than that of RT_5 in real space and smaller in the reciprocal space. 200 k –points in the reciprocal space of $R_2T_{14}B$ make a denser mesh than in RT_5 .

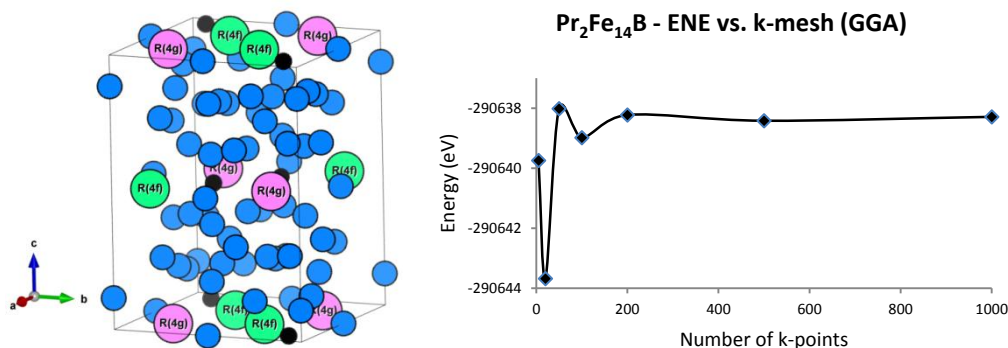


Fig. 5-15 Left: crystal structure of the $R_2T_{14}B$ phases ($Nd_2Fe_{14}B$ type, space group 136). $R(4g)$ sites are pink, $R(4f)$ are green, Fe sites are blue and B sites are black. Right: dependence of total free energy of $Pr_2T_{14}B$ on the number of k points used for the calculation (WIEN2k).

$Nd_2Fe_{14}B$ exhibits a spin reorientation and has a non-collinear magnetic structure at 4.2 K, but all other phases remain uniaxial down to 4.2 K [1991 Herbst] with the easy axis showing in [001] direction and the hard axis in [110]. To take into account the influence of SOC on symmetry of the spin polarized structures, in WIEN2k only the shared symmetries are used. This increases the number of inequivalent sites to 18. In VASP calculations all 68 sites are given as input and no symmetry is used.

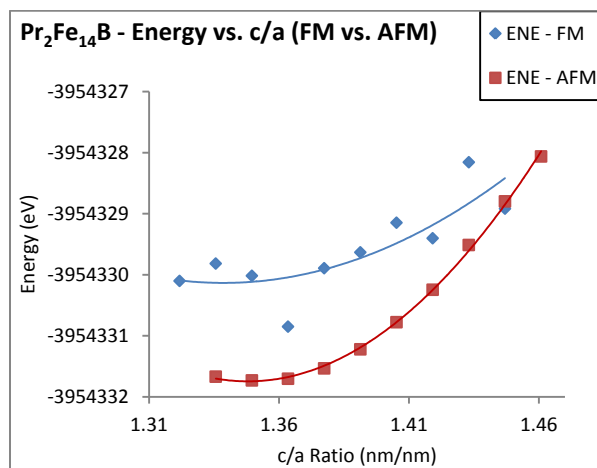


Fig. 5-16 Comparison of energy calculated for $Pr_2Fe_{14}B$, when the spin moments of Pr and Fe are antiferromagnetic (red squares) and ferromagnetic (blue diamonds). Lower energy indicates stable state.

While the coupling between R spin and T spin is experimentally well known as antiferromagnetic [1991 Herbst], from the point of view of first-principle methods, the correct coupling must be found through total free energy calculations. To this end, $Pr_2Fe_{14}B$ calculations were carried out with c/a ratio varied from 1.32 to 1.46 and the energy values are depicted in Fig. 5-16. It is evident that in all calculations close to energy minimum, the antiferromagnetic coupling results in a lower energy and is the

stable state. Individual calculations for $R = Nd$ and Dy also show a lower energy for antiferromagnetic coupling. In the initial substitution calculations, the energy values of substituted phases were lower than the non-substituted phase, hinting at the stability of 50% R –substitution. With larger number of k –points and a more accurate convergence criterion, energy of some substituted phases were higher than the non-substituted phases.

Results for $Y_2Fe_{14}B$: The starting point for investigating the $R_2Fe_{14}B$ compounds was with $R = Y$, as Y is non-magnetic and the SOC is a weak effect here. The first method tried was to start with the SRC calculation, then continue with the SOC (without $+U$). The initial calculations, both by LDA and PBE-GGA provided atomic magnetic moments for Fe , which were in good agreement with experimental results, but the value of MAE remained somewhat underestimated ($0.3 \text{ MJ}/m^3$). [Table 5.23](#) shows the atomic moments of individual sites, while the spin and orbital contributions of the three atoms to total magnetization are depicted in [Fig. 5-17, left](#). It is evident that most of the total magnetization stems from Fe –spin moment, while the sum of all Fe –orbital moments is less than $0.5 \mu_B$ in value, as is the total Y –spin moment. A notable feature seen is that the moment of Y arises mainly from the $4d$ –electrons.

$Y_2Fe_{14}B$	Fe (16k ₁)	Fe (16k ₂)	Fe (8j ₁)	Fe (8j ₂)	Fe (4c)	Fe (4e)	Fe-Avg.	R _{Spin} -Avg.
W (LDA)	2.26	2.21	2.13	2.71	2.34	2.01	2.28	-0.18
W (GGA)	2.34	2.27	2.25	2.72	2.07	2.42	2.35	-0.22
V (GGA)	2.42	2.33	2.35	2.77	2.50	2.11	2.42	-0.43
Exp. (a)	2.25	2.25	2.40	2.80	1.95	2.15	2.32	

Tab. 5-23 Total magnetic moments of Fe –sites, average Fe –moment and average Y –spin moment in $Y_2Fe_{14}B$. (a) = [[1985a Givord](#)]. (a; c) = (0.875; 1.202) W-LDA: k –mesh $6 \times 6 \times 4$; SRC \rightarrow SOC. W-GGA: k –mesh $8 \times 8 \times 6$; SRC \rightarrow SOC (1 it). V-GGA: (a; c) = (0.879; 1.22); k -mesh $G - 3 \times 3 \times 2$; $(U, J)_{Co-3d} = (1.2, 0.8)$.

In the following calculations, the first step was NSP, and then SRC and SOC were carried out, which increased MAE slightly, but not enough for agreement with experimental value. In VASP calculations, initially $(U; J)$ –potentials were applied to the $Y - 4f$ and separately to $Y - 4d$ electrons, though this did not result in any enhancement for the MAE value. In the next step, $(U; J) = (1.2; 0.8)$ were applied to $Fe - 3d$ –electrons and a better agreement with experimental value of MAE was found. The values of $(U; J)$ for $Fe - 3d$ –electrons are the same as for $Co - 3d$ –electrons of YCo_5 . [Table 5-24](#) shows the best results obtained by LAPW (LDA, GGA) and PAW (GGA).

	M_{Total} (Fe) (LAPW)	M_{Total} (Fe) (PAW)	M_{Total} (Fe) (Exp.)	MAE (LAPW)	MAE (PAW)	MAE (Exp.)
$Y_2Fe_{14}B$	31.9	33.9	32.5 (a)	0.62	0.65	0.77 (b)

Tab. 5-24 Sum of Fe –moments and MAE of $Y_2Fe_{14}B$ calculated with LAPW and PAW. (a) = [[1985a Givord](#)], (b) = [[1985 Hirosawa](#)]. LAPW: (a; c) = (0.875; 1.202); k –mesh $6 \times 6 \times 4$; LDA; SRC \rightarrow SOC. PAW: (a; c) = (0.879; 1.22); k –mesh $G - 3 \times 3 \times 2$; $(U, J)_{Co-3d} = (1.2, 0.8)$.

To consider the influence of strain on MAE, and based on the WIEN2k results, the c/a ratio was changed -8% to $+8\%$ of the initial values, with 1.5% steps, as shown in Fig. 5-17, right. The minimum of energy found corresponds to the lattice parameters from literature. The largest change per 1.5% change in c/a ratio is about 10% in MAE, which is a small change considering the small absolute value of MAE. The value of MAE hence remains nearly constant with c/a variation.

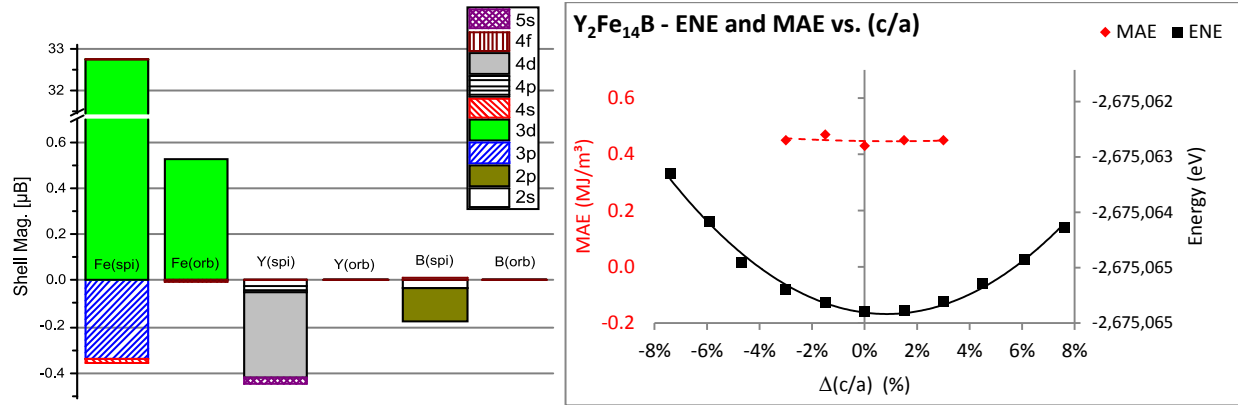


Fig. 5-17 Left: spin and orbital contribution of different electronic shells of each atom to total magnetization. Right: changes in energy and MAE of $Y_2Fe_{14}B$ due to variation of c/a ratio with a constant volume.

Results for $Pr_2Fe_{14}B$: The compound $Pr_2Fe_{14}B$ is very similar to $Nd_2Fe_{14}B$ while remaining uniaxial at low temperatures. It has a larger MAE, though a smaller saturation magnetization at room temperature. Starting with SRC calculations, then continuing with SOC provided severely underestimated MAE values both with LDA and PBE-GGA (both codes). On the other hand, calculating the orbital moment of Pr proved difficult. Fe and B –moments were calculated correctly. The Pr –spin moment is underestimated slightly by WIEN2k but strongly by VASP. The underestimation of Pr – orbital moments lowers both the total Pr –moment and total M_S . The latter error is small because of the large number of Fe –atoms compared to Pr . Table 5-25 lists the atomic magnetic moments of different Fe –sites, the average Fe –moment and the average spin moment of Pr –atoms.

$Pr_2Fe_{14}B$	$Fe(16k_1)$	$Fe(16k_2)$	$Fe(8j_1)$	$Fe(8j_2)$	$Fe(4c)$	$Fe(4e)$	Fe -Avg.	Pr_{Spin} -Avg.
W (LDA)	2.30	2.23	2.24	2.68	2.45	1.98	2.31	-2.03
W (GGA)	2.38	2.26	2.35	2.78	2.53	2.03	2.38	-0.46
V (GGA)	2.37	2.29	2.28	2.72	2.48	2.05	2.37	-0.82
Exp. (a)	2.07	2.15	2.01	2.37	1.77	2.18	2.11	

Tab. 5-25 Total and average Fe –moments and average Pr –spin moment. (a) = [1987 Fruchart]. W-LDA: $(a; c) = (0.880; 1.224)$; k –mesh $8 \times 8 \times 6$; LDA; SRC \rightarrow SOC. W-GGA: k –mesh $5 \times 5 \times 3$; SRC \rightarrow SOC \rightarrow SOC+U; $U_{eff} = 5.2$ eV. V-GGA: $(a; c) = (0.881; 1.227)$; k –mesh $G - 3 \times 3 \times 2$, $(U; J)_{Pr-Af} = (5.4, 0.7)$ eV.

As a single example, in [Tab. 5-26](#), and [Tab. 5-27](#), the calculated spin and orbital moments of each electronic shell for each atomic site are given as average, taken from an LDA calculation with LAPW. It is clear that the main contributions to magnetization stem from specific electronic shells. In particular, the spin moments of *Fe* stem from *d* –electrons and the spin and orbital moments of *Pr* stem from *f* –electrons, while the *Pr* – *d* –electrons have negligible orbital magnetization.

$Pr_2Fe_{14}B$	<i>Fe</i> (16 <i>k</i> ₁)	<i>Fe</i> (16 <i>k</i> ₂)	<i>Fe</i> (8 <i>j</i> ₁)	<i>Fe</i> (8 <i>j</i> ₂)	<i>Fe</i> (4 <i>c</i>)	<i>Fe</i> (4 <i>e</i>)	<i>Pr</i> (4 <i>f</i>)	<i>Pr</i> (4 <i>g</i>)
<i>s</i> –orbital	-0.002555	-0.00237	-0.002475	0.001415	0.00056	-0.00303	-0.012685	-0.01202
<i>p</i> –orbital	-0.021	-0.017255	-0.01935	-0.02024	-0.0155	-0.015865	-0.03021	-0.03587
<i>d</i> –orbital	2.290585	2.19541	2.225975	2.663585	2.411955	1.948875	-0.1669	-0.16893
<i>f</i> –orbital	0.0015	0.00096	0.00169	0.00068	0.00123	0.0008	-1.75679	-1.868315

Tab. 5-26 Spin magnetic moments (in μ_B) of individual electronic orbitals of individual atomic sites of $Pr_2Fe_{14}B$.

$Pr_2Fe_{14}B$	<i>Fe</i> (16 <i>k</i> ₁)	<i>Fe</i> (16 <i>k</i> ₂)	<i>Fe</i> (8 <i>j</i> ₁)	<i>Fe</i> (8 <i>j</i> ₂)	<i>Fe</i> (4 <i>c</i>)	<i>Fe</i> (4 <i>e</i>)	<i>Pr</i> (4 <i>f</i>)	<i>Pr</i> (4 <i>g</i>)
<i>p</i> –orbital	0.00018	0.00026	0.000005	-0.00007	0.00061	-0.000255	-0.00074	-0.001275
<i>d</i> –orbital	0.034035	0.05308	0.033735	0.037695	0.052265	0.050505	0.00522	0.004335
<i>f</i> –orbital	-0.00016	-0.00017	-0.00017	-0.00006	-0.00012	-0.00018	1.44155	1.649135

Tab. 5-27 Orbital magnetic moments (in μ_B) of individual electronic orbitals of individual atomic sites of $Pr_2Fe_{14}B$.

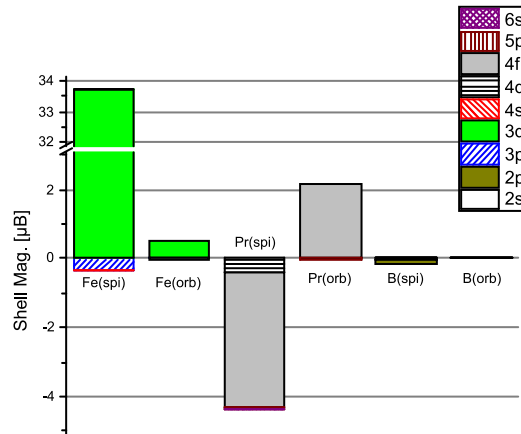


Fig. 5-18 Spin and orbital contribution of electronic shells of each atom to total magnetization in $Pr_2Fe_{14}B$.

[Figure 5-18](#) shows the sum of the contributions of magnetization from different electronic shells of all sites to the three elements in the structure. The *y* –axis is cut short between 2.5 and 32 μ_B . It is clear that *Fe* –spin moments produce the bulk of the magnetization, while *Fe* –orbital is quite small (contribution of all 56 *Fe* –atoms). There is a small negative spin moment originating from *Fe* – 3*p* –electrons. *Pr* –spin is anti-parallel to *Fe* –spin and most of it stems from *Pr* – 4*f* –orbital.

With the LAPW method, the best result for MAE was found by calculating the +*U* for one iteration after the convergence of NSP, SRC and SOC. Differing from the method of magnetic force theorem, where the SOC is calculated only for one iteration, here, due to the convergence of the SOC calculation, energy and charges are physically correct. For this one iteration, $U_{eff,Pr-4f} = 5.2 eV$ was used. Nonetheless, when

the same calculations were converged while including U_{eff} , it became evident that the first iteration of the $+U$ –calculation was not at energy minimum. For closer investigations, and using GGA+ U , the value of MAE was also calculated, when $4f$ –electrons were put in the core region, while the calculation steps and other parameters remained unchanged. In the PAW calculations, the $(U; J)$ –potentials were included from the beginning. The first step was NSP+ U , and after its convergence, SOC+ U was calculated to convergence. Similar to $SmCo_5$, $(U; J) = (5.4; 0.7)$ provided good results (Tab. 5-28).

Quantity	M_{Total} (Fe) (LAPW)	M_{Total} (Fe) (PAW)	M_{Total} (Fe) (Exp.)	MAE (LAPW)	MAE (PAW)	MAE (Exp.)
$Pr_2Fe_{14}B$	32.4	33.2	29.6 (a)	27.8	20.1	23.5 (b)

Tab. 5-28 Sum of Fe –moments and MAE for $Pr_2Fe_{14}B$ calculated with LAPW and PAW. (a) = [1985a Givord], (b) = [1985 Hiroswawa]. LAPW: (a; c) = (0.880; 1.224); k –mesh 8x8x6; LDA; Steps: SRC → SOC. PAW: (a; c) = (0.881; 1.227); k –mesh $G - 3 \times 3 \times 2$; $(U; J)_{Pr-4f} = (5.4, 0.7)eV$.

Based on the LDA and GGA+ U calculations with WIEN2k, the variation of energy with c/a ratio is shown in Fig. 5-19 for the interval of -6% to $+6\%$ for LDA and -5% to $+5\%$ for GGA+ U and with 1% steps. For both potentials the minimum of energy lies at smaller c/a ratios compared to literature lattice parameters and the trend of MAE, given only around energy minimum, is seen as a slight decrease.

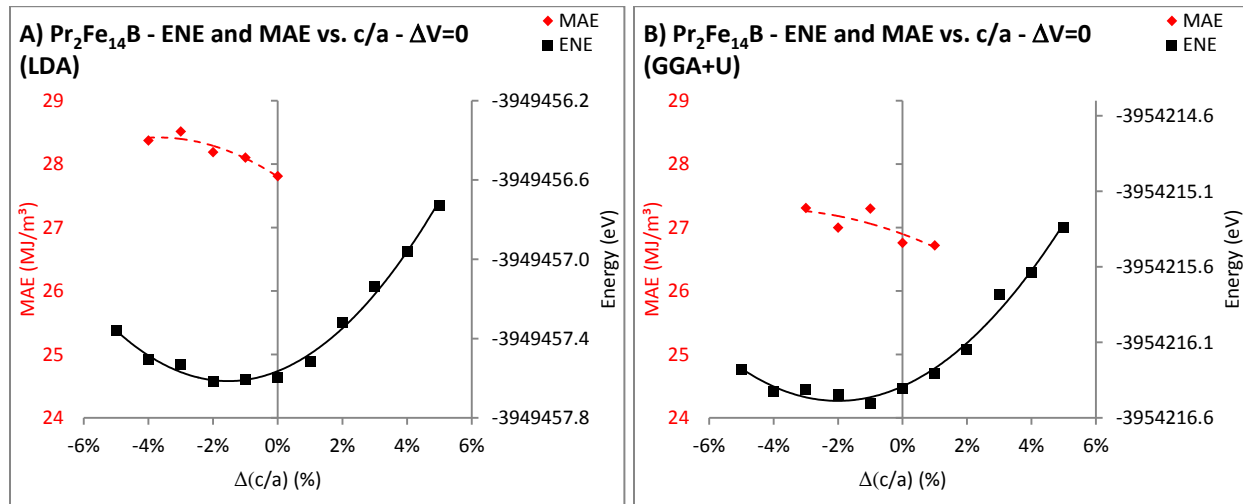


Fig. 5-19 Changes in energy and MAE due to variation of c/a ratio with a constant volume for $Pr_2Fe_{14}B$ with LDA (A) and GGA+ U (B) calculations.

With the LAPW calculations, the value of MAE changed considerably with U_{eff} after one iteration of $+U$ calculation (after SOC) from -0.3 to $27 MJ/m^3$, when the $4f$ –electrons were put in the core region. But by the convergence of $+U$ calculation, the MAE values was back at $-0.3 MJ/m^3$, showing that the U –potential does not influence MAE strongly, when the electrons it works on are in the core

region. To study the impact of the $+U_{eff}$ on energy, MAE and magnetization, in **Tab. 5-29** these values are compared after the convergence of SOC, after the first iteration of SOC+ U and after the convergence of SOC+ U , while the c/a ratio is varied. That considering $4f$ –electrons as core electrons delivers incorrect MAE values is visible again, but more interesting is the large change in MAE, after one iteration of SOC+ U . It is not surprising that after convergence of the SOC+ U calculation, the MAE values are very similar to the value after the convergence of SOC.

SOC	c/a	$d(c/a)$	SOC [001] (eV)	MAE [MJ/m ³]	MAG [μ B/fu]
w_e_311	1.3216	-5%	-3954216.3163806	-0.4	31.1
w_e_312	1.3355	-4%	-3954216.4641220	-0.3	31.2
w_e_313	1.3494	-3%	-3954216.4481823	-0.4	31.4
w_e_314	1.3634	-2%	-3954216.4804082	-0.4	31.5
w_e_315	1.3773	-1%	-3954216.5452727	-0.4	31.6
w_e_316	1.3912	0%	-3954216.4442298	-0.3	31.6
w_e_317	1.4051	+1%	-3954216.3424021	-0.3	31.6
w_e_318	1.4190	+2%	-3954216.1831690	-0.4	31.5
w_e_319	1.4329	+3%	-3954215.9268423	-0.4	31.5
w_e_320	1.4468	+4%	-3954215.6746653	-0.6	31.5
w_e_321	1.4607	+5%	-3954215.3732149	-0.6	31.5
+U(1 it)	c/a	$d(c/a)$	+U (1 it) [001] (eV)	MAE [MJ/m ³]	MAG [μ B/fu]
w_e_311	1.3216	-5%	-3954216.2778153	27.68	31.1
w_e_312	1.3355	-4%	-3954216.4257020	27.39	31.3
w_e_313	1.3494	-3%	-3954216.4098821	27.31	31.4
w_e_314	1.3634	-2%	-3954216.4425812	27.00	31.5
w_e_315	1.3773	-1%	-3954216.5074069	27.30	31.6
w_e_316	1.3912	0%	-3954216.4065390	26.76	31.6
w_e_317	1.4051	+1%	-3954216.3047752	26.72	31.6
w_e_318	1.4190	+2%	-3954216.1456352	26.70	31.5
w_e_319	1.4329	+3%	-3954215.7821325		31.5
w_e_320	1.4468	+4%	-3954215.6373247	27.81	31.5
w_e_321	1.4607	+5%	-3954215.3359265	27.65	31.5
+U(con)	c/a	$d(c/a)$	+U (con.) [001] (eV)	MAE [MJ/m ³]	MAG [μ B/fu]
w_e_311	1.3216	-5%	-3954216.2777245	-0.4	31.1
w_e_312	1.3355	-4%	-3954216.4256704	-0.3	31.3
w_e_313	1.3494	-3%	-3954216.4099463	-0.4	31.4
w_e_314	1.3634	-2%	-3954216.4425249	-0.3	31.5
w_e_315	1.3773	-1%	-3954216.5073812	-0.4	31.6
w_e_316	1.3912	0%	-3954216.4064721	-0.3	31.6
w_e_317	1.4051	+1%	-3954216.3047487	-0.3	31.6
w_e_318	1.4190	+2%	-3954216.1455974	-0.3	31.5
w_e_319	1.4329	+3%	-3954215.7818640	-0.4	31.5
w_e_320	1.4468	+4%	-3954215.6373077	-0.6	31.5
w_e_321	1.4607	+5%	-3954215.3359004	-0.6	31.5

Tab. 5-29 Change of energy, MAE and M_S with c/a ratio after SOC, first iteration of + U and convergence of + U in $Pr_2Fe_{14}B$. ($a; c$) = (0.880; 1.224); k –mesh $5 \times 5 \times 3$; $RK = 8$; $V = \text{const.}$; f –elect. = core, $U_{eff} = 5.2$ eV.

Results for $Nd_2Fe_{14}B$: The non-collinearity of this compound at 0 K introduces complications for the calculation of its MAE. $Nd_2Fe_{14}B$ is even more complex than $PrCo_5$, because the R –sites in $Nd_2Fe_{14}B$

do not have parallel spin moments. Not only they assume different angles θ compared to the easy axis in the z –direction at $z = 0$ and $z = 1/2$, but they also have different angles compared to the basal plane [1988 Cadogan]. The initial calculations with the LAPW method were carried out collinearly. Such a collinear calculation is expected to provide a larger MAE value, than a non-collinear one. The moments of Fe and B –sites are again described well, as seen in Tab. 5-30. For Nd , the correct coupling is found with PBE-GGA (negative spin moment), but the LDA calculations found a positive spin moment and a negative orbital moment. In both cases, the total moment is underestimated.

$Nd_2Fe_{14}B$	Fe (16k ₁)	Fe (16k ₂)	Fe (8j ₁)	Fe (8j ₂)	Fe (4c)	Fe (4e)	Fe-Avg.	R _{Spin} -Avg.
W (LDA)	2.35	2.28	2.29	2.72	2.48	2.04	2.36	1.98
W (GGA)	2.44	2.36	2.38	2.79	2.517	2.12	2.44	-3.28
V (GGA)	1.36	1.31	1.31	1.57	1.41	1.18	1.36	0.34
Exp. (a)	2.6	2.6	2.3	2.85	2.75	2.1	2.57	

Tab. 5-30 Total magnetic moments of Fe –sites, average Fe –moment and average Nd –spin moment in $Nd_2Fe_{14}B$. (a) = [1985a Givord]. “W” (a;c) = (0.880;1.220); k –mesh 6x6x4; SRC → SOC. “V” (a;c) = (0.881; 1.221); k –mesh 3x3x2; ($U;J$) _{$Nd-4f$} = (5.4; 0.7); SRC+ U → SOC+ U .

$Nd_2Fe_{14}B$	M_{Total} (Fe)	M_{Total} (Fe) (Exp.)	MAE (calc.)	MAE (Exp.)
W (CL) – LDA	30.9	34.8 (a)	13.9	11.2* (b)
W (CL) – GGA	34.2	34.8 (a)	3.6	11.2* (b)
V (NCL)	19.04	37.7 (c)	-14.5	-2.3 (d)

Tab. 5-31 Sum of Fe –moments and MAE of $Nd_2Fe_{14}B$. (a) = [1984 Sinnema] (powder), (b) = [1986 Grossinger] (powder, 50 K), (c) = [1986 Yamauchi], (d) = [1986 Yamada]. *Calculated from anisotropy field and M_5 . “W” (a;c)=(0.880;1.220); k -mesh 6x6x4; SRC → SOC. “V” (a;c)=(0.881;1.221); k -mesh 3x3x2; ($U;J$) _{$Nd-4f$} = (5.4; 0.7); SRC+ U → SOC+ U .

In collinear calculations, the total magnetization is comparable with neutron studies on powder samples, as such studies provide data only on the magnetic moments parallel to c –axis in $Nd_2Fe_{14}B$ [1987 Fruchart]. In reality the single phase of $Nd_2Fe_{14}B$ exhibits a negative MAE due to non-collinearity, but the collinear calculation should give a positive MAE. The PAW calculations were carried out with non-collinear magnetic couplings, which should in principle result in negative MAE values. This was indeed the case, though MAE was overestimated in value. Unlike the cases of $Y_2Fe_{14}B$ and $Pr_2Fe_{14}B$, here the best approach was found to start with the SRC calculation and not with the NSP calculation while including ($U;J$) –potentials, similar to $PrCo_5$. The reason is that energy values obtained from non-collinear and non spin-polarized calculations are too far from the correct minimum.

Based on the LDA calculations with WIEN2k, the dependence of MAE on changes of c/a ratio are shown in Fig. 5-20 for the interval of –5% to +5% with 1% steps. The effect of strain in $Nd_2Fe_{14}B$ shows an interesting feature, due to the non-collinear magnetic structure. When the strain is large enough and the c/a ratio is farther away from energy minimum, it is possible that MAE undergoes a sudden change. Non-collinearity comes to be due to a competition of CEF and anisotropy energies of Nd –atoms [1988 Cadogan]. Both energies change due to strain, but their changes do not follow the same trend.

Should the change result in considerable differences of these energies, it is possible that the magnetic structure experiences a change, which would result in an abrupt change of MAE, even though total energy changes, as before, with a smooth trend. This change in MAE is recognizable in [Fig. 5-20](#) between +1% and +2% of change in c/a ratio.

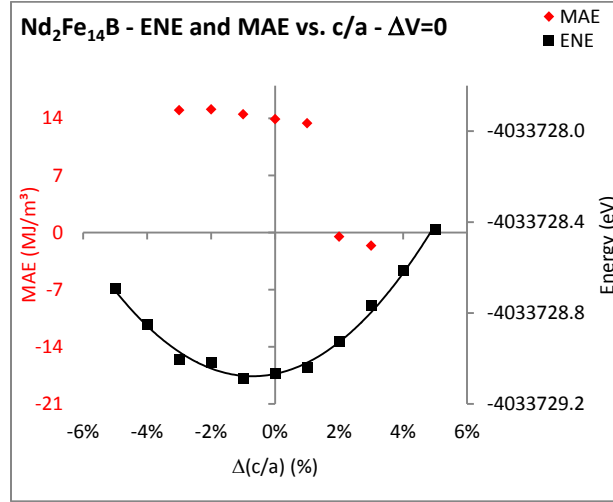


Fig. 5-20 Change of energy and MAE due to variation of c/a ratio with a constant volume in $Nd_2Fe_{14}B$ (LDA).

Results for $Dy_2Fe_{14}B$: In $Dy_2Fe_{14}B$, both spin and orbital moments of Dy are antiparallel to spin moments of Fe , and they have large absolute values. This means that the SOC and the $Fe - Dy$ coupling are strong. WIEN2k correctly calculates the coupling and the magnetic moments are calculated accurately, when PBE-GGA is used. As opposed, in VASP calculations with PBE-GGA+ U , the magnetic moments of Dy are underestimated largely ([Tab. 5-32](#)).

$Dy_2Fe_{14}B$	Fe (16 k_1)	Fe (16 k_2)	Fe (8 j_1)	Fe (8 j_2)	Fe (4c)	Fe (4e)	Fe-Avg.	R_{Spin} -Avg.
W (LDA)	2.24	2.20	2.10	2.70	2.30	2.01	2.26	-4.77
W (GGA)	2.34	2.26	2.24	2.73	2.38	2.07	2.34	-7.37
V (GGA)	2.39	2.30	2.34	2.73	2.07	2.44	2.39	-5.37
Exp. (a)	2.06	2.17	2.10	2.49	2.28	1.69	2.15	

Tab. 5-32 Total and average moments of Fe –sites, average Dy –spin moment in $Dy_2Fe_{14}B$. (a) = [[1987 Fruchart](#)]. W-LDA: $(a; c) = (0.876; 1.199)$; k –mesh $6 \times 6 \times 4$; SRC \rightarrow SOC. W-GGA: $(a; c) = (0.874; 1.183)$; k –mesh $5 \times 5 \times 3$; SOC=1 it. V: $(a; c) = (0.879; 1.199)$; k –mesh $3 \times 3 \times 2$; $(U, J)_{Dy-4f} = (5.4; 0.7)$.

The contributions of different electronic shells to magnetization in $Dy_2Fe_{14}B$ are shown in [Fig. 5-21](#). The ferromagnetic coupling of Dy –spin and Dy –orbital moments are visible, though the Dy –spin moment is overestimated. The best MAE value is obtained from GGA+ U of PAW calculations with $(U; J)_{Dy-4f} = (5.4; 0.7)$. Similar to $Pr_2Fe_{14}B$, for $Dy_2Fe_{14}B$ the first calculation step was NSP+ U , followed by and SOC+ U . [Table 5-33](#) shows the calculated total moments for Fe –sites and MAE values, and compares them to experimental results.

	M_{Total} (Fe) (LAPW)	M_{Total} (Fe) (PAW)	M_{Total} (Fe) (Exp.)	MAE (LAPW)	MAE (PAW)	MAE (exp.)
$Dy_2Fe_{14}B$	31.7	33.4	20.1 (a)	3.0	3.4	3.8 (b)

Tab. 5-33 Sum of Fe –moments, MAE in $Dy_2Fe_{14}B$ calculated with LAPW and PAW. (a) = [1987 Fruchart], (b) = [1985 Hirosawa]. ($a; c$) = (0.876; 1.199); LAPW: k –mesh $6 \times 6 \times 4$; SRC \rightarrow SOC. PAW: k –mesh $3 \times 3 \times 2$; $(U, J)_{Dy-4f}$ = (5.4; 0.7).

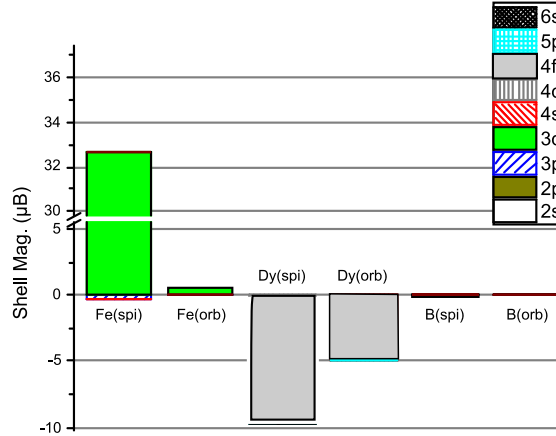


Fig. 5-21 Spin and orbital contribution of different electronic shells of atoms to total magnetization in $Dy_2Fe_{14}B$.

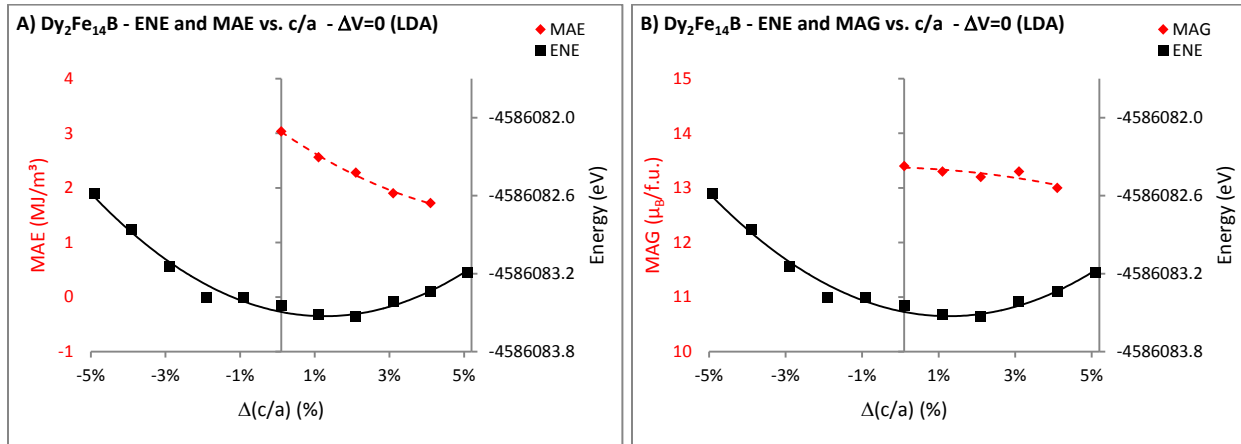


Fig. 5-22 Changes in energy and MAE (A) and energy and magnetization (B) of $Dy_2Fe_{14}B$ due to variation of c/a ratio with a constant volume.

When investigating the influence of strain, one sees that an increase in c/a ratio decreases MAE monotonously, but the changes in MAE are much larger for $Dy_2Fe_{14}B$ compared to $Pr_2Fe_{14}B$, up to 40% per 1% change of c/a (Fig. 5-22). Decreasing the c/a ratio up to 2% results in an increase of MAE. The total magnetization also shows a decreasing trend with increasing c/a , which is though very small.

Substitution Effects in $R_2Fe_{14}B$: One way of influencing intrinsic magnetic properties is through substitution of some of the R –atoms with a different R –element, as indicated for example by Huang et al. [1987 Huang] for $(NdPr)Fe_{14}B$. As R –atoms occupy two distinct sites, namely $R(4f)$ and $R(4g)$,

two cases for each compound are considered. The notation is so that $R(4f)$ is written first and $R(4g)$ second, i.e. $(R(4f)R(4g))Fe_{14}B$. This means that $(YDy)Fe_{14}B$ has its lattice parameters ($a; c$) taken from $Y_2Fe_{14}B$, while $(DyY)Fe_{14}B$ uses ($a; c$) from $Dy_2Fe_{14}B$. This also means that $(YNd)Fe_{14}B$ begins with the NSP+ U calculation, similar to $Y_2Fe_{14}B$, while as $(NdY)Fe_{14}B$ begins with SRC+ U , similar to $Nd_2Fe_{14}B$. Optimizing the structure and relaxing the atomic positions in the compounds were not undertaken, which is another difference between $(YDy)Fe_{14}B$ and $(DyY)Fe_{14}B$ phases. The calculated results for MAE of 50% R -substituted $(R(4f)R(4g))Fe_{14}B$ phases are tabulated in [Tab. 5-34](#). Also given are the change of MAE compared to the respective, non-substituted phase and the sum of Fe , B and interstitial magnetic moments. These calculations use GGA+ U of the PAW code.

Phase	MAE (cal) [MJ/m ³]	MAE (exp.) [MJ/m ³]	Diff. to $R_2Fe_{14}B$	$M_S^{Fe+B+INT}$ [μ_B]
$Y_2Fe_{14}B$	0.65	0.77 (a)		31.36
$(YPr)Fe_{14}B$	5.2		+700 %	31.48
$(YNd)Fe_{14}B$	0.5	-0.2* (b)	-23 %	32.28
$(YDy)Fe_{14}B$	1.5		+131 %	31.50
$Pr_2Fe_{14}B$	20.1	23.5 (a)		31.03
$(PrY)Fe_{14}B$	5.9		-71 %	31.27
$(PrNd)Fe_{14}B$	-2.8	-0.1* (c)	-114 %	32.54
$(PrDy)Fe_{14}B$	10.4		-48 %	30.63
$Nd_2Fe_{14}B$	-14.5	-2.3 (d)		18.86
$(NdY)Fe_{14}B$	-6.5	-0.2* (b)	+55 %	19.14
$(NdPr)Fe_{14}B$	-14.0	-0.1* (c)	+3 %	18.31
$Dy_2Fe_{14}B$	3.4	3.8 (a)		30.70
$(DyY)Fe_{14}B$	1.9		-44 %	31.12
$(DyPr)Fe_{14}B$	9.7		+185 %	30.95
$(DyNd)Fe_{14}B$	11.0		+479 %	32.03

Tab. 5-34 MAE, change in MAE due to substitution, difference between substituted and non-substituted phase, and calculated magnetization of $Fe + B$ -sites. * not single crystal. (a) = [\[1985 Hiroasawa\]](#), (b)= [\[1989 Zhang\]](#), (c) = [\[2016 Eslava\]](#), (d) = [\[1986 Yamauchi\]](#). Y -based: ($a; c$) = (0.879; 1.220); Pr -based ($a; c$) = (0.881; 1.227); Nd -based: ($a; c$) = (0.881; 1.221); Dy -based: ($a; c$) = (0.879; 1.199). k -mesh $G - 3 \times 3 \times 2$; ($U; J$) $_{R-4f}$ = (5.4; 0.7). In $Y_2Fe_{14}B$, (U, J) $_{Fe-3d}$ = (1.2; 0.8).

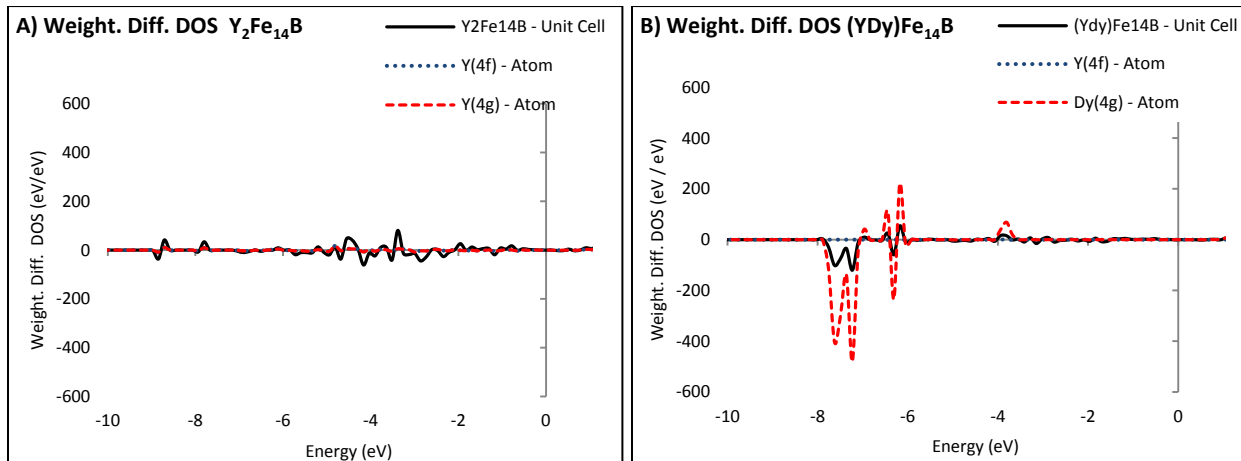
Any compound containing Y has a quite small MAE, with the largest being $5.9 \text{ MJ}/m^3$ and belonging to $(PrY)Fe_{14}B$. All $Nd_2Fe_{14}B$ based calculations have large, negative MAE values, hinting at the inaccuracy of this calculation method for describing this compound well. One see that $R(4g) = Pr$ and Dy increase MAE of $Y_2Fe_{14}B$, $R(4g) = Y$ and Dy strongly decrease MAE of $Pr_2Fe_{14}B$, and $R(4g) = Y$ decreases MAE of $Dy_2Fe_{14}B$, while Pr increases it.

The conclusion drawn by Herbst [\[1991 Herbst\]](#) and references therein that, while substituting, the R -atoms with smaller radii occupy $R(4f)$ sites is reflected in the results (configurations with lower total energy), with the exception of $(DyPr)Fe_{14}B$. Although, limited availability of experimental results for MAE of 50% R -substituted phases at low temperatures makes a direct comparison with experiment impossible. Among the investigated compounds, the phase $(PrY)Fe_{14}B$ is interesting, with a MAE of

nearly $6 \text{ MJ}/\text{m}^3$ at 0 K . The volume of this compound is slightly smaller than that of $\text{Y}_2\text{Fe}_{14}\text{B}$, while its magnetization is larger, due to addition of Pr . Another interesting phase is $(\text{PrDy})\text{Fe}_{14}\text{B}$. Based on the crystal field theory, one expects that Dy should increase MAE of $\text{Pr}_2\text{Fe}_{14}\text{B}$, because total angular momentum of Dy^{3+} is $J = 15/2$ as compared to $J = 4$ for Pr^{3+} . The total energy calculations though show a decrease in MAE with Dy substitution.

DOS Analysis of $\text{R}_2\text{Fe}_{14}\text{B}$: As pointed out in the discussion of RT_5 , DOS analysis helps achieving a better understanding of the influence of substitution on MAE. [Figure 5-23](#) shows the weighted difference of DOS between [110] and [001] axes of the phases $\text{Y}_2\text{Fe}_{14}\text{B}$, $(\text{YDy})\text{Fe}_{14}\text{B}$, $(\text{DyY})\text{Fe}_{14}\text{B}$ and $\text{Dy}_2\text{Fe}_{14}\text{B}$, as well as the contribution of $\text{R}(4f)$ and $\text{R}(4g)$ to MAE in the vicinity of Fermi Energy ($E_F = 0$), calculated based on [Eq. 5-2](#). From [Fig. 5-23\(A\)](#) it is evident that the Y –atoms have little or no considerable contribution to MAE in this interval [Fig. 5-23\(B, C\)](#). In comparison, Dy –atoms produce larger peaks. In all phases, the contribution of R –atoms to anisotropy originate from the same energy intervals. [Moze et al. \[1989 Moze\]](#) found a similar behavior in $\text{Pr}_2\text{Fe}_{14}\text{B}$. It is interesting to note that the contribution of Fe –atoms to MAE opposes the contribution of Dy –atoms in some intervals. This is seen for example in [Fig. 5-23\(B\)](#) and [Fig. 5-23 \(D\)](#) around -7 eV , where the contribution of Dy – atoms is strongly negative, while total MAE is not affected as strongly. This indicates that the influence of R –substitution on Fe –atoms and MAE originating from the Fe –atoms are not negligible.

When comparing [Fig. 5-23\(C\)](#) and [Fig. 5-23\(D\)](#), even though the element at $\text{R}(4f)$ site has remained unchanged (Dy –atom), its contribution to MAE has changed appreciably, indicating that the coupling with other R –elements and the change in CEF impact anisotropy considerably. For completion, the contributions of three selected Fe –sites, namely $16k_1$, $8j_2$ and $4c$, to MAE of $\text{Dy}_2\text{Fe}_{14}\text{B}$ are depicted in [Fig. 5-24](#) in an energy interval, where their peaks are largest (between -50 and -55 eV). The figure shows that these contributions take place at the same energy intervals and follow similar trends. This behavior is in contrast with SmCo_5 and YCo_5 , where the two different Co –sites ($\text{Co}(2c)$ and ($\text{Co}(3g)$) have very different contributions to MAE.



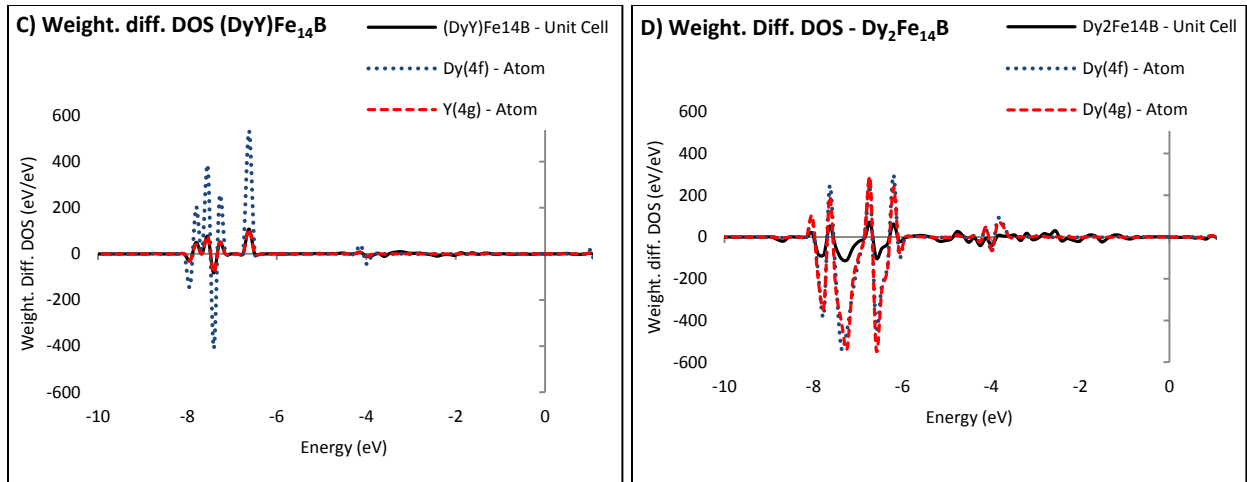


Fig. 5-23 Weighted difference of DOS between magnetization in $[110]$ and $[001]$ (solid black line) for $(R(4f)R(4g))Fe_{14}B$ with (A) Y_2 , (B) (YDy) , (C) (DyY) and (D) Dy_2 , close to Fermi Energy. Contributions of $R(4f)$ –sites (dotted, blue) and $R(4g)$ –sites (dashed, red) to MAE are also shown.

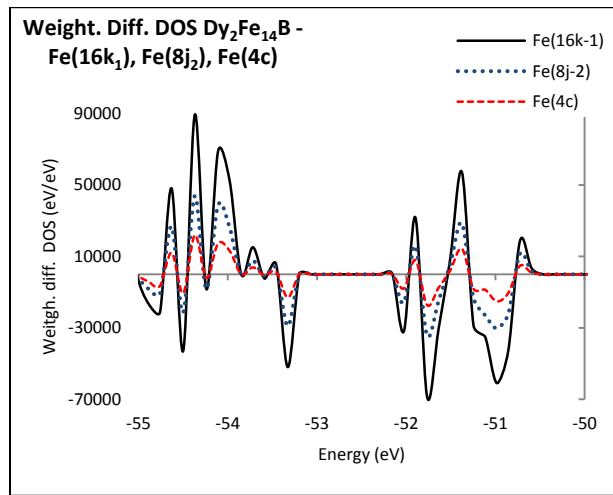


Fig. 5-24 Contribution of $Fe(16k_1)$ (black), $Fe(8j_2)$ (blue), and $Fe(4c)$ (red) to weight. diff. of DOS in $Dy_2Fe_{14}B$.

It should be mentioned that based on [Eq. 5-2](#), the reason the peaks of Fe –sites are much larger than those of Dy are depicted in [Fig. 5-23 \(D\)](#) is that the energy interval is further away from Fermi Energy and $|E|$ is larger here. These large peaks should not be interpreted as disproportionately large contribution of Fe –atoms to MAE.

Based on [Eq. 5-3](#) it is also possible to investigate the change in anisotropy due to substitution. Comparison has been drawn between $(YDy)Fe_{14}B$ and $Y_2Fe_{14}B$ to see the influence of substitution of Y by Dy . But it is also possible to compare $(DyY)Fe_{14}B$ (substituting Y in $Dy_2Fe_{14}B$) and $Y_2Fe_{14}B$. The four different cases for the $(Y - Dy)Fe_{14}B$ system are shown in [Fig. 5-25](#). The contribution of different

R – sites are also shown. In [Fig. 5-25\(A\)](#) for example, $R(4f)$ is Y in both phases, but $R(4g)$ is once Dy and once Y and one sees that Dy at $R(4g)$ changes MAE considerably, while as the contribution of Y does not change much. The same conclusion can be drawn from [Fig. 5-25\(B\)](#), while in this case Dy is at $R(4f)$. On the other hand, based on [Fig. 5-25\(C\)](#) and [Fig. 5-25\(D\)](#), the comparison with $Y_2Fe_{14}B$ shows that in those cases both $R(4f)$ and $R(4g)$ –sites see considerable changes in contribution to MAE.

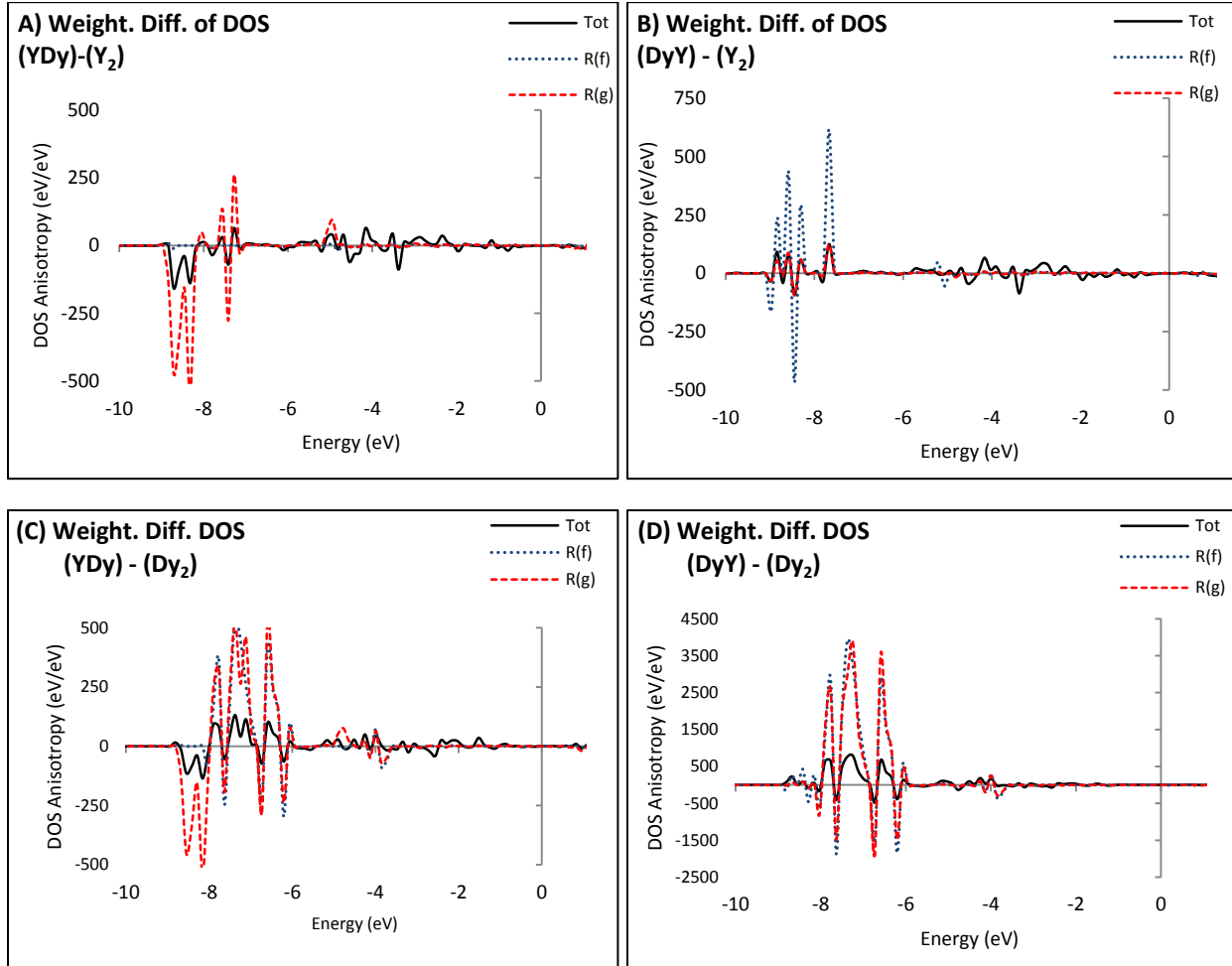


Fig. 5-25 Weighted difference of DOS between $[(YDy)Fe_{14}B$ (A, C), $(DyY)Fe_{14}B$ (B, D)] compared to $[Y_2Fe_{14}B$ (A, B), $Dy_2Fe_{14}B$ (C, D)].

[Figure 5-26\(A\)](#) shows the influence of substituting once Pr and once Nd in $R(4g)$ –site of $Y_2Fe_{14}B$ on weighted difference of DOS. Note that $(YNd)Fe_{14}B$ was calculated non-collinearly only at the SOC+ U phase. The change between $(YPr)Fe_{14}B$ and $Y_2Fe_{14}B$ has a larger positive portion than negative, and hence MAE is increased due to Pr –substitution. As opposed, the difference with $(YNd)Fe_{14}B$ is negative in total and hence MAE is expected to decrease. Close to Fermi Energy the weighted difference of DOS is not all too negative. This leads to the conclusion that MAE will be reduced, but not strongly.

This agrees with the findings of Zhang et al. [1989 Zhang], who obtain $-0.2 \text{ MJ}/\text{m}^3$ for $(\text{YNd})\text{Fe}_{14}\text{B}$. The MAE value obtained by current total energy calculation overestimates this reduction, possibly because the structure wasn't optimized.

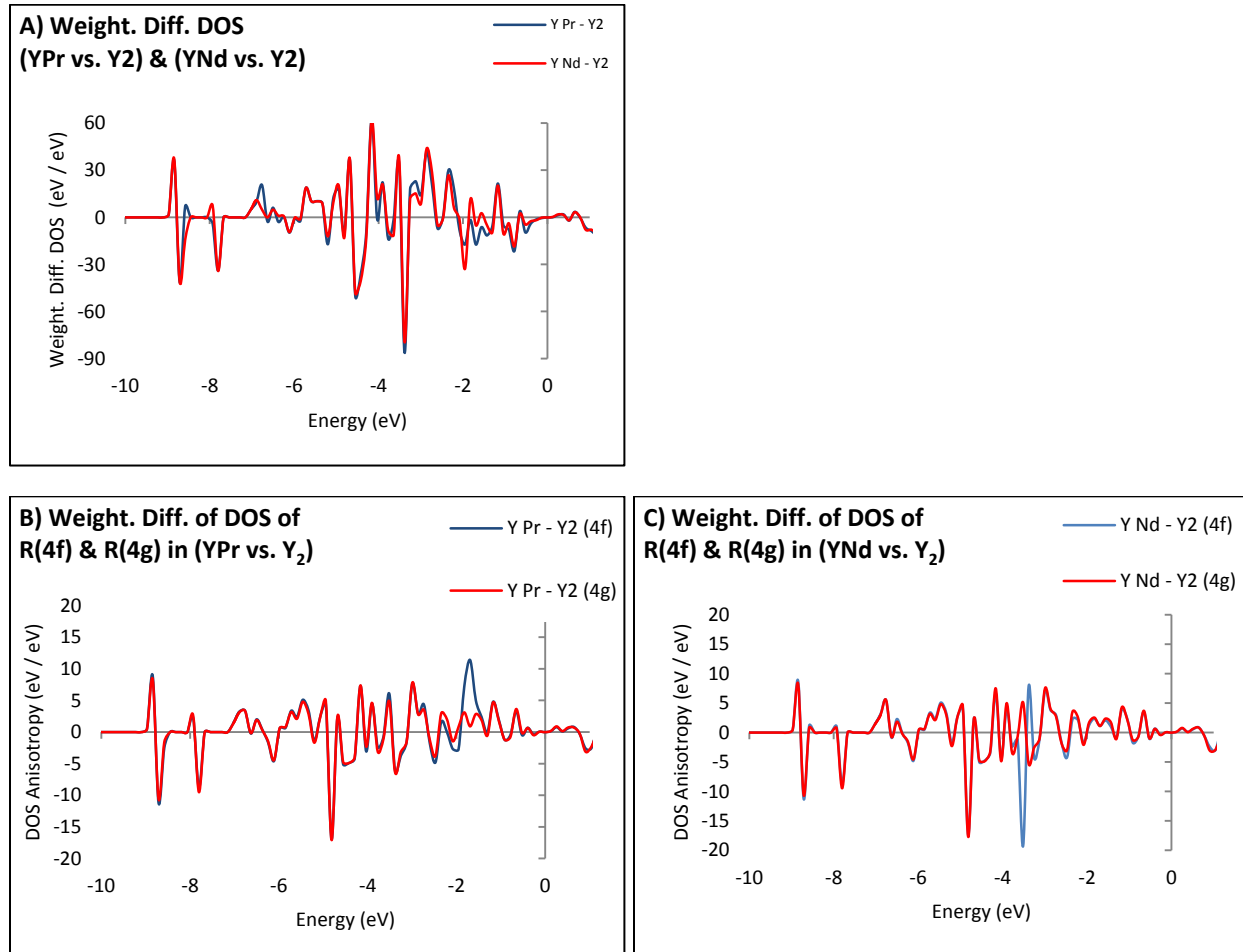


Fig. 5-26 Weighted difference of DOS of $(\text{YPr})\text{Fe}_{14}\text{B}$, $(\text{YNd})\text{Fe}_{14}\text{B}$ compared to $\text{Y}_2\text{Fe}_{14}\text{B}$ (A). Comparison of contribution of $R(4f)$ and $R(4g)$ –sites to the quantities Pr –substitution (B) and Nd –substitution (C).

[Figure 5-26\(B\)](#) and [Fig. 5-26\(C\)](#) show the contributions of the R –sites. The R –atom on the $R(4f)$ is always Y here. One sees that the $R(4f)$ sites are more important for the change of MAE, when Pr or Nd substitutes an Y –atom, even though the substituted atoms are placed at $R(4g)$ –sites. The large peaks of the $R(4f)$ curve around -2 eV show that Pr helps increase MAE, while Nd reduces it, in accordance to the calculation results of total energy. This shows that the effect of substitution in $\text{Y}_2\text{Fe}_{14}\text{B}$ on MAE is indirect, and comes to be due to the changes in anisotropy and CEF of Fe –atoms and $R(4f)$ –sites. In conclusion, the coupling with different R –atoms and the change in CEF impact the contribution of an atom to MAE notably. This large weighted difference of DOS of Y –atoms though is mostly canceled out by the opposing contribution of Fe –atoms.

Electronic Densities of $R_2Fe_{14}B$: The network of the Fe –atoms provides the massive magnetization in $R_2Fe_{14}B$ compounds and also contributes to MAE. Hence, it is of interest to investigate the electronic density and its influences on Fe –atoms, and the changes that occur due to R –substitution. The contour plots of the electronic densities provide a direct way for such studies. The first graph (Fig. 5-27) shows the position of atoms in the three different planes that are studied. The first two parts from left show the $\{001\}$ planes, which are perpendicular to the c –axis, once at $z = 0$ and once at $z = 1/6$. The third is the plane (110), at $x = y = 1/2$ of a –axis and b –axis.

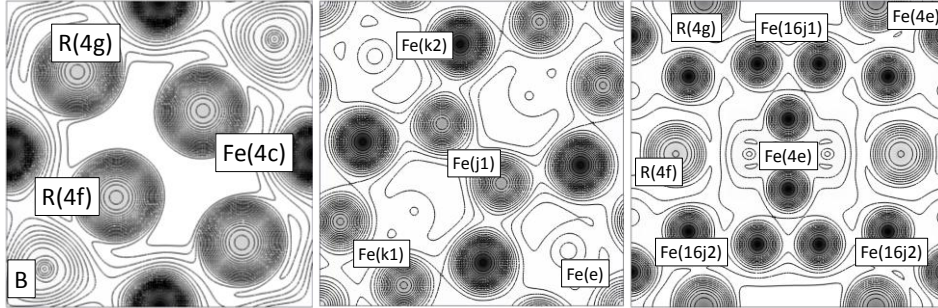


Fig. 5-27 The position of atoms on the three planes. Left: plane perpendicular to $[001]$ at $z = 0$. Upper left and lower right are $R(4g)$ and the sites closer to center are $R(4f)$. Lower left and upper right corners are $B(4c)$ and the four dark sites are $Fe(4c)$. Middle: plane perpendicular to $[001]$ at $z = 1/6$. Two sites in the middle are $Fe(8j_1)$, four darker ones are $Fe(16k_2)$, incomplete ones are $Fe(16k_1)$, corners are $Fe(4e)$. Right: plane perpendicular to $[110]$ at $x = y = 1$. The larger atoms halved by the edges on top and bottom are $R(4g)$, the large atoms on the middle horizontal line are $R(4f)$. The four dark atoms halved by the edges are $Fe(4e)$, the middle two are $Fe(4e)$, four darker atoms closest to central $Fe(4e)$ are $Fe(j_1)$, and four darker atoms close to $R(4f)$ are $Fe(j_2)$.

In Fig. 5-28 and Fig. 5-29 the electronic densities of $Y_2Fe_{14}B$, $Pr_2Fe_{14}B$, $Nd_2Fe_{14}B$ and $Dy_2Fe_{14}B$ phases are depicted at $z = 0$ and $z = 1/6$ perpendicular to the c –axis. The valence character of the R –atoms differ surprisingly strongly, despite these atoms having their main difference in $4f$ –electrons. The electronic density of B and Fe –atoms are unchanged, but the densities surrounding each R –atom change. From Fig. 5-29 it is evident that the electronic density close to the core of Fe is not influenced strongly by R – atoms, but the gradient of the density between the atoms changes considerably. This gradient influences the CEF and hence magnetization and anisotropy. This is in accordance with the findings of Fruchart et al. [1987 Fruchart], who asserted that the hyperfine fields of the Fe –sites of $R_2Fe_{14}B$ depend on the R – atom.

Further, to analyze the differences between $R(4f)$ and $R(4g)$ –sites and the impact of substitution on each site as well as the influence of exchanging the elements between specific sites, the electronic densities of the $(Y - Dy)Fe_{14}B$ system are also drawn, once at $z = 0$ of the c –axis (Fig. 5-30), once at $z = 1/6$ of the c –axis (Fig. 5-31), and once on the plane (110) (Fig. 5-32). All phases are magnetized in $[001]$ direction. Figure 5-30 serves as a comparison for the influence of different R –sites on the

electronic density. The density around the R –atoms, especially $R(4g)$ –sites, changes subtly. The changes caused by R –substitution are better appreciated in [Fig. 5-31](#), where the electronic density close to the core of Fe –atoms is not influenced by R –atoms, but the gradient of the density between the Fe –atoms changes notably.

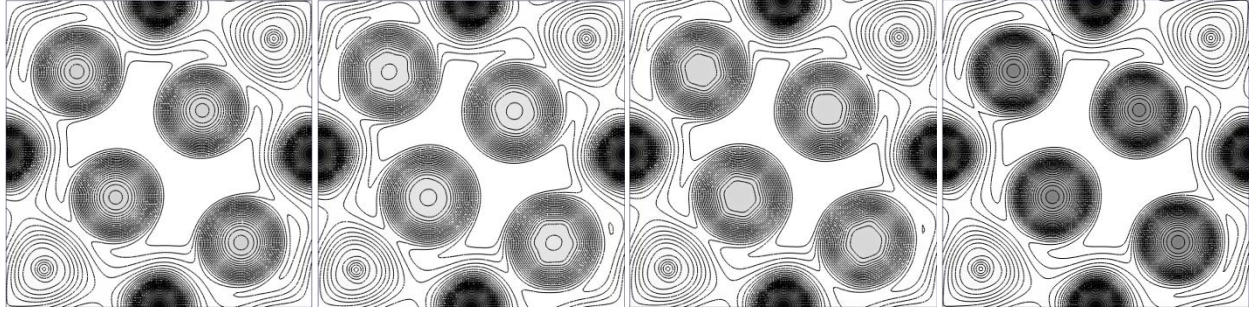


Fig. 5-28 Electronic density of $Y_2Fe_{14}B$, $Pr_2Fe_{14}B$, $Nd_2Fe_{14}B$ and $Dy_2Fe_{14}B$ (from left) at $z = 0$ of (001) plane.

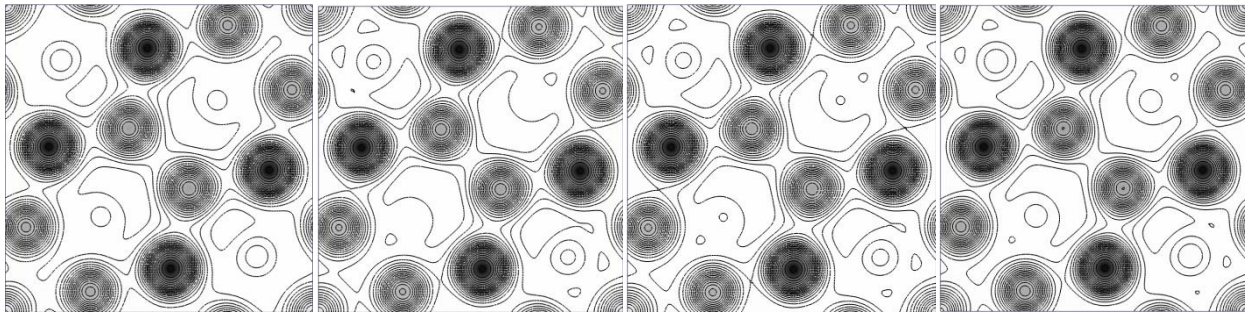


Fig. 5-29 Electronic density of $Y_2Fe_{14}B$, $Pr_2Fe_{14}B$, $Nd_2Fe_{14}B$ and $Dy_2Fe_{14}B$ (from left) at $z = 1/6$ on a plane parallel to (001).

One also observes that different R –atoms in the same site ($Dy(4g)$ in second and $Y(4g)$ in third parts of [Fig. 5-30](#) and [Fig. 5-31](#) from left) influence the Fe –network differently. Further, Dy impacts the Fe –atoms differently when it is coupled with a different element (once Y and once Dy), while it changes the electronic density stronger at $R(4g)$ than it does at $R(4f)$. The valence character of $R = Y$ and Dy also differs visibly, which is due to $4f$ –electrons. Based on [Fig. 5-32](#), the differences in density between $Fe(8j_1)$ and $Fe(8j_2)$ as well as between $Fe(8j_2)$ and $Fe(4e)$ sites are noteworthy. The changes along the c –axis are less pronounced compared to the changes perpendicular to it. Indeed, a change in MAE is only then achieved if the easy axis is influenced differently than the hard axis. Comparing second parts of [Fig. 5-31](#) and [Fig. 5-32](#) from left, it is evident that the substitution of Dy in $Y_2Fe_{14}B$ influences the plane perpendicular to [001] stronger than the plane perpendicular to [110]. This is to be expected, as the total magnetization per formula unit (calculated in [001]) is not influenced as strongly as MAE (difference of energy between [110] and [001]).

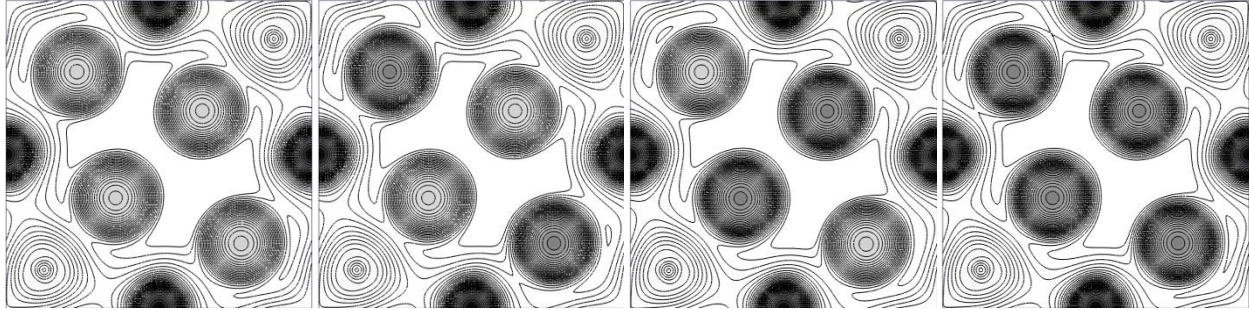


Fig. 5-30 Elect. density of $Y_2Fe_{14}B$, $(YDy)Fe_{14}B$, $(DyY)Fe_{14}B$ and $Dy_2Fe_{14}B$ (from left) on (001) plane at $z = 0$.

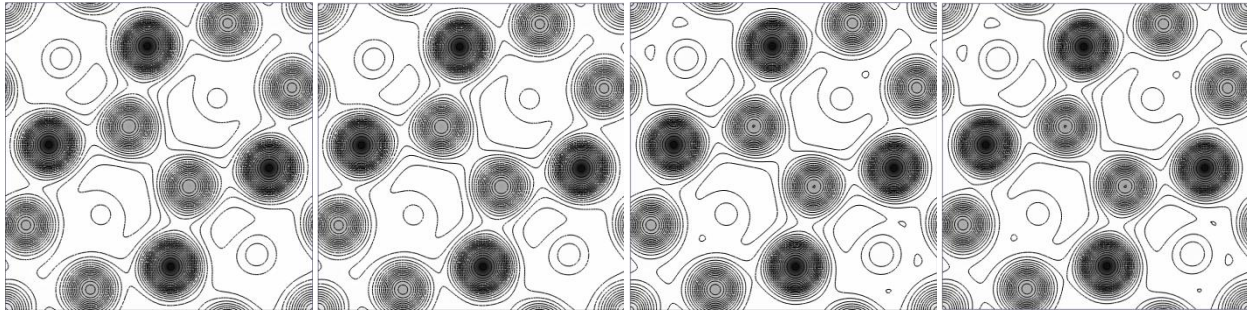


Fig. 5-31 Electronic density of $Y_2Fe_{14}B$, $(YDy)Fe_{14}B$, $(DyY)Fe_{14}B$ and $Dy_2Fe_{14}B$ (from left) on a plane parallel to (001) at $z = 1/6$ of c -axis.

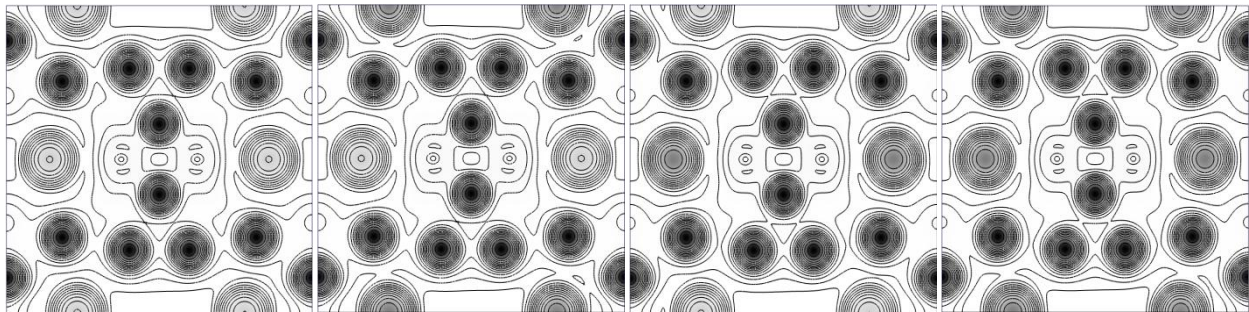


Fig. 5-32 Electronic density of $Y_2Fe_{14}B$, $(YDy)Fe_{14}B$, $(DyY)Fe_{14}B$ and $Dy_2Fe_{14}B$ (from left) at $x = y = 1$ on a plane perpendicular to $[110]$.

Another way of studying the changes caused by substitution is to compare the effect of the coupling that different R -atoms produce; hence in [Fig. 5-33](#), $R(4f)$ is always Y and $R(4g)$ is changed. The areas between Y and B or between Y and Fe remain unchanged with different atoms at $R(4g)$, but the parts surrounding the $R(4g)$ undergo visible changes, which shows that the coupling with different R -atoms is an important aspect of strong anisotropy. [Figure 5-34](#) shows similar graphs to [Fig. 5-31](#) for four selected substituted phases, namely $(PrNd)Fe_{14}B$, $(PrDy)Fe_{14}B$, $(NdY)Fe_{14}B$ and $(DyNd)Fe_{14}B$, on a plane parallel to (001) at $z = (1/6)c$. It is seen that the same R -atom in the same position (Pr in $R(4g)$ site in first two parts) influences the Fe -network differently, when it is coupled with a different

R –atom (Nd , as compared to Dy). The anti-parallel spin moments of Dy , compared to Pr , are one cause of this difference.

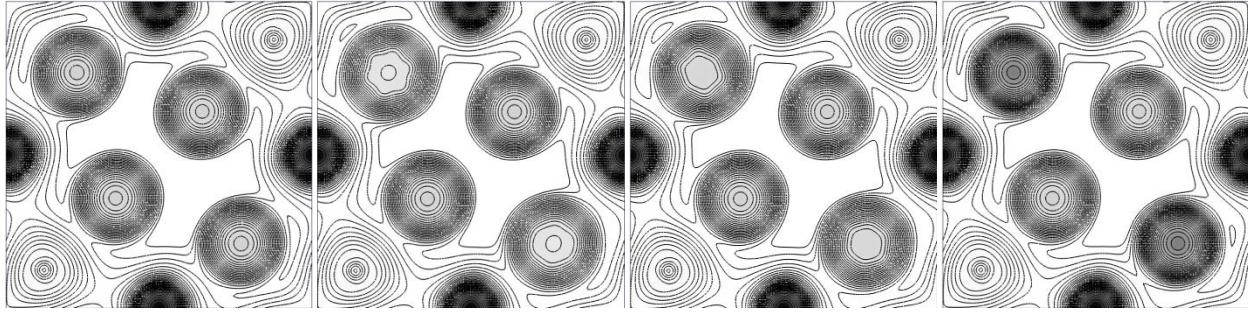


Fig. 5-33 Electronic density of $Y_2Fe_{14}B$, $(YPr)Fe_{14}B$, $(YNd)Fe_{14}B$ and $(YDy)Fe_{14}B$ (from left) at $z = 0$ of $[001]$.

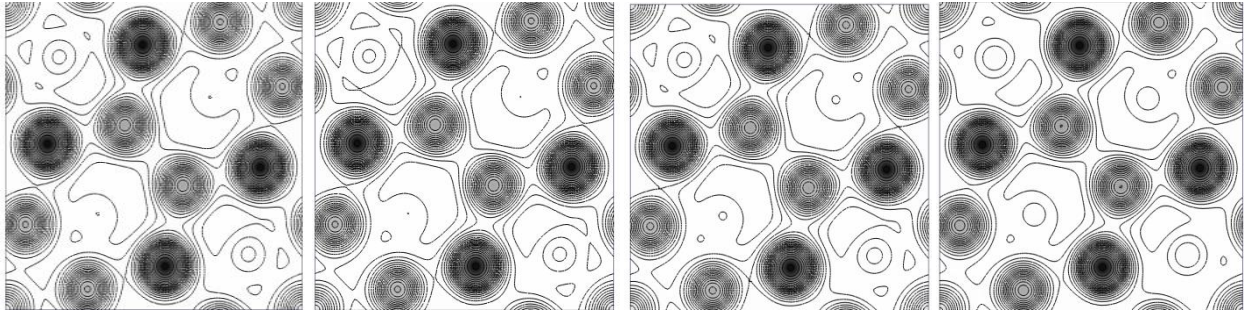


Fig. 5-34 Electronic density for $(PrNd)Fe_{14}B$, $(PrDy)Fe_{14}B$, $(NdY)Fe_{14}B$ and $(DyNd)Fe_{14}B$ (from left) at $z = 1/6$, parallel to (001) .

5-4 Nucleation Fields

Different approaches have been utilized to describe the microscopic mechanisms that determine coercive field, H_c , in real microstructures, especially in novel permanent magnets. The concept of microscopic, magnetic domains, as proposed by Weiss, was used as the outgoing point, and building upon earlier works, Brown developed a framework for numerical calculation of the coercive field within this concept [1940a Brown, 1940b Brown]. In real microstructures, the process of magnetization reversal does not occur suddenly and for the whole solid phase at once, but starts at individual domains and grows depending on the favorability of the magnetization direction in each domain. To derive a quantitative formulation for the coercive field in domains, which are much larger than individual atoms, continuum models were used instead of discrete energies. During further development, an important task of the micromagnetic calculations became the determination of local polarization [2007 Kronmuller]

$$J_S(\mathbf{r}) = \mu_0 \mathbf{M}_s(\mathbf{r}) = J_S(\mathbf{r}) \sum_{i=1}^3 \gamma_i(\mathbf{r}) \quad (5-4)$$

Here γ_i are the direction cosines of the moment vectors of magnetic moments, i.e. $\sum_{i=1}^3 \gamma_i^2 = 1$. The core idea is to minimize free energy, which consists of terms due to exchange (E_X), MCA (E_{MCA}), Zeeman

Splitting (E_Z), stray fields (E_S), and magnetostriction (E_{MS}). The minimization is undertaken with regard to γ_i . One hence faces a variational problem [2003 Kronmuller].

Landau et al. [Landau 1992] developed a framework to calculate exchange energy and concluded that it must depend on $(\nabla\gamma_i)^2$. For a tetragonal or a hexagonal structure with \mathbf{z} as the easy direction and A as exchange stiffness constant, one has for short-range exchange energy

$$E_{X,short} = A_{\perp} \sum_{i=x,y} (\nabla\gamma_i)^2 + A_{\parallel} (\nabla\gamma_z)^2. \quad (5-5)$$

Due to the RKKY interaction in ferromagnets, long-range couplings must also be taken into account, and hence there is an additional energy term, given by

$$E_{X,long}(\mathbf{r}) = -\frac{2}{(g\mu_B)^2} \int J_X(|\mathbf{r} - \mathbf{r}'|) M(\mathbf{r}) M(\mathbf{r}') d^3\mathbf{r}' \quad (5-6)$$

Aside from the external field that produces the Zeeman Splitting, the dipoles and the field they produce, $\mathbf{H}_S(\mathbf{r})$, are also a source of magnetostatic energies. Stray field energy is written as

$$E_S = \frac{1}{2} \mu_0 \int_S \sigma(\mathbf{r}) \cdot U(\mathbf{r}) df + \frac{1}{2} \mu_0 \int_{V_0} U(\mathbf{r}) \rho(\mathbf{r}) d^3\mathbf{r} \quad (5-7)$$

with σ as surface charge, U as the solution of the Poisson Equation ($\nabla^2 U = -\rho(\mathbf{r})$) and f the surface. By using $\gamma_1 = \sin(\theta) \cos(\varphi)$, $\gamma_2 = \sin(\theta) \sin(\varphi)$ and $\gamma_3 = \cos(\theta)$, one finally arrives at [2007 Kronmuller]

$$2A[\sin^2(\theta) \cdot \nabla^2 \varphi + \sin(2\theta) \cdot \nabla \varphi \cdot \nabla \theta] - \frac{\partial}{\partial \varphi} (E_{MCA} + E_S + E_{MS} - \mathbf{J}_S \cdot \mathbf{H}_{ext}) = 0 \quad (5-8)$$

In this equation E_S and E_{MS} are dependent on the shape of the specimen and its domain structure, but MAE (E_{MCA}) is intrinsic. The focus in this work has been to calculate this intrinsic value, in order to allow a more accurate determination of total energy and provide a better approximation for the coercive field. The importance of the works of Brown ([1940b Brown, 1941 Brown]) was that he solved this equation for the case of magnetic saturation in a ferromagnet.

Based on these works it became evident that the reversal processes depend on the intrinsic magnetic properties, such as M_S and MAE, as well as on the microstructural properties, such as grain size, orientation of grains, and composition of grain boundary layers. The long range dipolar interactions between misaligned grains are more pronounced in large-grained magnets, whereas short range exchange coupling reduces the coercive field in small-grained magnets. Most high energy density $Nd - Fe - B$ magnets are produced by sintering techniques [2002 Rodewald], which leads to grain sizes above $1\mu m$. Melt-spun magnet materials with a grain size ranging from 20 to 100 nm are used for bonded and hot deformed magnets.

If a microscopic grain consists of only one domain, then only one magnetic direction exists in it. The nucleation field, H_N , is the field which reverses the direction of magnetization in such a grain. It is possible to determine the limit of the coercivity, which is controlled by the nucleation field (H_N) of reversed domains during magnetization reversal processes. For a homogenous rotation of magnetization

during the reversal process, Stoner and Wohlfarth derived an initial estimation for the coercive field, H_C , as equal to the anisotropy field, H_A , of a single-domain, uniaxial particle [1948 Stoner]

$$H_{C,Theory} = H_A = 2 \cdot \frac{K_1}{J_S} \quad (5-9)$$

Here K_1 is the first anisotropy constant. In uniaxial phases $K_1 = \text{MAE}$. Experimental measurements though found much smaller values for H_N in permanent magnets. Kronmuller [1978 Kronmuller] concluded that demagnetization and local changes in anisotropy due to strain and surface effects are important factors and affect H_N .

In real magnets, the coercive field is controlled by the nucleation and expansion of reversed domains during magnetization reversal process. This knowledge has been used to investigate the possibility of enhancing permanent magnetic properties in novel magnets, e.g. [1986b Hirosawa]. As described by Kronmuller et al. [1988 Kronmuller, 2003 Kronmuller], in real microstructures, the nucleation field H_N is determined by the reduced local anisotropy field, H_A , and the local demagnetizing field, H_D . Inhomogeneous magnetization reversal processes lead to the nucleation of reversed domains if $H_D + H_{extern} > H_{A,reduced}$, which results in the experimental coercive field value

$$H_{C,real} = H_N = \alpha \frac{2 \cdot K_1}{J_S} - N_{eff} M_S \quad (5-10)$$

Here, α is a microstructural parameter corresponding to the influence of the real microstructure (grain size, grain orientation and nature of grain boundary phase) and N_{eff} the demagnetization factor. This equation shows the reason that substitution atoms have the potential to considerably influence the macroscopic permanent magnetic properties, as both MAE and M_S are sensitive to changes of the electronic structure close to Fermi Energy. The strain effects caused by substitution or possible other effects, also impact MAE and M_S . In the recent years, many theoretical and numerical studies have been carried out to investigate the real microstructure in permanent magnets, and the effect of substitution and strain on it, e.g. [2014 Hrkac], [2017 Saito] and [2017 Yi].

The micromagnetic model, which suggests that the reversal of magnetization starts at a nucleation site, and for which the Eq. (5-10) is obtained, has proven to be reliable, especially, as it is possible to further develop more accurate estimations for the parameters α and N_{eff} , e.g. [2017 Li]. Kou et al. [1994 Kou] undertook a detailed investigation on the coercive field of $Pr_2Fe_{14}B$ and compared the predictions of this micromagnetic model with those of a phenomenological model developed by Givord et al. [1988a Givord, 1988b Givord] and concluded the micromagnetic model agrees well with experimental measurements.

Further, a portion of anisotropy of R –atoms, which stems from the CEF, is dependent on exchange. Changing the number of magnetic electrons, e.g. $T - 3d$ or $R - 4f$ –electrons, results in different strength of exchange and hence of anisotropy. Hilzinger et al. [1976 Hilzinger] observed that the density of defects in crystals (e.g. impurities) influences the coercive field by impacting the domain walls. In

Subsection 5-2 it was shown that changes in the Co –network through substitution or strain, influence anisotropy. Such local changes in anisotropy influence energy of the domain walls. The possibility hence exists to enhance the coercive field by considerably reducing the number of magnetic atoms in the T –networks of the RT_5 and $R_2T_{14}B$ phases [1979 Oesterreicher]. Such a reduction in number of magnetic atoms though result in reduction of saturation magnetization.

RT_5 Compounds: Based on the calculated M_S and MAE for the RT_5 compounds, their nucleation fields (H_N) were studied. The parameters α and N_{eff} in Eq. 5-10 depend only on the microstructure, and hence the same sets of values are used for all RT_5 phases. Different microstructures have different parameters, and five different sets are compared in Fig. 5-35, with addition of two points for $hcp - Co$. The first two graphs show the effect of substitution in YCo_5 and $SmCo_5$ respectively, and the third compares Co_5 , Co_6 , YCo_5 and $SmCo_5$, as well as $hcp - Co$. The values of $(\alpha; N_{eff})$ used for $hcp - Co$ are $Co - 1 = (0.002; 0.33)$ [2016 Skomski] and $Co - 2 = (0.106; 0.138)$ [2017 Son], and for RT_5 , $B2 = (0.15; 0.4)$, $B3 = (0.3; 1.0)$, $B4 = (0.45; 1.8)$, adapted from [2014 Bhatt] and corresponding to $Sm - Co$ sputtered thin films, annealed at $500^\circ C$, $600^\circ C$ and $700^\circ C$ respectively, $C5 = (0.13; 2.22)$ obtained for strong textured $SmCo_5$ nanoflakes by Zuo et al. [2015 Zuo] and $D6 = (0.035; 0.61)$ obtained for melt-spun ribbons of $SmCo_5Fe_2$ by Tung et al. [1999 Tung]. It is noted that the calculations with substitution were optimized and relaxed, i.e. the effect of substitution on the crystal structure is taken into account.

In YCo_4Cu , the value of H_N is quite large despite its small MAE. The substituted phase with the largest H_N is $SmCo_4Fe$, which is not surprising, as it has a larger M_S than $SmCo_5$ and its MAE is also large. The microstructure has a visible impact on the nucleation field and for certain microstructures (e.g. annealed thin films) the changes in H_N due to substitution are larger. From Fig. 5-35(C), it is seen that for certain microstructures found in thin films, the nucleation field of YCo_5 is up to four times smaller than that of $SmCo_5$, even though YCo_5 has a considerably large MAE. The nucleation field of $PrCo_5$ is not included, because for this compound $K_1 \neq MAE$.

Oesterreicher et al. [1979 Oesterreicher] studied $SmCo_{5-x}Cu_x$ and found that the changes in coercive field with temperature in these compounds is described well by the model of domain wall propagation. Fidler [1982 Fidler] studied the behavior of magnetization reversal processes and the influence of the nucleation on the coercive field for Cu –substitution in $Sm - Co$ phases. One conclusion drawn from these and further studies (e.g. [1976 Perkins] and [1979 Nagel]) was that the exchange coupling and its variations influence the coercive field. Indeed one of the reasons that impurities and substitution influence the coercive field is because they impact exchange constants, as the change in number of valence electrons also changes the band structure.

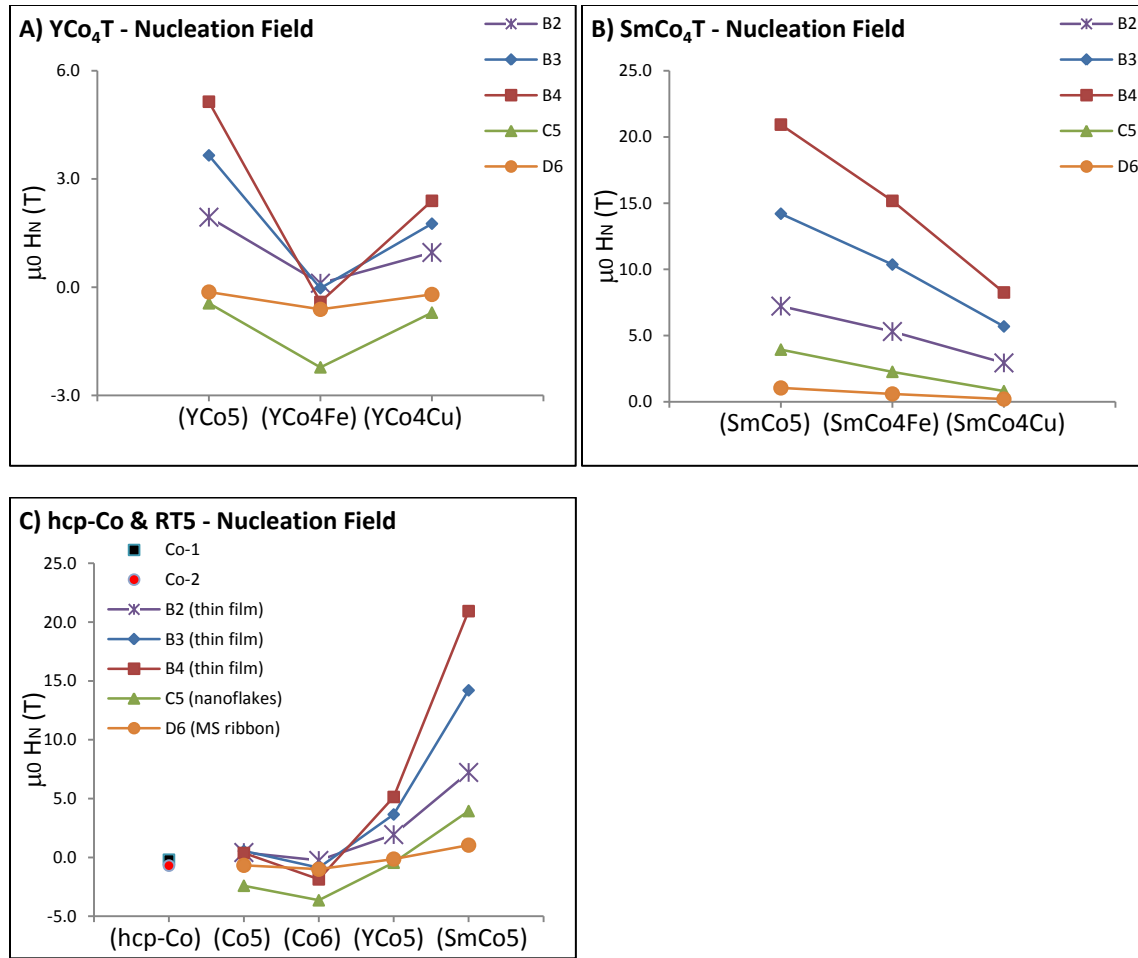


Fig. 5-35 Changes in nucleation field of YCo_5 with Fe or Cu substitution (A). Changes in nucleation field of $SmCo_5$ with Fe or Cu substitution (B). Comparing nucleation fields of $hcp-Co$, Co_5 , Co_6 , YCo_5 and $SmCo_5$ (C). The lines connecting the points are guides and do not represent calculation results. Only the dots represent calculation results.

$R_2Fe_{14}B$ Compounds: Experimental data on individual spin and orbital contribution to magnetism of $R_2Fe_{14}B$ near $0 K$ are scarce, especially for substituted compounds. Nevertheless based on total R –moments of $R_2Fe_{14}B$ single crystals, measured at $4.2 K$ by Hirosawa et al. [1986a Hirosawa], and assuming these values remain unchanged after substitution, it is possible to predict the total magnetization of substituted phases. The estimated total moments and polarization are given in Tab. 5-35, where the moments of Fe and B –sites and the interstitial region are taken from PAW calculations.

As α and N_{eff} of Eq. (5-10) depend only on the microstructure, the same set of values are used for all phases to draw a comparison. Several different sets of $(\alpha; N_{eff})$ values are considered, taken from literature. Especially interesting is to compare on one hand isotropic and anisotropic microstructures and on the other hand sintered, melt-spun and nanocrystalline specimens, as these processes result in markedly different microstructures. Figure 5-36 shows the calculated nucleation fields of $(Y - Pr)Fe_{14}B$,

$(Y - Dy)Fe_{14}B$ and $(Pr - Dy)Fe_{14}B$ systems. Each diagram compares the values for non-substituted and substituted phases of a different combination of R -atoms.

Phase	$M_S^{Fe+B+INT}$ [μ_B]	M_S^R (Exp.) [μ_B] (a)	M_S (Est.) [μ_B /f. u.]	J_S (Est.) [T] (0 K)	$J_S^{Exp.}$ [T] (b) (RT)
$Y_2Fe_{14}B$	31.36	0.0	31.36	1.59	1.36
$(YPr)Fe_{14}B$	31.48	3.1	34.58	1.75	
$(YDy)Fe_{14}B$	31.50	-10.1	21.40	1.08	
$Pr_2Fe_{14}B$	31.03	6.2	37.23	1.82	1.41
$(PrY)Fe_{14}B$	31.27	3.1	34.37	1.68	
$(PrDy)Fe_{14}B$	30.63	-7.0	23.63	1.16	
$Dy_2Fe_{14}B$	30.70	-20.2	10.50	0.52	0.67
$(DyY)Fe_{14}B$	31.12	-10.1	21.03	1.05	
$(DyPr)Fe_{14}B$	30.95	-7.0	23.95	1.19	

Tab. 5-35 Calculated $Fe + B$ magnetization, estimated total magnetization based on literature R -moments, estimated polarization at 0 K and experimental polarization at room temperature (RT). (a) = [1986a Hirose], (b) = [2008 Skomski].

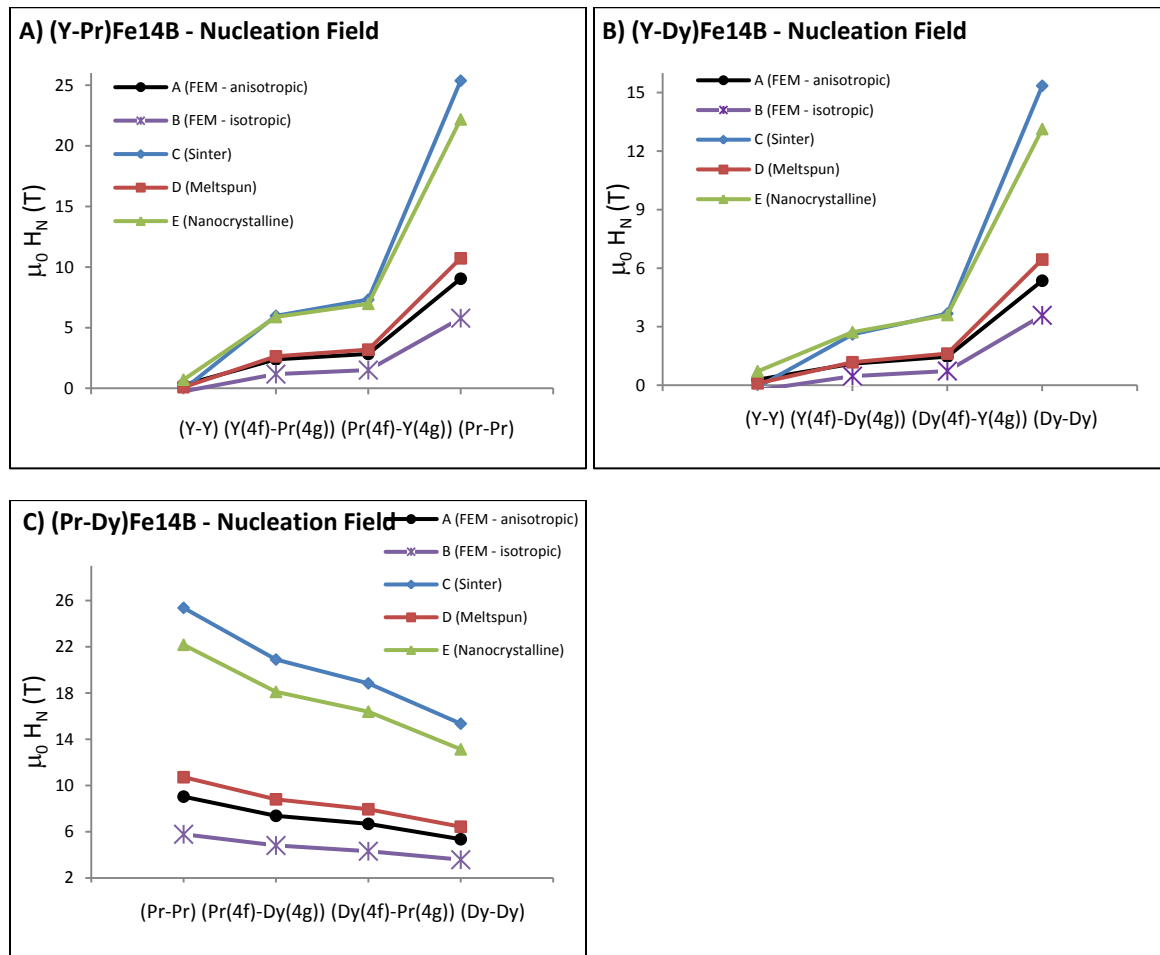


Fig. 5-36 Changes in nucleation field of $(Y - Pr)Fe_{14}B$, $(Y - Dy)Fe_{14}B$ and $(Pr - Dy)Fe_{14}B$ systems due to substitution, drawn for different types of microstructures (isotropic and anisotropic FEM simulation, sintered, melt-spun and nano-crystalline specimen). Only the dots represent calculation results. The lines are depicted for guidance.

Here $(\alpha; N_{eff})$ values of curve (A) = (0.33; 0.04) and (B) = (0.23; 0.30) are from finite element simulations of anisotropic and isotropic $NdFeB$ structures [2017 Zickler]. Curve (C) = (0.96; 0.68) is from sintered $Pr - Fe - B$ specimen studied by Kou et al. [1994 Kou], those of curve (D) = (0.40; 0.20) are obtained for anisotropic, melt-spun ribbons by Bance et al. [2014 Bance] and curve (E) = (0.81; 0.08) uses values from isotropic, melt-spun, nano-crystalline specimen [1998 Youhui].

The strong impact of sintering on the nucleation field is clear for both $Pr_2Fe_{14}B$ and $Dy_2Fe_{14}B$, with H_N being more than four times larger for the sintered specimen (data points C) compared to melt-spun (data points D). Durst et al. also observed larger H_N for sintered $Nd_2Fe_{14}B$ compared to melt-spun [1987 Durst]. Comparing the idealized anisotropic (data points A) and isotropic (data points B) phases, it is evident that orienting the grains positively influences the nucleation field. Data point E, which represents a specimen made of a nanocrystalline alloy, provides the most interesting case. Despite having an isotropic microstructure, its nucleation field is very large. As it is possible to further manipulate and change the microstructure of such specimen, they have the potential for further enhancement.

Among the substituted phases, $(PrDy)Fe_{14}B$ exhibits a large H_N at 0 K, despite having a clearly smaller MAE compared to $Pr_2Fe_{14}B$. As Hirosawa et al. indicated [1985 Hirosawa], the anisotropy constant K_1 of $Dy_2Fe_{14}B$ remains larger than that of $Pr_2Fe_{14}B$ at temperatures above 370 K. This leads to the conclusion that $(PrDy)Fe_{14}B$ is ought to exhibit a smaller loss of coercive field compared to $Pr_2Fe_{14}B$ above room temperature. Another visible feature is that phases containing $R = Y$ have much smaller nucleation fields compared to other compounds studied. Further, no type of microstructure enhances the nucleation field of $Y_2Fe_{14}B$ considerably, which remains below 1 T. This is not surprising due to yttrium's vanishing magnetic moment. An important factor for large MAE of $R_2Fe_{14}B$ is the indirect coupling of $4f$ -electrons of the R -atoms. When only one R -site has $4f$ -electrons, a large contribution to the SOC is absent. Hence, despite considerable MAE of $(YPr)Fe_{14}B$, due its low nucleation field, the phase is not deemed suitable for permanent magnet applications. Interestingly and as opposed to $Y_2Fe_{14}B$, the nucleation fields of $Pr_2Fe_{14}B$ and $Dy_2Fe_{14}B$ depend on the type of the microstructure of these phases. This is seen from the large variation of $\mu_0 H_N$ in these pure phases (for example between 5 and 25 T for $R = Pr$). The strain in the individual grains, caused by the substitution of atoms that diffuse from the boundary phases into the grains, also impact MAE and M_S of these grains, though these effects were not included in the current PAW calculations for the $R_2T_{14}B$.

When considering the real microstructure of $R_2T_{14}B$ phases, it is not only the presence of R -atoms, but also certain amounts of T -atoms, at grain boundaries that influence magnetic properties in industrially produced magnets. Yue et al. [2008 Yue] for example studied the influence of the concentration of $\alpha - Fe$ in $Nd_2Fe_{14}B/\alpha - Fe$ nanocomposites and observed a large (slight) increase of BH_{max} and a large (slight) decrease in coercive fields for isotropic (anisotropic) specimen. It is evident that the potential exists for enhancing the macroscopic properties through atomistic influences. Elizalde et al. [2009 Elizalde] for example used a temperature treatment for YCo_5 and $PrCo_5$ to achieve average grain sizes that are below 20 nm. They observed an enhancement of the coercive field at due to this feature.

6 – Conclusions and Outlook

Novel hard magnetic materials, consisting of compounds with complex $R - T$ intermetallic phases find many applications in industry. Enhancing their macroscopic properties, especially the coercive field H_C , and maximum energy product BH_{max} , is of scientific, technological and economic interest. The coercive field is strongly dependent on the microstructure of a magnet, that is, on the small magnetic grains, their sizes and orientations, the magnetic couplings inside and between these grains, and the properties of the magnetic domains. Aside from the microstructure, H_C also depends on certain intrinsic magnetic properties, most importantly, saturation magnetization, M_S , and MAE. The potential hence exists to enhance the macroscopic magnetic properties based on advanced materials design.

In this work, M_S and MAE of ideal crystals of RT_5 ($R = Y, Sm, Pr$; $T = Co, Fe, Cu$) and $R_2T_{14}B$ ($R = Y, Pr, Nd, Dy$; $T = Fe$) are investigated by numerical calculations, based on density functional theory (DFT) at 0 K. Due to their robust physical and mathematical foundation, DFT calculations allow the incorporation of relativistic effects (most importantly SOC), as well as inclusion of non ab-initio corrections, such as the ($U; J$) –potentials. Further, as DFT allows the construction of different phases, it was also possible to investigate the influence of strain effects and of substitution atoms on M_S and MAE. Electronic structure calculations and analyses of density of states and electronic density provide accurate and precise means to investigate the physics of magnetic properties on atomic scale and the possibilities of enhancing intrinsic properties. Finally, based on the calculated M_S and MAE, estimations are made for the nucleation field, H_N , which is related to H_C .

An important aim of the work was to find calculation procedures that are straightforward, easy to carry out and do not require advanced manipulation of the DFT codes, but allow an accurate and systematic study of the $R - T$ phases, with the fewest possible external variables. The results of thousands of calculations showed that in uniaxial systems, it is best to start the calculation with the non spin-polarized (NSP) structure, and then continue with the spin-polarized calculating including SOC. But in phases with non-collinear magnetic structures, one should start with the scalar relativistic calculation (SRC) and after its convergence continue to SOC. On the other hand, it became evident that the $+U$ potentials should be included in the calculation from the start. The values of $+U$ potentials were initially taken from literature and then varied slowly to obtain best agreement with experiments.

Optimizing and relaxing the crystal structure, that is, finding the lattice parameters and the atomic positions that minimize energy proved to be essential. Extensive tests on the RT_5 phases showed that all calculation steps, (NSP+U), (SRC+U) and (SOC+U) must be optimized and relaxed separately to achieve the most accurate outcome. Even small variations in lattice parameters and atomic positions that stem from optimization and relaxation, resulted in changes for MAE of $SmCo_5$. This was further confirmed by comparing YCo_5 with fictive phases Co_5 and Co_6 . By way of studying the dependence of MAE on the

changes in the crystallographic c/a ratio, it was concluded that strain effects have the potential to impact anisotropy without affecting magnetization.

Summary of results: The MAE values calculated at 0 K for RCO_5 ($R = Y, Sm$ and Pr) are 7.2, 25.4, and -0.7 MJ/m^3 respectively; to be compared with experimentally measured values (at 4.2 K) of 6.5 ... 10, 24 ... 29 and -0.8 MJ/m^3 . The MAE values calculated for $hcp - Co$, Co_5 , Co_6 , YCo_4Fe , YCo_4Cu , $SmCo_4Fe$ and $SmCo_4Cu$ are 0.77, 3.98, 2.30, 1.99, 2.81, 19.2, and 8.16 MJ/m^3 respectively. Substituting a Co -atom in YCo_5 by Fe or Cu reduces MAE strongly, while the reduction due to Fe is larger. Substituting a Co -atom in $SmCo_5$ by Cu very strongly reduces MAE, while the reduction due to Fe is much smaller and MAE remains over 19 MJ/m^3 . For both $SmCo_5$ and YCo_5 , MAE increases at first, then decreases again with increasing c/a ratio. Both increase and decrease are stronger in $SmCo_5$. Depending on the microstructure, YCo_4Cu exhibits a substantial nucleation field, despite having a considerably smaller MAE compared to YCo_5 . On the other hand, $SmCo_4Fe$ has an H_N that is only 25% smaller than that of $SmCo_5$, while its MAE is also large.

The MAE values calculated at 0 K for $R_2Fe_{14}B$ ($R = Y, Dy$ and Pr) are 23.5, 3.8, and 0.8 MJ/m^3 respectively; to be compared with experimentally measured values of 0.7, 3.0 and 23.5 MJ/m^3 . For all phases except $Nd_2Fe_{14}B$, MAE has been calculated accurately, while the $+(U, J)$ potentials have been the only free variable. It should be noted though that the values of the $(U; J)$ potentials were the same for $Co - 3d$ -electrons of YCo_5 and $Fe - 3d$ -electrons of $Y_2Fe_{14}B$. Similarly, the values were the same for $R - 4f$ -electrons of $SmCo_5$, $Pr_2Fe_{14}B$ and $Dy_2Fe_{14}B$, hinting at the possibility that general and similar $(U; J)$ values exist, which apply to isostructural, uniaxial $R - T$ compounds. In $Pr_2Fe_{14}B$, MAE decreases slightly with increasing c/a ratio, in $Dy_2Fe_{14}B$ it decreases strongly (up to 40%) and in $Y_2Fe_{14}B$ it remains nearly constant. Substituting Pr by Dy and Y strongly reduces MAE of $Pr_2Fe_{14}B$ and substituting Y by Pr and Dy increases MAE, while the effect of Pr is much stronger. Substituting Dy by Pr increases, and by Y decreases MAE of $Dy_2Fe_{14}B$. Among the different microstructure parameters (taken from literature), those for sintered specimen result in largest H_N values. Any $R_2T_{14}B$ phase containing Y has a much smaller H_N compared to phases without Y . The phase $(PrDy)Fe_{14}B$ has both a large MAE and a considerable H_N (only 20% smaller than $Pr_2Fe_{14}B$).

Regarding Phases: In YCo_5 , Y obtains a small magnetic moment, and as the comparison with Co_5 and Co_6 shows, also contributes to MAE, but the main contribution to MAE stems from $Co(2c)$ atoms. In YCo_5 , changing lattice parameter " c " up to 2%, without " a " being changed, which is possible in thin films, increases MAE. In $SmCo_5$, decreasing the c/a ratio up to 1%, with a constant volume, increases MAE. When substituting 20% of Co -atoms, Fe increases magnetization and Cu decreases it. Similar to YCo_5 , in $Y_2Fe_{14}B$, Y obtains a small magnetic moment. The variation of c/a ratio in $Y_2Fe_{14}B$ while the volume is constant, does not impact MAE, while it slightly decreases MAE in $Pr_2Fe_{14}B$ and strongly decreases it in $Dy_2Fe_{14}B$. In $Nd_2Fe_{14}B$ it is possible to observe a sudden change of MAE, in value and even sign, if the variation of c/a changes the non-collinear magnetic structure to a collinear structure.

$(PrDy)Fe_{14}B$ exhibits the largest nucleation field among the studied substituted phases and has a large magnetization and anisotropy as well.

Regarding Calculations: It is found that the magnetic force theorem is not suitable for calculation of MAE of complex magnetic phases, especially with $4f$ –electrons. Designating the $4f$ –electrons as core-electrons results in strongly underestimated MAE values in both codes, if the calculation is carried out to convergence, owing to the fact that these electrons are pushed away from Fermi Energy and have no influence on the Fermi Surface, which is important for MAE. Without the introduction of the $+U$ –potential, no combination or variation of settings in either code provided an accurate MAE value for phases with $4f$ –electrons. Accurate results were obtained, only when calculations were carried out with lowest or no symmetries, which indicates that the inclusion of symmetries for faster computation is a possible source of error in calculation of complex magnetic phases. Including all steps in one calculation, that is spin-polarization, scalar relativity, spin-orbit coupling and Hubbard Potential does not deliver good results. Despite its seemingly less important role, it is possible that changes in value of exchange potential (J) impact MAE.

Regarding Codes: The WIEN2k code is accurate and provides good results on the atomic level. An important feature to note is that the code calculates energies of the core electrons as well, which increases accuracy in general, but also means that stricter convergence criteria are required, as the absolute values of free energy are quite large. Running non-collinear calculations with WIEN2k is not straightforward and was not carried out. On the other hand, energy optimization and structure relaxation is also not easily done. The k –mesh is constructed automatically based on the structure and with regard to the compound. The WIEN2k team provides continuous scientific and technical help with the calculations, and the User Guide is quite helpful. Calculating DOS is easily done.

VASP calculates only valence and some semi-core electrons, which means the absolute value of free energy is smaller and hence calculating MAE is easier, but the accuracy of energy calculation is lower. For VASP calculations, small changes in k –mesh result in considerable changes in MAE values, which means energy convergence tests are required even for small and similar number of k –points. This is especially cumbersome, as VASP doesn't include a built-in k –mesh generator to find the best k –mesh for each phase. Further, the results of VASP calculations for energies at μeV level were strongly dependent on the machine parameters and parallelization configurations (even with convergence criterion $10^{-8} eV$), which should have no physical significance or influence. This is a strong drawback for calculation of MAE, and disallows simple comparison of results from different calculations. There is no real support from the VASP team and the User Guide is incomplete, but a practical online copy of the guide exists in “Wiki” style. Another drawback of VASP in regard to magnetic calculations is that the concept of spin up / down is replaced by a total spin density, when SOC included (even for collinear calculations). Further, the tool for calculating SOC is still in the “beta phase”. Obtaining DOS-data is not straightforward and was done through a different software.

References

1. [[Andoh 1982](#)] Y. Andoh, H. Fuji, H. Fujiwara, T. Okamoto, Magnetization and Magnetocrystalline Anisotropy of $Y_{1-x}R_xCo_5$ ($R = Pr$ and Sm), [J. Phys. Soc. Jpn.](#) **51** (1982), 435.
2. [[Andersen 1975](#)] O.K. Andersen, Linear methods in band theory, [Phys. Rev. B](#) **12** (1975), 3060.
3. [[Andersen 1977](#)] O.K. Andersen, J.Madsen, U.K. Poulsen, O. Jepsen, J. Kollár, Magnetic ground state properties of transition metals, [Physica B+C](#) **86** (1977), 249.
4. [[Anderson 1961](#)] P.W. Anderson, Localized Magnetic States in Metals, [Phys. Rev.](#) **124** (1961), 41.
5. [[Antropov 1995](#)] V.P. Antropov, M.I. Katsnelson, M. van Schilfgaarde, B.N. Harmon, Ab Initio Spin Dynamics in Magnets, [Phys. Rev. Lett.](#) **75** (1995), 729.
6. [[Antropov 1996](#)] V.P. Antropov, M.I. Katsnelson, B.N. Harmon, M. van Schilfgaarde, D. Kusnezov, Spin dynamics in magnets: Equation of motion and finite temperature effects, [Phys. Rev. B](#) **54** (1996), 1019.
7. [[Baberschke 2001](#)] K. Baberschke, Anisotropy in Magnetism, in [Lecture Notes in Physics](#) **580** (2001): [Band Ferromagnetism](#), 27, (Ed. K. Baberschke, W. Nolting, M. Donath), Springer, ISBN 978-3-540-44610-1.
8. [[Bance 2014](#)] S. Bance, B. Seebacher, T. Schrefl, L. Exl, M. Winklhofer, G. Hrkac, G. Zimanyi, T. Shoji, M. Yano, N. Sakuma, M. Ito, A. Kato, A. Manabe, Grain-size dependent demagnetizing factors in permanent magnets, [J. Appl. Phys.](#) **116** (2014), 233903.
9. [[Bihlmayer 2006](#)] G. Bihlmayer, Non-Collinear Magnetism: Exchange Parameter and T_C , [NIC Series](#) **31** (2006), 447, Publication Series of the John von Neumann Institute for Computing, ed. J. Grotendorst, S. Blugel, D. Marx, ISBN: 3-00-017350-1.
10. [[Bihlmayer 2007](#)] G. Bihlmayer, Density-functional Theory of Magnetism, [Handbook of Magnetism and Advanced Magnetic Materials](#), vol. 1, (Ed. H. Kronmuller, S. Parkin, J.E. Miltat, M.R. Scheinfein), Wiley (2007), ISBN: 978-0-470-02217-7.
11. [[Billas 1994](#)] I.M.L. Billas, A. Chatelain, W.A. de Heer, Magnetism from the Atom to the Bulk in Iron, Cobalt and Nickel Clusters, [Science](#) **265** (1994), 1682.
12. [[Bhatt 2014](#)] R. Bhatt, P. Bhatt, G. Schütz, Investigation of cellular microstructure and enhanced coercivity in sputtered $Sm_2(CoCuFeZr)_{17}$ film, [J. Appl. Phys.](#) **115** (2014), 103903.
13. [[Blaha 1990](#)] P. Blaha, K. Schwarz, P. Sorantin, S.B. Trickey, Full-potential, linearized augmented plane wave programs for crystalline systems, [Comput. Phys. Commun.](#) **59** (1990), 399.
14. [[Blaha 2018](#)] P. Blaha, K. Schwarz, G.K.H. Madsen, D. Kvasnicka, J. Luitz, R. Laskowski, F. Tran, L.D. Marks, WIEN2k, An Augmented Plane Wave + Local Orbitals Program for Calculating Crystal Properties, K. Schwarz, Techn. Universität Wien, Austria (2018), [ISBN 3-9501031-1-2](#).
15. [[Bloch 1928](#)] F. Bloch, Über die Quantenmechanik der Elektronen in Kristallgittern, [Z. Phys.](#) **52** (1928), 555.
16. [[Blochl 1994a](#)] P.E. Blochl, Projector augmented wave method, [Phys. Rev. B](#) **50** (1994), 17953.

17. [[Blochl 1994b](#)] P. E. Blochl, O. Jepsen, and O. K. Andersen, Improved tetrahedron method for Brillouin-zone integrations, [Phys. Rev. B](#) **49** (1994), 16223.
18. [[Blugel 2006](#)] S. Blugel, Full-Potential Linearized Augmented Planewave Method, [NIC Series](#) **31** (2006), 85, Publication Series of the John von Neumann Institute for Computing, ed. J. Grotendorst, S. Blugel, D. Marx, ISBN: 3-00-017350-1.
19. [[Born 1927](#)] M. Born, J.R. Oppenheimer, Zur Quantentheorie der Molekullen, [Ann. Phys.](#) **389**(1927), 457.
20. [[Brooks 1997](#)] M.S.S. Brooks, Conduction Electrons in Magnetic Metals, [Matematisk-Fysiske Meddelelser](#) **45** (1997), 291, Royal Danish Academy of Science and Letters, Copenhagen, ISBN: 87-7304-287-0.
21. [[Brown 1940a](#)] W.F. Brown, Jr., Ferromagnetic domains and the magnetization curve, [J. Appl. Phys.](#) **11** (1940), 160.
22. [[Brown 1940b](#)] W.F. Brown, Jr., Theory of the Approach to Magnetic Saturation, [Phys. Rev.](#) **58** (1940), 736.
23. [[Brown 1941](#)] W.F. Brown, Jr., The Effect of Dislocations on Magnetization Near Saturation, [Phys. Rev.](#) **60** (1941), 139.
24. [[Cadogan 1988](#)] J.M. Cadogan, J.P. Gavigan, D. Givord, H.S Li, A new approach to the analysis of magnetisation measurements in rare-earth/transition-metal compounds: application to $Nd_2Fe_{14}B$, [J Phys. F: Met. Phys.](#) **18** (1988) 779.
25. [[Cai 2015](#)] G. Cai, Z. Wu, F. Guo, Y. Wu, H. Li, Q. Liu, M. Fu, T. Chen, J. Kang, First-principles calculations of perpendicular magnetic anisotropy in $Fe_{1-x}Co_x/MgO(001)$ thin films, [Nanoscale Research Letters](#) (2015) 10:126.
26. [[Capelle 2006](#)] K. Capelle, A bird's eye view of density functional theory, v. 5 (2006) – arXiv: [cond-mat/0211443v5](#).
27. [[Cheng 2012](#)] W. Cheng, S. Zhao, X. Cheng, X. Miao, Magnetic Moments in $SmCo_5$ and $SmCo_{5-x}Cu_x$ Films, [J. Supercond. Nov. Magn.](#) **25** (2012) 1947.
28. [[Cococcioni 2012](#)] M. Cococcioni, The LDA+U Approach: A Simple Hubbard Correction for Correlated Ground States, Correlated Electrons: From Models to Materials (Ed. E. Pavarini, E. Koch, F. Anders, M. Jarrell), Forschungszentrum Julich (2012), [ISBN: 9783893367962](#).
29. [[Coey 2010](#)] J.M.D. Coey, Magnetism and Magnetic Materials, Cambridge University Press (2010), [ISBN: 978-0-511-67743-4](#).
30. [[Cullity 2009](#)] B.D. Cullity, C.D. Graham, Introduction to Magnetic Materials, Wiley-IEEE Press, (2009), [ISBN: 978-0-471-47741-9](#).
31. [[Daalderop 1990](#)] G.H.O. Daalderop, P.J. Kelly, M.F.H. Schuurmans, First-principles calculation of the magnetocrystalline anisotropy energy of iron, cobalt, and nickel, [Phys. Rev. B](#) **41** (1990), 11919.
32. [[Daalderop 1996](#)] G.H.O. Daalderop, P.J. Kelly, M.F.H. Schuurmans, Magnetocrystalline anisotropy of YCo_5 and related $RECo_5$ compounds, [Phys. Rev. B](#) **53** (1996), 14415.
33. [[Demtroder 2010](#)] W. Demtroder, Experimentalphysik 3 (German), 4th Ed., Springer (2010), [ISBN: 978-3-642-03911-9](#).

34. [[Deportes 1976](#)] J. Deportes, D. Givord, J. Schweizer, F. Tasset, Different contributions of the two cobalt sites to the magnetocrystalline anisotropy of YCo_5 and related compounds, [IEEE Trans. Mag. 12 \(1976\), 1000](#).
35. [[Dirac 2010](#)] P.A.M. Dirac, The Principles of Quantum Mechanics, 4th Ed. – Intl. Series Monogr. Phys. 27 (Ed. J. Birman, S.F. Edwards, R.H. Friend, C.H. Llewellyn Smith, M. Rees, G. Veneyiano), Oxford University Press (2010), [ISBN: 978-0-19-852011-5](#).
36. [[Dubay 2017](#)] O. Dubay, p4vasp, the VASP Visualization Tool, [p4vasp.at](#) (Mar. 2017).
37. [[Dugdale 2016](#)] S.B. Dugdale, Life on the edge: a beginner's guide to the Fermi energy, [Phys. Scr. 91 \(2016\), 053009](#).
38. [[Durst 1987](#)] K.D. Durst, H.Kronmüller, The coercive field of sintered and melt-spun NdFeB magnets, [J. Magn. Magn. Mat. 68 \(1987\), 63](#).
39. [[Elizalde 2009](#)] J.T. Elizalde Galindo, F.J. Rivera Gómez, J.A. Matutes Aquino, High temperature magnetic properties of nanocrystalline $PrCo_5$ and YCo_5 alloys obtained by mechanical milling, [J. Appl. Phys. 105 \(2009\), 07A725](#).
40. [[Ermolenko 1976](#)] A.S. Ermolenko, Magnetocrystalline anisotropy of rare earth intermetallics, [IEEE Trans. Mag. 12 \(1976\), 992](#).
41. [[Eslava 2016](#)] G.G. Eslava, M. Ito, M. Yano, N.M. Dempsey, D. Givord, Calculation of magnetic properties of pseudo-ternary $R_2Fe_{14}B$ intermetallic compounds (R = rare earth, M = Fe, Co), [J. Sci. Adv. Mat. Dev. 1 \(2016\), 158](#).
42. [[Fidler 1982](#)] J. Fidler, Coercivity of precipitation hardened cobalt rare earth 17:2 permanent magnets, [J. Magn. Magn. Mat. 30 \(1982\), 58](#).
43. [[Fermi 1928](#)] E. Fermi, Eine statistische Methode zur Bestimmung einiger Eigenschaften des Atoms und ihre Anwendung auf die Theorie des periodischen Systems der Elemente, [Z. Physik. 48 \(1928\), 73](#).
44. [[Fock 1930](#)] V. Fock, Näherungsmethode zur Lösung des quantenmechanischen Mehrkörperproblems, [Z. Phys. 61 \(1930\), 126](#).
45. [[Frank 1932](#)] A. Frank, Temperature Variation of the Magnetic Susceptibility, Gyromagnetic Ratio, and Heat Capacity in Sm^{+++} and Eu^{+++} , [Phys. Rev. 39 \(1932\), 119](#).
46. [[Fruchart 1987](#)] R. Fruchart, P. L'Heritier, P. Dalmas de Reotier, D. Fruchart, P. Wolfers, J.M.D. Coey, L.P. Ferreira, R. Guillen, P. Vulliet, A. Yaouanc, Mossbauer Spectroscopy of $R_2Fe_{14}B$, [J. Phys. F: Met. Phys. 17 \(1987\) 483](#).
47. [[Gaspar 1954](#)] R. Gaspar, Über eine Approximation des Hartree-Fockschen Potentials Durch eine Universelle Potentialfunktion, [Acta. Phys. Hung. 3 \(1954\), 263](#).
48. [[Gerlach 1924](#)] W. Gerlach, O. Stern, Über die Richtungsquantelung im Magnetfeld, [Ann. Phys. 379 \(1924\), 673](#).
49. [[Givord 1979](#)] D. Givord, J. Laforest, J. Schweizer, F. Tasset, Temperature dependence of the samarium magnetic form factor in $SmCo_5$, [J. Appl. Phys. 50 \(1979\), 2008](#).

50. [[Givord 1985](#)] D. Givord, H.S. Li, Polarized neutron study of the compounds $Y_2Fe_{14}B$ and $Nd_2Fe_{14}B$, [J. Appl. Phys.](#) **57** (1985), 4100.
51. [[Givord 1988a](#)] D. Givord, P. Tenaud, T. Viadieu, Coercivity mechanisms in ferrites and rare earth transition metal sintered magnets ($SmCo_5$, Nd-Fe-B), [IEEE Trans. Magn.](#) **24** (1988), 1921.
52. [[Givord 1988b](#)] D. Givord, P.Tenaud, T.Viadieu, Angular dependence of coercivity in sintered magnets, [J. Magn. Magn. Mat.](#) **72** (1988), 247.
53. [[Grossinger 1986](#)] R.Grossinger, X.K.Sun, R.Eibler, K.H.J.Buschow, H.R.Kirchmayr, Temperature dependence of anisotropy fields and initial susceptibilities in $R_2Fe_{14}B$ compounds, [J. Magn. Magn. Mat.](#) **58** (1986), 55.
54. [[Gunnarson 1975](#)] O. Gunnarsson, H. Hjelmberg, Hydrogen Chemisorption by the Spin-density Functional Formalism. I, [Phys. Scr.](#) **11** (1975), 97).
55. [[Gunnarson 1976](#)] O. Gunnarsson, B. I. Lundqvist, Exchange and correlation in atoms, molecules, and solids by the spin-density-functional formalism, [Phys. Rev. B](#) **13** (1976), 4274.
56. [[Hartree 1928](#)] D.R. Hartree, The Wave Mechanics of an Atom with a Non-Coulomb Central Field. Part I. Theory and Methods, [Math. Proc. Camb. Philos. Soc.](#) **24** (1928), 89.
57. [[Heisenberg 1926](#)] W. Heisenberg, Mehrkörperproblem und Resonanz in der Quantenmechanik, [Z. Phys.](#) **38** (1926), 411.
58. [[Heisenberg 1928](#)] W. Heisenberg, Zur Theorie des Ferromagnetismus, [Z. Phys.](#) **49** (1928), 619.
59. [[Heitler 1927](#)] W. Heitler, F. London, Wechselwirkung neutraler Atome und homöopolare Bindung nach der Quantenmechanik, [Z. Phys.](#) **44** (1927), 455.
60. [[Herbst 1991](#)] J.F. Herbst, $Nd_2Fe_{14}B$ materials: Intrinsic properties and technological aspects, [Rev. Mod. Phys.](#) **63** (1991), 819.
61. [[Herring 1940](#)] C. Herring, A New Method for Calculating Wave Functions in Crystals, [Phys. Rev.](#) **57** (1940), 1169.
62. [[Hilzinger 1975](#)] H.R. Hilzinger, H. Kronmuller, Statistical theory of the pinning of Bloch walls by randomly distributed defects, [J. Magn. Magn. Mat.](#) **2** (1975), 11.
63. [[Hirosawa 1985](#)] S. Hirosawa, Y. Matsuura, H. Yamamoto, S. Fujimura, M. Sagawa, H. Yamauchi, Single Crystal Measurements of Anisotropy Constants of $R_2Fe_{14}B$, [Jpn. J. Appl. Phys.](#) **24** (1985), L803.
64. [[Hirosawa 1986a](#)] S. Hirosawa, Y. Matsuura, H. Yamamoto, S. Fujimura, M. Sagawa, H. Yamauchi, Magnetization and magnetic anisotropy of $R_2Fe_{14}B$ measured on single crystals, [J. Appl. Phys.](#) **59** (1986), 873.
65. [[Hirosawa 1986b](#)] S. Hirosawa, K. Tokuhara, Y. Matsuura, H. Yamamoto, S. Fujimura, M. Sagawa, The dependence of coercivity on anisotropy in sintered R-Fe-B permanent magnets, [J. Magn. Magn. Mat.](#) **61** (1986), 363.
66. [[Hoffer 1967](#)] G. Hoffer, K. Strnat, Magnetocrystalline Anisotropy of Two Yttrium-Cobalt Compounds, [J. Appl. Phys.](#) **38** (1967) 1377.

67. [[Hohenberg 1964](#)] P. Hohenberg, W. Kohn, Inhomogeneous Electron Gas, [Phys. Rev. **136** \(1964\), B864](#).
68. [[Hono 2018](#)] K. Hono, H. Sepehri-Amin, Prospect for HRE-free high coercivity Nd-Fe-B permanent magnets, [Scri. Mat. **151** \(2018\), 6](#).
69. [[Hrkac 2014](#)] G. Hrkac, K. Butler, T.G. Woodcock, L. Saharan, T. Schrefl, O. Gutfleisch, Modeling of Nd-Oxide Grain Boundary Phases in Nd-Fe-B Sintered Magnets, [JOM **66** \(2014\), 1138](#).
70. [[Huang 1987](#)] Y. Huang, C.H. Wu, Y. Chuang, F. Yang, F.R. de Boer, First-order magnetic transition in $(Nd, Pr)_2Fe_{14}B$, [J. Less Comm. Met. **132** \(1987\) 317](#).
71. [[Hubbard 1960](#)] W.M. Hubbard, E. Adams, J.V. Gilfrich, Magnetic Moments of Alloys of Gadolinium with Some of the Transition Elements, [J. Appl. Phys. **31** \(1960\), S365](#).
72. [[Hubbard 1963](#)] J. Hubbard, Electron correlations in narrow energy bands, [Proc. Roy. Soc. Lon. **A276** \(1963\), 238](#).
73. [[Hubbard 1979](#)] J. Hubbard, The magnetism of iron, [Phys. Rev. B **19** \(1979\), 2626](#).
74. [[Hutchings 1964](#)] M.T. Hutchings, Point-Charge Calculations of Energy Levels of Magnetic Ions in Crystalline Electric Fields, [Solid State Phys. Vol. **16** \(1964\), p. 227](#), Ed. F. Seitz, D. Turnbull, Academic Press.
75. [[INKSCAPE 1991](#)] [Inkscape: Vector Graph Freeware](#) (GNU General Public License), Copyright 1991 Free Software Foundation, Inc., 51 Franklin Street, Fifth Floor, Boston, MA 02110-1301, USA.
76. [[Jiles 1998](#)] D. Jiles, Introduction to magnetism and magnetic materials, 2nd Ed., Taylor & Francis (1998) – [ISBN 978-0-412-79860-3](#).
77. [[Johnson 1988](#)] D.D. Johnson, Modified Broyden's method for accelerating convergence in self-consistent calculations, [Phys. Rev. B **38** \(1988\), 12807](#).
78. [[Johansson 1979](#)] B. Johansson, Energy Position of 4f Levels in Rare-Earth Metals, [Phys. Rev. B **20** \(1979\), 1315](#).
79. [[Jones 2006](#)] R.O. Jones, Introduction to Density functional Theory and Exchange-Correlation Energy Functionals, [NIC Series **31** \(2006\), 45](#), Publication Series of the John von Neumann Institute for Computing, ed. J. Grotendorst, S. Blugel, D. Marx, ISBN: 3-00-017350-1.
80. [[Kasuya 1956](#)] T. Kasuya, A Theory of Metallic Ferro- and Antiferromagnetism on Zener's Model, [Prog. Theor. Phys. **16** \(1965\), 45](#).
81. [[Kittel 1987](#)] Ch. Kittel, Quantum Theory of Solids, 2nd Ed., Wiley (1987), [ISBN 978-0-471-62412-7](#).
82. [[Kittel 2006](#)] Ch. Kittel, Einführung in die Festkörperphysik, 14. Überarbeitete und erweiterte Auflage, (German) – Oldenburg (2006). Transl. from John Wiley & Sons, Inc. (2005) by S. Hunklinger, [ISBN: 978-3-486-57723-5](#).
83. [[Kleinmann 1983](#)] L. Kleinmann, Error in the tetrahedron integration scheme, [Phys. Rev. B **28** \(1983\), 1139\(R\)](#).
84. [[Koelling 1975](#)] D.D. Koelling, G.O. Arbman, Use of energy derivative of the radial solution in an augmented plane wave method: application to copper, [J. Phys. F: Metal Phys. **5** \(1975\), 2041](#).

85. [[Koelling 1977](#)] D.D. Koelling, B.N. Harmon, A technique for relativistic spin-polarised calculations, [J. Phys. C: Sol. Stat. Phys.](#) **10** (1977), 3107.
86. [[Kohn 1965](#)] W. Kohn, L.J. Sham, Self-Consistent Equations Including Exchange and Correlation Effects, [Phys. Rev.](#) **140** (1965), A1133.
87. [[Kou 1994](#)] X.C. Kou, H. Kronmuller, D. Givord, M.F. Rossignol, Coercivity mechanism of sintered $Pr_{17}Fe_{75}B_8$ and $Pr_{17}Fe_{53}B_{30}$ permanent magnets, [Phys. Rev. B](#) **50** (1994), 3849.
88. [[Krakauer 1979](#)] H. Krakauer, M. Posternak, A.J. Freeman, Linearized augmented plane-wave method for the electronic band structure of thin films, [Phys. Rev. B](#) **19** (1979), 1706.
89. [[Kresse 1996](#)] G. Kresse, J. Furthmuller, Efficient iterative schemes for ab initio total-energy calculations using a plane-wave basis set, [Phys. Rev. B](#) **54** (1996), 11169.
90. [[Kresse 1999](#)] G. Kresse, D. Joubert, From ultrasoft pseudopotentials to the projector augmented-wave method, [Phys. Rev. B](#) **59** (1999), 1758.
91. [[Kresse 2016](#)] G. Kresse, M. Marsman, J. Furthmuller, VASP the Guide, [Faculty of Physics, Universitat Wien \(2016\), Wien, Austria](#).
92. [[Kronmuller 1978](#)] H. Kronmuller, Micromagnetism in hard magnetic materials, [J. Magn. Magn. Mat.](#) **7** (1978), 341.
93. [[Kronmuller 1988](#)] H. Kronmuller, K.D. Durst, M. Sagawa, Analysis of the magnetic hardening mechanism in RE-FeB permanent magnets, [J. Magn. Magn. Mat.](#) **74** (1988), 291.
94. [[Kronmuller 2003](#)] H. Kronmuller, M. Fahnle, Micromagnetism and the Microstructure of Ferromagnetic Solids, Cambridge University Press (2003), [ISBN: 0521331358](#).
95. [[Kronmuller 2007](#)] H. Kronmuller, General Micromagnetic Theory, [Handbook of Magnetism and Advanced Magnetic Materials, vol. 2](#) (Ed. H. Kronmuller, S. Parkin, J.E. Miltat, M.R. Scheinfein), Wiley (2007), ISBN: 978-0-470-02217-7.
96. [[Kurth 2006](#)] S. Kurth, S. Pittalis, The Optimized Effective Potential Method and LDA+U, [NIC Series 31 \(2006\), 299](#), Publication Series of the John von Neumann Institute for Computing, ed. J. Grotendorst, S. Blugel, D. Marx, ISBN: 3-00-017350-1.
97. [[Lajaghre 2016](#)] K. Lajaghre et al., Reproducibility in density functional theory calculation of solids, [Science](#) **351** (2016), aad3000.
98. [[Landa 2018](#)] A. Landa, P. Soderlind, D. Parker, D. Aberg, V. Lordi, A. Perron, P.E.A. Turchi, R.K. Chouhan, D. Paudyal, T.A. Lograsso, Thermodynamics of $SmCo_5$ compound doped with Fe and Ni: An ab initio study, [J. Alloys Comp.](#) **765** (2018), 659.
99. [[Landau 1930](#)] L.D. Landau, Diamagnetismus der Metalle, [Z. Phys.](#) **64** (1930), 629.
100. [[Landau 1974](#)] L.L. Landau, E.M. Lifschitz: „*Lehrbuch der Theoretischen Physik, Vol. III: Quantenmechanik, 9. Auflage*“ (German) – Verlag Harri Deutsch (2007). Translation from Russian (Nauka, Moscow 1974) by A. Kühnel, [ISBN: 978-3-8171-1328-6](#).

101. [[Landau 1992](#)] L. Landau, E. Lifschitz, [3 - On the theory of the dispersion of magnetic permeability in ferromagnetic bodies](#), in Perspectives in Theoretical Physics (Ed. L.P. Pitaevski), Pergamon (1992), ISBN: 978-0-08-036364-6.
102. [[Lande 1923](#)] E. Lande, Termstruktur und Zeemaneffekt der Multipletts, [Z. Phys. 15 \(1923\), 189](#).
103. [[Langevin 1906](#)] P. Langevin, The Relations of Physics of Electrons to Other Branches of Science, Trans. B. Davis, [Cong. Arts Sci., Univ. Expos., St. Louis 1904, vol. 4 \(1906\), 121](#).
104. [[Langreth 1975](#)] D.C. Langreth, J.P. Perdew, The exchange-correlation energy of a metallic surface, [Solid State Commun. 17 \(1975\), 1425](#).
105. [[Larmor 1897](#)] J. Larmor, LXIII On the theory of the magnetic influence on spectra; and on the radiation from moving ions, [LED Phil. Mag. J. Sci. 44:271 \(1897\), 503](#).
106. [[Larson 2003a](#)] P. Larson, I.I. Mazin, D.A. Papaconstantopoulos, Calculation of magnetic anisotropy energy in $SmCo_5$, [Phys. Rev. B 67 \(2003\), 214405](#).
107. [[Larson 2003b](#)] P. Larson, I.I. Mazin, Calculation of magnetic anisotropy energy in YCo_5 , [J. Magn. Magn. Mat. 264 \(2003\), 7](#).
108. [[Larson 2004](#)] P. Larson, I.I. Mazin, D.A. Papaconstantopoulos, Effects of doping on the magnetic anisotropy energy in $SmCo_{5-x}Fe_x$ and $YCo_{5-x}Fe_x$, [Phys. Rev. B 69 \(2004\), 134408](#).
109. [[Li 2017](#)] H. Li, Y. Liang, X. Tan, H. Xu, P. Hu, K. Ren, Coercivity Mechanism of $(Nd_{0.8}Ce_{0.2})_{2.4}Fe_{12}Co_2B$ Ribbons with Ferromagnetic Grain Boundary Phase, [Materials 10 \(2017\), 1062](#).
110. [[Lifschitz 1980](#)] I.M. Lifshitz, M.I. Kaganov, Geometric concepts in electron theory of metals, in Electrons at Fermi Surface (Ed. M. Springford), Cambridge University Press (1980), ISBN: 9780521175067.
111. [[MacDonald 1980](#)] A.H. MacDonald, W.E. Pickett and D.D. Koelling, A linearised relativistic augmented-plane-wave method utilising approximate pure spin basis functions, [J. Phys. C: Sol. Stat. Phys. 13, 2675 \(1980\)](#).
112. [[Marcus 1967](#)] P.M. Marcus, Variational Methods in the Computation of Energy Bands, [Int. J. Quantum Chem. Suppl. 1, 567 \(1967\)](#).
113. [[Martin 2012](#)] R.M. Martin, Electronic Structure: Basic Theory and Practical Methods, Cambridge University Press (2012), ISBN: 9780511805769.
114. [[Methfessel 1989](#)] M. Methfessel, A.T. Paxton, High-precision sampling for Brillouin-zone integration in metals, [Phys. Rev. B 40 \(1989\) 3616](#).
115. [[Meyer 2006](#)] B. Meyer, The Pseudopotential Plane Wave Approach, [NIC Series 31 \(2006\), 71](#), Publication Series of the John von Neumann Institute for Computing, ed. J. Grotendorst, S. Blugel, D. Marx, ISBN: 3-00-017350-1.
116. [[Mitchel 1989](#)] I.V. Mitchell, J.M.D. Coey, D. Givord, I.R. Harris, R. Hanitsch, Concerted European Action on Magnets (CEAM) (Eds.), [Springer Dordrecht \(1989\)](#).
117. [[Miyake 2018](#)] T. Miyake, H. Akai, Quantum Theory of Rare-Earth Magnets, [J. Phys. Soc. Jpn. 87 \(2018\) 041009](#).

118. [[Mohn 2005](#)] P. Mohn, Magnetism in the Solid State, Springer Series in Solid State Sci. 134, Springer, 2nd Ed., (2005), [ISBN: 978-3-540-30981-9](#).
119. [[Momma 2011](#)] K. Momma, F. Izumi, VESTA 3 for three-dimensional visualization of crystal, volumetric and morphology data, [J. Appl. Crystallogr.](#) **44** (2011) 1272.
120. [[Monkhorst 1976](#)], H.J. Monkhorst, J.D. Pack, Special points for Brillouin-zone integrations, [Phys. Rev. B.](#) **13** (1976), 5188.
121. [[Moriya 1965](#)] T. Moriya, Spin Polarization in Dilute Magnetic Alloys: With Particular Reference to Palladium Alloys, [Prog. Theor. Phys.](#) **34** (1965), 329.
122. [[Morrish 2001](#)] A. H. Morrish, The Physical Principles of Magnetism, IEEE Press (2001), [ISBN: 978-0-7803-6029-7](#).
123. [[Moze 1989](#)] O. Moze, L. Pareti, G. Marusi, M. Solzi, W.I.F. David, Preferential site occupation in *Y* and *La* substituted $Pr_2Fe_{14}B$ intermetallic compounds, [Physica B](#) **156-157** (1989), 747.
124. [[Muller 2006](#)] Th. Muller, Basis Sets, Accuracy, and Calibration in Quantum Chemistry, [NIC Series](#) **31** (2006), 19, Publication Series of the John von Neumann Institute for Computing, ed. J. Grotendorst, S. Blugel, D. Marx, ISBN: 3-00-017350-1.
125. [[Nagel 1979](#)] H. Nagel, Coercivity and microstructure of $Sm(Co_{0.87}Cu_{0.13})_{7.8}$, [J. Appl. Phys.](#) **50** (1979), 1026.
126. [[Narasimhan 1974](#)] Narasimhan K.S.V.L., Wallace W.E., Hutchens R.D.: Effect of Tm and Er Substitution on the Magnetic Anisotropy of $NdCo_5$ and $PrCo_5$; Proc. Rare Earth Res. Conf., **11** (1974) 487-491.
127. [[Nesbitt 1959](#)] E.A. Nesbitt, J.H. Wernick, E. Corenzwit, Magnetic Moments of Alloys and Compounds of Iron and Cobalt with Rare Earth Metal Additions, [J. Appl. Phys.](#) **30** (1959), 365.
128. [[Nesbitt 1962](#)] E.A. Nesbitt, H.J. Williams, J.H. Wernick, R.C. Sherwood, Magnetic Moments of Intermetallic Compounds of Transition and Rare Earth Elements, [J. Appl. Phys.](#) **33** (1962) 1674.
129. [[Nguyen 2018](#)] M.C. Nguyen, Y. Yao, C.Z. Wang, K. Ho, V.P. Antropov, Magnetocrystalline anisotropy in cobalt based magnets: a choice of correlation parameters and the relativistic effects, [J. Phys.: Cond. Matter](#) **30** (2018), 195801.
130. [[Nordstrom 1992](#)] L. Nordstrom, M.S.S. Brooks, B. Johansson, Calculation of orbital magnetism and magnetocrystalline anisotropy energy in YCo_5 , [J. Phys.: Condens. Matter](#) **4** (1992), 3261.
131. [[Novak 2002](#)] P. Novák, Orbital Package in WIEN, Institute of Physics, Prague, Czech Republic (2002), available online at [WIEN2k Website](#).
132. [[Novak 2003](#)] P. Novak, J. Kunes, W.E. Pickett, W. Ku, F.R. Wagner, Self-interaction correction and contact hyperfine field, [Phys. Rev. B](#) **67** (2003), R140403.
133. [[Oesterreicher 1979](#)] H. Oesterreicher, F.T. Parker, M. Misroch, Giant intrinsic magnetic hardness in $SmCo_{5-x}Cu_x$, [J. Appl. Phys.](#) **50** (1979), 4273.
134. [[Ono 1981](#)] F. Ono, Magnetic Field Dependence of the Magnetocrystalline Anisotropy Energy in hcp Co, [J. Phys. Soc. Jpn.](#) **50** (1981), 2564.

135. [Owen 1955] J. Owen, The colours and magnetic properties of hydrated iron group salts, and evidence for covalent bonding, [Proc. Roy. Phys. Soc. A227 \(1955\), 183](#).
136. [Paige 1984] D.M. Paige, B. Szpunar, B.K. Tanner, The magnetocrystalline anisotropy of cobalt, [J. Magn. Magn. Mat. 44 \(1984\) 239](#).
137. [Pauli 1927] W. Pauli, Über Gasentartung und Paramagnetismus, [Z. Physik 41 \(1927\), 81](#).
138. [Pauling 1938] L. Pauling, The Nature of the Interatomic Forces in Metals, [Phys. Rev. 54 \(1938\), 899](#).
139. [Perdew 1996] J.P. Perdew, K. Burke, M. Ernzerhof, Generalized Gradient Approximation Made Simple, [Phys. Rev. Lett. 77 \(1996\), 3865](#).
140. [Perkins 1976] R.S. Perkins, J. Bernasconi, H.J. Wiesmann, Magnetic properties of Sm(Co,Cu) alloys. II. Coercivity mechanism, [J. Appl. Phys. 47 \(1976\), 2679](#).
141. [Perry 1975] A.J. Perry, A. Menth, Permanent magnets based on Sm(Co,Cu,Fe)_z, [IEEE Trans. Magn. 11 \(1975\), 1423](#).
142. [Pines 1954] D. Pines, Paramagnetic Susceptibility of Conduction Electrons, [Phys. Rev. 95 \(1954\), 1090](#).
143. [Pollack 2002] G.L. Pollack, D.R. Stump, Electromagnetism, Addison Wesley (2002), [ISBN: 978-0-8053-8567-0](#).
144. [Richter 1998] M. Richter, Band Structure Theory of Magnetism in 3d – 4f Compounds, [J. Phys. D: Appl. Phys. 31 \(1998\), 1017](#).
145. [Rodewald 2002] W. Rodewald, B. Wall, M. Katter, K. Uestuener, Top Nd-Fe-B Magnets with Greater Than 56 MGOe Energy Density and 9.8 kOe Coercivity, [IEEE Trans. Magn. 38 \(2002\), 2955](#).
146. [Rossignol 2005] M-F. Rossignol, J-P. Yonnet, Permanent Magnets, from Magnetism: Materials and Applications (Ed. E. du Trémolet de Lacheisserie, D. Gignoux, M. Schlenker), Springer-Verlag New York (2005), [ISBN: 978-0-387-23000-9](#).
147. [Rudermann 1954] M.A. Rudermann, C. Kittel, Indirect Exchange Coupling of Nuclear Magnetic Moments by Conduction Electrons, [Phys. Rev. 96 \(1954\), 99](#).
148. [Russell 1925] H.N. Russell, F.A. Saunders, New Regularities in the Spectra of the Alkaline Earths, [Astrophys. J. 61 \(1925\), 38](#).
149. [Saito 2014] T. Saito, D. Nishio-Hamane, Magnetic properties of SmCo_{5-x}Fe_x (x = 0 – 4) melt-spun ribbon, [J. All. Comp. 585 \(2014\), 423](#).
150. [Saito 2017] K. Saito, S. Doi, T. Abe, K. Ono, Quantitative evaluation of site preference in Dy-substituted Nd₂Fe₁₄B, [J. Alloy. Comp. 721 \(2017\), 476](#).
151. [Schwabl 2006] F. Schwabl, Statistische Mechanik (German), 3rd Ed., Springer (2006), [ISBN: 978-3-540-31095-2](#).
152. [Schwarz 2003] K. Schwarz, P. Blaha, Solid State Calculations Using WIEN2k, [Comput. Mat. Sci. 28 \(2003\), 259](#).

153. [[Schweizer 1980](#)] J. Schweizer, F. Tasset, Polarized neutron study of the RCO_5 intermetallic compounds. I. The cobalt magnetization in YCo_5 , [J. Phy. F Metal Phys. 10 \(1980\) 2799](#).
154. [[Schutz 1987](#)] G. Schutz, W. Wagner, W. Wilhelm, P. Kienle, R. Zeller, R. Frahm, G. Materlik, Absorption of circularly polarized x rays in iron, [Phys. Rev. Letters 58 \(1987\), 737](#).
155. [[Singh 2006](#)] D.J. Singh, L. Nordstrom, Planewaves, Pseudopotentials and the LAPW Method, 2nd Ed., Springer-Verlag US (2006), [ISBN: 978-0-387-29684-5](#).
156. [[Sinnema 1984](#)] S. Sinnema, R.J. Radwanski, J.J.M. Franse, D.B.de Mooij, K.H.J. Buschow, Magnetic properties of ternary rare-earth compounds of the type $R_2Fe_{14}B$, [J. Magn. Magn. Mat. 44 \(1984\), 333](#).
157. [[Slater 1929](#)] J.C. Slater, The Theory of Complex Spectra, [Phys. Rev. 34 \(1929\), 1293](#).
158. [[Slater 1937a](#)] J.C. Slater, Wave Functions in a Periodic Potential, [Phys. Rev. 51 \(1937\), 846](#).
159. [[Slater 1937b](#)] J.C. Slater, Electronic Structure of Alloys, [J. Appl. Phys. 8 \(1937\), 385](#).
160. [[Slater 1951a](#)] J.C. Slater, A Simplification of the Hartree-Fock Method, [Phys. Rev. 81 \(1951\), 385](#).
161. [[Slater 1951b](#)] J.C. Slater, Magnetic Effects and the Hartree-Fock Equation, [Phys. Rev. 82 \(1951\), 538](#).
162. [[Skokov 2018](#)] K.P. Skokov, O. Gutfleisch, Heavy rare earth free, free rare earth and rare earth free magnets - Vision and reality, [Scri. Mat. 154 \(2018\), 289](#).
163. [[Skomski 2008](#)] R. Skomski, Simple Models of Magnetism, Oxford University Press (2008), [ISBN: 9780198570752](#).
164. [[Skomski 2009](#)] R. Skomski, D.J. Sellmyer, Anisotropy of rare-earth magnets, [J. Rare Earths 27 \(2009\), 675](#).
165. [[Skomski 2016](#)] R. Skomski, Permanent Magnets: History, Current Research, and Outlook. Novel Functional Magnetic Materials (Ed. A. Zhukov), [Springer Series in Materials Science, vol 231](#). Springer (2016).
166. [[Soderlind 1994](#)] P. Soderlind, R. Ahuja, O. Eriksson, J.M. Wills, and B. Johansson, Crystal structure and elastic-constant anomalies in the magnetic $3d$ transition metals, [Phys. Rev. B 50 \(1994\), 5918](#).
167. [[Soderlind 2017](#)] P. Soderlind, A. Landa, I.L.M. Locht, A. Aberg, Y. Kvashnin, M. Pereiro, M. Dane, P.E.A. Turchi, V.P. Antropov, O. Eriksson, Prediction of the new efficient permanent magnet $SmCoNiFe_3$, [Phys. Rev. B 96 \(2017\), 100404R](#).
168. [[Son 2017](#)] K. Son, Tailored magnetic properties of exchange-spring and ultra hard nanomagnets ([Dissertation](#)), [Stuttgart University \(2017\)](#).
169. [[Staemmler 2006](#)] V. Staemmler, Introduction to Hartree-Fock and CI Methods, [NIC Series 31 \(2006\), 1](#), Publication Series of the John von Neumann Institute for Computing, ed. J. Grotendorst, S. Blugel, D. Marx, ISBN: 3-00-017350-1.
170. [[Steinbeck 2001](#)] L. Steinbeck, M. Richter, H. Eschrig, Itinerant-electron magnetocrystalline anisotropy energy of YCo_5 , [Phys. Rev. B 63 \(2001\), 184431](#).
171. [[Stevens 1951](#)] K.W.H. Stevens, Matrix Elements and Operator Equivalents Connected with the Magnetic Properties of Rare Earth Ions, [Proc. Phys. Soc. 65A \(1951\), 209](#).

172. [[Stoner 1933](#)] E.C. Stoner, Atomic moments in ferromagnetic metals and alloys with non-ferromagnetic elements, [LED Phil. Mag.](#) **15** (1933), 1018.
173. [[Stoner 1948](#)] E.C. Stoner, E.P. Wohlfarth, A mechanism of magnetic hysteresis in heterogeneous alloys, [Phil. Trans. Roy. Soc.](#) **240** (1948) 599.
174. [[Tatsumoto 1971](#)] E. Tatsumoto, T. Okamoto, H. Fuji, C. Inoue, Saturation magnetic moment and crystalline anisotropy of single crystals of light rare earth cobalt compounds RCo_5 , [J. Phys. Colloq.](#) **32** (1971), 550.
175. [[Thomas 1927](#)] L.H. Thomas, The calculation of atomic fields, [Math. Proc. Cambridge Philos. Soc.](#) **23** (1927), 542.
176. [[Toson 2016](#)] P. Toson, G.A. Zickler, J.Fidler, Do micromagnetic simulations correctly predict hard magnetic hysteresis properties?, [Physica B](#) **486** (2016), 142.
177. [[Tung 1982](#)] C.J. Tung, I. Said, G.E. Everett, Magnetic anisotropy constants of Fe and Ni at 77, 4.2, and 1.09 K: Interdomain configuration transitions in Ni, [J. Appl. Phys.](#) **53** (1982), 2044.
178. [[Tung 1999](#)] IC. Tung, HW. Zhang, SY. Yao, JC. Shih, BG. Shen, TS. Chin, Hard magnetic properties and microstructures of melt-spun $SmCo_5Fe_x$ ($x = 0, 1$ and 2) ribbons, [J. Phys. D: Appl. Phys.](#) **32** (1999), 1587.
179. [[van der Marel 1988](#)] D. van der Marel, G.A. Sawatzky, Electron-electron interaction and localization in d and f transition metals, [Phys. Rev. B](#) **37** (1988) 10674.
180. [[Van Vleck 1932](#)] J.H. Van Vleck, The Theory of Electric and Magnetic Susceptibilities, (Ed. R.H. Fowler, P. Kapitza), Oxford University Press (1932), [ISBN: 978-0-198-51243-1](#).
181. [[Velge 1968](#)] W.A.J.J. Velge, K.H.J. Buschow, Magnetic and Crystallographic Properties of Some Rare Earth Cobalt Compounds with $CaZn_5$ Structure, [J. Appl. Phys.](#) **39** (1968) 1717.
182. [[von Barth 1972](#)] U. von Barth, L. Hedin, A local exchange-correlation potential for the spin polarized case. I, [J. Phys. C: Solid State Physics](#) **5** (1972), 1629.
183. [[Wang 1996](#)] X. Wang, D. Wang, R. Wu, and A. J. Freeman, Validity of the force theorem for magnetocrystalline anisotropy, [J. Magn. Magn. Mat.](#) **159** (1996), 337.
184. [[Wernick 1959](#)] J.H. Wernick, S. Geller, Transition element-rare earth compounds Cu_5Ca structure, [Acta Cryst.](#) **12** (1959) 662-665.
185. [[Williams 1981](#)] A.R. Williams, R. Zeller, V.L. Moruzzi, C.D. Gelatt Jr., J. Kubler, Covalent magnetism: An alternative to the Stoner model, [J. Appl. Phys.](#) **52** (1981), 2067.
186. [[WP 2010](#)] Graph taken from [Wikipedia's article on magnetic hysteresis](#) (creator of graph: [RockMagnetist](#)), file created 09.2010 under CC1.0 , accessed 04.2019.
187. [[Yamada 1986](#)] O.Yamada, H.Tokuhara, F.Ono, M.Sagawa, Y.Matsuura, Magnetocrystalline anisotropy in $Nd_2Fe_{14}B$ intermetallic compound, [J. Magn. Magn. Mat.](#) **54-57** (1986), 585.
188. [[Yamauchi 1986](#)] H. Yamauchi, Magnetic Properties of $R_2Fe_{14}B$ Compounds, [JMMM](#) **54-57** (1986), 575.
189. [[Yi 2017](#)] M. Yi, H. Zhang, O. Gutfleisch, B.X. Xu, Multiscale Examination of Strain Effects in Nd-Fe-B Permanent Magnets, [Phys. Rev. Applied](#) **8** (2017), 014011.

190. [[Yin 2013](#)] S.Q. Yin, H. Wang, H.B. Zhao, Y. Jiang, J.P. Wang, The effects of Cu doping on crystalline structure and magnetic properties of $SmCo_{5-x}Cu_x$ thin films grown on Ru (0002), [J. Appl. Phys. 114 \(2013\), 213908](#).
191. [[Yosida 1957](#)] K. Yosida, Magnetic Properties of $Cu - Mn$ Alloys, [Phys. Rev. 106 \(1957\), 893](#).
192. [[Youhui 1998](#)] G. Youhui, Z. Jinghan, W. Yuqing, The nucleation process and magnetic interaction in nanocrystalline alloy $Nd_4Fe_{77}Co_3B_{16}$, [J. Appl. Phys. 84 \(1998\) 4388](#).
193. [[Yue 2008](#)] M. Yue, P.L. Niu, Y.L. Li, D.T. Zhang, W.Q. Liu, J.X. Zhang, C.H. Chen, S. Liu, D. Lee, A. Higgins, Structure and magnetic properties of bulk isotropic and anisotropic $Nd_2Fe_{14}B / \alpha - Fe$ nanocomposite permanent magnets with different $\alpha - Fe$ contents, [J. Appl. Phys. 103 \(2008\), 07E101](#).
194. [[Zeeman 1897](#)] P. Zeeman, On the influence of magnetism on the nature of the light emitted by a substance, [LED Phil. Mag. J. Sci. 43:262 \(1897\), 226](#).
195. [[Zeller 2006](#)] R. Zeller, Spin-Polarized DFT Calculations and Magnetism, [NIC Series 31 \(2006\), 419](#), Publication Series of the John von Neumann Institute for Computing, ed. J. Grotendorst, S. Blugel, D. Marx, ISBN: 3-00-017350-1.
196. [[Zickler 2016](#)] G.A. Zickler, J. Fidler, J. Bernardi, T. Schrefl, A. Asali, A Combined TEM/STEM and Micromagnetic Study of the Anisotropic Nature of Grain Boundaries and Coercivity in Nd-Fe-B Magnets, [Adv. Mat. Sci. Engin. vol. 2017, 6412042](#).
197. [[Zickler 2017](#)] G.A. Zickler, Influence of the real microstructure on hysteresis properties of novel hard magnets ([Dissertation Thesis, TU Wien, 2017](#)).
198. [[Zhang 1989](#)] Z. Zhang, Y. Huang, X.K. Sun, Y.C. Chuang, F. Yang, F.R. de Boer, R.J. Radwanski, Magnetic properties of $(Nd, Y)_2Fe_{14}B$ and $(Nd, Gd)_2Fe_{14}B$, [J. Less Comm. Met. 152 \(1989\), 67](#).
199. [[Zheng 2018](#)] M. Zheng, YK. Fang, LW. Song, R. Han, M-G. Zhu, W. Li, Magnetic properties and structures of Y-substituted Nd–Y–Fe–B melt-spun ribbons, [Rare Met. 2018](#).
200. [[Zitnan 1994](#)] P. Zitnan, The Rayleigh-Ritz method still competitive, [J. Comp. Appl. Math. 54 \(1994\), 297](#).
201. [[Zuo 2015](#)] WL. Zuo, X. Zhao, JF. Xiong, M. Zhang, TY. Zhao, FX. Hu, JR. Sun, BG. Shen, Strong textured $SmCo_5$ nanoflakes with ultrahigh coercivity prepared by multistep (three steps) surfactant-assisted ball milling, [Sci. Rep. 5 \(2015\) 13117](#).

List of Publications

- 1) A. Asali, J. Fidler, Influence of strain and substitution on magnetocrystalline anisotropy of $R_2Fe_{14}B$ ($R = Pr, Dy$ and Y), *J. Magn. Magn. Mat.* **488** (2019), 165370.
Article retrievable at <https://authors.elsevier.com/a/1Z8zJ15Kgb9u~e>.
- 2) Asali, J. Fidler, D. Suess, Influence of changes in electronic structure on magnetocrystalline anisotropy of YCo_5 and related compounds, *J. Magn. Magn. Mat.* **485** (2019), 61.
Article retrievable at <https://authors.elsevier.com/a/1Yw-B15Kgb6BHJ>.
- 3) G.A. Zickler, J. Fidler, J. Bernardi, T. Schrefl, A. Asali, A Combined TEM/STEM and Micromagnetic Study of the Anisotropic Nature of Grain Boundaries and Coercivity in Nd-Fe-B Magnets, *Adv. Mat. Sci. Eng.* (2017), 6412042.
- 4) P. McGuinness et al., Replacement and Original Magnet Engineering Options (ROME0): A European Seventh Framework Project to Develop Advanced Permanent Magnets Without, or with Reduced Use of, Critical Raw Materials, *JOM* **67** (2015), 1306.
- 5) P. Toson, A. Asali, G.A. Zickler, J. Fidler, Ab-Initio Study on the Hard Magnetic Properties of MnBi, *Phys. Proc.* **75** (2015), 1410.
- 6) G.A. Zickler, P. Toson, A. Asali, J. Fidler, Nanoanalytical TEM Studies and Micromagnetic Modelling of Nd-Fe-B Magnets, *Phys. Proc.* **75** (2015), 1442.
- 7) P. Toson, A. Asali, W. Wallisch, G. Zickler, J. Fidler, Nanostructured Hard Magnets: A Micromagnetic Study, *IEEE Trans. Magn.* **51** (2015), 7400104.
- 8) A. Asali, P. Toson, P. Blaha, J. Fidler, Dependence of Magnetic Anisotropy Energy on c/a Ratio of $X_2Fe_{14}B$ ($X = Y, Pr, Dy$), *IEEE Trans. Mag.* **50** (2014), 7027504.
- 9) P. Toson, W. Wallisch, A. Asali, J. Fidler, Modelling of Packed Co Nanorods for Hard Magnetic Applications, *EPJ Web of Conferences* **75** (2014), 03002.

List of Conference Contributions

- 1) A. Asali, G.A. Zickler, J. Fidler, Calculation of Magnetic Moments of Hard Magnetic $RECo_5$ Compounds, Junior European Congress and Exhibition on Advanced Materials and Processes 2016 (Junior EUROMAT, Lausanne, Switzerland).
- 2) G.A. Zickler, J. Fidler, A. Asali, D. Brown, J. Bernardi, [TEM/STEM study of rapidly quenched hard magnetic Nd-Fe-B ribbons \(poster\)](#), European Microscopy Congress 2016 (Lyon, France).
- 3) J. Fidler, G.A. Zickler, P. Toson, A. Asali, Combined TEM analysis and micromagnetic modelling of $Nd_2Fe_{14}B$ magnets, MMM INTERMAG Joint Conference 2016 (San Diego, USA).
- 4) G.A. Zickler, P. Toson, A. Asali, P. Tozman, M. Venkatesan, J.M.D. Coey, J. Fidler, Microstructural TEM-analysis of novel rare earth free permanent magnets (oral), 5th ASEM Workshop 2015 (ASEM, Graz, Austria).
- 5) G.A. Zickler, P. Toson, A. Asali, J. Bernardi, J. Fidler, Grain boundary chemistry of heavy rare earth free Nd-Fe-B permanent magnets (poster), 12th Multinational Congress on Microscopy 2015 (Eger, Hungary), Hungarian Academy of Sciences 2015, pp. 585-586.
- 6) J. Fidler, P. Toson, G.A. Zickler, A. Asali, Multiscale modelling of hard magnetic nanostructures (oral), International Workshop of the ARISTEIA Project 2015 (COMANA, Aegina, Greece).
- 7) G.A. Zickler, P. Toson, A. Asali, J. Fidler, Nanoanalytical TEM studies and micromagnetic modelling of (Nd,Pr)-Fe-B magnets (poster), 20th International Conference on Magnetism 2015 (ICM, Barcelona, Spain).
- 8) P. Toson, A. Asali, G.A. Zickler, J. Fidler, Ab-initio study on the hard magnetic properties of $MnBi$ (poster), 20th International Conference on Magnetism 2015 (ICM, Barcelona, Spain).
- 9) A. Asali, P. Toson, G.A. Zickler, J. Fidler, Comparison of potential approximations in electronic structure calculations of magnetic anisotropy energy of $PrCo_5$ and $Pr_2Fe_{14}B$ (poster), 20th International Conference on Magnetism 2015 (ICM, Barcelona, Spain).
- 10) J. Fidler, G.A. Zickler, P. Toson, A. Asali, Do Micromagnetic Simulations Correctly Predict Hard Magnetic Hysteresis Properties (oral), 10th International Symposium on Hysteresis Modelling and Micromagnetics 2015 (HMM, Isai, Romania).
- 11) J. Fidler, G.A. Zickler, A. Asali, P. Toson, Nanoanalytical TEM studies and multiscale modelling of Nd-Fe-B magnets (oral), G8 Symposium on Next Generation Permanent Magnets 2015 (ESICMM, Tsukuba, Japan).
- 12) J. Fidler, A. Asali, G.A. Zickler, P. Toson, M. Hajduga, T. Schrefl, Ab-Initio and Micromagnetic Calculations on Permanent Magnets, Intl. Workshop on Rare Earth and Future Permanent Magnets and Their Applications 2014 (REPM, Annapolis, USA), G. Hadjipanayis (Ed.), p. 231.
- 13) J. Fidler, A. Asali, P. Toson, G.A. Zickler, K. Zagar, Modelling of anisotropy and coercivity in novel hard magnets (oral), International Conferences on Modern Materials & Technology 2014 (CIMTEC, Montecatini, Italy).
- 14) P. Toson, A. Asali, W. Wallisch, G.A. Zickler, J. Fidler, Nanostructured Hard Magnets: A Micromagnetic Study (poster), 10th European Conference on Magnetic Sensors and Actuators 2014 (EMSA, Vienna, Austria).

- 15) J. Fidler, G.A. Zickler, P. Toson, A. Asali, Do micromagnetic simulations correctly predict hard magnetic hysteresis properties? (oral), Materials Science and Engineering Conference 2014 (MSE, Darmstadt, Germany).
- 16) J. Fidler, A. Asali, P. Toson, W. Wallisch, G.A. Zickler, K. Zagar, Advanced Hard Magnetic Materials Based on Shape and Crystal Anisotropy (oral), Materials Science and Engineering Conference 2014 (MSE, Darmstadt, Germany).
- 17) J. Fidler, A. Asali, P. Toson, G.A. Zickler, D. Suess, Modelling of anisotropy and coercivity in $RE_2Fe_{14}B$ ($RE = Pr, Dy$) magnets by electronic structure and micromagnetic calculations (oral), 59th Annual Magnetism and Magnetic Materials Conference 2014 (MMM, Honolulu, USA).
- 18) P. Toson, A. Asali, J. Fidler, R. Salikhov, M. Spasova, M. Farle, Magnetic Hardening of Nanorods with Antiferromagnetic Caps (oral), IEEE International Magnetism Conference 2014 (INTERMAG, Dresden, Germany).
- 19) A. Asali, P. Toson, P. Blaha, J. Fidler, Dependence of Magnetic Anisotropy Energy on c/a Ratio of $X_2Fe_{14}B$ ($X = Y, Pr, Dy$) (poster), IEEE International Magnetism Conference 2014 (INTERMAG, Dresden, Germany).
- 20) P. Toson, W. Wallisch, J. Fidler, A. Asali, Modelling of Packed Co Nanorod Structures for Hard Magnetic Applications (oral), Joint European Magnetic Symposia 2013 (JEMS, Rhodes, Greece).
- 21) W. Wallisch, P. Toson, A. Asali, H. Sassik, J. Fidler, Synthesis and analysis of $(Fe, Co)_{2-3}B$ microcrystalline alloys (poster), Joint European Magnetic Symposia 2013 (JEMS, Rhodes, Greece).

Curriculum Vitae

Personal Information

Name: Ahmad Asali
Current Residence: Vienna, Austria
Date of Birth: 22/Feb/1988
Place of Birth: Tehran, Iran
Nationality: Austria / Iran
Gender: Male

Work Experience

2017/10 – 2018/10 Project assistant (University of Vienna), tasks: atomistic numerical calculations of permanent magnets with DFT codes.
2013/05 – 2017/09 Project assistant (TU Vienna), tasks: atomistic numerical calculations of permanent magnetic properties of certain magnets, taking part in research projects, supervising a bachelor's students, writing master's and doctorate's theses.
2013/05 – 2014/12 Participation in two EU-FP7 projects on permanent magnets (ROME0, REFREPERMAG). Goal of the projects: development of new or improvement of currently produced permanent magnets to reduce use of strategic elements especially.

Education

2015/10 – 2019/06 Doctorate (Vienna University of Technology)
Tools: Density Functional Theory based codes "WIEN2k" and "VASP".
Thesis Subject: atomistic calculations of intrinsic magnetic properties in certain rare earth – transition metal compounds.
2012/11 – 2015/06 Master's (Vienna University of Technology).
Tool: The code "WIEN2k".
Thesis Subject: atomistic calculation of intrinsic properties of permanent magnets and their variation due to external strain effects.
2009/10 – 2012/11 Bachelor's (Vienna University of Technology).
Final project on "Magnetic measurement methods in technology"
2008/09 – 2009/06 University College (University of Leipzig) – course of technical studies

Appendix - Tabulated Results of Calculations

A-1 Results of WIEN2k Calculations

Lattice parameters in *nm*. EC: energy convergence (in *eV*), CC: charge convergence (in *C*) NCL: non-collinear, NSP: non-spin polarized, SR: scalar-relativistic, SOC: spin-orbit coupling, RK: RK_{max} , NM: non-magnetic, FM: ferromagnetic, AFM: anti-ferromagnetic, OPT: optimized, REL: relaxed, OPEL: optimization and relaxation, f.u.: formula unit, ENCUT= 500 *eV*, unless specified.

$Pr_2Fe_{14}B$

Here MAE is obtained from two calculations, one magnetized in [001] from start and the other in [110] from start.

Q	c/a	d(c)	ENE-SOC[001] (eV)	MAE [MJ/m ³]	MAG [μ B/fu]
q_4	1.3414	-3.58%	-3949506.6675720	-6.4	25.1
q_6	1.3913	0%	-3949500.8961249	4.6	29.7
q_3	1.4412	+3.58%	-3949492.1211012	6.6	30.8

1) $Pr_2Fe_{14}B$ "w_Q" – (a;c)=(0.880;1.224); 5, 50 k-pts.; RK=7; LDA; d(a)=0; d(c)≠0; AFM; SOC=1 it.

C1	c/a	d(c)	ENE-SOC[001] (eV)	MAE [MJ/m ³]	Total-MAG [μ B/fu]
c_101	1.3217	-5%	-3954334.9658184	-17.5	29.5
c_102	1.3356	-4%	-3954336.2260845	16.2	28.8
c_103	1.3496	-3%	-3954336.2888588	15.1	29.0
c_104	1.3635	-2%	-3954336.2126958	14.5	29.2
c_105	1.3774	-1%	-3954335.0547470	54.4	29.9
c_106	1.3913	0%	-3954335.6868240	9.2	29.7
c_107	1.4052	+1%	-3954335.2725848	6.9	29.8
c_108	1.4191	+2%	-3954334.6728142	19.9	30.2
c_109	1.4330	+3%	-3954334.0350718	-25.5	30.3
c_110	1.4469	+4%	-3954332.5296032	-27.0	31.5
c_111	1.4609	+5%	-3954332.4599835	-1.6	30.8

2) $Pr_2Fe_{14}B$ "w_C1" – (a;c)=(0.880;1.224); 100 k-pts.; RK=8; GGA; RLO=Pr; d(a)=0; d(c)≠0; AFM; SOC=1 it.

D3	c/a	d(c/a)	SOC [001] (eV)	MAE [MJ/m ³]	MAG [μ B/fu]
d_301	1.3216	-5%	-3949457.3618751	6.2	30.0
d_302	1.3355	-4%	-3949457.5139505	6.2	30.1
d_303	1.3494	-3%	-3949457.5731138	6.2	30.2
d_304	1.3634	-2%	-3949457.6493535	6.0	30.4
d_305	1.3773	-1%	-3949457.6847822	5.8	29.9
d_306	1.3912	0%	-3949457.6452484	5.6	30.5
d_307	1.4051	+1%	-3949457.5975963	3.9	30.3
d_308	1.4190	+2%			
d_309	1.4329	+3%	-3949457.3208730	5.1	30.5
d_310	1.4468	+4%	-3949457.1566088	5.2	30.3
d_311	1.4607	+5%	-3949456.9534808	5.9	30.0

3) $Pr_2Fe_{14}B$ "w_D1, D3" – (a;c)=(0.880;1.224); 500 k-pts.; RK=8; LDA; d(V)=0; AFM; SOC conv.; 4 cores.

E1	c/a	d(c/a)	SOC [001] (eV)	MAE [MJ/m ³]	MAG [μ B/fu]
e_101	1.3216	-5%	-3954335.6222990		29.5
e_102	1.3355	-4%	-3954335.8123189		29.7
e_103	1.3494	-3%	-3954335.8961257		29.7
e_104	1.3634	-2%	-3954335.9709971		
e_105	1.3773	-1%	-3954336.0303355		
e_106	1.3912	0%	-3954335.9846743		29.7
e_107	1.4051	+1%	-3956929.0236364		
e_108	1.4190	+2%			

e_109	1.4329	+3%	-3954335.5989644		29.9
e_110	1.4468	+4%	-3954335.3693124		29.7
e_111	1.4607	+5%	-3954333.5229144		31.8

4) $Pr_2Fe_{14}B$ “w_E1” – (a;c)=(0.880;1.224); 200 k-pts.; RK=8; GGA; d(V)=0; AFM; SOC=conv.

Instead of giving both U and J , the method uses $U_{eff} = (U - J)$ with $J = 0$. 4f –electrons considered as valence.

E30-SOC	c/a	U_eff	SOC [001] (eV)	MAE [MJ/m ³]	MAG [μB/fu]
e_301	1.3912	1 eV	-3954335.6420954	0.6	29.8
e_302	1.3912	2 eV	-3954335.6420912	0.6	29.7
e_303	1.3912	3 eV	-3954335.6420814	0.6	29.8
e_304	1.3912	4 eV	-3954335.6420825	0.6	29.8
e_305	1.3912	5 eV	-3954335.6420808		29.8
E30+U	c/a	U_eff	SOC+U [001] (eV)	MAE [MJ/m ³]	MAG [μB/fu]
e_301	1.3912	1 eV	-3954332.8950820	-11.6	29.6
e_302	1.3912	2 eV	-3954335.6420842	729.7	28.3
e_303	1.3912	3 eV	-3954330.2450421	-14.3	29.6
e_304	1.3912	4 eV	-3954329.4152999	-21.6	29.7
e_305	1.3912	5 eV	-3954328.7249775	-13.4	29.6

5) $Pr_2Fe_{14}B$ “w_E30” – (a;c)=(0.880;1.224); 200 k-pts.; RK=8; GGA(+U); AFM; SOC+U=conv.

$Pr_2Co_{14}B$

B1-FM	c/a	d(c/a)	SOC (1 it) [001] (eV)	MAE [MJ/m ³]	MAG [μB/fu]
b_101	1.3079	-5%	-4138332.7932320	-15.8	20.1
b_102	1.3216	-4%	-4138323.6446781	-11.0	20.5
b_103	1.3354	-3%	-4138293.7908043	-15.2	20.2
b_104	1.3492	-2%	-4138300.9403629	-16.3	20.3
b_105	1.3629	-1%	-4138225.9109903	5.1	21.1
b_106	1.3767	0%	-4138284.6976276	4.9	20.9
b_107	1.3905	+1%	-4138225.5893384	-2.2	21.8
b_108	1.4042	+2%	-4138269.1974049	0.2	23.0
b_109	1.4180	+3%	-4138280.1799908	-0.1	21.6
b_110	1.4318	+4%	-4138281.2383159	-1.7	21.2
b_111	1.4455	+5%	-4138274.7340544	-0.4	22.5
B2-AFM	c/a	d(c/a)	SOC (1 it) [001] (eV)	MAE [MJ/m ³]	MAG [μB/fu]
b_201	1.3079	-5%	-4138298.7314024	-14.4	17.4
b_202	1.3216	-4%	-4138294.4829163	41.0	17.3
b_203	1.3354	-3%	-4138315.6443547	-14.3	17.6
b_204	1.3492	-2%	-4138324.3594296	-15.7	17.6
b_205	1.3629	-1%	-4138224.6093053	3.1	18.2
b_206	1.3767	0%	-4138283.6118090	1.0	18.4
b_207	1.3905	+1%	-4138224.7408502	-1.9	18.6
b_208	1.4042	+2%	-4138226.2120151	3.3	19.7
b_209	1.4180	+3%	-4138282.2365404	0.5	19.0
b_210	1.4318	+4%	-4138271.6345557	0.3	19.1
b_211	1.4455	+5%	-4138284.7607193	-0.2	19.6

1) $Pr_2Co_{14}B$ “w_B1, B2” – (a;c)=(0.864;1.189); 20 k-pts.; RK=7; GGA; d(a)=0; d(c)≠0; RLO=Pr; SOC=1 it.

$Nd_2Fe_{14}B$ (calculated collinearly)

A1-GGA	c/a	d(c/a)	SOC (conv) [001] (eV)	MAE [MJ/m ³]	MAG [μB/fu]
a_101	1.3164	-5%	-4038643.6548039	3.7	28.3
a_102	1.3303	-4%	-4038643.7034656	1.2	30.9
a_103	1.3441	-3%	-4038643.8184929	7.8	28.5
a_104	1.3580	-2%	-4038643.9846478	3.5	28.5
a_105	1.3719	-1%	-4038644.0511199	4.6	28.4
a_106	1.3857	0%	-4038643.8822166	3.6	28.5
a_107	1.3996	+1%	-4038644.0784847	2.0	28.4

a_108	1.4134	+2%	-4038643.9409787	3.2	30.1
a_109	1.4273	+3%	-4038643.7855600	2.8	28.5
a_110	1.4411	+4%	-4038643.5588747	4.5	28.5
a_111	1.4550	+5%	-4038643.2942943	3.2	28.6
A2-LDA	c/a	d(c/a)	SOC (conv) [001] (eV)	MAE [MJ/m ³]	MAG [μB/fu]
a_201	1.3164	-5%	-4033728.6912696	15.6	30.5
a_202	1.3303	-4%	-4033728.8523805	14.6	30.6
a_203	1.3441	-3%	-4033729.0028666	15.0	30.7
a_204	1.3580	-2%	-4033729.0166186	15.1	30.7
a_205	1.3719	-1%	-4033729.0898780	14.5	30.8
a_206	1.3857	0%	-4033729.0662195	13.9	30.9
a_207	1.3996	+1%	-4033729.0380960	13.4	30.9
a_208	1.4134	+2%	-4033728.9240755	-0.5	30.4
a_209	1.4273	+3%	-4033728.7658587	-1.6	30.3
a_210	1.4411	+4%	-4033728.6150007	2.9	30.0
a_211	1.4550	+5%	-4033728.4343476	5.7	29.5

1) $Nd_2Fe_{14}B$ "w_A2" – (a;c)=(0.880;1.220); 200 k-pts.; RK=7; LDA; AFM; SOC=conv.; d(a)=0; d(c)≠0.

$Dy_2Fe_{14}B$

B2	c/a	d(c/a)	SOC (1 it) [001] (eV)	MAE [MJ/m ³]	MAG [μB/fu]
b_201	1.2859	-5%	-4591212.7843448	21.2	14.7
b_202	1.2994	-4%	-4591213.5041921	-22.6	15.7
b_203	1.3129	-3%	-4591214.2857498	8.3	15.9
b_204	1.3265	-2%	-4591214.6926758	-23.2	16.4
b_205	1.3400	-1%	-4591215.5349898	8.4	16.5
b_206	1.3535	0%	-4591215.6838587	-1.0	17.3
b_207	1.3671	+1%	-4591215.8518040	20.2	17.2
b_208	1.3801	+2%	-4591215.7338301	14.3	17.9
b_209	1.3941	+3%	-4591215.3531787	18.3	17.3
b_210	1.4077	+4%	-4591215.0468715	21.0	17.8
b_211	1.4212	+5%	-4591214.5880301	17.9	18.0
C2	c/a	d(c/a)	SOC (1 it) [001] (eV)	MAE [MJ/m ³]	MAG [μB/fu]
c_202	1.2994	-4%	-4591213.3939083	-21.5	15.4
c_203	1.3129	-3%	-4591214.6135519	-13.0	16.1
c_204	1.3265	-2%	-4591215.2374850	13.8	16.7
c_205	1.3400	-1%	-4591215.6320044	11.8	24.2
c_206	1.3535	0%	-4591215.6644254	24.0	16.7
c_207	1.3671	+1%	-4590495.6581477	19.8	21.0
c_208	1.3801	+2%	-4591216.0176425	22.5	24.4
c_209	1.3941	+3%	-4591215.7074900	6.8	17.9
c_210	1.4077	+4%	-4591215.0024463	10.2	25.1
c_211	1.4212	+5%	-4591214.4928556	-10.1	25.5
C5	c/a	d(c/a)	SOC (1 it) [001] (eV)	MAE [MJ/m ³]	MAG [μB/fu]
c_501	1.2859	-5%	-4591212.7372415	-17.3	15.5
c_502	1.2994	-4%	-4591213.6276446	18.2	15.4
c_503	1.3129	-3%	-4591214.6830581	3.7	16.1
c_504	1.3265	-2%	-4591215.0289034	-24.6	23.8
c_505	1.3400	-1%	-4591215.4353101	5.3	16.6
c_506	1.3535	0%	-4591215.6510383	-2.8	17.7
c_507	1.3671	+1%	-4591215.7080363	12.2	21.1
c_508	1.3801	+2%	-4591215.8366056	-1.5	24.4
c_509	1.3941	+3%	-4591215.6765222	-12.0	25.4
c_510	1.4077	+4%	-4591214.9785622	-3.3	25.5
c_511	1.4212	+5%	-4591214.5891525	12.8	25.2

1) $Dy_2Fe_{14}B$ "w_B2, C2, C5" – (a;c)=(0.874;1.183); 50(B2) + 100 (C2) + 500(C5) k-pts.; RK=7; GGA; d(a)=0; d(c)≠0; AFM; SOC=1 it.

$Dy_2Co_{14}B$

B1	c/a	d(c/a)	SOC (1 it) [001] (eV)	MAE [MJ/m ³]	MAG [μB/fu]
b_101	1.2678	-5%	-4775178.8599826	13.2	27.7
b_102	1.2811	-4%	-4775227.8710517	-21.5	22.3
b_103	1.2945	-3%	-4775244.8060822	5.4	23.3
b_104	1.3078	-2%	-4775155.1539938	11.0	24.5
b_105	1.3211	-1%	-4775227.0537849	-15.7	25.0
b_106	1.3345	0%	-4775221.4384663	16.0	24.4
b_107	1.3478	+1%	-4775215.7865369	8.5	24.1
b_108	1.3612	+2%	-4775110.5746937	3.5	28.5
b_109	1.3745	+3%	-4775165.3827187	-2.7	30.0
b_110	1.3879	+4%	-4775181.4514147	9.7	27.0
b_111	1.4012	+5%	-4775165.5687160	-3.2	29.4

1) $Dy_2Co_{14}B$ "w_B1" – (a;c)=(0.874;1.183); 20 k-pts.; RK=7; GGA; RLO=Dy; d(a)=0; d(c)≠0; AFM; SOC=1 it.

$Y_2Fe_{14}B$

B1	c/a	d(c)	SOC (1 it) [001] (eV)	MAE [MJ/m ³]	MAG [μB/fu]
b_101	1.3046	-5%	-2679298.0795432	0.79	29.2
b_102	1.3183	-4%	-2679299.1011586	0.50	30.0
b_103	1.3320	-3%	-2679299.5434122	0.31	30.5
b_104	1.3458	-2%	-2679299.8099817	0.39	31.0
b_105	1.3595	-1%	-2679299.4295264	0.44	31.1
b_106	1.3732	0%	-2679299.3803053	0.42	31.3
b_107	1.3870	+1%	-2679299.5326083	0.41	31.5
b_108	1.4007	+2%	-2679299.1931323	0.41	31.7
b_109	1.4144	+3%	-2679298.7157697	0.45	31.8
b_110	1.4282	+4%	-2679298.1418185	0.43	31.9
b_111	1.4419	+5%	-2679297.4643824	0.44	32.2

1) $Y_2Fe_{14}B$ "w_A1, B1" – (a;c)=(0.875;1.202); 20 k-pts.; RK=9; GGA; RLO=Y+Fe; d(a)=0; d(c)≠0; SRC=conv.

C2	c/a	d(c)	SOC (1 it) [001] (eV)	MAE [MJ/m ³]	MAG [μB/fu]
c_201	1.3046	-5%	-2679298.5081024	0.66	30.5
c_202	1.3183	-4%	-2679299.1022668	0.51	30.5
c_203	1.3320	-3%	-2679299.5395181	0.40	30.7
c_204	1.3458	-2%	-2679299.7962066	0.42	30.9
c_205	1.3595	-1%	-2679300.2108976	0.44	31.2
c_206	1.3732	0%	-2679299.8244544	0.49	31.5
c_207	1.3870	+1%	-2679299.6278220	0.50	31.6
c_208	1.4007	+2%	-2679299.3075701	0.46	31.8
c_209	1.4144	+3%	-2679298.8502488	0.48	32.0
c_210	1.4282	+4%	-2679298.5729069	0.46	32.2
c_211	1.4419	+5%	-2679297.8515054	0.46	32.4
C5	c/a	d(c/a)	SOC (1 it) [001] (eV)	MAE [MJ/m ³]	MAG [μB/fu]
c_501	1.3046	-5%	-2679310.9758788	-0.66	30.0
c_502	1.3183	-4%	-2679311.5463673	-0.23	30.3
c_503	1.3320	-3%	-2679312.2935966	-0.47	30.7
c_504	1.3458	-2%	-2679311.6965401	-0.18	31.1
c_505	1.3595	-1%	-2679300.2290959	0.43	31.3
c_506	1.3732	0%	-2679313.0942733	0.79	31.5
c_507	1.3870	+1%	-2679299.6588982	0.44	31.6
c_508	1.4007	+2%	-2679315.1424340	0.09	31.8
c_509	1.4144	+3%	-2679312.8613967	1.16	32.0
c_510	1.4282	+4%	-36453921.816229	1.03	32.2
c_511	1.4419	+5%	-2679301.3382974	-0.01	26.1

2) $Y_2Fe_{14}B$ "w_C2, C5" – (a;c)=(0.875;1.202); 100 (C2) + 500 (C5) k-pts.; RK=7; GGA; d(V)=0; SRC=conv.

$Y_2Co_{14}B$

B1	c/a	d(c)	SOC (1 it) [001] (eV)	MAE [MJ/m ³]	MAG [μB/fu]
----	-----	------	-----------------------	--------------------------	-------------

b_101	1.2953	-5%	-2863188.0961478	0.7	18.7
b_102	1.3090	-4%	-38955672.742048	16.5	19.0
b_103	1.3226	-3%	-2863261.2776861	438.0	18.9
b_104	1.3363	-2%	-2863188.7816153	0.7	18.8
b_105	1.3499	-1%	-2863190.4651147	10.2	19.0
b_106	1.3636	0%	-2863196.4988774	1.1	19.8
b_107	1.3772	+1%	-38955787.067050	1.0	20.2
b_108	1.3908	+2%	-2863191.4611762	1.1	20.3
b_109	1.4044	+3%	-2863243.7813381	0.4	20.6
b_110	1.4181	+4%	-2863253.3272696	6.5	20.9
b_111	1.4317	+5%	-2863244.9480076	6.4	21.2

1) $Y_2Co_{14}B$ “w_B1” – (a;c)=(0.861;1.174); 20 k-pts.; RK=7; GGA; RLO=Y; d(a)=0; d(c)≠0; SRC=conv.

PrCo₅

A	XC	Coupling	SOC (conv) [001] (eV)	MAE [MJ/m ³]	MAG [μB/fu]
a_1	LDA	AFM	-440602.70536217	-4.3	7.1
a_2	LDA	FM	-440602.71709885	-4.9	7.1
a_3	GGA	AFM	-441102.32808412	8.7	7.0
a_4	GGA	FM	-441102.34696638	2.4	7.0

1) $PrCo_5$ “w_A” – (a;c)=(0.5025;0.3943); 5000 k-pts.; RK=8; LDA; GGA; RLO=Pr; FM+AFM; SOC=conv.

B4-SOC	U (eV)	SOC (conv) [001] (eV)	MAE [MJ/m ³]	Spin-MAG [μB/fu]
b_401	4.15	-441102.30676794	0.59	4.99
b_402	4.25	-441102.30676780	0.59	4.99
b_403	4.35	-441102.30677338	0.61	4.99
b_404	4.45	-441102.30677229	0.52	4.99
b_405	4.55	-441102.30677229	0.60	4.99
b_406	4.65	-441102.30677243	0.61	4.99
b_407	4.75	-441102.30677325	0.61	4.99
B4+U	U (eV)	+U (conv) [001] (eV)	MAE [MJ/m ³]	Total-MAG [μB/fu]
b_401	4.15	-441101.25394324	-117.2	7.50
b_402	4.25	-441102.30676780	185.7	6.69
b_403	4.35	-441101.23158472	-120.0	7.50
b_404	4.45	-441101.22139637	-121.4	7.50
b_405	4.55	-441101.21152856	-122.4	7.50
b_406	4.65	-441101.20038142	-123.4	7.47
b_407	4.75	-441101.19083239	-124.7	6.74

2) $PrCo_5$ “w_B4” – (a;c)=(0.5025;0.3943); 5000 k-pts.; RK=8; GGA(+U), RLO=none, AFM, f-electrons: valence, +U=conv, U=4.15, 4.25, 4.35, 4.45, 4.55, 4.65, 4.75 eV.

B5-SOC	U (eV)	SOC (conv) [001] (eV)	MAE [MJ/m ³]	Spin-MAG [μB/fu]
b_501	4.15	-441087.16682007	0.07	6.47
b_502	4.25	-441087.16682047	0.07	6.47
b_503	4.35	-441087.16682020	0.07	6.47
b_504	4.45	-441087.16682088	0.07	6.47
b_505	4.55	-441087.16682020	0.07	6.47
b_506	4.65	-441087.16682088	0.07	6.47
b_507	4.75	-441087.16682007	0.07	6.47
B5+U	U (eV)	+U (conv) [001] (eV)	MAE [MJ/m ³]	Total-MAG [μB/fu]
b_501	4.15	-441087.11778050	0.31	6.95
b_502	4.25	-441087.11660878	0.15	6.95
b_503	4.35	-441087.11536957	0.15	6.95
b_504	4.45	-441087.11428778	0.15	6.95
b_505	4.55	-441087.11320736	0.15	6.95
b_506	4.65	-441087.11196407	0.13	6.95
b_507	4.75	-441087.11089901	0.15	6.95

3) $PrCo_5$ “w_B5” – (a;c)=(0.503;0.394); 5000 k-pts.; RK=8; GGA(+U); RLO=none; AFM; f-elect.: core; +U=conv.

SmCo₅

U1	k-points	SOC (1 it) [001] (eV)	MAE [MJ/m ³]	Total-MAG [μB/fu]
u_101	50	-473433.33887675	-1.67	11.2
u_102	100	-473433.30602171	1.74	10.4
u_103	500	-473433.29198825	0.73	10.5
u_104	1000	-473433.28976644	0.31	10.6
u_105	5000	-473433.29055652	0.31	10.6
u_106	10,000	-473433.29069870	0.32	10.6
u_107	20,000	-473433.29058169	0.35	10.6

1) SmCo₅ “w_U1” – (a;c)=(0.5002;0.3961); 50 ... 20,000 k-pts.; RK=9; GGA; RLO=none; AFM; SR=conv.

T1	c/a	d(c/a)	SOC (1 it) [001] (eV)	MAE [MJ/m ³]	Total-MAG [μB/fu]
t_11	0.7636	+3.8%	-473432.18554295	-9.6	10.2
t_12	0.7920	0%	-473432.63882399	-16.9	10.4
t_13	0.8204	-3.8%	-473433.33008570	-8.3	10.6
T2	c/a	d(c/a)	SOC (1 it) [001] (eV)	MAE [MJ/m ³]	Total-MAG [μB/fu]
t_21	0.7636	+3.8%	-473432.44712855	23.8	10.0
t_22	0.7920	0%	-473432.85198950	70.3	10.2
t_23	0.8204	-3.8%	-473432.32478321	16.2	10.1

2) SmCo₅ “w_T1, T2” – (a;c)=(0.500;0.396); 5000(T1) + 50000(T2) k-pts.; RK=7; GGA; d(a)=0; d(c)≠0; RLO=Sm+Co; FM; SR=conv.

A0	RK	SOC (1 it) [001] (eV)	MAE [MJ/m ³]	Total-MAG [μB/fu]
a_01	7	-473433.59424210	0.44	10.5
a_02	8	-473433.63316024	0.52	10.5

3) SmCo₅ “w_A0” – (a;c)=(0.499;0.3968) (10,000 k-pts.; RK=7+8; GGA; RLO=none; AFM; SR=conv.

B1-AFM	b_101 (RK 7)		b_102 (RK 8)		b_103 (RK 9)	
d(c/a)	SCF (conv)	Spin	SCF (conv)	Spin	SCF (conv)	Spin
-10%	-473535.13318363	13.2	-473536.35412019	13.2	-473536.59672462	13.0
-5%	-473535.29949777	13.1	-473536.47100539	13.1	-473536.74821727	13.0
0%	-473535.32871996	13.0	-473536.48839524	13.1	-473536.77979310	12.9
+5%	-473535.27995850	12.9	-473536.43300086	12.9	-473536.71817248	12.9
+10%	-473535.11312583	12.8	-473536.26540179	12.9	-473536.55968270	12.8

4) SmCo₅ “w_B1” – (a;c)=(0.499;0.3968); 10,000 k-pts.; RK=7+8+9; GGA; RLO=none; AFM; SR=conv.

B2-GGA	c/a	d(c/a)	SOC (1 it) [001] (eV)	MAE [MJ/m ³]	MAG [μB/fu]
b_201	0.7554	-5%	-473432.11199395	0.01	10.3
b_202	0.7634	-4%	-473432.16122304	-0.15	10.3
b_203	0.7713	-3%	-473432.19070699	0.07	10.4
b_204	0.7793	-2%	-473432.22659338	0.41	10.4
b_205	0.7873	-1%	-473432.22450232	1.02	10.5
b_206	0.7952	0%	-473432.22762755	1.36	10.5
b_207	0.8031	+1%	-473432.19937627	1.83	10.5
b_208	0.8111	+2%	-473432.17791233	2.44	10.7
b_209	0.8190	+3%	-473432.12720974	2.54	10.7
b_210	0.8270	+4%	-473432.03971150	2.44	10.8
b_211	0.8350	+5%	-473431.96203358	2.53	10.8
B3-LDA	c/a	d(c/a)	SOC (1 it) [001] (eV)	MAE [MJ/m ³]	MAG [μB/fu]
b_307	0.7554	-5%	-473536.42031613	33.3	11.3
b_308	0.7634	-4%	-473536.44953151	-161.1	11.2
b_309	0.7713	-3%	-473535.20804177	-2724.5	10.9
b_310	0.7793	-2%	-473536.53378044	-248.7	10.9
b_311	0.7873	-1%	-473536.69363161	13.3	10.9
b_301	0.7952	0%	-473536.61801114	-351.5	11.3
b_302	0.8031	+1%	-473536.68307427	-19.8	11.7
b_303	0.8111	+2%	-473536.70936225	26.7	11.3
b_304	0.8190	+3%	-473536.60886948	-192.3	12.3

b_305	0.8270	+4%	-473536.62430038	-1.0	11.7
b_306	0.8350	+5%	-473536.56955010	14.5	12.4

5) $SmCo_5$ “w_B2, B3” – (a;c)=(0.499;0.3968); 10,000 k-pts.; RK=7; d(a)=0; d(c)≠0; RLO=Sm+Co; FM; SRC=con.

B4-RK8	c/a	d(c/a)	SOC (1 it) [001] (eV)	MAE [MJ/m ³]	Spin-MAG [μB/fu]
b_401	0.7554	-5%	-473432.11262362	0.00	9.9
b_402	0.7634	-4%	-473432.16122317	-0.15	9.9
b_403	0.7713	-3%	-473432.19070699	0.07	9.9
b_404	0.7793	-2%	-473432.22659338	0.41	10.0
b_405	0.7873	-1%	-473432.22450232	1.02	10.1
b_406	0.7952	0%	-473432.22762755	1.36	10.1
b_407	0.8031	+1%	-473432.19937627	1.83	10.2
b_408	0.8111	+2%	-473432.17751654	2.40	10.3
b_409	0.8190	+3%	-473432.12720974	2.54	10.3
b_410	0.8270	+4%	-473432.04872990	2.61	10.3
b_411	0.8350	+5%	-473431.96203358	2.53	10.3
B6-RK7	c/a	d(c/a)	SOC (1 it) [001] (eV)	MAE [MJ/m ³]	Spin-MAG [μB/fu]
b_601	0.7554	-5%	-473432.19374555	0.10	9.96
b_602	0.7634	-4%	-473432.25252094	-0.05	9.98
b_603	0.7713	-3%	-473432.27825884	0.19	9.99
b_604	0.7793	-2%	-473536.57428733	-20.9	1.81
b_605	0.7873	-1%	-473432.29512964	0.81	10.1
b_606	0.7952	0%	-473432.28561735	1.33	10.1
b_607	0.8031	+1%	-473432.25387879	1.94	10.2
b_608	0.8111	+2%	-473432.21621645	2.38	10.2
b_609	0.8190	+3%	-473432.16033445	2.48	10.3
b_610	0.8270	+4%	-473432.08401601	2.50	10.3
b_611	0.8350	+5%	-473431.99860882	2.34	10.3

6) $SmCo_5$ “w_B4, 6” – (a;c)=(0.499;0.3968); 10,000 k-pts.; GGA; d(a)=0; d(c)≠0; RLO=Sm+Co; FM; SRC=conv.

Calculations initialized in three different directions ([001], [100] and [010]).

F2	Init. in	SOC (conv) [001] (eV)	MAE(100) [MJ/m ³]	MAE(010) [MJ/m ³]	MAG [μB/fu]
f_201	[001]	-473537.66821647	-14.1	-14.2	3.7
f_202	[100]	-473537.66821675	-14.1	-14.2	3.8
f_203	[010]	-473537.66821661	-14.1	-14.2	3.7

7) $SmCo_5$ “w_F2” – (a;c)=(0.5002;0.3961); 5000 k-pts.; RK=8; GGA; RLO=none; AFM; SOC=conv.

G1	k-pts.	SOC (conv) [001] (eV)	MAE [MJ/m ³]	MAG [μB/fu]
g_111	100	-473537.66847621	-17.6	3.9
g_112	200	-473537.67389971	-17.2	3.7
g_113	500	-473537.66672719	-16.2	3.9
g_114	1000	-473537.66760776	-16.8	3.7
g_115	5000	-473537.66893717	-16.3	3.8
g_116*	500	-473537.67535021	-0.05	4.0
G1	Core / semi-core	SOC (conv) [001] (eV)	MAE [MJ/m ³]	MAG [μB/fu]
g_120	Sm_4f	-473433.32287767	3.6	7.1
g_121	Sm_4f + Co_3d [100]	-473433.32248202	2.3	10.5
g_122	Sm_4f + Co_3d [001]	-473537.66672420	-16.2	4.0
g_123	Sm_4f&_3d + Co_3d	-473433.32127533		7.1

8) $SmCo_5$ “w_G1” – (a;c)=(0.5002;0.3961); 100, 200, 500, 1000, 5000 k-pts.; RK=8; GGA; RLO=none; AFM; SOC=conv; Sm-4f-elect.=core; Co-3d-elect.=semi-core. *separate in [001] and in [100].

G2-SOC	RK_max	SOC (conv) [001] (eV)	MAE [MJ/m ³]	MAG [μB/fu]
g_201	7.0	-473536.63890283	-16.2	3.9
g_202	7.5	-473537.32404483	-16.5	3.9
g_203	8.0	-473537.66664542	-16.4	3.9
g_204	8.5	-473537.83117886	-16.2	3.9
g_205	9.0	-473537.91142880	-1.62	3.9

G2-+U	RK_max	SOC+U (conv) [001] (eV)	MAE [MJ/m ³]	MAG [μB/fu]
g_201	7.0	-473535.42849857	-37.3	3.9
g_202	7.5	-473536.11488073	-37.0	3.9
g_203	8.0	-473536.46008137	-36.8	3.9
g_204	8.5	-473536.62524693	-36.3	3.8
g_205	9.0	-473536.70491849	-40.0	3.9

9) $SmCo_5$ “w_G2” – (a;c)=(0.5002;0.3961); 500 k-pts.; RK=7+7.5+8+8.5+9; GGA; RLO=none; AFM; +U=conv.

G3-SOC	Initialized in	SRC in	SOC (conv) [001] (eV)	MAE [MJ/m ³]	MAG [μB/fu]
g_301	[001]	[001]	-473433.32296026	3.7	10.5
g_302	[001]	[100]	-473433.32287781	3.6	10.5
g_303	[100]	[001]	-473433.32247930	2.3	10.5
g_304	[100]	[100]	-473433.32248025	2.3	
g_305	[001],[100]	[001]	-473537.66672488	-16.2	4.0
g_306	[001],[100]	[100]	-473537.66672570	-16.2	4.0
g_307	[001],[100],[110]	[001]	-473537.67400529	-17.8	3.8
g_308	[001],[100],[110]	[100]	-473433.32110417	1.5	10.5
g_309	[001],[100],[110]	[110]	-473537.67400543	-17.8	4.0
G3-+U	Initialized in	SRC in	+U (conv) [001] (eV)	MAE [MJ/m ³]	MAG [μB/fu]
g_301	[001]	[001]	-473433.27906923		10.5
g_302	[001]	[100]	-473433.27904651		
g_303	[100]	[001]	-473433.27860963	2.3	10.5
g_304	[100]	[100]	-473433.27860949	2.3	10.6
g_305	[001],[100]	[001]	-473536.46008736	-36.9	3.8
g_306	[001],[100]	[100]	-473536.46008994	-36.9	4.1
g_307	[001],[100],[110]	[001]	-473536.46526446		3.8
g_308	[001],[100],[110]	[100]	-473433.27713219	1.3	10.5
g_309	[001],[100],[110]	[110]	-473536.46514147	-37.0	4.2

10) $SmCo_5$ “w_G3” – (a;c)=(0.5002;0.3961); 500 k-pts.; RK=8; GGA; RLO=none; AFM; +U=conv.

G4-+U	Started with	f-electrons	+U (conv) [001] (eV)	MAE [MJ/m ³]	MAG [μB/fu]
g_401	SOC	Valence	-473536.46151133	-36.9	3.9
g_402	SOC	Core	-473433.27620401	1.0	10.6
g_403	+U	Valence	-473536.44984458	-58.7	4.7
g_404	+U	Core	-473433.27630387	1.0	10.6

11) $SmCo_5$ “w_G4” – (a;c)=(0.5002;0.3961); 500 k-pts.; RK=8; GGA; AFM; +U=conv.; f-elect.: core + valence.

G52-SOC	U_eff	SOC (conv) [001] (eV)	MAE [MJ/m ³]	MAG [μB/fu]
g_521	4.15	-473537.66893771	16.2	3.80
g_522	4.25	-473537.66893703	16.2	3.80
g_523	4.35	-473537.66893717	16.2	3.80
g_524	4.45	-473537.66893730	16.2	3.80
g_525	4.55	-473537.66893703	16.2	3.80
g_526	4.65	-473537.66893281	16.2	3.80
g_527	4.75	-473537.66893730	16.2	3.80
G52-+U	U_eff	+U (conv) [001] (eV)	MAE [MJ/m ³]	MAG [μB/fu]
g_521	4.15	-473536.50817588	35.7	3.82
g_522	4.25	-473536.49159911	36.0	3.83
g_523	4.35	-473536.47301998	36.4	3.84
g_524	4.45	-473536.45708254	36.8	3.86
g_525	4.55	-473536.44144034	37.2	3.87
g_526	4.65	-473536.42389198	37.9	3.88
g_527	4.75	-473536.40891810	38.3	3.89

12) $SmCo_5$ “w_G52” – (a;c)=(0.5002;0.3961); 5000 k-pts.; RK=8; GGA; AFM; SOC(+U)=conv..

H2-SOC	c/a ratio	d(c/a)	SOC (conv) [001] (eV)	MAE [MJ/m ³]	MAG [μB/fu]
h_201	0.7524	-5%	-473434.52036795	-2.3	10.6
h_202	0.7603	-4%	-473538.66547482	-14.6	3.8
h_205	0.7841	-1%	-473434.67828942	-1.1	10.5

h_209	0.8158	+3%	-473434.75295967	3.7	10.6
h_210	0.8237	+4%	-473434.76450724	3.7	10.5
h_211	0.8316	+5%	-473434.77717482	3.5	10.5
h_212	0.8395	+6%	-473434.77080654	2.5	10.7
h_213	0.8474	+7%	-473434.77059456	3.0	10.6
h_214	0.8554	+8%	-473434.76743369	3.3	10.5
h_215	0.8633	+9%	-473434.76086703	4.6	10.5
h_216	0.8712	+10%	-473434.74361582	4.8	10.4
H2-+U	c/a ratio	d(c/a)	+U (conv) [001] (eV)	MAE [MJ/m³]	MAG [μB/fu]
h_201	0.7524	-5%	-473434.47985535	-2.2	10.6
h_202	0.7603	-4%	-473537.46616097	-36.2	3.9
h_205	0.7841	-1%	-473434.63514317	-1.0	10.5
h_209	0.8158	+3%	-473434.70657104	3.9	10.6
h_210	0.8237	+4%	-473434.71740553	3.5	10.5
h_211	0.8316	+5%	-473434.72929528	4.0	10.5
h_212	0.8395	+6%	-473434.72152561	2.2	10.7
h_213	0.8474	+7%	-473434.72053294	2.7	10.6
h_214	0.8554	+8%	-473434.71656674	1.7	10.5
h_215	0.8633	+9%	-473434.70881993	4.7	10.5
h_216	0.8712	+10%	-473434.69076530	5.0	10.5

13) $SmCo_5$ “w_H2” – (a;c)=(0.500;0.396); 200 k-pts.; RK=9; GGA; RLO=Sm; d(V)=0; AFM; +U =conv.; f –elect.: valence; $U_{eff} = 4.42$ eV.

H3-SOC	c/a ratio	d(c/a)	SOC (conv) [001] (eV)	MAE [MJ/m³]	MAG [μB/fu]
h_301	0.7524	-5%	-473538.62768418	19.1	3.92
h_302	0.7603	-4%	-473538.65043522	18.9	3.87
h_303	0.7682	-3%	-473538.66400581	20.3	3.88
h_304	0.7762	-2%	-473538.67523582	17.6	3.89
h_305	0.7841	-1%	-473538.68759483	17.9	3.87
h_306	0.7920	0%	-473538.69008250	17.8	3.80
h_307	0.7992	+1%	-473538.68743741	17.8	3.78
h_308	0.8078	+2%	-473538.67877793	19.1	3.78
h_309	0.8158	+3%	-473538.67079968	20.5	3.81
h_310	0.8237	+4%	-473538.65732270	23.8	3.83
h_311	0.8316	+5%	-473538.64508859	26.7	3.82
H3-+U	c/a ratio	d(c/a)	+U (conv) [001] (eV)	MAE [MJ/m³]	MAG [μB/fu]
h_301	0.7524	-5%	-473537.42617315	40.1	4.06
h_302	0.7603	-4%	-473537.45049115	41.8	3.99
h_303	0.7682	-3%	-473537.46683663	41.5	3.98
h_304	0.7762	-2%	-473537.47874053	37.5	4.01
h_305	0.7841	-1%	-473537.48854846	39.5	4.43
h_306	0.7920	0%	-473537.49370380	39.0	3.87
h_307	0.7992	+1%	-473537.49118580	37.1	3.79
h_308	0.8078	+2%	-473537.48325259	36.0	3.75
h_309	0.8158	+3%	-473537.47534332	36.3	3.75
h_310	0.8237	+4%	-473537.46235315	37.0	3.73
h_311	0.8316	+5%	-473537.44292149	23.4	4.66

14) $SmCo_5$ “w_H3” – (a;c)=(0.5002;0.3961); 200 k-pts.; RK=9; GGA; RLO=Sm; d(V)=0; AFM; +U=conv.; f-elect.: valence; $U_{eff} = 4.42$ eV; Space group is simple hexagonal (H).

H4-SOC	c/a ratio	d(c/a)	SOC (conv) [001] (eV)	MAE [MJ/m³]	MAG [μB/fu]
h_401	0.7524	-5%	-473434.52792333	-1.5	10.5
h_402	0.7603	-4%	-473434.57757256	-0.7	10.4
h_403	0.7682	-3%	-473434.61610295	0.03	10.4
h_404	0.7762	-2%	-473434.64808396	-0.4	10.4
h_405	0.7841	-1%	-473434.68181684	1.2	10.4
h_406	0.7920	0%	-473434.70439563	1.8	10.4
h_407	0.7992	+1%	-473434.72167745	2.3	10.4
h_408	0.8078	+2%	-473434.73449266	2.6	10.4

h_409	0.8158	+3%	-473434.74916654	3.2	10.5
h_410	0.8237	+4%	-473434.75919040	3.0	10.5
h_411	0.8316	+5%	-473434.77130070	2.8	10.5
H4+U	c/a ratio	d(c/a)	+U (conv) [001] (eV)	MAE [MJ/m³]	MAG [μB/fu]
h_401	0.7524	-5%	-473434.48753196	-1.0	10.5
h_402	0.7603	-4%	-473434.53650485	-0.7	10.4
h_403	0.7682	-3%	-473434.57421563	-0.4	10.4
h_404	0.7762	-2%	-473434.60560751	-0.4	10.4
h_405	0.7841	-1%	-473434.63866283	1.2	10.4
h_406	0.7920	0%	-473434.66033983	1.4	10.4
h_407	0.7992	+1%	-473434.67693579	2.0	10.4
h_408	0.8078	+2%	-473434.68891602	2.4	10.5
h_409	0.8158	+3%	-473434.70267505	3.1	10.5
h_410	0.8237	+4%	-473434.71170951	2.3	10.5
h_411	0.8316	+5%	-473434.72306523	2.2	10.5

15) $SmCo_5$ “w_H4” – (a;c)=(0.5002;0.3961); 200 k-pts.; RK=9; GGA; d(V)=0; RLO=Sm; AFM; +U=conv; f-elect.: core; U_{eff} = 4.42; Space group is simple hexagonal (H).

H5-SOC	c/a ratio	d(c/a)	SOC (conv) [001] (eV)	MAE [MJ/m³]	MAG [μB/fu]
h_501	0.7524	-5%	-473538.63158670	-15.5	3.86
h_502	0.7603	-4%	-473538.65444455	-14.9	3.84
h_503	0.7682	-3%	-473537.36916010	-15.9	3.84
h_504	0.7762	-2%	-473538.67702647	-15.6	3.80
h_505	0.7841	-1%	-473538.68880614	-15.7	3.80
h_506	0.7920	0%	-473538.68904833	-16.7	3.80
h_507	0.7992	+1%	-473538.68468199	-16.7	3.81
h_508	0.8078	+2%	-473538.67401253	-18.4	3.79
h_509	0.8158	+3%	-473538.66454610	-20.3	3.80
h_510	0.8237	+4%	-473538.64928826	-23.7	3.80
h_511	0.8316	+5%	-473434.77761741	3.1	
H5+U	c/a ratio	d(c/a)	+U (conv) [001] (eV)	MAE [MJ/m³]	MAG [μB/fu]
h_501	0.7524	-5%	-473537.25106441	-0.02	5.39
h_502	0.7603	-4%	-473537.44914610	-40.6	3.94
h_503	0.7682	-3%	-473536.16193372	-38.9	3.95
h_504	0.7762	-2%	-473537.46607648	-54.8	4.74
h_505	0.7841	-1%	-473537.48653714	-38.8	3.87
h_506	0.7920	0%	-473537.48664354	-38.5	4.21
h_507	0.7992	+1%	-473537.48202522	-5.3	3.86
h_508	0.8078	+2%	-473537.47225646	-36.2	3.84
h_509	0.8158	+3%	-473537.46357725	-36.8	3.83
h_510	0.8237	+4%	-473537.44925127	-36.2	3.83
h_511	0.8316	+5%	-473434.72944141	3.7	10.57

16) $SmCo_5$ “w_H5” – (a;c)=(0.5002;0.3961); 5000 k-pts.; RK=9; GGA; RLO=Sm; d(V)=0; AFM; +U=conv.; f-elect.: valence; U_{eff} = 4.42 eV; Space group is simple hexagonal (H); Also charge and force convergence.

YCo₅

R1- GGA	c/a ratio	d(c/a)	SOC (1 it.) [001] (eV)	MAE [MJ/m³]	MAG [μB/fu]
r_101	0.8033	-0.5%	-281724.07824549	-117.9	7.78
r_102	0.8041	-0.4%	-281724.11090515	-55.4	7.78
r_103	0.8050	-0.3%	-281724.08828731	-120.1	7.78
r_104	0.8058	-0.2%	-281724.07244497	-104.9	7.79
r_105	0.8066	-0.1%	-281724.06652922	-118.7	7.80
r_106	0.8074	0%	-281724.15118074	-109.0	7.80
r_107	0.8082	+0.1%	-281724.14133919	22.0	7.81
r_108	0.8090	+0.2%	-281724.15452434	-88.7	7.81
r_109	0.8098	+0.3%	-281724.14773537	-75.5	7.82
r_110	0.8106	+0.4%	-281724.27378345	-104.6	7.82
r_111	0.8114	+0.5%	-281724.28423834	-71.4	7.83

R2-LDA	c/a ratio	d(c/a)	SOC (1 it.) [001] (eV)	MAE [MJ/m ³]	MAG [μB/fu]
r_201	0.8033	-0.5%	-281305.42102044	-44.9	7.59
r_202	0.8041	-0.4%	-281305.46162991	-36.5	7.60
r_203	0.8050	-0.3%	-281305.45996444	-36.4	7.61
r_204	0.8058	-0.2%	-281305.46239197	-0.33	7.54
r_205	0.8066	-0.1%	-281305.38266135	-0.01	7.54
r_206	0.8074	0%	-281305.63256578	0.09	7.50
r_207	0.8082	+0.1%	-281305.61597227	-6.3	7.56
r_208	0.8090	+0.2%	-281305.63036819	-22.3	7.64
r_209	0.8098	+0.3%	-281305.60687482	5.2	7.64
r_210	0.8106	+0.4%	-281305.58535374	-7.3	7.64
r_211	0.8114	+0.5%	-281305.60260767	-13.7	7.65

1) YCo_5 “w_R1 & R2” – (a;c)=(0.494;0.399); 10,000 k-pts.; RK=9; LDA; d(a)=0; d(c)≠0; RLO=Y+Co; SRC=conv.

B1	b_103 (RK 9 – RLO Y+Co)		b_104 (RK 7 - RLO Y)		b_110 (RK 7 – RLO Y+Co)	
d(c/a)	SCF (conv)	Spin	SCF (conv)	Spin	SCF (conv)	Spin
-10%	-281722.96821223	7.4	-281721.79017579	7.4	-281721.65328288	7.4
-5%	-281723.13294377	7.3	-281721.95859882	7.3	-281721.82179149	7.3
0%	-281723.18010574	7.2	-281722.00752001	7.2	-281721.87024641	7.2
+5%	-281723.10273463	7.2	-281721.93142158	7.2	-281721.79447642	7.2
+10%	-281722.90350149	7.2	-281721.73363554	7.2	-281721.59732182	7.2
B2	b_203 (RK 7)		b_204 (RK 8)		b_210 (RK 9)	
d(c/a)	SCF (conv)	Spin	SCF (conv)	Spin	SCF (conv)	Spin
-10%	-281301.74281494	7.2	-281302.85021372	7.2	-281303.10552859	7.1
-5%	-281301.88300587	7.1	-281302.98617506	7.1	-281303.24057127	7.1
0%	-281301.91269228	7.0	-281303.01456185	7.0	-281303.26993590	7.0
+5%	-281301.82941874	7.0	-281302.92962284	7.0	-281303.18538751	7.0
+10%	-281301.63341723	7.0	-281302.73018099	7.0	-281302.98621560	7.0

2) YCo_5 “w_B1, B2” – (a;c)=(0.4937;0.3986); 10,000 k-pts.; RK=7+8+9; GGA; RLO=Y+Co.

F1	k-pkt.	SOC (conv) [001] (eV)	MAE [MJ/m ³]	MAG [μB/fu]
f_101	100	-281723.08898308	2.88	8.10
f_102	200	-281723.08615023	2.72	7.93
f_103	500	-281723.08159654	1.97	7.90
f_104	1,000	-281723.08034019	1.64	7.73
f_105	5,000	-281723.08262731	1.78	7.76

3) YCo_5 “w_F1” – (a;c)=(0.4937;0.3986); RK=8; GGA; RLO=none; SOC=conv.; CC=0.001 C.

F2	Steps	SOC (conv) [001] (eV)	MAE [MJ/m ³]	MAG [μB/fu]
f_201	SRC → SOC → +U	-281723.03175411	2.09	7.68
f_202	SOC → +U	-281723.03172200	2.06	7.68
f_203	+U	-281723.08262146	9.88	7.76

4) YCo_5 “w_F2” – (a;c)=(0.4937;0.3986); 5000 k-pts.; RK=8; GGA; +U=conv.; CC=0.001 C.

N	c/a ratio	d(c/a)	SOC (1 it) [001] (eV)	MAE [MJ/m ³]	MAG [μB/fu]
n_0	0.7254	-10%	-281722.57815986	0.2	7.70
n_2	0.7658	-5%	-281723.47415059	4.1	7.70
n_3	0.8060	0%	-281723.40733206	4.4	7.76
n_5	0.8463	+5%	-281723.49414893	2.8	7.73

5) YCo_5 “w_N” – (a;c)=(0.4928;0.3972) (3000 k-pts.; RK=7; GGA; d(a)=0; d(c)≠0; SRC=conv.

A-2 Results VASP Calculation

$Y_2Fe_{14}B$

V_A1	no +U	+U for 3d	+U for 4d	+U for 3d+4d
NSP+U [eV]	-68.32377652	-61.5893331547*	-68.06710480	-61.3028852556*
V_A4	Y2 (U_4d)	YPr (U_4f)	YNd (U_4f)	YDy (U_4f)
NSP+U [eV]	-509.69523231	-528.59620137*	-526.37725777*	-529.87388610*

2) $Y_2Fe_{14}B$ “v_A4” – (a;c)=(0.879;1.20); G-6x6x5 k-pts.; GGA; ISMEAR=1; EC=10⁻⁶; 1 f.u. (A1) + 4 f.u. (A4); GGA_COMPAT; ADDGRID; LASPH; 3d-(U;J)=(1.2;0.8), 4f-(U;J)=(5.4;0.7); *Not converged.

V_A5	SOC [001] (conv) (eV)	MAE [MJ/m ³]	Total-MAG [μB/fu]
v_a5_01 – Y2	-534.17802993	0.44	33.2
v_a5_02 – YPr	-551.46657263	2.11	31.1
v_a5_03 – YNd	-558.53759960	1.11	30.2
v_a5_04 – YDy	-573.24296683	4.14	28.0

3) $Y_2Fe_{14}B$ “v_A5” – (a;c)=(0.879;1.22); G-3x3x2 k-pts.; GGA; SOC+U=conv.; ISMEAR=1; EC=10⁻⁵; 4 f.u.; GGA_COMPAT; ADDGRID; LASPH; 3d-(U;J)=(1.2;0.8), 4f-(U;J)=(5.4;0.7); @VSC3.

V_A6	k-mesh	SOC [001] (conv) (eV)	MAE [MJ/m ³]	Total-MAG [μB/fu]
v_a6_01	2x2x1	-526.20232191	-0.1	20.9
v_a6_02	1x1x1	-534.77725070	-0.3	32.9
v_a6_03	3x3x2	-534.18246661	0.4	32.2

4) $Y_2Fe_{14}B$ “v_A6” – (a;c)=(0.879;1.22); GGA; SOC+U=Conv.; ISMEAR=1; EC=10⁻⁵; 4 f.u.; GGA_COMPAT; ADDGRID; LASPH; 3d-(U;J)=(1.2;0.8); @FX.

$Pr_2Fe_{14}B$

V_A1	k-mesh	Cores	Remark	SRC (eV)	Spin [μB/fu]
v_al_01a	1x1x1	1-core		-534.09059534	34.0
v_al_01b	1x1x1	16-cores		-534.09024646	34.0
v_al_01c	1x1x1	16-cores	Conv. Criterion 10 ⁻⁷ eV	-534.09024662	34.0
v_al_01d	1x1x1	16-cores	Conv. Criterion 10 ⁻⁶ eV	-534.09015004	34.0
v_al_02	1x1x1	2-cores		-534.09058862	34.0
v_al_03	2x2x1	16-cores		-533.29337693	31.5
v_al_04a	3x3x2	16-cores		-533.62761801	31.3
v_al_04b	3x3x2	32-cores		-533.62761798	31.3
v_al_04c	3x3x2	48-cores		-533.62761800	31.3
v_al_05	1x1x1	1-core	2xNBAND	-534.09058862	34.0
v_al_06	Γ-1x1x1	1-core	2xNBAND	-534.09058911	34.0
v_al_07a	1x1x1	2-cores	4GB RAM	-534.09058862	
v_al_07b	1x1x1	2-cores	16GB RAM	-534.09058862	34.0
v_al_07c	1x1x1	4-cores	4 GB RAM / NPAR=2	-534.09058862	34.0
v_al_07d	1x1x1	4-cores	4 GB RAM / NPAR=4	-534.09058862	34.0
v_al_04e	1x1x1	8-cores	1 GB RAM / NPAR=8	-534.09058862	34.0
v_al_07f	1x1x1	8-cores	2 GB RAM / NPAR=8	-534.09058862	34.0
v_al_07g	1x1x1	8-cores	4 GB RAM / NPAR=8	-534.09058862	34.0
v_al_08a	1x1x1	2-cores	4 GB RAM / (NG)X,Y,Z	-534.08878147	
v_al_08b	1x1x1	1-core	16 GB RAM / (NG)X,Y,Z	-534.08878147	34.0
v_al_09d	2x2x1	16-cores	SCALAPACK-IFORT 3 code	-533.29159269	
v_al_10d	2x2x1	32-cores	SCALAPACK-IFORT 3 code	-533.29159270	34.0
v_al_11d	1x1x1	32-cores	NCL from start (vasp 5.2.)	-534.08844109	34.0
v_al_11k	1x1x1	1-core	NCL from start (vasp 5.3.)	-534.08843865	34.0
v_al_12a	1x1x1	2-cores		-546.47888824	30.0
v_al_12b	2x1x1	2-cores		-546.63333472	27.5
v_al_12c	2x2x1	2-cores		-545.96636322	27.5

1) $Pr_2Fe_{14}B$ “v_A1” – (a;c)=(0.8799;1.241); ENCUT=390; GGA; SR=conv.; ISMEAR=1; 4 f.u.; EC 10⁻⁸.

V_A2	Potential Files	Potential Type	SRC (conv) [eV]	Spin [μ B/fu]
v_a2_01	Fe, Pr, B	0.52 PBE	-546.48617745	30.0
v_a2_02	Fe, Pr_3, B	0.52 PBE	-521.91146109	24.2
v_a2_03	Fe_pv, Nd, B	0.52 PBE	-547.85775765	29.0
v_a2_04	Fe_pv, Pr_3, B	0.52 PBE	-531.06503362	34.0
v_a2_05	Fe, Nd, B	PBE	-546.48203679	30.0
v_a2_06	Fe, Pr_3, B	PBE	-521.87070885	24.2
v_a2_07	Fe_pv, Nd, B	PBE	-547.85776131	29.0
v_a2_08	Fe_pv, Pr_3, B	PBE	-531.06503362	34.0
v_a2_09	Fe, Nd, B	PW 91	-541.33127080	27.5
v_a2_10	Fe, Nd_3, B	PW 91	-525.02276821	32.5
v_a2_11	Fe_pv, Nd, B	PW 91	-539.01514158	27.5
v_a2_12	Fe_pv, Nd_3, B	PW 91	-522.70967610	32.0
V_A3	Potential Files	Potential Type	SRC (conv) [eV]	Spin [μ B/fu]
v_a3_01	Fe, Pr, B	0.52 PBE		
v_a3_02	Fe, Pr_3, B	0.52 PBE	-529.00489748	
v_a3_03	Fe_pv, Nd, B	0.52 PBE	-547.58847347	
v_a3_04	Fe_pv, Pr_3, B	0.52 PBE	-530.43611343	
v_a3_05	Fe, Nd, B	PBE	-546.18956891	
v_a3_06	Fe, Pr_3, B	PBE	-529.00489748	
v_a3_07	Fe_pv, Nd, B	PBE	-547.58847306	
v_a3_08	Fe_pv, Pr_3, B	PBE	-530.43611343	
v_a3_09	Fe, Nd, B	PW 91	-540.22201069	
v_a3_10	Fe, Nd_3, B	PW 91	-524.82893920	
v_a3_11	Fe_pv, Nd, B	PW 91	-538.92550566	
v_a3_12	Fe_pv, Nd_3, B	PW 91	-522.54771863	

3) $Pr_2Fe_{14}B$ “v_A2, A3” – (a;c)=(0.8799;1.241); ENCUT=320; 1x1x1 k-pts.; GGA; SRC=conv.; ISMEAR=1 (A2), -5 (A3); 4 f.u.; EC 10^{-6} ; GGA_COMPAT; NG(X;Y;Z)=114;114;158.

V_A4 @FX	Potential Files	Potential Type	SRC (conv) [eV]	Spin [μ B/fu]
v_a4_01	Fe, Pr, B	0.52 PBE	-546.48765819	30.0
v_a4_01*	Fe, Pr, B	0.52 PBE	-546.48644324	30.0
v_a4_02	Fe, Pr_3, B	0.52 PBE	-522.86162411	24.8
v_a4_03	Fe_pv, Nd, B	0.52 PBE	-547.86533314	29.0
v_a4_04	Fe_pv, Pr_3, B	0.52 PBE	-531.07257588	34.0
v_a4_05	Fe, Nd, B	PBE	-546.48768014	30.0
v_a4_06	Fe, Pr_3, B	PBE	-522.75945884	25.3
v_a4_07	Fe_pv, Nd, B	PBE	-547.86533316	29.0
v_a4_08	Fe_pv, Pr_3, B	PBE	-531.07257588	34.0
v_a4_09	Fe, Nd, B	PW 91	-541.33119827	27.5
v_a4_10	Fe, Nd_3, B	PW 91	-525.02292092	32.5
v_a4_11	Fe_pv, Nd, B	PW 91	-539.02125179	27.5
v_a4_12	Fe_pv, Nd_3, B	PW 91	-522.71614122	32.0
V_A5 @VSC2	Potential Files	Potential Type	SRC (conv) [eV]	Spin [μ B/fu]
v_a5_01	Fe, Pr, B	0.52 PBE	-543.65418477	30.3
v_a5_02	Fe, Pr_3, B	0.52 PBE	-529.00433557	31.0
v_a5_03	Fe_pv, Nd, B	0.52 PBE	-547.58778804	27.5
v_a5_04	Fe_pv, Pr_3, B	0.52 PBE	-530.43531829	31.0
v_a5_05	Fe, Nd, B	PBE		
v_a5_06	Fe, Pr_3, B	PBE	-529.00433557	31.0
v_a5_07	Fe_pv, Nd, B	PBE	-547.58778786	27.5
v_a5_08	Fe_pv, Pr_3, B	PBE	-530.43531852	31.0
v_a5_09	Fe, Nd, B	PW 91	-541.23544588	26.5
v_a5_10	Fe, Nd_3, B	PW 91	-524.82864801	30.5
v_a5_11	Fe_pv, Nd, B	PW 91	-536.71469073	29.7
v_a5_12	Fe_pv, Nd_3, B	PW 91	-522.54718617	30.5

5) $Pr_2Fe_{14}B$ “v_A5” – (a;c)=(0.8799;1.241); ENCUT=320; 1x1x1 k-pts.; GGA; SRC=conv.; ISMEAR=1; 4 f.u.; EC= 10^{-6} ; GGA_COMPAT; NG(X;Y;Z)=114;114;158; LMAXMIX=6. * no LMAXMIX.

V_B1	Potential Files	Potential Type	SRC (conv) [eV]	Spin-MAG [μ B/fu]
v_b1_01	Fe, Pr, B	0.52 PBE – STD	-546.48267104	30.0
v_b1_02	Fe, Pr_3, B	0.52 PBE – STD	-522.75945735	25.3
v_b1_03	Fe, Pr, B	0.52 PBE – NCL	-546.48267581	30.0
v_b1_04	Fe, Pr_3, B	0.52 PBE – NCL	-523.99115569	23.7
v_b1_05	Fe, Pr, B	0.52 PBE – GAMMA	-546.48654041	30.0
v_b1_06	Fe, Pr_3, B	0.52 PBE – GAMMA	-523.16661431	24.5

6) $Pr_2Fe_{14}B$ “v_B1” – (a;c)=(0.8799;1.241); ENCUT=320; 1x1x1 k-pts.; GGA; SRC=conv.; ISMEAR=1+0; 4 f.u.; EC=10⁻⁶; GGA_COMPAT; NG(X;Y;Z)=114;114;158; LMAXMIX = 6.

“v_b4_02”: 1st SRC (IBRION; ISIF) = (2;1), 2nd (1;7). “v_b4_03”: 1st (IBRION; ISIF) = (2;2), 2nd (1; 7).

V_B4	SRC (1st) [eV]	Spin (1st)	(a,c) [Ang.]	SRC (2nd) [eV]	Spin (2nd)	(a,c) [Ang.]
v_b4_02	-542.28464997	22.1	8.799; 12.241	-526.46071916	2.8	8.799; 12.241
v_b4_03 - M	-546.31417297	27.5	8.799; 12.241	-546.31417297	26.8	8.686; 12.083
v_b4_03 - G	-545.50015288	27.7	8.799; 12.241	-546.55369365	26.1	8.615; 11.984

7) $Pr_2Fe_{14}B$ “v_B4” – (a;c)=(0.8799;1.241); ENCUT=320; G+M-3x3x2 k-pts.; GGA; SRC=conv.; ISMEAR=0; 68 4 f.u.; EC=10⁻⁶; GGA_COMPAT; NG(X;Y;Z)=114;114;158; LMAXMIX=6.

V_B5	k-mesh	Remark, ISYM	SRC [001] (eV)	Spin-MAG [μ B/fu]
v_b5_01	5x5x3		-1	-546.24518863
v_b5_02	4x4x4		-1	-541.23854549
v_b5_03	5x5x4		No	-546.22043810
v_b5_04	5x5x4	LMAXMIX, -1		-546.22043550
v_b5_05	5x5x4	LMAXMIX, no		-546.22043456
v_b5_06	5x5x4	MAGMOM, -1		-546.22043807
v_b5_07	5x5x4	MAGMOM, no		-546.22043802
v_b5_08	5x5x4	MAGMOM, LMAXMIX, -1		-545.56080533
v_b5_09	5x5x4	MAGMOM, LMAXMIX, no		-546.22043803
V_B5	k-mesh	SOC [001] (eV)	MAE [MJ/m ³]	Total-MAG [μ B/fu]
v_b5_01	5x5x3	-550.84765657	111.9	32.0
v_b5_02	4x4x4	-545.93957652	8.0	24.4
v_b5_04	5x5x4	-550.82634742	6.2	32.1
v_b5_06	5x5x4	-550.82310249	5.7	32.1

8) $Pr_2Fe_{14}B$ “v_B5” – (a;c)=(0.8799;1.241); ENCUT=320; GGA; SRC=conv.; ISMEAR=1; 4 f.u.; EC=10⁻⁶; GGA_COMPAT; NG(X;Y;Z)=114;114;158; LMAXMIX=6 (default 2); MAGMOM (Fe;Pr)=(2.6;-2.2)

“v_b6_03 is relaxed but not optimized. B6_v_08 is relaxed and optimized (6th SRC).

V_B6	SRC (1st) [eV]	SRC (2nd) [eV]	SRC (3rd) [eV]	SRC (4th) [eV]	SRC (5th) [eV]
b6_v_03	-546.21107757	-546.21107874	-546.21108012	-546.21107883	-546.21107819
b6_v_08	-546.21107788	-546.21107848	-546.21107855	-546.40419354	-546.42271371
V_B6	SRC (6th) [eV]	SOC [001] [eV]	MAE [MJ/m ³]	Total-MAG [μ B/fu]	
b6_v_03		-550.81779906	6.1		33.0
b6_v_08	-546.2677884	-550.87477961	6.0		32.9

9) $Pr_2Fe_{14}B$ “v_B6” – (a;c)=(0.8799;1.241); ENCUT=320; M-3x3x2 k-pts.; GGA; SRC=conv.; ISMEAR=0; 4 f.u.; EC=10⁻⁶; GGA_COMPAT.

V_C3	Pr2	PrY	PrNd	PrDy
NSP+U [eV]	-517.21729633	-525.64159898	-512.35011488	-519.56529751

10) $Pr_2Fe_{14}B$ “v_C3” – (a;c)=(0.876;1.199); G-6x6x5 k-pts.; GGA+U; NSP=conv.; ISMEAR=1; EC=10⁻⁶; 4 f.u.; GGA_COMPAT; ADDGRID; LASPH; R-4f-(U;J)=(5.4;0.7).

V_C5	k-mesh	SOC [001] (conv) (eV)	MAE [MJ/m ³]	Total-MAG [μ B/fu]
v_c5_01 – Pr2	1x1x1	-548.80183094		33.2
v_c5_02 – Pr2	3x3x2	-551.02151156		29.9

12) $Pr_2Fe_{14}B$ “v_C5” – (a;c)=(0.881;1.227); SOC+U=conv.; ISMEAR=1; EC=10⁻⁵; 4 f.u.; GGA_COMPAT; ADDGRID; LASPH; Pr-4f-(U;J)=(5.4;0.7).

Nd₂Fe₁₄B

V_A1	Potential Files	Potential Type	SRC (conv) [eV]	Spin-MAG [μ B/fu]
v_a_01	Fe, Nd, B	0.52 PBE	-554.87821263	26.5
v_a_02	Fe, Nd_3, B	0.52 PBE	-530.40817251	34.0
v_a_03	Fe_pv, Nd, B	0.52 PBE	-555.71442126	28.0
v_a_04	Fe_pv, Nd_3, B	0.52 PBE	-531.81556686	34.0
v_a_05	Fe, Nd, B	PBE	-554.27827747	28.0
v_a_07	Fe_pv, Nd, B	PBE	-555.75030646	28.0
v_a_09	Fe, Nd, B	PW 91	-548.37307347	28.5
v_a_10	Fe, Nd_3, B	PW 91	-525.61827494	32.0
v_a_11	Fe_pv, Nd, B	PW 91	-546.60278085	27.9
v_a_12	Fe_pv, Nd_3, B	PW 91	-523.37927614	32.0

1) *Nd₂Fe₁₄B* “v_A1” – (a;c)=(0.8799;1.2241); ENCUT=320; 1x1x1 k-pts.; GGA; SRC=conv.; ISMEAR=1.

V_A2	# cores; f-elect.	SOC (conv) [001] [eV]	MAE [MJ/m ³]	MAG [μ B/fu]
v_a_01	2; valence	-558.30972244	11.2	34.0
v_a_12	4; core	-526.36712484	0.3	33.6

2) *Nd₂Fe₁₄B* “v_A2” – (a;c)=(0.8799;1.2241); ENCUT=320; 1x1x1 k-pts.; SOC=conv; ISMEAR=-5.

V_B4	SOC+U [001] (eV)	MAE [MJ/m ³]	MAG [μ B/fu]
v_b4_05 - Nd2	-561.85453826		20.3

5) *Nd₂Fe₁₄B* “v_B5” – (a;c)=(0.881;1.221); 1x1x1 k-pts.; GGA; +U=conv.; ISMEAR=1; 4 f.u.

Dy₂Fe₁₄B

V_A1	+U for none	+U for Co-3d	+U for Dy-4f	+U for Co-3d & Dy-4f
NSP [eV]	-69.15502601	-62.41231355	-67.33927410	-60.62963359
SRC [eV]			-94.93841422	-91.14912357

1) *Dy₂Fe₁₄B* “v_A1” – (a;c)=(0.879;1.199); 6x6x5 k-pts.; ISMEAR=1; 3d-(U,J)=(1.2;0.8); 4f-(U,J)=(5.4;0.7);.

V_A3 @VSC2	Dy2	DyY	DyPr	DyNd
NSP [eV]	-517.80482100	-527.44032006	-518.08077424	-518.11691703
V_A4 @VSC3	Dy2	DyY	DyPr	DyNd
NSP [eV]	-518.601101959	-527.177839509	-518.196974018	-515.302750411

3) *Dy₂Fe₁₄B* “v_A3, A4” – (a;c)=(0.879;1.199); 6x6x5 k-pts.; ISMEAR=1; 4 f.u.; ISYM=-1; Dy-4f-(U,J)=(5.4;0.7).

V_A6	SOC+U (conv) [001] (eV)	MAE [MJ/m ³]	MAG [μ B/fu]
v_a6_01 Dy2	-591.401232050	12.9	22.1
V_A8	SOC+U (conv) [eV]	MAE [MJ/m ³]	MAG [μ B/fu]
Dy2	[001]: -590.87739509	5.3	18.1
DyY	[001]: -572.59930368	16.1	28.5
DyPr	[110]: -568.90758141		*29.0
DyNd	[001]: -576.07757826	545.8	23.8

6) *Dy₂Fe₁₄B* “v_A6, A8” – (a;c)=(0.879;1.199); 1x1x1(A6) + 3x3x2(A8) k-pts.; GGA+U; SOC+U=conv.; ISMEAR=1; R-4f-(U,J)=(5.4;0.7). * ENE and MAG in [110].

hcp - Co

V_A1	SRC, MAGMOM	+U [001] (conv) (eV)	MAE (100)	MAE (210)	MAG [μ B/fu]
v_a1_01	No, 3.2	-2.97152795	-2.4	-0.5	0.9 - 0.01
v_a1_03	Yes, 3.2	-2.97240678	1.6	1.6	0.9 - 0.01
v_a1_04	Yes, 1.6	-2.97238877	1.6	1.7	0.8 - 0.01
v_a1_05	Yes, 3.2	-2.97447109	-2.6	-1.9	1.2 - 0.004
v_a1_06	Yes, 1.6	-2.97447942	-2.5	-1.9	1.2 - 0.005

01) *hcp - Co* “v_A1” (a;c)=(0.2503;0.4057); M-5x5x7 k-mesh; ISMEAR=1; +U=conv.; EC=10⁻⁶; LMAXMIX=6; LREAL; LASPH; ADDGIRD, ISYM=-1; Co-3d-(U,J)=(1.2;0.8); NSP+U → (SRC+U) → SOC+U.

V_A2a	k-mesh, U-Potential	+U [001] (conv) (eV)	MAE (MJ/m ³)	MAG [μ B/fu]
v_a2_01	5x5x5, (1.2;0.8)	-13.49378705	0.3	
v_a2_02	5x5x7, (1.2;0.8)	-13.48290819	-39.5	
v_a2_03	5x5x8, (1.2;0.8)	-13.49403330	23.8	
v_a2_04	7x7x5, (1.2;0.8)	-13.50616242	-0.1	
v_a2_05a	8x8x5, (1.2; 0.45)	-12.89764265	1.4	
v_a2_05b	8x8x5, (1.2;0.8)	-13.55932417	4.1	
v_a2_06	7x7x7, (1.2;0.8)	-13.50487640	-0.2	
v_a2_07	8x8x6, (1.2;0.8)	-13.56048280	-2.6	
v_a2_08	5x5x5, (1.2;0.8)	-13.49614885	0.3	
v_a2_09	7x7x7, (1.2;0.8)	-13.50487649	-0.2	
V_A2b	k-mesh, Setup	+U [001] (conv) (eV)	MAE (MJ/m ³)	MAG [μ B/fu]
v_a2_10	8x8x5, U = (2.8; 1.0)	-10.94684918	-1.4	3.5 + 0.3
v_a2_11	7x7x7, U = (2.8; 1.0)	-10.92152696	-85.5	3.6 + 0.3
v_a2_12	9x9x9, U = (2.8; 1.0)	-10.91371630	8.6	3.6 + 0.3
v_a2_13	8x8x6, U = (2.8; 1.0)	-10.92909786	-28.8	3.4 + 0.3
v_a2_14	9x9x9, U = (1.2;0.8)	-13.52662386	-0.5	3.1 + 0.1
v_a2_15	10x10x10, U= (1.2;0.8)	-13.54334960	1.1	3.3 + 0.2
v_a2_16	11x11x11, U= (1.2;0.8)	-13.54176579	0.1	3.2 + 0.2
v_a2_17a	8x8x5 – ISIF = 3	-13.55662871	4.0	3.3 + 0.2
v_a2_17b	8x8x5 – ISIF = 0	-13.55658193	4.2	3.3 + 0.2
v_a2_18a	8x8x6 – ISIF = 3	-13.55815657	-2.5	3.2 + 0.2
v_a2_18b	8x8x6 – ISIF = 0	-13.55735514	-2.8	3.2 + 0.2
v_a2_19	8x8x4, U = (1.2;0.8)	-13.54326532	* [210]-[001] 2.1	3.3 + 0.2

02) *hcp* – Co “v_A2” (a;c)=(0.2503;0.4057); ISMEAR=1; EC=10⁻⁶; “Co_sv”; LMAXMIX=6; LREAL; LASPH; ADDGIRD; GGA_COMPAT; ISYM=-1; A2a) NSP+U → NSP+U-OPT → NSP+U-REL → SOC+U → SOC+U-OPT → SOC+U-REL; A2b) NSP+U → NSP+U-OPT → NSP+U-REL → SOC+U → SOC+U-OPT → SOC+U-REL.

Co₅, Co₆

V_F8a	Phase	+U [001] (conv) (eV)	MAE (100)	MAG [μ B/fu]
v_f8_01	Co ₆	-37.79914974	1.25	11.3 + 0.7
v_f8_03	Co ₅	-30.11309345	2.66	9.7 + 0.6
V_F8b	Phase	+U [001] (conv) (eV)	MAE (100)	MAG [μ B/fu]
v_f8_04	Co ₆	-38.23611000	1.84	11.0 + 0.6
V_F8c	Phase	+U [001] (conv) (eV)	MAE (100)	MAG [μ B/fu]
v_f8_07	Co ₅	-30.29766282	3.98	9.2 + 0.5

Co₅ & Co₆ “v_F8” – (a;c)=(0.4937;0.3986); M-5x5x7 k-pts.; ISMEAR=1; +U=conv.; EC=10⁻⁶; “Co_sv”; LMAXMIX=6; LREAL; LASPH; ADDGIRD; ISYM=-1; MAGMOM=(1.6;0.0); Co-3d-(U;J)=(1.2;0.8). F8a) NSP+U → SOC+U; F8b) NSP+U → NSP+U-OPT → SOC+U → SOC+U-OPT; F8c) NSP+U → NSP+U-OPT → NSP+U-REL → SOC+U → SOC+U-OPT → SOC+U-REL.

YCo₅

V_A2	Potential type – Files	SRC (con) (eV)	Spin-MAG [μ B/fu]
v_a2_01	.52 LDA – Co; Y_sv	-45.65151161	6.6
v_a2_02	.52 LDA – Co; Y_sv_GW	-47.74139530	6.6
v_a2_03	.52 LDA – Co_GW; Y_sv	-24.27915215	6.4
v_a2_04	.52 LDA – Co_GW; Y_sv_GW	-26.39930469	6.4
v_a2_05	.52 LDA – Co_pv; Y_sv	-42.26662501	6.6
v_a2_06	.52 LDA – Co_pv; Y_sv_GW	-44.36399225	6.6
v_a2_07	.52 LDA – Co_sv; Y_sv	772.508155	0.4
v_a2_08	.52 LDA – Co_sv; Y_sv_GW	769.4152919	0.4
v_a2_09	.52 LDA – Co_sv_GW; Y_sv	89.75878283	5.0
v_a2_10	.52 LDA – Co_sv_GW; Y_sv_GW	87.49599663	5.0
v_a2_11	.52 PBE – Co; Y_sv	-40.02478056	6.8
v_a2_12	.52 PBE – Co; Y_sv_GW	-42.11366247	6.8
v_a2_13	.52 PBE – Co_GW; Y_sv	-20.69453007	6.6

v_a2_14	.52 PBE – Co_GW; Y_sv_GW	-22.81722999	6.6
v_a2_15	.52 PBE – Co_pv; Y_sv	-36.60798129	6.8
v_a2_16	.52 PBE – Co_pv; Y_sv_GW	-38.7050645	6.8
v_a2_17	.52 PBE – Co_sv; Y_sv	662.6377578	1.2
v_a2_18	.52 PBE – Co_sv; Y_sv_GW	659.6721704	2.4
v_a2_19	.52 PBE – Co_sv_GW; Y_sv	93.82563216	5.1
v_a2_20	.52 PBE – Co_sv_GW; Y_sv_GW	91.54965793	5.1
v_a2_21	LDA – Co; Y_sv	-45.65151161	6.6
v_a2_23	LDA – Co_GW; Y_sv	-24.27915215	6.4
v_a2_24	LDA – Co_GW; Y_sv_GW	-26.21500365	6.3
v_a2_25	LDA – Co_pv; Y_sv	-42.26662501	6.6
v_a2_26	LDA – Co_pv; Y_sv_GW	-43.57454898	0.0
v_a2_27	LDA – Co_sv; Y_sv	772.508155	0.4
v_a2_28	LDA – Co_sv; Y_sv_GW	771.0250183	0.3
v_a2_29	LDA – Co_sv_GW; Y_sv	801.2959718	0.0
v_a2_30	LDA – Co_sv_GW; Y_sv_GW	798.714683	0.0
v_a2_31	PBE – Co; Y_sv	-40.02478056	6.8
v_a2_32	PBE – Co; Y_sv_GW	-41.19704404	0.7
v_a2_33	PBE – Co_GW; Y_sv	-20.69453007	6.6
v_a2_34	PBE – Co_GW; Y_sv_GW	-22.79263883	6.6
v_a2_35	PBE – Co_pv; Y_sv	-36.60798129	6.8
v_a2_36	PBE – Co_pv; Y_sv_GW	-37.76795871	0.2
v_a2_37	PBE – Co_sv; Y_sv	662.6377579	1.2
v_a2_38	PBE – Co_sv; Y_sv_GW	660.4445523	2.4
v_a2_39	PBE – Co_sv_GW; Y_sv	804.9144553	0.0
v_a2_40	PBE – Co_sv_GW; Y_sv_GW	802.0166935	0.0
v_a2_41	PAW_PW91 – Co; Y_sv	-39.7216862	6.8
v_a2_42	USPP_LDA – Co; Y	-47.58800966	6.8
v_a2_43	USPP_LDA – Co; Y_pv	-47.38736222	6.8
v_a2_44	USPP_PW91 – Co; Y	-41.96509747	7.1
v_a2_45	USPP_PW91 – Co; Y_pv	-41.78494429	7.1

1) YCo₅ “v_A2” – (a;c)=(0.4937;0.3986); ENCUT=200; G-11x11x11; ISMEAR=1; GGA; SRC=conv.; EC=10⁻⁸.

V_A5	ISMEAR	SOC [001] (con) (eV)	MAE (100)	MAE (210)	MAG [μB/fu]
v_a5_01	-5	-42.33209978	2.1	2.1	7.1 + 0.6
v_a5_02	-4	-42.31513912	1.1	1.1	7.1 + 0.6
v_a5_03	-2	-42.30700577	-0.1	-0.1	7.1 + 0.6
v_a5_04	-1	-42.48935782	1.9	1.8	7.1 + 0.6
v_a5_05	0	-42.35867647	2.4	2.4	7.1 + 0.6
v_a5_06	1	-42.33413024	2.5	2.5	7.1 + 0.6

3) YCo₅ “v_A5” – (a;c)=(0.4937;0.3986); ENCUT=265; G-5x5x5; SOC=conv.; EC=10⁻⁸; .52 PBE-“Co”+“Y_sv”.

V_B2	SRC-Optimization	SOC [001] (con) (eV)	MAE (100)	MAE (210)	MAG [μB/fu]
v_b2_01	No optimization	-42.29186144	1.8	1.8	7.3 + 0.6
v_b2_04_I	ISIF = 0	-40.50918470	3.6	4.3	4.2 + 0.4
v_b2_04_II	ISIF = 0	-40.50921879	3.7	4.6	4.2 + 0.4
v_b2_05_I	ISIF = 1	-40.50918470	3.7	4.3	4.2 + 0.4
v_b2_05_II	ISIF = 1	-40.50921879	3.7	4.6	4.2 + 0.4
v_b2_06_I	ISIF = 2	-40.50918470	3.7	4.3	4.2 + 0.4
v_b2_06_II	ISIF = 2	-40.50921879	3.7	4.6	4.2 + 0.4
v_b2_07_I	ISIF = 3	-45.49602754	-0.02	0.0	0.0 + 0.0
v_b2_07_II	ISIF = 3	-45.49640201	0.0	0.0	0.0 + 0.0
v_b2_08_I	ISIF = 4	-46.18675148	-1.3	-1.4	0.01 + 0.02
v_b2_08_II	ISIF = 4	-46.32030233	6.0	6.1	2.0 – 0.03
v_b2_09_I	ISIF = 5, LVTOT	-43.76809946	10.6	1.9	4.1 + 0.3
v_b2_09_II	ISIF = 5, LVTOT	-44.21771844	-3.2	-3.3	0.1 + 0.1
v_b2_10_I	ISIF = 6, LVTOT	-44.91973964	-1.5	-1.2	2.0 + 0.2
v_b2_10_II	ISIF = 6, LVTOT	-44.80023447	-0.7	-0.7	2.0 + 0.2
v_b2_11_I	ISIF = 7, LVTOT	-40.50359089	13.4	16.9	2.1 – 0.3

v_b2_11_II	ISIF = 7, LVTOT	-40.51312801	12.9	13.9	4.1 + 0.6
V_B4-SRC	SRC-Optimization	SOC [001] (con) (eV)	MAE (100)	MAE (210)	MAG [μ B/fu]
v_b4_06_I	ISIF = 2	-42.29186154	1.8	1.8	7.1 + 0.6
v_b4_06_II	ISIF = 2	-42.29186305	1.8	1.8	7.2 + 0.6
v_b4_07_I	ISIF = 3	-42.29533897	0.8	0.7	6.7 + 0.6
v_b4_07_II	ISIF = 3	-42.29540596	0.8	0.8	6.7 + 0.6
v_b4_10_I	ISIF = 6	-42.29566287	0.8	0.8	6.8 + 0.6
v_b4_10_II	ISIF = 6	-42.29526536	0.8	0.7	6.7 + 0.6
v_b4_11_I	ISIF = 7	-42.29456551	1.1	1.1	6.7 + 0.6
v_b4_11_II	ISIF = 7	-42.29588000	1.2	1.1	6.7 + 0.6

6) YCo_5 “v_B4” – (a;c)=(0.4937;0.3986); ENCUT=270; G-8x8x6; ISMEAR=1; GGA; SOC=conv.; EC = 10^{-6} ; .52 PBE-“Co”+“Y_sv”; ORBITALMAG=T; LVTOT=TRUE; LMAXMIX=6; NG(X,Y,Z); “I”: (ISTART 0, ICHARG 2); “II”: (ISTART 1, ICHARG 1). (SRC) → SRC-OPEL 1 → SRC-OPEL 2 → SRC-OPEL 3 → SOC.

V_B5	k-mesh	SRC (con) (eV)	Spin-MAG [μ B/fu]		
v_b5_01	G – 5x5x5	-42.22515898	7.1		
v_b5_02	M – 5x5x5	-42.22515898	7.1		
v_b5_03	G – 8x8x6	-42.19423945	7.1		
v_b5_04	G – 8x8x6	-42.22631240	7.2		
v_b5_05	G – 2x2x3	-42.22799685	5.8		
v_b5_06	G – 2x3x3	-42.28724349	7.7		
v_b5_07	G – 5x5x6	-42.21710480	7.0		
v_b5_08	G – 5x5x6	-42.23809483	7.2		
V_B5	Setup	SOC [001] (con) (eV)	MAE (100)	MAE (210)	MAG [μ B/fu]
v_b5_10_0	G – 5x5x5	-42.32112337	1.8	1.8	7.4 + 0.6
v_b5_10_1	G – 5x5x56	-42.33429705	2.0	2.0	7.2 + 0.6
v_b5_10_2	_0 + LREAL	-42.33204324	1.8	1.8	7.1 + 0.6
v_b5_10_4	_0 + NG(X,Y,Z)	-42.33204385	1.8	1.8	7.1 + 0.6
v_b5_10_7	_0 + LREAL + NGX	-42.33204322	1.8	1.8	7.1 + 0.6
v_b5_10_14	_0 + LREAL + NGX+LMAXMIX	-42.33204383	1.8	1.8	7.1 + 0.6
v_b5_10_17	G – 5x5x7, LREAL	-42.33165615	3.6	3.6	7.3 + 0.6

7) YCo_5 “v_B5” – (a;c)=(0.4937;0.3986); ENCUT=270; ISMEAR=1; GGA; SOC=conv.; EC= 10^{-6} ; “Co”+“Y_sv”.

V_B7	Setup	SOC [001] (con) (eV)	MAE (100)	MAE (210)	MAG [μ B/fu]
v_b7_01	M-5x5x7	-42.28827389	3.5	3.5	7.3 + 0.6
v_b7_02	M-5x5x7, MAGM	-42.28827352	3.5	3.5	7.3 + 0.6
v_b7_03	M-5x5x7, LMAX 4	-42.28827235	3.5	3.5	7.3 + 0.6
v_b7_04	M-7x7x9	-42.26136667	1.4	1.3	7.2 + 0.6
v_b7_05	M-7x7x9, MAGM	-42.26136413	1.3	1.3	7.2 + 0.6
v_b7_06	M-7x7x9, LMAX 4	-42.26136599	1.4	1.3	7.2 + 0.6
v_b7_07	M-9x9x11	-42.26358933	0.7	0.7	7.0 + 0.6
v_b7_08	M-9x9x11, MAGM	-42.26359104	0.7	0.7	7.0 + 0.6
v_b7_09	M-9x9x11, LMAX 4	-42.26359078	0.7	0.7	7.0 + 0.6
v_b7_10	M-5x5x6	-42.29032389	1.8	1.8	7.2 + 0.6
v_b7_11	M-5x5x6, MAGM	-42.29032497	1.8	1.8	7.2 + 0.6
v_b7_12	M-5x5x6, LMAX 4	-42.29032682	1.8	1.8	7.2 + 0.6
V_B8	k-mesh	SOC [001] (con) (eV)	MAE (100)	MAE (210)	MAG [μ B/fu]
v_b8_01	M-5x5x5	-42.28629072	1.7	1.7	7.4 + 0.6
v_b8_02	M-5x5x6	-42.29032583	1.8	1.8	7.5 + 0.6
v_b8_03	M-5x5x7	-42.28827299	3.5	3.5	7.6 + 0.6
v_b8_04	M-7x7x7	-42.26931078	1.2	1.2	7.5 + 0.6
v_b8_05	M-7x7x8	-42.26009679	1.8	1.8	7.6 + 0.6
v_b8_06	M-7x7x9	-42.26136588	1.4	1.3	7.3 + 0.6
v_b8_07	M-9x9x9	-42.26339146	1.5	1.5	7.3 + 0.6
v_b8_08	M-9x9x10	-42.26500553	0.6	0.7	7.3 + 0.6
v_b8_09	M-9x9x11	-42.2635908	0.7	0.7	7.5 + 0.6
v_b8_10	M-5x10x6	-42.28004897	1.2	1.2	7.4 + 0.6
v_b8_11	M-5x10x7	-42.24457482	0.4	0.5	7.4 + 0.6

v_b8_12	M-7x4x9	-42.27904912	1.1	1.0	7.4 + 06
v_b8_13	M-7x5x9	-42.26712117	1.5	1.6	7.4 + 06
v_b8_14	M-7x6x9	-42.26361952	1.1	0.9	7.4 + 06
v_b8_15	M-7x8x9	-42.26609034	1.1	1.1	7.4 + 06
v_b8_16	M-7x9x9	-42.26136498	1.0	0.9	7.4 + 06
v_b8_17	M-7x10x9	-42.26387065	1.3	1.2	7.4 + 06
v_b8_18	M-7x11x9	-42.26416182	1.1	1.1	7.4 + 06
v_b8_19	M-7x12x9	-42.26345846	1.0	1.0	7.4 + 06
v_b8_20	M-7x13x9	-42.26406108	1.2	1.3	7.4 + 06
v_b8_21	M-7x14x9	-42.26462347	1.1	1.0	7.4 + 06
v_b8_22	M-6x6x7	-42.30461276	0.8	0.8	7.4 + 06

10) YCo_5 “v_B7, B8” – (a;c)=(0.4937;0.3986); ENCUT=270; M-5x5x7 k-pts.; ISMEAR=1; SOC=conv.; EC = 10^{-6} .

V_C1	k-points / ENCUT	SOC [001] (con) (eV)	MAE (100)	MAE (210)	MAG [μ B/fu]
v_c1_01	6 (manual) / 275	-42.49069070	1.0	2.2	3.0 + 0.4
v_c1_02	6 (manual) / 355	-42.56103891	0.8	2.2	3.0 + 0.4
v_c1_03	150 (line) / 275	-42.09710519	-5.6	-4.9	3.1 + 0.3
v_c1_04	150 (line) / 355	-42.17831004	-5.6	-5.0	3.1 + 0.3
v_c1_05	100 (auto) / 275	-42.29830888	0.8	0.8	7.1 + 0.6
v_c1_07	5x5x7-G / 275	-42.32288666	3.6	3.5	7.3 + 0.6
v_c1_08	5x5x7-G / 355	-42.42745556	3.5	3.5	7.3 + 0.6
v_c1_09	10 (auto) / 275	-42.30112147	-1.4	-1.8	5.8 + 0.7
v_c1_10	10 (auto) / 355	-42.41568416	-1.5	-1.8	5.8 + 0.7
v_c1_11	20 (auto) / 275	-42.32371857	1.8	1.8	7.1 + 0.6
v_c1_12	20 (auto) / 355	-42.42903559	1.9	1.9	7.1 + 0.6
v_c1_13	30 (auto) / 275	-42.29607701	0.9	0.9	7.2 + 0.6
v_c1_14	30 (auto) / 355	-42.40040381	1.1	1.1	7.2 + 0.6
v_c1_15	40 (auto) / 275	-42.29499928	1.1	1.2	7.1 + 0.6
v_c1_16	40 (auto) / 355	-42.40086075	1.1	1.1	7.1 + 0.6

11) YCo_5 “v_C1” – (a;c)=(0.4937;0.3986); ENCUT=275+355; ISMEAR=1; SOC=conv.; EC= 10^{-6} ; LREAL.

V_C2	LREAL/ ENCUT	SOC [001] (con) (eV)	MAE (100)	MAE (210)	MAG [μ B/fu]
v_c2_01	auto / 275	-42.32034005	3.6	3.6	7.3 + 0.6
v_c2_02	auto / 355	-42.42690583	3.5	3.5	7.3 + 0.6
v_c2_03	on / 275	-42.35264890	3.5	3.5	7.3 + 0.6
v_c2_04	on / 275	-42.38367199	3.6	3.6	7.3 + 0.6
v_c2_05	false / 275	-42.32288522	3.6	3.6	7.3 + 0.6
v_c2_06	false / 275	-42.42745814	3.5	3.5	7.3 + 0.6
v_c2_07	true / 275	-42.34923482	3.5	3.5	7.3 + 0.6
v_c2_08	true / 275	-42.35910559	3.6	3.6	7.3 + 0.6

12) YCo_5 “v_C2” – (a;c)=(0.4937;0.3986); G-5x5x7 k-pts., ISMEAR=1; GGA; SOC=conv; EC= 10^{-6} ; .52 PBE-“Co”+“Y_sv”; “LMAXMIX=4”; ISYM=-1.

V_C3	ENCUT (eV)	SOC [001] (eV)	MAE (100)	MAE (210)	MAG [μ B/fu]
v_c3_01	200	-36.72941974	0.3	0.3	7.1 + 0.6
v_c3_02	225	-40.62249166	4.4	4.3	7.3 + 0.6
v_c3_03	250	-41.99172261	3.4	3.4	7.3 + 0.6
v_c3_04	275	-42.34023436	3.5	3.6	7.3 + 0.6
v_c3_05	300	-42.34023436	3.5	3.6	7.3 + 0.6
v_c3_06	325	-42.45371690	3.5	3.5	7.3 + 0.6
v_c3_07	350	-42.43175162	3.5	3.5	7.3 + 0.6
v_c3_08	375	-42.41190781	3.4	3.4	7.3 + 0.6
v_c3_09	400	-42.40518525	3.4	3.4	7.3 + 0.6
v_c3_10	425	-42.40360334	3.5	3.5	7.3 + 0.6
v_c3_11	450	-42.40784743	3.5	3.5	7.3 + 0.6
v_c3_12	475	-42.41125478	3.5	3.5	7.3 + 0.6
v_c3_13	500	-42.41351933	3.6	3.5	7.3 + 0.6
v_c3_14	525	-42.41452192	3.5	3.5	7.3 + 0.6
v_c3_15	550	-42.41416944	3.4	3.5	7.3 + 0.6

v_c3_16	575	-42.41367837	3.5	3.5	7.3 + 0.6
v_c3_17	600	-42.41286852	3.5	3.5	7.3 + 0.6
v_c3_18	625	-42.41233060	3.5	3.5	7.3 + 0.6
v_c3_19	650	-42.41250695	3.5	3.5	7.3 + 0.6
v_c3_20	675	-42.41294626	3.5	3.5	7.3 + 0.6
v_c3_21	700	-42.41362348	3.5	3.5	7.3 + 0.6
v_c3_22	725	-42.41417437	3.5	3.5	7.3 + 0.6
v_c3_23	750	-42.41465053	3.5	3.5	7.3 + 0.6
v_c3_24	775	-42.41505626	3.5	3.5	7.3 + 0.6
v_c3_25	800	-42.41519626	3.5	3.5	7.3 + 0.6
v_c3_26	825	-42.41518206	3.5	3.5	7.3 + 0.6
v_c3_27	850	-42.41509668	3.5	3.5	7.3 + 0.6
v_c3_28	875	-42.41491435	3.5	3.5	7.3 + 0.6
v_c3_29	900	-42.41471708	3.5	3.5	7.3 + 0.6
v_c3_30	925	-42.41460786	3.5	3.5	7.3 + 0.6
v_c3_31	950	-42.41451210	3.5	3.5	7.3 + 0.6
v_c3_32	975	-42.41414130	3.6	3.6	7.3 + 0.6
v_c3_33A	1000	-42.41377552	3.5	3.5	7.3 + 0.6
v_c3_33B	1000, no NSP	-42.41377572	3.5	3.5	7.3 + 0.6
v_c3_33C	1000, COMP	-42.41370258	3.5	3.5	7.3 + 0.6
v_c3_33D	1000, COMP, no NSP	-42.41370391	3.5	3.5	7.3 + 0.6

13) YCo_5 “v_C3” – (a;c)=(0.4937;0.3986); G-5x5x7 k-pts.; ISMEAR=1; SOC=conv.; EC= 10^{-6} ; .52 PBE-“Co”+“Y_sv”; LMAXMIX=4; ISYM=-1; GGA_COMPAT=TRUE (except for 2); NSP → SRC → SOC.

V_C4	Setup	SOC [001] (con) (eV)	MAE (100)	MAE (210)	MAG [μ B/fu]
v_c4_00	ENCUT 400	-42.40518525	3.4	3.4	7.3 + 0.6
v_c4_01	00 + COMPAT	-42.40463938	3.4	3.4	7.3 + 0.6
v_c4_02	01 + ADDGRID	-42.40478618	3.4	3.4	7.3 + 0.6
v_c4_03	02; ICHG 0	-41.58953515	9.5	0.0	0.0 + 0.0
v_c4_03B	02; ICHG 0 (src)	-42.40478608	3.4	3.4	7.3 + 0.6
v_c4_05B	02; ICHG 10 (src)	-42.40537076	3.6	3.6	7.3 + 0.7
v_c4_06	02; ICHG 11	-41.72955497	-3.8	-3.7	6.0 + 0.3
v_c4_06B	02; ICHG 11 (src)	-42.40538545	3.6	3.6	7.6 + 0.6
v_c4_07	02; ICHG 12	-48.27166158	0.0	0.0	6.0 + 0.3
v_c4_07B	02; ICHG 12 (src)	-48.27166158	3.6	0.0	6.0 + 0.3
v_c4_10	ENCUT 500	-42.41351933	3.6	3.5	7.3 + 0.6
v_c4_11	10 + COMPAT	-42.41305457	3.5	3.5	7.3 + 0.6
v_c4_12	11 + ADDGRID	-42.41306451	3.5	3.5	7.3 + 0.6
v_c4_13	12; ICHG 0	-41.59898137	0.0	-0.01	0.0 + 0.0
v_c4_16	12; ICHG 11	-41.73840326	-3.8	-3.8	6.0 + 0.5
v_c4_21*	ICHG 1	-42.40399490	0.1	-0.1	4.3 + 0.4
v_c4_23*	ICHG 1, nband 110	-42.40414412	0.4	0.2	4.6 + 0.4

14) YCo_5 “v_C4” (a;c)=(0.4937;0.3986); ENCUT=400+500; G-5x5x7 k-pts.; ISMEAR=1; SOC=conv.; EC= 10^{-6} ; .52 PBE-“Co”+“Y_sv”; LMAXMIX=4; LREAL=FALSE; ISYM=-1; NSP → SRC → SOC; * SRC → SOC.

V_C5	Potential type – Files	SOC [001] (con) (eV)	MAE (100)	MAE (210)	MAG [μ B/fu]
v_c5_01	Co; Y_sv	-42.34778100	3.7	3.7	7.3 + 0.6
v_c5_02	Co; Y_sv_GW	-44.49343004	3.7	3.7	7.3 + 0.6
v_c5_03	Co_GW; Y_sv	-42.42421781	3.7	3.8	7.3 + 0.6
v_c5_04	Co_GW; Y_sv_GW	-44.56979129	3.8	3.7	7.3 + 0.6
v_c5_05	Co_pv; Y_sv	-42.41351896	3.6	3.5	7.3 + 0.6
v_c5_06	Co_pv; Y_sv_GW	-44.56001027	3.5	3.5	7.3 + 0.6
v_c5_07	Co_sv; Y_sv	-42.87687941	3.7	3.7	7.3 + 0.6
v_c5_08	Co_sv; Y_sv_GW	-45.02352486	3.7	3.7	7.3 + 0.6
v_c5_09	Co_sv_GW; Y_sv	-48.18125628	3.6	3.7	7.3 + 0.6
v_c5_10	Co_sv_GW; Y_sv_GW	-50.32790019	3.4	3.4	7.3 + 0.6

15) YCo_5 “v_C5” – (a;c)=(0.4937;0.3986); ENCUT=500; G-5x5x7 k-pts.; ISMEAR=1; SOC=conv.; EC= 10^{-6} ; .52 PBE-“Co”+“Y_sv”; LMAXMIX=4; LREAL=FALSE; ISYM=-1; NSP → SRC → SOC.

V_D1	k-mesh type / Fe-site	SOC [001] (con) (eV)	MAE (100)	MAE (210)	MAG [μ B/fu]
v_d1_01	M – no Fe	-42.42103722	3.5	3.5	7.3 + 0.6
v_d1_02	M – TM1 (2c)	-43.72976026	1.5	1.4	8.2 + 0.6
v_d1_03	M – TM2 (2c)	-43.72976024	1.5	1.4	8.2 + 0.6
v_d1_04	M – TM3 (3g)	-43.65167487	0.5	0.8	8.2 + 0.6
v_d1_05	M – TM4 (3g)	-43.6516722	1.5	1.0	8.2 + 0.6
v_d1_06	M – TM5 (3g)	-43.65167403	1.5	1.7	8.2 + 0.6
v_d1_11	G – no Fe	-42.42103722	3.5	3.5	7.3 + 0.6
v_d1_12	G – TM1 (2c)	-43.72976146	1.5	1.4	8.2 + 0.6
v_d1_13	G – TM2 (2c)	-43.72976036	1.5	1.4	8.2 + 0.6
v_d1_14	G – TM3 (3g)	-43.65166984	0.5	0.8	8.2 + 0.6
v_d1_15	G – TM4 (3g)	-43.65167386	1.5	1.0	8.2 + 0.6
v_d1_16	G – TM5 (3g)	-43.65167403	1.5	1.7	8.2 + 0.6

16) YCo_5 , YCo_4Fe “v_D1” – (a;c)=(0.4937;0.3986); G&M-5x5x7 k-pts.; ISMEAR=1; SOC=con.; EC= 10^{-6} ; ISYM =-1; LREAL; LMAXMIX=4; GGA_COMPAT; ADDGIRD; SRC→SRC-OPT(ISIF 7)→SRC-REL (ISIF 2)→SOC.

V_E1	Steps; MAGMOM	SOC [001] (con) (eV)	MAE (100)	MAE (210)	MAG [μ B/fu]
v_e1_01	NSP → SOC; none.	-42.89051166	4.3	4.3	7.3 + 0.6
v_e1_02	NSP → SOC; AFM	-42.89051083	4.3	4.3	7.3 + 0.6
v_e1_03	NSP → SOC; FM	-42.89051147	4.3	4.3	7.3 + 0.6
V_E1	MAGMOM	SOC [001] (con) (eV)	MAE (100)	MAE (210)	MAG [μ B/fu]
v_e1_07	None	* -42.88908427			4.8 + 0.4
v_e1_08	AFM	-42.89051154	4.3	4.3	7.3 + 0.6
v_e1_09	FM	-42.89051127	4.3	4.3	7.3 + 0.6

17) YCo_5 “v_E1” – (a;c)=(0.4937;0.3986); M-5x5x7 k-pts.; ISMEAR=1; SOC=conv.; EC = 10^{-6} ; LMAXMIX=4; LREA; GGA_COMPAT; LASPH; ADDGIRD; ISYM=-1. NSP → SRC → SOC. * Given in [100].

V_E2	Steps	SOC [001] (con) (eV)	MAE (100)	MAE (210)	MAG [μ B/fu]
v_e2_01	nsp -> src -> soc	-42.89051101	4.3	4.3	7.3 + 0.6
v_e2_02	src -> soc	-42.88822893	4.3	4.3	7.3 + 0.6

18) YCo_5 “v_E2” – (a;c)=(0.4937;0.3986); M-5x5x7 k-pts.; ISMEAR=1; SOC=conv.; EC = 10^{-6} ; PBE-“Co”+“Y_sv”; LMAXMIX=4; LREAL; GGA_COMPAT=TRUE; LASPH; ADDGIRD; ISYM=-1.

V_E5	MAGMOM	SOC [001] (1 it) (eV)	MAE (100)	MAE (210)	MAG [μ B/fu]
v_e5_03	No MAGMOM	-42.89179989	4.7	4.7	7.3 + 0.6
v_e5_02	3.2 ; 0.0	-42.89025004	-0.2	0.0	4.4 + 0.4
v_e5_04	1.6 ; 0.0	-42.89179984	4.7	4.7	7.3 + 0.6

19) YCo_5 “v_E5” – (a;c)=(0.4937;0.3986); ENCUT=500; M-5x5x7 k-pts.; ISMEAR=1; SOC=1 it; EC = 10^{-6} ; “Co_sv”+“Y_sv”; LMAXMIX=6; LREAL; GGA_COMBAT; LASPH; ADDGIRD; ISYM=-1. NSP → SOC.

V_E3_a	MAGMOM	SOC [001] (1 it) (eV)	MAE (100)	MAE (210)	MAG [μ B/fu]
v_e3_a_01	1.6 ; -0.5	-42.50316756	-0.1	-0.1	7.1 + 0.5
v_e3_a_02	1.8 ; -0.5	-42.45406090	0.9	0.9	7.3 + 0.5
v_e3_a_03	2.0 ; -0.5	-42.33340236	0.9	1.3	7.2 + 0.5
v_e3_a_04	2.2 ; -0.5	-42.14472443	1.9	2.0	7.4 + 0.5
v_e3_a_05	2.2 ; -0.2	-42.14428192	2.9	2.7	7.2 + 0.5
v_e3_a_06	No MAGMOM	-41.83680137	-1.1	-1.2	7.3 + 0.5
v_e3_a_07	2.2 ; 0.0	-42.12856114	3.5	3.3	7.4 + 0.5
v_e3_a_08	2.5 ; 0.0	-41.70479507	2.5	2.8	7.5 + 0.5
v_e3_a_09	3.0 ; 0.0	-40.70225010	4.0		8.0 + 0.6
v_e3_a_10	3.3 ; 0.0	-40.34056489	7.4	7.5	7.4 + 0.5
v_e3_a_11	3.5 ; 0.0	-39.26915695	7.7	7.9	8.8 + 0.5
V_E3_b	MAGMOM	SOC [001] (1 it) (eV)	MAE (100)	MAE (210)	MAG [μ B/fu]
v_e3_b_02	1.6 ; -0.5	-42.88887012	4.0	4.0	7.3 + 0.6
v_e3_b_03	1.8 ; -0.5	-42.88886778	4.0	4.0	7.3 + 0.6
v_e3_b_04	2.0 ; -0.5	-42.88887227	4.0	4.0	7.3 + 0.6
v_e3_b_05	2.2 ; -0.5	-42.88887252	4.0	4.0	7.3 + 0.6
v_e3_b_06	1.6 ; -2.0	-42.88886976	4.0	4.0	7.3 + 0.6

v_e3_b_07	2.2 ; -0.2	-42.88887459	4.0	4.0	7.3 + 0.6
v_e3_b_08	2.2 ; 0.0	-42.88887105	4.0	4.0	7.3 + 0.6
v_e3_b_09	2.5 ; 0.0	-42.88897781	4.0	4.0	7.3 + 0.6

20) YCo_5 “v_E3” – (a;c)=(0.4937;0.3986); M-5x5x7 k-pts.; ISMEAR=1; GGA; SOC=1 it.; EC=10⁻⁶; LREAL; LMAXMIX=6; GGA_COMPAT; LASPH; ADDGIRD; ISYM=-1. E3a) NSP → NSP-OPT 1 → NSP-REL 1 → NSP-OPT 2 → NSP-REL 2 → SOC; E3b) NSP → NSP-OPT → NSP-REL → SRC → SRC-OPT → SRC-REL → SOC.

V_E4_A	MAGMOM	SOC [001] (1 it) (eV)	MAE (100)	MAE (210)	MAG [μ B/fu]
v_e4_a_01	1.6 ; -0.2	-42.51577776	1.0	0.9	7.2 + 0.5
v_e4_a_02	1.8 ; -0.2	-42.46181291	0.7	0.7	7.2 + 0.5
v_e4_a_03	2.0 ; -0.2	-42.33790357	1.2	1.3	7.2 + 0.5
v_e4_a_04	2.2 ; -0.2	-42.14533289	2.9	2.8	7.2 + 0.5
v_e4_a_05	2.2 ; 0.0	-42.13001172	3.5	3.1	7.2 + 0.5
v_e4_a_06	2.5 ; 0.0	-41.70747878	4.8	5.0	7.2 + 0.5
v_e4_a_07	3.0 ; 0.0	-40.68275492	6.1	6.1	7.2 + 0.5
v_e4_a_08	3.5 ; 0.0	-39.27052783	6.8	6.9	7.2 + 0.5
v_e4_a_09	3.8 ; 0.0	-38.22988756	5.3	4.8	7.2 + 0.5
v_e4_a_10	4.0 ; 0.0	-37.46692926	5.1	5.3	7.2 + 0.5
V_E4_B	MAGMOM	SOC [001] (1 it) (eV)	MAE (100)	MAE (210)	MAG [μ B/fu]
v_e4_b_01	1.6 ; -0.2	-42.88904074	4.3	4.3	7.3 + 0.6
v_e4_b_02	1.8 ; -0.2	-42.88901384	4.3	4.3	7.3 + 0.6
v_e4_b_03	2.0 ; -0.2	-42.88904074	4.3	4.3	7.3 + 0.6
v_e4_b_04	2.2 ; -0.2	-42.88909672	4.3	4.3	7.3 + 0.6
v_e4_b_05	2.2 ; 0.0	-42.88903311	4.3	4.3	7.3 + 0.6
v_e4_b_06	2.5 ; 0.0	-42.88903289	4.3	4.3	7.3 + 0.6
v_e4_b_07	3.0 ; 0.0	-42.89071159	4.0	4.0	7.3 + 0.6
v_e4_b_08	3.5 ; 0.0	-42.89088244	4.0	4.0	7.3 + 0.6

21) YCo_5 “v_E4” – (a;c)=(0.4937;0.3986); M-5x5x7 k-pts.; ISMEAR=1; GGA; SOC=1 it.; EC =10⁻⁶; PBE-“Co_sv”+“Y_sv”; LMAXMIX=6; LREAL; LASPH; ADDGIRD; ISYM=-1; OPT: ISIF=7; REL: ISIF=0. E4a) NSP → NSP-OPT 1 → NSP-REL 1 → NSP-OPT 2 → NSP-REL 2 → SOC; E4b) NSP → NSP-OPT → NSP-REL → SRC → SRC-OPT → SRC-REL → SOC.

V_E6	Fe-site	SOC [001] (conv) (eV)	MAE (100)	MAE (210)	MAG [μ B/fu]
v_e6_01	No Fe	-42.76320361	2.2	2.2	7.2 + 0.5
v_e6_04	TM3 (3g)	-43.93631791	3.3	-0.1	7.8 + 0.5
v_e6_05	TM4 (3g)	-43.93583632	1.7	0.7	7.8 + 0.5
v_e6_06	TM5 (3g)	-43.93561650	1.7	2.2	7.8 + 0.5

22) YCo_5 & YCo_4Fe “v_E6” – (a;c)=(0.4937;0.3986); M-5x5x7 k-pts.; ISMEAR=1; SOC=conv.; EC=10⁻⁶; “Co_sv”+“Fe_sv”+“Y_sv”; LMAXMIX=6; GGA_COMBAT; LREAL; LASPH; ADDGIRD; ISYM=-1; MAGMOM (Co;Fe;Y)=(3.2;4.4;0.0). NSP → NSP-OPT 1 → NSP-REL 1 → NSP-OPT 2 → NSP-REL 2 → SOC.

V_E8_1	MAGMOM / U	+U [001] (conv) (eV)	MAE (100)	MAE (210)	MAG [μ B/fu]
v_e8_01a	1.6; 0.0 / U_4f	-42.79739607	3.8	3.8	7.7 + 0.6
v_e8_01b	3.2; 0.0 / U_4f	-42.79739591	3.8	3.8	7.7 + 0.6
v_e8_01c	1.6; 0.0 / U_3d	-39.54552473	8.9	8.9	7.9 + 0.8
v_e8_01d	3.2; 0.0 / U_3d	-39.54552652	8.9	8.9	7.9 + 0.8
V_E8_2	MAGMOM / U	+U [001] (conv) (eV)	MAE (100)	MAE (210)	MAG [μ B/fu]
v_e8_02a	1.6; 0.0 / U_4f	-42.79739572	3.8	3.8	7.3 + 0.6
v_e8_02c	1.6; 0.0 / U_3d	-39.54552306	8.9	8.9	7.5 + 0.8
V_E8_3	MAGMOM / U	+U [001] (conv) (eV)	MAE (100)	MAE (210)	MAG [μ B/fu]
v_e8_03a	1.6; 0.0 / U_4f	-42.79739737	3.8	3.8	7.3 + 0.6
v_e8_03b	3.2; 0.0 / U_4f	-42.79739647	3.8	3.8	7.3 + 0.6
v_e8_03c	1.6; 0.0 / U_3d	-39.54552641	8.9	8.9	7.5 + 0.8
v_e8_03d	3.2; 0.0 / U_3d	-39.54552367	8.9	8.9	7.5 + 0.8
V_E8_4	MAGMOM / U	+U [001] (conv) (eV)	MAE (100)	MAE (210)	MAG [μ B/fu]
v_e8_04a	1.6; 0.0 / U_4f	-42.79739659	3.8	3.8	7.7 + 0.6
v_e8_04b	3.2; 0.0 / U_4f	-42.81461477	3.9	3.9	7.7 + 0.6
v_e8_04c	1.6; 0.0 / U_3d	-39.54552418	8.9	8.9	7.5 + 0.8
v_e8_04d	3.2; 0.0 / U_3d	-35.82695312	22.6	22.5	7.7 + 1.2

V_E8_6	MAGMOM / U	+U [001] (conv) (eV)	MAE (100)	MAE (210)	MAG [μ B/fu]
v_e8_06a	1.6; 0.0 / U_4f	-42.79739511	3.8	3.8	7.3 + 0.6
v_e8_06b	3.2; 0.0 / U_4f	-42.79739673	3.8	3.8	7.3 + 0.6
v_e8_06c	1.6; 0.0 / U_3d	-39.54552956	8.9	8.9	7.5 + 0.8
v_e8_06d	3.2; 0.0 / U_3d	-39.54552956	8.9	8.9	7.5 + 0.8
V_E8_7	MAGMOM / U	+U [001] (conv) (eV)	MAE (100)	MAE (210)	MAG [μ B/fu]
v_e8_07a	1.6; 0.0 / U_4f	-42.79739589	3.8	3.8	7.3 + 0.6
v_e8_07b	3.2; 0.0 / U_4f	-42.79739674	3.8	3.8	7.3 + 0.6
v_e8_07c	1.6; 0.0 / U_3d	-39.54552277	8.9	8.9	7.5 + 0.8
v_e8_07d	3.2; 0.0 / U_3d	-39.54552401	8.9	9.0	7.5 + 0.8
V_E8_8	U	+U [001] (conv) (eV)	MAE (100)	MAE (210)	MAG [μ B/fu]
v_e8_08a	4f (6.8 ; 0.7)	-42.79739656	3.8	3.8	7.7 + 0.6
v_e8_08b	4f (6.8 ; 0.7)	-42.81461549	3.9	3.9	7.7 + 0.6
v_e8_08d	3d (1.5 ; 0.8)	-39.54555225	8.9	9.1	7.5 + 0.8
v_e8_08h	3d (1.5 ; 0.8) *	-39.52470995	6.8	6.8	7.5 + 0.8
v_e8_08i	3d (1.6 ; 0.8)	-39.07456043	10.3	10.4	7.5 + 0.9
v_e8_08j	3d (0.8 ; 0.0)	-39.07456043	10.3	10.4	7.5 + 0.9

23) YCo_5 “v_E8” – (a;c)=(0.4937;0.3986); M-5x5x7 k-pts.; ISMEAR=1; +U=conv.; EC= 10^{-6} ; LMAXMIX=6; LREAL; GGA_COMBAT; LASPH; ADDGIRD; ISYM=-1; MAGMOM=(3.2;0.0) (except a=(1.6;0.0)). * k-mesh: 7x7x8. E8_1) NSP → SRC → SOC → +U; E8_2) NSP → SOC → +U; E8_3) NSP → SRC → SOC+U; E8_4) NSP → SOC+U; E8_6) SOC → +U; E8_7) SRC → SOC+U; E8_8) SOC+U.

V_E9	OPT / REL	+U [001] (conv) (eV)	MAE (100)	MAE (210)	MAG [μ B/fu]
v_e9_01	No optim.	-39.52472054	6.8	6.9	7.5 + 0.8
v_e9_02	OPT	-39.51966125	5.6	5.6	7.5 + 0.7
v_e9_03	OPT+REL (3)	-39.51434773	5.4	5.5	7.4 + 0.7
v_e9_04	OPT+REL (6)	-39.51441679	5.4	5.4	7.4 + 0.7

24) YCo_5 “v_E9” – (a;c)=(0.4937;0.3986); M-5x5x7 k-pts.; ISMEAR=1; GGA, +U=conv.; EC = 10^{-6} ; ADDGIRD; LMAXMIX=6; LREAL; GGA_COMPAT; LASPH; ISYM=-1; MAGMOM=(1.6;0.8). Co-3d-(U;J)=(1.5;0.8); NSP → (NSP-OPT) → (NSP-REL) → SRC → (SRC-OPT) → (SRC-REL) → (SOC+U).

V_F1	Setup	+U [001] (conv) (eV)	MAE (100)	MAE (210)	MAG [μ B/fu]
v_f1_01	-5; 5x5x7; 10^{-7}	-39.54552644	8.9	9.0	7.5 + 0.8
v_f1_02	1; 5x5x7; 10^{-7}	-39.54451513	9.0	9.1	7.5 + 0.8
v_f1_03	-5; 7x7x8; 10^{-7}	-39.52470990	6.8	7.1	7.6 + 0.8
v_f1_04	1; 7x7x8; 10^{-7}	-39.52356387	6.8	6.8	7.5 + 0.8
v_f1_05	-5; 5x5x7; 10^{-6}	-39.54552342	9.1	9.0	7.5 + 0.8
v_f1_06	1; 5x5x7; 10^{-6}	-39.54451305	8.9	9.0	7.5 + 0.8
v_f1_07	-5; 7x7x8; 10^{-6}	-39.52470164	6.8	7.2	7.5 + 0.8
v_f1_08	1; 7x7x8; 10^{-6}	-39.52356446	6.8	6.8	7.5 + 0.8
v_f1_09	=_06; 8x cores	-39.54451321	9.0	9.0	7.5 + 0.8

25) YCo_5 “v_F1” – (a;c)=(0.4937;0.3986); ISMEAR=-5+1; GGA; +U=conv.; EC= $10^{-6}+10^{-7}$; PBE- “Co_sv”+“Y_sv”; LMAXMIX=6; LREAL; GGA_COMPAT; LASPH; ADDGIRD; ISYM=-1; MAGMOM= (1.6;0.8). Co-3d-(U;J)=(1.5;0.8); REL 1: ISIF=3; REL 2: ISIF=6. NSP → SRC → (SOC+U).

V_F2	Co-3d-(U;J)	+U [001] (conv) (eV)	MAE (100)	MAG [μ B/fu]
v_f2_01	1.2; 0.8	-40.96821418	7.1	7.3 + 0.7
v_f2_02	1.3; 0.8	-40.49082209	7.6	7.3 + 0.8
v_f2_03	1.4; 0.8	-40.01690766	7.7	7.5 + 0.8
v_f2_04	1.5; 0.8	-39.54451305	8.9	7.5 + 0.8
v_f2_05	1.6; 0.8	-39.07375729	10.5	7.5 + 0.8
v_f2_06	1.7; 0.8	-38.60440598	11.8	7.5 + 0.9
v_f2_07	1.8; 0.8	-38.13653737	12.7	7.5 + 0.9

27) YCo_5 “v_F2” – (a;c)=(0.4937;0.3986); M-5x5x7 k-pts.; ISMEAR=1; +U=conv.; EC= 10^{-6} ; LMAXMIX=6; LREAL; GGA_COMPAT; LASPH; ADDGIRD; ISYM=-1; NSP+U → SRC+U → SOC+U.

V_F4	Latt. Par. “c” (Δc)	+U [001] (conv) (eV)	MAE (100)	MAG [μ B/fu]
v_f4_01	0.3906 (-2.0 %)	-40.97367941	6.9	7.3 + 0.7

v_f4_02	0.3926 (-1.5 %)	-40.97852320	7.2	7.3 + 0.7
v_f4_03	0.3946 (-1.0 %)	-40.97900352	7.1	7.3 + 0.7
v_f4_04	0.3966 (-0.5 %)	-40.97557148	6.9	7.3 + 0.7
v_f4_05	0.3986 (0.0 %)	-40.96821181	7.1	7.3 + 0.7
v_f4_06	0.4006 (+0.5 %)	-40.95835230	7.6	7.3 + 0.8
v_f4_07	0.4026 (+1.0 %)	-40.94589667	7.6	7.5 + 0.8
v_f4_08	0.4046 (+1.5 %)	-40.93021702	7.1	7.5 + 0.8
v_f4_09	0.4066 (+2.0 %)	-40.91072994	7.6	7.5 + 0.8

28) YCo_5 “v_F4” – (a;c)=(0.4937;0.3986); M-5x5x7 k-pts.; ISMEAR=1; d(a)=0; d(c)≠0; GGA; EC=10⁻⁶; LMAXMIX=6; LREAL; GGA_COM; LASPH; ADDGIRD; ISYM=-1; Co-3d-(U;J)=(1.2;0.8). NSP+U → SOC+U.

V_F5_A	OPEL	+U [001] (conv) (eV)	MAE (100)	MAG [μ B/fu]
v_f5a_01	ISIF 3	-40.97837491	7.1	7.3 + 0.7
v_f5a_02	ISIF 4	-40.97749917	7.5	7.3 + 0.7
V_F5_B	Latt. Par. “c” (Δ c)	+U [001] (conv) (eV)	MAE (100)	MAG [μ B/fu]
v_f5b_01	0.3849 (-2.0 %)	-40.92244874	5.6	7.3 + 0.7
v_f5b_02	0.3869 (-1.5 %)	-40.94189417	6.1	7.3 + 0.7
v_f5b_03	0.3888 (-1.0 %)	-40.95647821	6.9	7.3 + 0.7
v_f5b_04	0.3908 (-0.5 %)	-40.96771084	7.2	7.3 + 0.7
v_f5b_05	0.3927 (0.0 %)	-40.97470481	7.1	7.3 + 0.7
v_f5b_06	0.3947 (+0.5 %)	-40.97763761	6.9	7.3 + 0.7
v_f5b_07	0.3967 (+1.0 %)	-40.97620597	6.8	7.3 + 0.7
v_f5b_08	0.3986 (+1.5 %)	-40.97147467	7.4	7.3 + 0.7
v_f5b_09	0.4006 (+2.0 %)	-40.96366067	7.7	7.3 + 0.7

29) YCo_5 “v_F5_B” – (a;c)=(0.4937;0.3986); M-5x5x7 k-pts.; ISMEAR=1; d(a)=0; d(c)≠0;GGA; EC=10⁻⁶; LMAXMIX=6; LREAL; GGA_COMPAT; LASPH; ADDGIRD; ISYM=-1; MAGMOM=(1.6;0.0); Co-3d-(U;J)=(1.2; 0.8). F5a) NSP+U → NSP+U-OPT → NSP+U-OPEL → SOC+U → SOC+U-OPT → SOC+U-OPEL; F5b) NSP+U → SOC+U.

V_F6	Fe-site, U-potential	+U [001] (conv) (eV)	MAE (100)	MAG [μ B/fu]
v_f6_01	No Fe, U_3d-Co	-40.96821181	7.1	7.3 + 0.7
v_f6_02	TM1 (2c), U_3d-Co	-42.68860997	3.4	8.3 + 0.6
v_f6_03	TM4 (3g), U_3d-Co	-42.59528116	3.5	8.3 + 0.6
v_f6_04	TM1 (2c), U_3d-Co & 3d-Fe	-42.32027835	3.5	8.3 + 0.6
v_f6_05	TM4 (3g), U_3d-Co & 3d-Fe	-42.22926698	3.8	8.3 + 0.6
V_F7a	Cu-site	+U [001] (conv) (eV)	MAE (100)	MAG [μ B/fu]
v_f7_01	No Cu	-40.96821181	7.1	7.3 + 0.7
v_f7_02	TM1 (2c)	-37.88422161	2.0	5.3 + 0.5
v_f7_03	TM4 (3g)	-37.80079407	1.6	5.6 + 0.5
V_F7c	Fe-site, U_3d-Cu	+U [001] (conv) (eV)	MAE (100)	MAG [μ B/fu]
v_f7_09	TM1 (2c), (1.2; 0.8)	-37.73348402	2.3	5.3 + 0.5
v_f7_10	TM4 (3g), (1.2; 0.8)	-37.80784474	-7.6	5.5 + 0.4

30) YCo_5 , YCo_4Cu “v_F7” – (a;c)=(0.491599;0.392744); M-5x5x7 k-pts.; ISMEAR=1; +U=con; EC=10⁻⁶; LREAL; LASPH; LMAXMIX=6; GGA_COMPAT; ADDGIRD; ISYM=-1; MAGM=(1.6;0.0); Co-3d-(U;J)= (1.2;0.8). F6) NSP+U → SOC+U; F7a) no Cu-3d-(U;J); F7b) NSP+U → SOC+U → SOC+U-OPT → SOC+U-REL.

V_G2-d(c/a)	LP Ratio “c/a” (Δ c/a)	+U [001] (conv) (eV)	MAE (100)	MAG [μ B/fu]
v_g2_01	0.7829 (-2.0 %)	-40.96111116	6.0	7.3 + 0.7
v_g2_02	0.7869 (-1.5 %)	-40.96666266	6.5	7.3 + 0.7
v_g2_03	0.7909 (-1.0 %)	-40.96929305	5.6	7.3 + 0.7
v_g2_04	0.7949 (-0.5 %)	-40.97395673	6.2	7.0 + 0.6
v_g2_05	0.7989 (0.0 %)	-40.97471221	7.1	7.3 + 0.7
v_g2_06	0.8029 (+0.5 %)	-40.97381823	6.6	7.3 + 0.7
v_g2_07	0.8069 (+1.0 %)	-40.97189289	6.6	7.3 + 0.7
v_g2_08	0.8109 (+1.5 %)	-40.96901315	6.9	7.3 + 0.7
v_g2_09	0.8149 (+2.0 %)	-40.96365630	7.1	7.3 + 0.7

31) YCo_5 “v_G1, G2” – (a;c)=(0.49159943;0.39274376); M-5x5x7 k-pts.; ISMEAR=1; d(V)=0; +U=conv.; EC=10⁻⁶; PBE-“Co_sv”+“Y_sv”; LMAXMIX=6; LREAL; GGA_COMPAT; LASPH; ADDGIRD; ISYM=-1; Co-3d-(U;J)=(1.2;0.8). NSP+U → NSP+U-REL → SOC+U → SOC+U-REL.

PrCo₅

V_A1	Pot. Files	Pot. Type	SOC [001] (conv) (eV)	MAE [MJ/m ³]	MAG [μ B/fu]
v_a1_01	Co, Pr	.52 PBE	-42.97790316	1795.3	5.5 + 2.4
v_a1_02	Co, Pr_3	.52 PBE	-40.27621176	1476.4	7.5 + 0.7
v_a1_03	Co_pv, Pr	.52 PBE	-42.95569855	1785.7	5.5 + 2.4
v_a1_04	Co_pv, Pr_3	.52 PBE	-40.28540306	1467.8	7.5 + 0.7
v_a1_05	Co, Pr	PBE	-42.97790248	1795.3	5.5 + 2.5
v_a1_06	Co, Pr_3	PBE	-40.27621176	1476.4	7.5 + 0.7
v_a1_07	Co_pv, Pr	PBE	-42.95569872	1784.3	5.5 + 2.4
v_a1_08	Co_pv, Pr_3	PBE	-40.28540306	1467.8	7.5 + 0.7
v_a1_10	Co, Pr_3	PW 91	-40.15603255	1147.6	7.2 + 0.6

1) PrCo₅ “v_A1” – (a;c)=(0.5025;0.3943); ENCUT=275; M-5x5x5 k-pts.; ISMEAR=1, EC =10⁻⁶; NBAND=100.

V_A2		VASP File	SRC (conv) (eV)	Spin [μ B/fu]
v_a2_01	Co, Pr	impi 4.1. scalapack ifort 3	-42.44273729	5.0
v_a2_02	Co, Pr_3	impi 4.1. wannier90 ifort 3	-40.04534349	7.0
v_a2_03	Co_pv, Pr	impi 4.0. scalapack ifort 3	-41.84875597	7.9
v_a2_04	Co_pv, Pr_3	non cl- impi 4.0. scalap. ifort 3	-39.98320393	7.0

2) PrCo₅ “v_A2” – (a;c)=(0.5025;0.3943); ENCUT=275; M-2x2x2 k-pts.; SOC=Conv.; ISMEAR=1; EC =10⁻⁶; NBAND=100; @VSC2; .52 PBE-“Co_sv”+“Pr”.

V_A3	Pot. Files	Pot. Type	SOC [001] (conv) (eV)	MAE [MJ/m ³]	S+O-MAG [μ B/fu]
v_a3_01	Co, Pr	.52 PBE	-41.73368811	-3.8	7.3 – 0.3
v_a3_02	Co, Pr_3	.52 PBE	-39.28210618	16.1	4.3 + 0.7
v_a3_03	Co_pv, Pr	.52 PBE	-41.53993441	-8.3	4.4 + 1.1
v_a3_04	Co_pv, Pr_3	.52 PBE	-39.27435458	18.3	4.3 + 0.7
v_a3_05	Co, Pr	PBE	-41.73368449	4.4	7.3 – 0.3
v_a3_06	Co, Pr_3	PBE	-39.28210618	16.1	4.3 + 0.7
v_a3_07	Co_pv, Pr	PBE	-41.53474087	20.8	4.4 + 1.2
v_a3_08	Co_pv, Pr_3	PBE	-39.27435458	18.3	4.3 + 0.7
v_a3_10	Co, Pr_3	PW 91	-39.24885139	58.9	2.6 – 0.6

3) PrCo₅ “v_A3” – (a;c)=(0.5025;0.3943); ENCUT=275; M-1x1x1 k-pts.; GGA; SOC=Conv.; ISMEAR=1; ISYM= -1; GGA_COMPAT; N(X;Y;Z)=(54;54,48); EC=10⁻⁶; NBAND=100; NCL from start.

V_A4	Pot. Files	Pot. Type	SOC [001] (conv) (eV)	MAE [MJ/m ³]	S+O-MAG [μ B/fu]
v_a4_01	Co, Pr	.52 PBE	-42.97790530	0.006	5.5 + 2.4
v_a4_02	Co, Pr_3	.52 PBE	-40.27621241	-0.001	7.5 + 0.7
v_a4_03	Co_pv, Pr	.52 PBE	-42.95569678	-0.005	5.5 + 2.4
v_a4_04	Co_pv, Pr_3	.52 PBE	-40.28540226	0.001	7.5 + 0.7
v_a4_05	Co, Pr	PBE	-42.97790424	0.004	5.5 + 2.4
v_a4_06	Co, Pr_3	PBE	-40.27621241	-0.0001	7.5 + 0.7
v_a4_07	Co_pv, Pr	PBE	-42.95569678	-0.005	5.5 + 2.4
v_a4_08	Co_pv, Pr_3	PBE	-40.28540226	0.001	7.5 + 0.7
v_a4_10	Co, Pr	PW 91	-42.76927959	0.001	5.3 + 2.4
v_a4_10	Co, Pr_3	PW 91	-40.15603280	-0.001	7.2 + 0.7

V_A5	Pot. Files	Pot. Type	SOC [001] (conv) (eV)	MAE [MJ/m ³]	S+O-MAG [μ B/fu]
v_a5_01	Co, Pr	.52 PBE	-42.9779281	-1.8	5.5 + 2.4

5) PrCo₅ “v_A5” – (a;c)=(0.5025;0.3943); ENCUT=275; M-5x5x5 k-pts.; GGA; SOC=Conv.; ISMEAR=1; ISYM= -1; EC=10⁻⁶; NBAND=100; SOC, NCL from start. A5) LREAL.

Testing different VASP binary files. The NCL binaries are A: “vasp 5.2.12 – noncoll impi 4.0.3 elpa ifort13”; B: “vasp 5.2.12 noncoll impi 4.0.3 scalapack ifort13”; C: “vasp noncoll impi 4.1.0 wannier90 scalapack ifort13.1”; D: “vasp 5.2.12 noncoll impi 5.1.1 scalapack ifort16”; E: “vasp 5.3 – noncoll”; F: “vasp 5.4 – noncoll”.

V_A6	SRC binary	SOC [001] (conv) (eV)	MAE [MJ/m ³]	MAG [μ B/fu]
v_a6_03b	Vasp 5.2 mvapich2 scalapack ifort13	-43.02234791	-6.74	5.5 + 2.2
v_a6_03c		-43.02234791	-6.74	5.5 + 2.2

v_a6_05b	Vasp 5.2 impi 4.0.1 scalapack ifort13	-43.02234692	-6.75	5.0 + 2.2
v_a6_05c		-43.02234692	-6.75	5.0 + 2.2
v_a6_07b	Vasp 5.2 impi 4.0.1.007 mkl	-43.02234702	-6.72	5.0 + 2.2
v_a6_07c		-43.02234702	-6.72	5.0 + 2.2
v_a6_09b	Vasp 5.2 impi 4.0.3 scalapack ifort13	-43.02234724	-6.75	5.0 + 2.2
v_a6_09c		-43.02234724	-6.75	5.0 + 2.2
v_a6_10b	Vasp 5.2 impi 4.1.024 scalapack ifort13.1	-43.02234756	-6.76	5.0 + 2.2
v_a6_10c		-43.02234756	-6.76	5.0 + 2.2
v_a6_11b	Vasp 5.3 impi 4.1.0 sca mkl vtst3.0b	-43.02234757	-6.76	5.0 + 2.2
v_a6_11c		-43.02234757	-6.76	5.0 + 2.2
v_a6_13b	Vasp 5.2 noncoll impi 4.0.3 scalapack ifort13	-43.02234761	-6.76	5.0 + 2.2
v_a6_13c		-43.02234761	-6.76	5.0 + 2.2
v_a6_14b	Vasp 5.2 ncl impi 4.1 wannier 90 sca ifort13.1	-43.02235003	-6.72	5.0 + 2.2
v_a6_14c		-43.02235003	-6.72	5.0 + 2.2
v_a6_16e	Vasp 5.3.3	-43.02234721	-6.72	5.0 + 2.2
v_a6_18e	Vasp 5.3.3 ncl	-43.02234825	-6.75	5.0 + 2.2

6) $PrCo_5$ “v_A6” – (a;c)=(0.5025;0.3943); ENCUT=275; M-3x3x3 k-pts.; SOC=Conv.; ISMEAR=-5; ISYM=-1; EC=10⁻⁶; NBAND; NG(X;Y;Z); LREAL; LMAXMIX=6.

V_B1	ISMEAR, Type	SOC [001] (conv) (eV)	MAE (100)	MAE (210)	S+O-MAG [μB/fu]
v_b1_01	1, standard	-42.96403208	-1.97	-2.04	5.5 + 2.4
v_b1_02	1, non col.	-42.96403252	-1.97	-2.04	5.5 + 2.4
v_b1_04	-5, non col.	-42.96368016	-3.45	-4.14	5.4 + 2.5

7) $PrCo_5$ “v_B1” – (a;c)=(0.5025;0.3943); ENCUT=275; M-3x3x3 k-pts.; GGA; SOC=Conv.; ISMEAR=-5+1; ISYM=-1; EC=10⁻⁶; NBAND; NG(X;Y;Z); LREAL; LMAXMIX=6.

V_B2	.52 PBE Files	SOC [001] (conv) (eV)	MAE (100)	MAE (210)	S+O-MAG [μB/fu]
v_b2_01	Co, Pr	-42.98040842	0.20	0.28	5.5 + 2.4
v_b2_02	Co, Pr_3	-40.27409224	1.85	1.86	7.4 + 0.6
v_b2_03	Co_pv, Pr	-42.96063885	0.18	0.31	5.5 + 2.4
v_b2_04	Co_pv, Pr_3	-40.28691224	1.58	1.58	7.5 + 0.7

8) $PrCo_5$ “v_B2” – (a;c)=(0.5025;0.3943); ENCUT=275; M-5x5x7 k-pts.; ISMEAR=1; ISYM=-1; LREAL.

V_C1a	Data Files	SOC [001] (conv) (eV)	MAE (100)	MAE (210)	S+O-MAG [μB/fu]
v_c1_01	Co, Pr	-42.98259798	0.15	0.24	4.9 + 2.4
v_c1_02	Co_pv, Pr	-43.04894062	0.21	0.28	4.9 + 2.4
v_c1_03	Co_sv, Pr	-43.50269531	1.52	1.51	4.9 + 2.4
v_c1_04	Co, Pr_3	-40.28409481	1.71	1.70	7.1 + 0.7
v_c1_05	Co_pv, Pr_3	-40.37183892	1.79	1.77	7.1 + 0.7
v_c1_06	Co_sv, Pr_3	-40.82598795	2.40	2.40	7.1 + 0.6
V_C1b	Data Files	SOC [001] (conv) (eV)	MAE (100)	MAE (210)	S+O-MAG [μB/fu]
v_c1_11	Co, Pr				
v_c1_12	Co_pv, Pr	-43.04806686	-0.06	-0.04	3.1 + 1.4
v_c1_13	Co_sv, Pr	-43.50164508	0.23	0.02	1.7 + 0.7
v_c1_14	Co, Pr_3	-40.28349807	0.04	0.01	4.2 + 0.4
v_c1_15	Co_pv, Pr_3	-40.37120989	-0.02	0.002	4.2 + 0.4
v_c1_16	Co_sv, Pr_3	-40.82513897	0.01	-0.01	4.2 + 0.4
V_C1c	Data Files	SOC [001] (conv) (eV)	MAE (100)	MAE (210)	S+O-MAG [μB/fu]
v_c1_11	Co, Pr				
v_c1_12	Co_pv, Pr	-43.04807514	-0.04	0.001	3.1 + 1.4
v_c1_13	Co_sv, Pr	-43.50152957	-0.32	-0.28	2.7 + 1.2
v_c1_14	Co, Pr_3	-40.28349810	0.04	0.01	4.2 + 0.4
v_c1_15	Co_pv, Pr_3	-40.37120989	-0.01	0.001	4.2 + 0.4
v_c1_16	Co_sv, Pr_3	-40.82513897	0.01	0.03	4.2 + 0.4

9) $PrCo_5$ “v_C1” – (a;c)=(0.5025;0.3943); M-5x5x7 k-pts.; SOC=Conv.; ISMEAR=1; ISYM=-1; EC=10⁻⁷; LREAL; LMAXMIX=6. C1a) ISPIN=2; C1b) LNONCOLL, ISPIN=2; C1c) LNONCOLL; ISPIN=1.

V_C2a	Data Files	SOC [001] (conv) (eV)	MAE (100)	MAE (210)	S+O-MAG [μB/fu]
-------	------------	-----------------------	-----------	-----------	-----------------

v_c2_01	Co, Pr	-42.23783709				3.4 - 0.2
v_c2_03	Co_sv, Pr	-42.83547301	2.21	2.24		0.7 - 0.03
v_c2_04	Co, Pr_3	-40.28314030	1.76	1.77		7.1 + 0.7
v_c2_05	Co_pv, Pr_3	-40.37109024	1.75	1.76		7.1 + 0.7
v_c2_06	Co_sv, Pr_3	-40.81951846	2.08	2.13		7.1 + 0.6
V_C2b	Data Files	SOC [001] (conv) (eV)	MAE (100)	MAE (210)		S+O-MAG [μ B/fu]
v_c1_14	Co, Pr_3	-40.28345970	-0.003	-0.004		4.1 + 0.4
v_c1_16	Co_sv, Pr_3	-40.81986386	0.005	-0.001		4.1 + 0.4
V_C2	Data Files	SOC [001] (conv) (eV)	MAE (100)	MAE (210)		S+O-MAG [μ B/fu]
v_c1_22	Co_pv, Pr	-43.08795374	0.04	0.03		2.9 + 1.3
v_c1_25	Co_pv, Pr_3	-40.37141426	0.01	0.06		4.3 + 0.4
v_c1_26	Co_sv, Pr_3	-40.81999139	-0.002	-0.002		4.2 + 0.4

10) $PrCo_5$ "v_C2" - (a;c)=(0.5025;0.3943); M-5x5x7 k-pts.; ISMEAR=1; ISYM =-1; EC= 10^{-7} ; LREAL; LMAXMIX=6; SRC(OPT;REL). C2a) LNONCOLL, ISPIN; C2b) LNONCOLL, ISPIN=2; C2c) LNONCOLL.

V_D1	SRC-SOC /MAG	SOC[100] (con) (eV)	MAE (100)	MAE (210)	MAG [μ B/fu]
v_d1_01	separate - no MAG				
v_d1_02	separate - AFM	-43.56799952	2.2	2.3	5.0 + 2.0
v_d1_03	separate - FM	-43.02718392	8.0	6.1	8.4 - 0.5
v_d1_07	together - no MAG	-43.01129320			4.4 - 0.3
v_d1_08	together - AFM	-43.56800686	2.1	2.3	5.0 + 2.0
v_d1_09	together - FM	-43.00966543			7.6 - 0.4
V_D2	SRC-SOC /MAG	SOC[001] (con) (eV)	MAE (100)	MAE (210)	MAG [μ B/fu]
v_d2_01	separate - no MAG	-43.56733074	-0.02	-0.01	3.1 + 1.2
v_d2_02	separate - AFM	-43.56732782	-0.1	-0.02	3.1 + 1.2
v_d2_03	separate - FM	-43.56733136	-0.01	-0.01	3.1 + 1.2
v_d2_07	together - no MAG	-43.56732965	-0.02	-0.01	3.1 + 1.2
v_d2_08	together - AFM	-43.56732965	-0.02	-0.01	3.1 + 1.2
v_d2_09	together - FM	-43.56732965	-0.02	-0.01	3.1 + 1.2

12) $PrCo_5$ "v_D1, 2" - (a;c)=(0.5025;0.3943); G-5x5x7 k-pts.; SOC=Conv.; ISMEAR=1; ISYM =-1; EC= 10^{-7} ; LREAL; LMAXMIX=6; NSP \rightarrow SRC (\rightarrow) SOC. D1) SRC=collin., D2) SRC=NCL.

V_D3	k-points	SOC[001] (con) (eV)	MAE (100)	MAE (210)	S+O-MAG [μ B/fu]
v_d3_03	5x5x7	-43.38346672	-2.96	-3.01	4.7 + 1.8
v_d3_08*	5x5x9	-42.79209385	-3.14	-149.2	0.1 - 0.01
v_d3_09	5x5x10	-43.59474224	-0.4	-0.2	4.8 + 2.0

13) $PrCo_5$ "v_D3" - (a;c)=(0.5025;0.3943); SOC=Conv.; ISMEAR=1; ISYM=-1; EC= 10^{-7} ; LREAL; LMAXMIX=6; AFM; NSP \rightarrow SRC \rightarrow SOC; "Co_sv"+"Pr"; *SRC+SOC(OPT; REL).

V_D51	MAG (Co; Pr) μ_B	SOC[001] (1 it) (eV)	MAE (100)	MAE (210)	MAG [μ B/fu]
v_d51_01	1.6; -4.6	-44.09136749	15.2	15.2	4.6 + 1.0
v_d51_02	1.6; -4.0	-44.06445293	15.9	15.9	4.6 + 1.8
v_d51_03	1.6; -3.6	-44.01826090	17.1	16.6	4.5 + 2.8
v_d51_04	1.6; -2.6	-43.82237427	1.2	3.9	4.7 + 2.5
v_d51_05	1.6; -1.6	-43.54833669	-6.3	-6.8	4.8 + 3.0
v_d51_06	1.6; -1.4	-43.48494665	-6.5	-7.0	4.7 + 2.9
v_d51_07	1.6; -1.2	-43.41961304	-6.3	-6.4	4.9 + 2.4
v_d51_08	1.6; -1.0	-43.35354572	-4.8	-4.5	4.9 + 2.2
v_d51_09	1.6; -0.8	-43.28784090	-2.9	-2.5	4.7 + 2.6
v_d51_10	1.6; -0.6	-43.22470867	-0.6	-0.4	4.7 + 2.5
v_d51_11	1.6; -0.4	-43.16614255	1.2	1.1	4.5 + 2.7
v_d51_12	1.6; -0.2	-43.11360429	-0.8	-1.0	5.5 + 2.2
v_d51_13	1.6; 0.0	-43.06337957	-7.8	-8.0	5.7 - 1.6
V_D52	MAG (Co; Pr) μ_B	SOC[001] (1 it) (eV)	MAE (100)	MAE (210)	MAG [μ B/fu]
v_d52_01	1.6; -4.6	-44.21181951	5.9	5.4	4.6 + 0.6
v_d52_02	1.6; -4.0	-44.08364908	8.1	8.8	4.9 + 0.7
v_d52_03	1.6; -3.6	-43.95928087	8.1	9.0	4.6 + 0.6
v_d52_04	1.6; -2.6	-43.53763151	24.7	24.7	4.6 + 0.6

v_d52_05	1.6; -1.6		-43.00409472	29.3	26.9	4.5 + 0.6
v_d52_06	1.6; -1.4		-42.89616544	26.5	25.1	4.5 + 0.6
v_d52_07	1.6; -1.2		-42.79376397	22.9	22.9	4.7 + 0.6
v_d52_08	1.6; -1.0		-42.69489883	0.2	15.3	4.8 + 0.7
v_d52_09	1.6; -0.8		-42.60537388	3.5	4.1	5.0 + 0.6
v_d52_10	1.6; -0.6		-42.52740747	-9.1	-9.6	5.0 + 0.5
v_d52_11	1.6; -0.4		-42.46295463	-15.8	-16.2	5.0 + 0.5
v_d52_12	1.6; -0.2		-42.41186283	-17.5	-17.9	5.5 + 0.5
v_d52_13	1.6; 0.0		-42.37235701	-17.8	-17.4	5.4 + 0.5
V_D53	MAG (Co; Pr) μ_B	SOC[001] (1 it) (eV)	MAE (100)	MAE (210)	MAG [μ_B /fu]	
v_d53_01	3.2; -3.6		-43.54870058	0.4	0.4	5.1 + 2.0
v_d53_02	3.2; -2.6		-43.55302177	2.4	0.8	5.1 + 2.0
v_d53_03	3.2; -1.6		-43.55283471	0.9	0.5	5.0 + 1.9
v_d53_04	1.6; -3.6		-43.49214353	-43.3	-45.0	5.0 + 2.2
v_d53_05	1.6; -1.6		-43.54869838	0.4	0.5	5.1 + 2.0

14) $PrCo_5$ “v_D51 & D52 & D53” – (a;c)=(0.5025;0.3943); G-5x5x7 k-pts.; SOC=1 it.; ISMEAR=-5; ISYM=-1; EC=10⁻⁷; LREAL; LMAXMIX=6; D51, 52) NSP → SOC; D53) NSP → SRC → SOC.

V_D61	MAG (Co; Pr) μ_B	SOC[001] (1 it) (eV)	MAE (100)	MAE (210)	S+O-MAG [μ_B /fu]	
v_d61_01	3.2; -0.2		-41.59011429	-17.1	-16.6	4.3 + 0.6
v_d61_02	3.2; -0.4		-41.64813573	-9.9	-9.8	4.3 + 0.6
v_d61_03	3.2; -0.6		-41.71669168	-1.0	-1.3	4.3 + 0.6
v_d61_04	3.2; -0.8		-41.79505845	8.3	48.5	4.1 + 0.6
v_d61_05	3.2; -1.0		-41.88159042	16.2	1.7	4.2 + 0.7
v_d61_06	3.2; -1.2		-41.97423174	21.8	22.5	4.3 + 0.7
v_d61_07	3.2; -1.4		-42.07070141	25.7	27.4	4.2 + 0.7
v_d61_08	3.2; -1.6		-42.16809248	27.7	29.3	4.2 + 0.7
v_d61_09	no MAGMOM		-42.66961625	0.1	0.1	3.9 – 0.7
v_d61_10	1.6; -0.2		-42.91797570	0.7	0.5	4.4 + 1.3
v_d61_11	1.6; -0.4		-42.96499372	-2.6	-3.0	4.4 + 1.4
v_d61_12	1.6; -0.6		-43.01511814	-8.1	-8.0	4.4 + 1.4
v_d61_13	1.6; -0.8		-43.06757276	-13.4	-13.1	4.4 + 1.3
v_d61_14	1.6; -1.0		-43.12065460	-18.3	-18.1	4.4 + 1.2
v_d61_15	1.6; -1.2		-43.17305754	-21.9	-21.5	4.5 + 1.4
v_d61_16	1.6; -1.4		-43.22344980	-25.1	-25.1	4.8 + 1.9
v_d61_17	1.6; -1.6		-43.27239310	-25.8	-26.2	4.7 + 1.5
v_d61_18	1.6; -1.8		-43.31959900	-24.7	-25.3	4.7 + 1.4

15) $PrCo_5$ “v_D61” – (a;c)=(0.5025;0.3943); G-5x5x7 k-pts.; SOC=1 it.; ISMEAR=-5; ISYM=-1; EC=10⁻⁷; LREAL; LMAXMIX=6; NSP → NSP-OPT 1 → NSP-REL 1 → NSP-OPT 2 → NSP-REL 2 → SOC.

V_D62	Fe-site	SOC[001] (1 it) (eV)	MAE (100)	MAE (210)	S+O-MAG [μ_B /fu]	
v_d62_01	No Fe		-41.71669168	-1.0	-1.3	4.3 + 0.6
v_d62_02	TM(2c1)		-42.10202682	0.7	0.9	5.2 + 1.7
v_d62_03	TM(2c2)		-42.10766460	-4.2	-4.0	5.2 + 2.0
v_d62_04	TM(3g1)		-42.18821412	15.7	18.1	5.4 + 1.8
v_d62_05	TM(3g2)		-42.18851016	16.6	18.4	5.4 + 1.8
v_d62_06	TM(3g3)		-42.18838998	16.7	15.0	5.4 + 1.8

16) $PrCo_5$ “v_D62” – based on “v_d61_03”; (a;c)=(0.5025;0.3943); MAGMOM (Co;Fe;Pr)=(3.2;4.4;-0.6).

V_E1a	k-mesh / U_3d?	(U,J) of R_4f	SOC[001] (con) (eV)	MAE (100)	S+O-MAG [μ_B /fu]
v_e1_01	5x5x7 / no	6.8, 0.7	-42.39568769	-15.4	5.1 + 1.6
v_e1_02	5x5x7 / no	6.0, 0.7	-42.32732911	-52.8	5.1 + 1.1
v_e1_03	5x5x7 / yes	6.8, 0.7	-39.05424596	18.6	5.4 + 2.1
v_e1_04	5x5x7 / yes	6.0, 0.7	-39.00611613	-59.3	5.4 + 1.3
v_e1_05	7x7x8 / no	6.8, 0.7	-41.98981723	-82.5	5.0 + 0.6
v_e1_06	7x7x8 / no	6.0, 0.7	-42.44778573	15.2	5.1 + 1.9
V_E1b	k-mesh / U_3d?	(U,J) of R_4f	SOC[001] (con) (eV)	MAE (100)	S+O-MAG [μ_B /fu]
v_e1_07	5x5x7 / no	6.8, 0.7	-42.40978013		5.1 + 1.9
v_e1_08	5x5x7 / no	6.0, 0.7	-42.32630265	-139.7	5.1 + 1.3

v_e1_23	5x5x7 / no	5.2, 0.7	-42.52570591	-86.9	5.1 + 2.5
v_e1_24	5x5x7 / no	4.8, 0.7	-42.56443290	-115.8	5.1 + 2.5
v_e1_09	7x7x8 / no	6.8, 0.7	-41.98974819	-82.1	5.0 + 0.6
v_e1_10	7x7x8 / no	6.0, 0.7	-42.44856146	15.4	5.1 + 1.9
V_E1c	k-mesh / U_3d?	(U,J) of R_4f	SOC[001] (con) (eV)	MAE (100)	S+O-MAG [μ B/fu]
v_e1_11	5x5x7 / no	6.8, 0.7	-42.46888966	-0.9	5.1 + 1.6
v_e1_12	5x5x7 / no	6.0, 0.7	-42.38262001	22.6	5.1 + 1.7
v_e1_13	7x7x8 / no	6.8, 0.7	-42.45549829	14.3	5.2 + 1.7
v_e1_14	7x7x8 / no	6.0, 0.7	-42.36496624	19.3	5.2 + 1.7
V_E1d	k-mesh / U_3d?	(U,J) of R_4f	SOC[001] (con) (eV)	MAE (100)	S+O-MAG [μ B/fu]
v_e1_15	5x5x7 / no	6.8, 0.7	-42.39988698	34.8	5.1 + 2.5
v_e1_16	5x5x7 / no	6.0, 0.7	-42.45671853	-33.2	5.1 + 2.5
v_e1_17	7x7x8 / no	6.8, 0.7	-42.38631474	-19.5	5.2 + 2.5
v_e1_18	7x7x8 / no	6.0, 0.7	-42.44421539	-37.8	5.2 + 2.5
v_e1_19	7x7x8 / no	6.5, 0.7	-42.40694790	-114.2	5.2 + 2.5
v_e1_20	7x7x8 / no	7.0, 0.7	-42.00796260	-689.9	5.3 + 3.4
v_e1_21	7x7x8 / yes	6.8, 0.7	-39.14378040	-702.7	5.6 + 3.7
v_e1_22	7x7x8 / yes	6.0, 0.7	-39.56194949	-28.3	5.5 + 2.7

17) $PrCo_5$ "v_E1" - (a;c)=(0.5025;0.3943); ISMEAR=1; ISYM=-1; EC = 10^{-6} ; LREAL; LMAXMIX=6; Co-3d-(U;J)=(1.5;0.8).
 E1a) NSP+U \rightarrow SRC+U \rightarrow SOC+U; E1b) NSP+U \rightarrow SOC+U; E1c) SRC+U \rightarrow SOC+U; E1d) SOC+U.

V_E2a	k-mesh / U_3d?	(U,J) of R_4f	SOC[001] (con) (eV)	MAE (100)	S+O-MAG [μ B/fu]
v_e2_01	5x5x7 / no	6.8, 0.7	-42.18581366	-324.3	5.1 + 2.2
v_e2_02	5x5x7 / no	6.0, 0.7	-42.44120183	-15.0	5.1 + 1.6
v_e2_03	5x5x7 / yes	6.8, 0.7	-38.71258312	-125.8	5.5 + 0.8
v_e2_04	5x5x7 / yes	6.0, 0.7	-39.09760191	15.0	5.4 + 2.1
v_e2_05	7x7x8 / no	6.8, 0.7	-42.39393193	-15.5	5.1 + 1.5
V_E2b	k-mesh / EC	(U,J) of R_4f	SOC[001] (con) (eV)	MAE (100)	S+O-MAG [μ B/fu]
v_e2_07	5x5x7 / 10^{-6}	6.8, 0.7	-42.02705142	-221.9	5.1 + 3.5
v_e2_07b	5x5x7 / 10^{-7}	6.8, 0.7	-42.02628100	-220.6	5.1 + 3.5
v_e2_08	5x5x7 / 10^{-6}	6.0, 0.7	-42.43781004	-10.9	5.1 + 1.6
v_e2_19	5x5x7 / 10^{-6}	5.2, 0.7	-42.52569353	-81.0	5.1 + 2.5
v_e2_19b	5x5x7 / 10^{-7}	5.2, 0.7	-42.52569221		5.1 + 2.5
v_e2_09	7x7x8 / 10^{-6}	6.8, 0.7	-42.39460275	502.0	5.1 + 1.6
v_e2_10	7x7x8 / 10^{-6}	6.0, 0.7	-42.44745847	132.3	5.1 + 1.8
V_E2c	k-mesh / U_3d?	(U,J) of R_4f	SOC[001] (con) (eV)	MAE (100)	S+O-MAG [μ B/fu]
v_e2_16	5x5x7 / no	6.0, 0.7	-42.45775283	-33.0	5.1 + 2.5
v_e2_20	5x5x7 / no	5.2, 0.7	-42.57506039	67.2	5.1 + 1.5
v_e2_17	7x7x8 / no	6.8, 0.7	-42.38604076		5.2 + 2.5
v_e2_18	7x7x8 / no	6.0, 0.7	-42.44438998	-29.7	5.2 + 2.5

18) $PrCo_5$ "v_E2" - (a;c)=(0.5025;0.3943); SOC+U=conv. ; ISMEAR=1; ISYM=-1; EC = 10^{-6} ; LREAL; LMAXMIX=6. E2a) Co-3d-(U;J)=(1.5;0.8); NSP+U \rightarrow SRC+U \rightarrow SOC+U; E2b) no Co-3d-(U;J); NSP+U \rightarrow SOC+U; E2c) no Co-3d-(U;J); SOC+U.

V_E3a	Steps	(U,J) R_4f	SOC[001] (con) (eV)	MAE (100)	MAG [μ B/fu]
v_e3_19	SOC+U	6.8, 0.7	-42.41353698	-82.3	5.1 + 2.5
v_e3_20	NSP+U \rightarrow SOC+U	6.8, 0.7	-42.43041702	-20.1	5.1 + 1.7
v_e3_21	NSP+U \rightarrow SOC+U	6.0, 0.7	-42.32649229	-136.5	5.1 + 1.1
V_E3b	(U,J) T_3d	(U,J) R_4f	SOC[001] (con) (eV)	MAE (100)	MAG [μ B/fu]
v_e3_06	1.2, 0.8	7.0, 0.7	-40.38085359	11.3	5.2 + 1.6
v_e3_22	1.2, 0.8	6.9, 0.7	-40.44705326	149.9	5.2 + 2.5
v_e3_07	1.2, 0.8	6.8, 0.7	-40.49592959	1797.2	5.2 + 2.6
v_e3_08	1.2, 0.8	6.6, 0.7	-39.62896061	240.7	5.1 + 1.9
v_e3_09	1.2, 0.8	6.4, 0.7	-40.56200103	-96.5	5.2 + 2.3
V_E3c	(U,J) T_3d	(U,J) R_4f	SOC[001] (con) (eV)	MAE (100)	MAG [μ B/fu]
v_e3_11	1.8, 0.8	7.0, 0.7	-37.66313380	11.0	5.5 + 1.9
v_e3_13	1.8, 0.8	6.8, 0.7	-37.68166779	1616.4	5.4 + 2.8
v_e3_14	1.8, 0.8	6.6, 0.7	-37.77701222	3.7	5.4 + 1.8
v_e3_15	1.8, 0.8	6.4, 0.7	-37.79888924	259.0	5.4 + 1.9

19) $PrCo_5$ “v_E3” – (a:c)=(0.5025;0.3943); G-5x5x7 k-pts.; SOC+U=conv.; ISMEAR=1; ISYM=-1; EC=10⁻⁶; LREAL; LMAXMIX=6. E3a) no Co-3d-(U;J); E3b) SRC+U → SOC+U; E3c) SRC+U → SOC+U.

V_E4	Steps, k-mesh	(U,J) Co_3d	+U[001] (con) (eV)	MAE (100)	MAG [μB/fu]
v_e4_01	SRC-> SOC – G	None	-42.45511630	13.6	5.2 + 1.7
v_e4_02	SRC-> SOC – M	None	-42.28090146		5.2 + 1.8
v_e4_03	SOC – G	1.8, 0.8 eV	-37.35444995	-673.4	5.6 + 3.8
v_e4_04	SRC-> SOC – M	1.8, 0.8 eV	-37.63826802	49.3	5.5 + 2.2
v_e4_05	SRC-> SOC – G	1.8, 0.8 eV	-37.63679546	37.2	5.5 + 2.2
V_E5	Steps, k-mesh	(U,J) Co_3d	+U[001] (con) (eV)	MAE (100)	MAG [μB/fu]
v_e5_04	SRC-> SOC – M	1.8, 0.8 eV	-37.70725471	1642.1	5.5 + 2.8
v_e5_05	SRC-> SOC – G	1.8, 0.8 eV	-37.70384993	1637.5	5.5 + 2.7

20) $PrCo_5$ “v_E4 & E5” – (a:c)=(0.5025;0.3943); G+M 7x7x8 k-pts.; ISMEAR=1; ISYM=-1; EC=10⁻⁶; LREAL; LMAXMIX=6; Pr-4f-(U;J)=(6.8, 0.7); NCORE=4; @VSC2. E4) SRC+U → SOC+U; E5) SRC+U → SOC+U.

V_E6a	(U,J) Pr_4f	SOC[001] (con) (eV)	MAE (100)	MAG [μB/fu]
v_e6a_01	7.0, 0.7 eV	-42.43627839	2207.0	5.1 + 1.8
v_e6a_02	6.8, 0.7 eV	-42.29037080	-315.6	5.1 + 1.8
v_e6a_03	6.6, 0.7 eV	-42.03893684	-794.9	5.2 + 3.4
v_e6a_08	6.5, 0.7 eV	-41.39745869	261.0	5.0 + 1.7
v_e6a_04	6.4, 0.7 eV	-42.47080801	-10.6	5.1 + 1.5
v_e6a_07	6.3, 0.7 eV	-42.42456988	1729.4	5.1 + 2.5
v_e6a_07*	(EC 10 ⁻⁷) 6.3, 0.7 eV	-42.42457591	1939.8	5.1 + 2.5
v_e6a_05	6.2, 0.7 eV	-42.50052910	16.0	5.1 + 1.8
v_e6a_06	6.0, 0.7 eV	-41.54448269	241.1	5.0 + 1.7
V_E6b	(U,J) Pr_4f	SOC[001] (con) (eV)	MAE (100)	MAG [μB/fu]
v_e6b_01	7.0, 0.7 eV	-42.01139751	-718.0	5.2 + 3.4
v_e6b_02	6.8, 0.7 eV	-42.38935478	-33.2	5.1 + 2.5
v_e6b_03	6.6, 0.7 eV	-42.03905439	-711.9	5.2 + 3.5
v_e6b_04	6.4, 0.7 eV	-42.41727036	35.3	5.1 + 2.5
v_e6b_05	6.2, 0.7 eV	-42.43203405	-36.9	5.1 + 2.5
v_e6b_11	6.1, 0.7 eV	-42.43963050	-110.6	5.1 + 2.5
v_e6b_06	6.0, 0.7 eV	-42.44737418	2.8	5.1 + 2.5
v_e6b_12	5.9, 0.7 eV	-42.45524677	-34.4	5.1 + 2.5
v_e6b_07	5.8, 0.7 eV	-42.49712286	-31.3	5.0 + 1.7
v_e6b_08	5.6, 0.7 eV	-42.47987166	1423.6	5.1 + 2.5
v_e6b_09	5.4, 0.7 eV	-42.49723385	1398.4	5.1 + 2.5
v_e6b_10	5.2, 0.7 eV	-42.51616622	-93.4	5.1 + 2.5
V_E6c	(U,J) Pr_4f	SOC[001] (con) (eV)	MAE (100)	MAG [μB/fu]
v_e6c_01*	7.0, 0.7 eV	*[110] -42.13354815		*[110] 5.1 + 2.5
v_e6c_02	6.8, 0.7 eV	-42.31956638	-127.8	5.1 + 1.3
v_e6c_03	6.6, 0.7 eV	-42.45898778	2091.6	5.1 + 1.6
v_e6c_04	6.4, 0.7 eV	-42.42201072	12.6	5.1 + 1.9
v_e6c_05	6.3, 0.7 eV	-42.09274949	-128.7	5.1 + 0.6
v_e6c_06	6.2, 0.7 eV	-42.10134682	-132.5	5.1 + 0.6
v_e6c_07	6.1, 0.7 eV	-42.48797076	649.4	5.1 + 2.0

21) $PrCo_5$ “v_E6” – (a:c)=(0.5025;0.3943); M-5x5x7 k-pts.; GGA; SOC+U=conv.; ISMEAR=1; LREAL; ISYM=-1; EC=10⁻⁶; LMAXMIX=6; NCORE=4; @VSC3. E6a) SRC+U→SOC+U; E6b) SOC+U; E6c) NSP+U→SOC+U.

V_E7	Steps	SOC[001] (con) (eV)	MAE (100)	MAG [μB/fu]
v_e7_02	SRC→OPT→OPEL→ SOC→OPT→OPEL	-42.33467152	-182.3	5.1 + 1.8
v_e7_03	SRC→SOC→OPT→OPEL	-42.41242124	-34.5	5.1 + 2.5
v_e7_04	SRC→ SOC→OPT→REL	-42.40802622	33.0	5.1 + 2.5

22) $PrCo_5$ “v_E7” – (a:c)=(0.5025;0.3943); M-5x5x7 k-pts.; GGA; SOC+U=conv.; ISMEAR=1; ISYM=-1; EC=10⁻⁶+10⁻⁷; LREAL; LMAXMIX=6; PBE-“Co_sv”+“Pr”; Pr-4f-(U;J)=(6.8,0.7).

V_E8	(U, J) Pr_4f - comment	SOC[001] (con) (eV)	MAE (100)	MAG [μB/fu]
v_e8_01	6.4; 1.0	-42.43963068	185.6	5.1 + 2.5

v_e8_02	6.4; 0.9	-42.50046423	16.1	5.1 + 1.9
v_e8_03	6.4; 0.8	-42.42455853	1726.1	5.1 + 2.5
v_e8_04	6.4; 0.7	-42.47080801	-10.6	5.1 + 1.5
v_e8_05	6.4; 0.6	-41.39766282	262.7	5.0 + 1.7
v_e8_06	6.4; 0.5	-42.34409445	-33.4	5.1 + 1.6
v_e8_07	6.4; 0.4	-42.44725699	-7.0	5.1 + 1.5
v_e8_07b	6.4; 0.4 – NBAND 61	-42.44701174	-10.8	5.1 + 1.6
v_e8_07c*	6.4; 0.4 – NBAND 122	-41.94650620	-14.3	5.1 + 1.6
v_e8_07d	6.4; 0.4 – Co_3d (0.8; 0.7)	-40.46475840	211.2	5.2 + 2.6
v_e8_07e	6.4; 0.4 – Co_3d (1.2; 0.7)	-42.03162461	-794.3	5.2 + 3.4
v_e8_08	6.4; 0.3	-42.33212056	-8.0	5.1 + 2.3
v_e8_09	6.4; 0.2	-42.29816471	11.5	5.1 + 1.7
v_e8_10	6.4; 0.1	-42.44294407	2247.9	5.1 + 1.8
v_e8_11	6.4; 0.0	-42.31937260	-13.8	5.1 + 1.9

23) $PrCo_5$ “v_E8” – (a;c)=(0.5025;0.3943); M-5x5x7 k-pts.; SOC+U=conv.; ISMEAR=1; ISYM=-1; EC=10⁻⁶; LREAL; LMAXMIX=6; “Co_sv”+“Pr”; SRC+U → SOC+U. * only (SOC+U), no (SRC+U).

V_F1	(U, J) Pr_4f	SOC[001] (con) (eV)	MAE (100)	MAG [μ B/fu]
v_f1_09	7.4 ; 0.4	-42.25094553	21.4	9.1 – 0.5
v_f1_10	7.3 ; 0.4	-42.38400091	-35.8	5.1 + 1.6
v_f1_01	7.2 ; 0.4	-42.26530482	-8.6	9.1 – 0.4
v_f1_02	7.0 ; 0.4	-41.93067204	-743.8	7.1 + 0.3
v_f1_03	6.7 ; 0.4	-42.41759577	2103.7	5.1 + 2.4
v_f1_04	6.4 ; 0.4	-42.44725699	-7.0	5.1 + 1.5
v_f1_11	6.2 ; 0.4	-41.40137516	268.0	5.0 + 1.6
v_f1_05	6.1 ; 0.4	-42.47244176	5.1	5.1 + 1.6
v_f1_06	5.8 ; 0.4	-42.43963173	1856.2	5.1 + 2.5
v_f1_07	5.5 ; 0.4	-42.52995968	16.0	5.1 + 1.8
v_f1_08	No U	-43.55874747	2.1	5.0 + 2.0
V_F2	(U, J) Pr_4f	SOC[001] (con) (eV)	MAE (100)	MAG [μ B/fu]
v_f2_01	7.2 ; 0.0	-41.88703506	-3.6	7.1 + 0.02
v_f2_02	7.2 ; 0.1	-42.24976416	25.3	9.1 – 0.6
v_f2_03	7.2 ; 0.2	-42.25192411	23.6	9.1 – 0.5
v_f2_04	7.2 ; 0.3	-41.91893464	-7.1	7.0 + 0.2
v_f2_05	7.2 ; 0.4	-42.26530482	-8.6	9.1 – 0.4
v_f2_06	7.2 ; 0.5	-42.40635560	180.2	5.0 + 1.5
v_f2_07	7.2 ; 0.6	-42.42287961	6.5	5.1 + 1.6
v_f2_08	7.2 ; 0.7	-42.40892110	-14.5	5.1 + 1.5
v_f2_09	7.2 ; 0.8	-42.32080737	-103.1	5.1 + 2.4
v_f2_10	7.2 ; 0.9	-42.44722803	2240.4	5.1 + 2.8
v_f2_11	7.2 ; 1.0	-42.29614807	12.9	5.1 + 1.5

25) $PrCo_5$ “v_F1, F2” – (a;c)=(0.5025;0.3943); M-5x5x7 k-pts.; GGA; SOC+U=conv.; ISMEAR=1; ISYM=-1; EC=10⁻⁶; LREAL; LMAXMIX=6; PBE-“Co_sv”+“Pr”; SRC+U → SOC+U.

SmCo₅

V_A2	Files	SRC (con) (eV)	Spin [μ B/fu]
v_a2_01	ISYM = 2, ISMEAR = 1	-40.15581905	7.1
v_a2_02	ISYM = -1, ISMEAR = 1	-40.18012068	7.1
v_a2_03	ISYM = -1, ISMEAR = -5	-40.17710586	7.1
v_a2_04	ISYM = -1, ISMEAR = -5, LORBMOM	-40.17710587	7.1
v_a2_06	ISYM = -1, ISMEAR = -5, VSC2	-40.17710401	7.1

2) $SmCo_5$ “v_A2” – (a;c)=(0.5002;0.3961); M-5x5x5 k-pts.; GGA; SRC=conv.; LREAL; EC=10⁻⁸; “Co”+“Sm_3”.

V_A3	Setup	SOC [001] (con) (eV)	MAE (MJ/m ³)	MAG [μ B/fu]
v_a3_01	.52 PBE, ISMEAR 1, SRC->SOC	-40.55135109	3.7	7.1 + 0.7
v_a3_02	.52 PBE, ISMEAR -5, SRC->SOC	-40.55176445	2.5	7.1 + 0.6
v_a3_03	.52 PBE, ISMEAR 1, SOC	-40.55135113	0.000	7.1 + 0.7

v_a3_04	.52 PBE, ISMEAR -5, SOC	-40.55176446	0.0001	7.1 + 0.6
v_a3_05	PBE, ISMEAR 1, SOC	-40.55135109	0.000	7.1 + 0.7
v_a3_06	PBE, ISMEAR -5, SOC	-40.55176441	0.0001	7.1 + 0.6

3) $SmCo_5$ “v_A3” – (a;c)=(0.5002;0.3961); ENCUT=265; M-5x5x5 k-pts.; SOC=conv.; LREAL; GGA_COMPAT; LMAXMIX=6; ISYM=0; EC=10⁻⁸; PBE-“Co”+“Sm_3”.

V_B2	Files	SOC [001] (con) (eV)	MAE (100)	MAE (210)	MAG [μ B/fu]
v_b2_02	Co, Sm_3	-40.55918849	3.1	3.1	7.2 + 0.7
v_b2_04	Co_pv, Sm_3	-40.56858015	2.9	2.9	7.2 + 0.7

04) $SmCo_5$ “v_B2” – (a;c)=(0.5002;0.3961); ENCUT=270; M-5x5x7 k-pts.; SOC=conv.; LREAL; GGA_COMPAT; ISMEAR=1; LMAXMIX=2; ISYM=-1; EC=10⁻⁶; .52 PBE.

V_C5	Files	SOC [001] (con) (eV)	MAE (100)	MAE (210)	MAG [μ B/fu]
v_c5_04	Co, Sm_3	-40.58216422	1.9	1.9	7.1 + 0.7
v_c5_05	Co_pv, Sm_3	-40.66245416	2.0	2.0	7.1 + 0.7
v_c5_06	Co_sv, Sm_3	-41.11768772	2.6	2.6	7.1 + 0.6

05) $SmCo_5$ “v_C5” – (a;c)=(0.5002;0.3961); G-5x5x7 k-pts.; SOC=conv.; LREAL; GGA_COMPAT; ISMEAR=1; LMAXMIX=6; ISYM=-1; EC=10⁻⁷; ADDGRID; .52 PBE. SRC-OPT: ISIF = 7; SRC-REL: ISIF=0.

V_C6	Coupling	SOC [001] (1 it) (eV)	MAE (100)	MAE (210)	MAG [μ B/fu]
v_c6_02	AFM	-47.69867445	-55.3	-55.6	1.9 + 2.1
v_c6_03	FM	-47.09410582	9.2	-13.2	12.8 – 1.9

06) $SmCo_5$ “v_C6” – (a;c)=(0.5002;0.3961); G-5x5x7 k-pts.; SOC=1 it.; LREAL=FALSE; GGA_COMPAT; ISMEAR=1; LMAXMIX=2; ISYM=-1; EC=10⁻⁷; ADDGRID; PBE-“Sm”+“Co_sv”.

V_C8	Steps; Coupling	SRC (conv) (eV)	Spin [μ B/fu]
v_c8_01	NSP → SRC; None	-46.18799891	12.9
v_c8_02	NSP → SRC; AFM	-46.92194545	1.9
v_c8_03	NSP → SRC; FM	-46.19433776	12.9
V_C8	Steps; Coupling; NCORE	SRC (conv) (eV)	Spin [μ B/fu]
v_c8_04	SRC; None	-43.15765041	7.3
v_c8_05	SRC; AFM; NCORE = 4	-42.44383134	0.7
v_c8_06	SRC; FM; NCORE = 4	-46.19449664	12.9
v_c8_07	SRC; AFM; NCORE = 7	-43.14892107	7.3
v_c8_08	SRC; FM; NCORE = 7	-42.37122275	1.5

08) $SmCo_5$ “v_C8” – (a;c)=(0.5002;0.3961); G-5x5x7 k-pts.; GGA; SOC=1 it.; LREAL; GGA_COMPAT; ISMEAR=1; LMAXMIX=6; ISYM=-1; EC=10⁻⁷; ADDGRID; “Sm”+“Co_sv”. @VSC2.

V_D1	Fe-site	SOC [001] (conv) (eV)	MAE [MJ/m ³]	MAG [μ B/fu]
v_d1_03	TM 2 – Fe_sv	-48.92459327	-32.5	3.0 + 2.1
v_d1_13	TM 3 – Fe_pv	-49.01310629	-32.3	3.0 + 2.0
v_d1_14	TM 4 – Fe_pv	-48.91720755	-29.0	2.8 + 2.1
v_d1_06	TM 5 – Fe_sv	-45.43925707		8.4 – 0.2

09) $SmCo_5$ “v_D1” – (a;c)=(0.5002;0.3961); G-5x5x7 k-pts.; GGA; SRC=conv.; LREAL; GGA_COMPAT; ISMEAR=1; LMAXMIX=6; ISYM=-1; EC=10⁻⁷; ADDGRID; @VSC2.

V_D2	Fe-site	SRC (conv) (eV)	MAG [μ B/fu]
v_d2_01	No Fe	-46.92194542	1.9
v_d2_03	TM 2 – Fe_pv	-48.15923524	2.9
v_d2_05	TM 4 – Fe_pv	-43.63580408	0.6
v_d2_06	TM 5 – Fe_sv	-46.96241501	9.3

10) $SmCo_5$ “v_D2” – (a;c)=(0.5002;0.3961); G-5x5x7 k-pts.; SOC=1 it.; LREAL; GGA_COMPAT; ISMEAR=1; LMAXMIX=6; ISYM=-1; EC=10⁻⁷; ADDGRID; “Sm”+“Co_sv”+“Fe_sv”+“Fe_pv”.

V_D11	Fe-site	SOC [001] (conv) (eV)	MAE (210)	MAG [μ B/fu]
v_d11_01	No Fe	-47.74081932	-16.1	2.6 + 2.0
v_d11_02	TM 1 – Fe_sv	-49.05406195	-23.8	3.5 + 1.8

v_d11_03	TM 2 – Fe_sv	-49.05406271	-23.8	3.5 + 1.8
v_d11_04	TM 3 – Fe_sv	-48.94381092	-21.3	3.4 + 2.0
v_d11_05	TM 4 – Fe_sv	-48.93315293	-38.6	3.4 + 2.0
v_d11_06	TM 5 – Fe_sv	-48.94381131	-12.9	3.4 + 2.0

11) $SmCo_5$ “v_D11” (a;c)=(0.5002;0.3961); G-5x5x7 k-pts.; SOC=conv.; LREAL; GGA_COMPAT; ISMEAR=1; LMAXMIX=6; ISYM=-1; EC=10⁻⁷; ADDGRID; “Sm”+“Co_sv” “Fe_sv”+“Fe_pv”.

V_D12	Steps	SOC [001] (conv) (eV)	MAE (100)	MAG [μ B/fu]
v_d12_10	nsp->soc	-47.71792674	-15.4	1.8 + 1.8
v_d12_12	nsp->soc, cc = 10 ⁻⁷ eV	-47.46441548	-16.0	1.7 + 1.7
v_d12_01a	nsp->rel->soc	-47.46441518	-16.0	1.7 + 1.7
v_d12_01b	nsp->rel->opt->soc	-47.46441628	-16.0	5.3 – 1.3
v_d12_03	nsp->opt->rel->soc	-47.46964171	-16.0	1.7 + 1.7
v_d12_04	opt->rel->soc	-47.46801790	-16.0	1.7 + 1.7
v_d12_01d	nsp->rel->opt->rel->opt->soc	-47.46441552	-16.0	1.8 + 2.6

12) $SmCo_5$ “v_D12” – (a;c)=(0.5002;0.3961); G-5x5x7 k-pts.; GGA; SOC=conv.; LREAL; GGA_COMPAT; ISMEAR=1; LMAXMIX=6; ISYM=-1; EC=10⁻⁶; ADDGRID; PBE- “Sm”+“Co_sv”.

V_E1a	Coupling	SOC+U [001] (conv) (eV)	MAE (100)	MAE (210)	MAG [μ B/fu]
v_e1_01	None	-46.41630624	7.8	29.4	12.5 – 1.5
v_e1_02	AFM	-46.71578180	43.1	462.9	2.7 + 1.9
v_e1_03	FM	-46.40365756		-14.2	12.6 – 1.7
V_E1b	Coupling	SOC+U [001] (conv) (eV)	MAE (100)	MAE (210)	MAG [μ B/fu]
v_e1_04	None	-46.41834751	3.8	11.7	11.8 – 1.4
v_e1_05	AFM	-46.41046305	-103.8	-107.3	2.6 + 1.3
v_e1_06	FM	-46.38712742	-43.02	-45.0	12.6 – 0.8
V_E1c	Coupling	SOC+U [001] (conv) (eV)	MAE (210)		MAG [μ B/fu]
v_e1_07	None	* [100]	-46.38159382		8.8 – 0.9
v_e1_08	AFM		-46.71578238	462.3	2.7 + 1.9
v_e1_09	FM		-46.41820521	88.6	11.5 – 1.3
V_E1d	Coupling	SOC+U [001] (conv) (eV)	MAE (100)	MAE (210)	MAG [μ B/fu]
v_e1_10	None	-46.39346781	-467.6		11.0 – 1.2
v_e1_11	AFM	-43.14110257	-6616.8	-1451.8	7.6 – 0.2
v_e1_12	FM	-43.60734060	-524.2	706.1	7.0 + 0.9
V_E1e	Coupling	SOC+U [001] (conv) (eV)	MAE (100)	MAE (210)	MAG [μ B/fu]
v_e1_13	None	-45.83653025	* -1.4	* 3.3	5.9 – 1.4
v_e1_14	AFM	* (SOC) -44.04365153	* -494.9	* 62.4	1.9 + 0.05
v_e1_15	FM	-46.70658838	447.9	20.5	2.0 + 2.1
V_E1f	Coupling	SOC [001] (eV)	MAE (100)	MAE (210)	MAG [μ B/fu]
v_e1_16 *	None	-45.81910499	6240.3	4955.9	5.3 – 0.3
v_e1_17 *	AFM	-44.13662615	1697.5	1700.8	2.2 – 1.0
v_e1_18	FM	-46.70708614	355.74	28.1	2.1 + 2.7

13) $SmCo_5$ “v_E1” – (a;c)=(0.5002;0.3961); G-5x5x7 k-pts.; GGA; SOC=conv.; LREAL; GGA_COMPAT; ISMEAR=1; LASPH; LMAXMIX=6; ISYM=-1; EC=10⁻⁶; ADDGRID; Sm-4f-(U_eff)=4.45. E1a) NSP → SRC → SOC → +U; E1b) NSP → SRC → (SOC+U); E1c) NSP → SOC → +U; E1d) NSP → (SOC+U); E1e) SRC → SOC → +U; E1f) SRC → (SOC+U). * not converged.

V_E4	Setup	SOC [001] (1 it) (eV)	MAE (100)	MAE (210)	MAG [μ B/fu]
v_e4_01a	M(1.6, -2)	-44.83588992	25.1	28.0	2.4 + 3.0
v_e4_01b	M(3.2, -1.6)	-43.37911208	22.6	15.4	6.1 – 3.1
v_e4_02	Fe (TM1)	-45.83282647	28.3	30.0	3.5 + 2.7
v_e4_02b	ISIF = 5	-71.64980907	13.9	13.9	5.2 – 0.2
v_e4_03	Fe (TM2)	-45.82085266	28.2	29.8	3.1 + 2.1
v_e4_04	Fe (TM3)	-45.81125705	18.6	18.2	2.7 + 2.7
v_e4_04b	ISIF = 5	-45.82811620	19.4	19.0	2.7 + 2.7
v_e4_05	Fe (TM4)	-45.81333468	12.9	17.1	2.4 + 2.0
v_e4_06	Fe (TM5)	-45.81223803	13.0	15.7	3.0 + 2.7

14) $SmCo_5$ & $SmCo_4Fe$ “v_E4” – (a;c)=(0.5002;0.3961); G-5x5x7 k-pts.; SOC=1 it.; LREAL; GGA_COMPAT; ISMEAR=1; LASPH; LMAXMIX=6; ISYM=-1; EC = 10^{-6} ; ADDGRID, MAGMOM (Co;Cu;Sm)=(2.0;2.5;-2.0). NSP → NSP_REL I → NSP_OPT I → NSP_REL II → NSP_OPT II → SOC.

V_E5	Setup	SOC [001] (1 it) (eV)	MAE (100)	MAE (210)	MAG [μ B/fu]
v_e5_01	No Cu	-44.83588992	25.1	28.0	2.4 + 3.0
v_e5_02	Cu (TM1)	-41.32854062	8.9	9.0	5.6 + 0.5
v_e5_03	Cu (TM2)	-41.32713814	9.0	9.2	7.9 + 0.3
v_e5_04	Cu (TM3)	-41.50013662	23.4	26.9	2.3 + 0.2
v_e5_05	Cu (TM4)	-41.51345505	27.2	26.9	2.8 + 0.4
v_e5_06	Cu (TM5)	-41.51272642	26.9	31.1	3.3 + 0.5

15) $SmCo_5$ & $SmCo_4Cu$ “v_E5” – (a;c)=(0.5002;0.3961); G-5x5x7 k-pts.; GGA; SOC=1 it.; LREAL; GGA_COMPAT; ISMEAR=1; LASPH; LMAXMIX=6; ISYM=-1; EC= 10^{-6} ; ADDGRID; MAGMOM=(2.0;0.2;-2.0). NSP → NSP_REL I → NSP_OPT I → NSP_REL II → NSP_OPT II → SOC (1 it).

V_E6a	Setup	SOC [001] (1 it) (eV)	MAE (100)	MAE (210)	MAG [μ B/fu]
v_e6_01	No Fe	-44.82596789		30.8	1.9 + 1.4
v_e6_02	Fe (TM1)	-45.78654930	28.2	31.8	1.8 + 2.1
v_e6_03	Fe (TM2)	-45.78402971	28.7	31.7	1.8 + 2.1
v_e6_04	Fe (TM3)	-45.76680805	17.2	17.4	1.8 + 2.8
v_e6_05	Fe (TM4)	-45.76400576	11.3	17.0	1.8 + 2.8
v_e6_06	Fe (TM5)	-43.88101884	28.4	23.3	3.3 + 3.1
V_E6b	Setup	SOC [001] (1 it) (eV)	MAE (100)	MAE (210)	MAG [μ B/fu]
v_e6_01	No Fe	-43.39167018	32.7	26.2	1.9 + 1.4
v_e6_02	Fe (TM1)	-43.61936032	84.9	83.6	3.1 + 1.2
v_e6_03	Fe (TM2)	-43.61573777	86.2	83.8	2.7 + 1.7
v_e6_04	Fe (TM3)	-43.60940460	31.6	21.3	2.4 + 2.4
v_e6_05	Fe (TM4)	-43.60552280	19.8	19.7	2.4 + 2.5
v_e6_06	Fe (TM5)	-43.61181708	20.3	14.2	2.4 + 2.4
V_E6c	MAGMOM	SOC [001] (1 it) (eV)	MAE (210) [MJ/m ³]		MAG [μ B/fu]
v_e6_02b	3.0; -2.0	-43.96747584	58.2		2.3 + 2.7
v_e6_03c	2.1; -3.2	-45.65288077	16.4		2.2 + 1.7
v_e6_04d	2.8; -2.0	-44.24952434	63.0		2.3 + 2.5
v_e6_05e	2.1; -2.6	-45.24717195	21.9		2.3 + 1.8
v_e6_06g	2.2; -2.6	-45.20024245	21.8		2.2 + 1.7
v_e6_06h	1.6; -5.0	-46.51568489	7.8		2.2 + 1.7
v_e6_06i	2.1; -5.0	-46.57727392	7.5		2.3 + 1.7
v_e6_06j	1.9; -2.4	-45.15659187	25.4		2.3 + 1.9
v_e6_06k	3.2; 0.0	-42.82212813	-16.3		5.8 – 0.2
v_e6_06l	3.2; -1.6	-43.39167018	26.2		1.9 + 1.4
v_e6_06m	3.5; -2.0	-42.98074111	33.4		2.7 + 2.8
v_e6_06n	3.5; -3.0	-43.54490295	75.2		2.3 + 2.2
v_e6_06o	3.5; -3.5	-43.8067322	74.2		2.1 + 1.4
v_e6_06p	3.0; -2.0	-43.96747583	58.2		2.3 + 2.7
v_e6_06q	3.2; -2.0	-43.62193478	48.0		2.6 + 2.9
v_e6_06r	3.5; -4.4	-44.23682885	42.1		2.2 + 1.6
v_e6_06s	3.5; -4.7	-44.36263582	27.4		1.8 + 0.8
v_e6_06t	1.6; -5.2	-46.03840118	-0.2		13.4 – 1.7
v_e6_06u	1.6; -5.6	-46.68086069	6.4		2.3 + 1.6
v_e6_06v	3.2; -8.0	-45.51388476	0.7		1.9 + 0.9
v_e6_06w	3.2; -10.0	-44.5980115	3.1		1.9 + 0.7
v_e6_06x	1.6; -0.85	-44.14378669	-4.0		6.7 + 0.4
v_e6_06y	3.2; -1.9	-43.56380582	43.4		2.3 + 1.7
V_E6_06	MAGMOM	SOC [001] (1 it) (eV)	MAE (210) [MJ/m ³]		MAG [μ B/fu]
v_e6_06_3	2.0; 2.4; -0.5	-45.01624224	-2.5		8.4 + 0.3
v_e6_06_5	2.4; 2.8; -0.5	-44.82821081	-7.0		2.9 + 2.9
v_e6_06_9	3.2; 3.6; -0.5	-43.77649992	-3.1		2.2 – 1.7
v_e6_06_10	3.5; 3.8; -0.5	-43.17828172	-3.4		0.8 – 0.3

v_e6_06_12	1.8; 2.2; -1.0	-45.22429340	-0.5	2.5 + 2.7
v_e6_06_14	2.2; 2.6; -1.0	-45.13520517	1.9	3.1 + 3.0
v_e6_06_18	3.0; 3.4; -1.0	-44.32827338	12.1	3.8 + 1.4
v_e6_06_19	3.2; 3.6; -1.0	-43.97016138	7.4	2.8 + 3.2
v_e6_06_21	1.6; 2.0; -2.0	-45.82227087	13.8	2.9 + 2.6
v_e6_06_27	2.8; 3.2; -2.0	-45.21722961	23.3	2.7 + 1.9
v_e6_06_28	3.0; 3.4; -2.0	-44.91377588	27.7	3.1 + 2.6
v_e6_06_29	3.2; 3.6; -2.0	-44.54976034	38.0	3.1 + 2.9
v_e6_06_30	3.5; 3.8; -2.0	-43.93766816	42.2	2.5 + 1.5
v_e6_06_31	1.6; 2.2; -2.0	-45.82278345	12.6	3.0 + 0.02
v_e6_06_32	2.0; 2.2; -2.0	-45.82363946	13.3	3.9 - 0.1
v_e6_06_33	2.0; 2.2; -1.0	-45.19622483	0.5	6.1 - 0.6
v_e6_06_34	3.0; 3.2; -2.0	-44.98360003	26.0	2.8 + 2.0
v_e6_06_35	3.0; 3.5; -2.0	-44.87572874	29.2	3.1 + 2.5
v_e6_06_36	3.2; 3.4; -2.0	-44.63255768	36.6	3.2 + 3.2
v_e6_06_37	3.0; 3.6; -2.0	-44.83572879	30.3	3.1 + 2.5
v_e6_06_38	1.6; 2.2; -2.0	-45.82278344	12.6	
v_e6_06_39	2.0; 2.2; -1.0	-45.21168474	1.6	2.2 + 2.2
v_e6_06_40	2.1; 2.9; -3.2	-46.59711651	7.1	2.7 + 1.7
v_e6_06_41	2.1; 2.9; -2.6	-46.18493044	10.5	
v_e6_06_42	2.1; 2.9; -2.0	-45.75262170	13.8	1.7 + 2.9
v_e6_06_43	2.1; 2.9; -1.0	-45.12455441	1.4	1.9 + 3.1
v_e6_06_44	2.1; 2.9; -0.5	-44.93501643	-5.9	7.1 - 0.4
v_e6_06_45	2.1; 2.2; -2.0	-45.81781130	13.3	1.7 + 2.9
v_e6_06_46	2.1; 2.4; -2.0	-45.80937763	13.5	1.8 + 2.8
v_e6_06_47	2.1; 2.6; -2.0	-45.79291840	14.0	1.8 + 2.8
v_e6_06_49	2.1; 3.0; -2.0	-45.73504120	14.0	1.7 + 2.9
v_e6_06_50	2.2; 2.8; -2.6	-46.16615250	10.4	1.9 + 3.1
v_e6_06_51	1.6; 2.2; -5.0	-47.50183792	1.5	2.0 + 2.9
v_e6_06_52	2.1; 2.8; -5.0	-47.53956943	0.3	2.1 + 3.0
v_e6_06_53	1.9; 2.7; -2.4	-46.10390359	11.4	2.2 + 1.7
v_e6_06_54	3.5; 4.8; -2.0	-43.30683115	30.1	2.1 + 3.4
v_e6_06_57	3.5; 4.6; -2.0	-43.45271988	34.7	1.9 + 3.3
v_e6_06_58	3.5; 4.9; -2.0	-43.23019010	28.5	2.4 + 3.0
v_e6_06_59	3.5; 5.1; -2.0	-43.06877440	24.7	2.5 + 2.1
v_e6_06_60	3.5; 5.2; -2.0	-42.98370433	22.2	2.3 + 2.1
v_e6_06_62	3.2; 4.4; -1.6	-43.88101884	23.3	1.9 + 3.4

16) $SmCo_5$ & $SmCo_4Fe$ “v_E6” – (a;c)=(0.5002;0.3961); G-5x5x7 k-pts.; SOC=1 it.; LREAL; GGA_COMPAT; ISMEAR=-5; LASPH; LMAXMIX=6; ISYM=-1; EC=10⁻⁶; ADDGRID; NSP → NSP-REL → NSP-OPT → NSP-REL → NSP-OPT → SOC. E6a) MAGMOM=(2.1;2.8;-2.0); E6b) MAGMOM=(3.2;4.8;-1.6).

V_E7	Setup	SOC [001] (1 it) (eV)	MAE (100)	MAE (210)	MAG [μ B/fu]
v_e7_01	No Cu	-43.39167018	29.5	23.6	1.9 + 1.4
v_e7_02	Cu (TM1)	-40.03135218	6.8	7.3	0.2 + 2.2
v_e7_03	Cu (TM2)	-40.01956701	9.5	9.6	0.2 + 2.1
v_e7_04	Cu (TM3)	-40.28798590	23.5	12.7	0.5 + 1.7
v_e7_05	Cu (TM4)	-40.28267838	9.5	10.8	0.5 + 1.7
v_e7_06	Cu (TM5)	-40.28677254	10.1	5.2	0.5 + 1.6

17) $SmCo_5$ & $SmCo_4Cu$ “v_E7” – (a;c)=(0.5002;0.3961); G-5x5x7 k-pts.; SOC=1 it.; LREAL; GGA_COMPAT; ISMEAR=-5; LASPH; LMAXMIX=6; ISYM=-1; EC=10⁻⁶; ADDGRID; “Sm”+“Co_sv”+ “Cu_pv”; MAGMOM=(3.2;0.0;-1.6). NSP → NSP-REL → NSP-OPT → NSP-REL → NSP-OPT → SOC.

V_E8_01	MAGMOM	SOC [001] (1 it) (eV)	MAE (100)	MAE (210)	MAG [μ B/fu]
v_e8_01_a	1.6; -2.0	-44.83802216	25.2	27.9	2.1 + 1.1
v_e8_01_e	1.6; -1.6	-44.56556331	23.7	29.9	2.2 + 1.8
v_e8_01_f	3.2; -2.0	-43.59337859	42.7	36.9	1.6 + 1.2
v_e8_01_g	3.2; -3.2	-44.28738933	53.1	52.7	1.7 + 0.9
v_e8_01_h	3.5; -3.5	-43.77061949	61.0	62.6	1.7 + 1.2

v_e8_01_i	3.2; 0.0	-42.79629542	-15.4	-14.9	5.2 + 0.1
v_e8_01_j	3.2; -1.6	-43.36251866	21.9	14.2	1.9 + 1.7
v_e8_01_k	3.5; -2.0	-42.94488699		20.9	1.6 + 2.7
v_e8_01_l	3.0; -2.0	-43.94444102	54.1	48.9	5.1 - 2.5
V_E8_04	MAGMOM	SOC [001] (1 it) (eV)	MAE (100)	MAE (210)	MAG [μ B/fu]
v_e8_04_a	1.6; 2.2; -2.0	-45.82274041	24.4	20.5	3.0 + 2.0
v_e8_04_b	1.6; 2.2; -1.6	-45.55134876	21.7	17.5	3.1 + 3.1
v_e8_04_c	1.8; 2.2; -2.0	-45.84388118	19.5	18.9	3.1 - 0.1
v_e8_04_d	1.8; 2.2; -5.0	-45.02387187	2.8	-0.9	6.5 - 0.1
v_e8_04_e	3.0; 3.5; -2.0	-44.87352824	36.5	32.2	5.2 - 1.7

18) $SmCo_4Cu$ “v_E8” – (a;c)=(0.5002;0.3961); G-5x5x7 k-pts.; GGA; SOC=1 it.; LREAL; GGA_COMPAT; ISMEAR=1; LASPH; LMAXMIX=6; ISYM=-1; EC=10⁻⁶eV; ADDGRID; PBE- “Sm”+“Co_sv”+“Cu_pv”. NSP → NSP-OPT → NSP-REL → NSP-OPT → NSP-REL → SOC.

V_F1	Setup	SOC [001] (1 it) (eV)	MAE (100)	MAE (210)	MAG [μ B/fu]
v_f1_01	No Fe	-43.39604401	22.5	16.2	1.6 + 2.8
v_f1_02	Fe (TM1)	-69.29971385	21.2	21.5	3.7 + 0.2
v_f1_03	Fe (TM2)	-69.33852054	21.5	21.1	3.4 - 0.2
v_f1_04	Fe (TM3)	-43.72974693	44.9	35.6	2.1 + 3.2
v_f1_05	Fe (TM4)	-43.73733585	33.7	32.4	2.1 + 3.2
v_f1_06	Fe (TM5)	-43.73646329	34.5	30.6	2.1 + 3.2
V_F2	Setup	SOC [001] (1 it) (eV)	MAE (100)	MAE (210)	MAG [μ B/fu]
v_f2_01	No Fe	-43.37137341	21.9	15.7	2.2 + 2.3
v_f2_02	Fe (TM1)	-69.39460146	21.6	22.0	4.8 - 0.2
v_f2_03	Fe (TM2)	-43.87580114	86.1	84.5	2.8 + 1.4
v_f2_04	Fe (TM3)	-43.80977163	42.8	33.3	3.2 + 3.5
v_f2_05	Fe (TM4)	-43.80439157	33.4	32.4	3.2 + 3.3
v_f2_06	Fe (TM5)	-43.80807858	33.3	29.1	3.2 + 3.3
V_F4	Setup	SOC [001] (1 it) (eV)	MAE (100)	MAE (210)	MAG [μ B/fu]
v_f4_01	No Fe	-43.37256687	21.9	15.7	2.0 + 1.8
v_f4_02	Fe (TM1)	-69.39226949	21.1	21.7	4.7 - 0.2
v_f4_03	Fe (TM2)	-43.87452702	86.1	84.5	2.8 + 1.4
v_f4_04	Fe (TM3)	-43.80148892	43.5	34.3	3.2 + 3.2
v_f4_05	Fe (TM4)	-43.79274285	32.3	31.1	3.2 + 3.4
v_f4_06	Fe (TM5)	-43.79802923	32.7	28.7	3.2 + 3.3

19) $SmCo_5$ & $SmCo_4Fe$ “v_F1, F2, F4” (a;c)=(0.5002;0.3961); G-5x5x7 k-pts.; SOC=1 it.; LREAL; LASPH; GGA_COMPAT; ISMEAR=-5; LMAXMIX=6; ISYM=-1; EC=10⁻⁶; ADDGRID; MAGMOM=(3.2;4.4;-1.6). NSP → SRC → SRC-OPT → SRC-REL → SRC-OPT → SRC-REL → SOC. OPT 2: F1) ISIF=5; F2) =6; F4) =7.

V_F5	ISIF	SOC [001] (1 it) (eV)	MAE (100)	MAE (210)	MAG [μ B/fu]
v_f5_01	7; 0; 7; 0	-47.46200431	-16.2	-16.7	2.3 + 1.7
v_f5_02	7; 0; 6; 0	-47.44410421	-26.6	-27.0	2.3 + 1.9
v_f5_03	7; 0; 5; 0	-47.46786039	-26.7	-27.2	2.3 + 1.9
v_f5_04	7; 0; 3	-47.44487671	-26.6	-27.0	2.3 + 1.9

20) $SmCo_5$ “v_F5” – (a;c)=(0.5002;0.3961); G-5x5x7 k-pts.; SOC=conv.; LREAL; GGA_COMPAT; ISMEAR=-5; LASPH; LMAXMIX=6; ISYM=-1; EC=10⁻⁶; ADDGRID; MAGMOM=(1.6;-5.6); NSP → NSP-OPT → NSP-REL → NSP-OPT → NSP-REL → SOC; or NSP → NSP-OPT → NSP-REL → NSP-OPT+REL → SOC.

V_F7_02a	MAGMOM	SOC [001] (con) (eV)	MAE (100)	MAE (210)	MAG [μ B/fu]
v_f7_02a	1.6; -0.9	-47.74164115	-15.7	-16.4	1.9 + 1.9
v_f7_02b	1.6; -1.6	-47.74163230	-15.7	-16.4	1.9 + 1.9
v_f7_02c	1.6; -2.0	-47.74160896	-15.7	-16.5	1.9 + 1.9
v_f7_02e	3.2; -1.6	-47.73705481	-24.2	-25.0	1.9 + 2.2
v_f7_02f	3.2; -2.0	-47.74164170	-15.7	-16.4	1.9 + 1.9
v_f7_02g	1.6; -5.0	-47.74163430	-15.7	-16.4	1.9 + 1.9
V_F7_02b	MAGMOM, U	+U [001] (1 it) (eV)	MAE (100)	MAE (210)	MAG [μ B/fu]
v_f7_02a	1.6; -0.9	-45.31383249	-456.8	-469.1	2.1 + 2.0
v_f7_02b	1.6; -1.6	-45.31370823	-457.1	-469.3	2.1 + 2.0

v_f7_02c	1.6; -2.0	-45.31356415	-457.4	-469.5	2.1 + 2.0
v_f7_02e	3.2; -1.6	-45.44034568	-231.6	-243.8	2.1 + 2.4
v_f7_02f	3.2; -2.0	-45.32168522	-453.1	-465.3	2.1 + 2.0
v_f7_02g1	1.6; -5.0, (6.8; 0.7)	-45.31370507	-457.1	-469.2	2.1 + 2.0
v_f7_02g2	1.6; -5.0, (6.4; 0.7)	-45.45129179	-426.1	-437.0	2.1 + 2.0
v_f7_02g3	1.6; -5.0, (6.0; 0.7)	-45.58999297	-395.9	-405.2	2.1 + 2.0
v_f7_02g4	1.6; -5.0, (5.6; 0.7)	-45.73101687	-364.2	-372.2	2.1 + 2.0
v_f7_02g5	1.6; -5.0, (5.2; 0.7)	-45.87327119	-333.2	-340.1	2.1 + 2.0
V_F7_04	MAGMOM	SOC [001] (con) (eV)	MAE (100)	MAE (210)	MAG [μ B/fu]
v_f7_04a	1.6; -0.9	-47.73398282	5613.9	5511.7	1.9 + 2.1
v_f7_04b	1.6; -1.6	-47.74163749	-15.7	-16.4	1.9 + 1.9
v_f7_04c	1.6; -2.0	-47.74163785	-15.7	-16.4	1.9 + 1.9
v_f7_04d	3.2; -0.9	-47.73705802	-7.0	-24.9	1.9 + 2.2
v_f7_04e	3.2; -1.6	-47.73399231	-29.9	-30.7	1.9 + 2.1
v_f7_04f	3.2; -2.0	-47.73406897	-29.8	-30.5	1.9 + 2.1
v_f7_04g	1.6; -5.0	-47.74163437	-15.7	-16.4	1.9 + 1.9
V_F7_04+U	MAGMOM, U	+U [001] (1 it) (eV)	MAE (100)	MAE (210)	MAG [μ B/fu]
v_f7_04a	1.6; -0.9	-45.51120067	4578.7		1.8 + 3.3
v_f7_04b	1.6; -1.6	-45.31379817	-456.8	-469.1	2.1 + 2.0
v_f7_04c	1.6; -2.0	-45.31379008	-456.9	-469.0	2.1 + 2.0
v_f7_04d	3.2; -0.9	-45.43187850	106.5	-248.3	2.1 + 3.9
v_f7_04e	3.2; -1.6	-45.51116224	-88.4	-100.7	1.8 + 3.3
v_f7_04f	3.2; -2.0	-45.51123153	-88.2	-100.5	1.8 + 3.3
V_F7_06	MAGMOM, U	+U [001] (con) (eV)	MAE (100)	MAE (210)	MAG [μ B/fu]
v_f7_06a	1.6; -0.9	-46.54708687	-42.0	-41.0	2.1 + 2.0
v_f7_06b	1.6; -1.6	-46.54706447	-42.0	-41.1	2.1 + 2.0
v_f7_06c	1.6; -2.0	-46.54708842	-42.0	-41.0	2.1 + 2.0
v_f7_06d	3.2; -0.9	-46.54708669	-41.6	-41.1	2.1 + 2.0
v_f7_06f	3.2; -2.0	-46.54708769	-42.0	-41.0	2.1 + 2.0
v_f7_06g1	1.6; -5.0, (6.8; 0.7)	-46.54708713	-42.0	-41.0	2.1 + 2.0
v_f7_06g2	1.6; -5.0, (6.4; 0.7)	-46.57892653		607.2	2.1 + 2.0
v_f7_06g3	1.6; -5.0, (6.0; 0.7)	-46.61622343	561.0	559.7	2.0 + 1.9
v_f7_06g4	1.6; -5.0, (5.6; 0.7)	-46.32525959	-110.3	-110.1	1.9 + 1.2
v_f7_06g5	1.6; -5.0, (5.2; 0.7)	-46.39932876	-109.8		1.9 + 1.2

21) $SmCo_5$ "v_F7" – (a;c)=(0.5002;0.3961); G-5x5x7 k-pts.; SOC=conv.; +U=1 it.; LREAL; GGA_COMPAT; ISMEAR=-5; LASPH; LMAXMIX=6; ISYM=-1; EC= 10^{-6} ; ADDGRID; Sm-4f-(U;J)=(6.8;0.7). F7_02a) NSP → SRC → SOC → +U; F7_02b) NSP → SRC → SOC → +U; F7_04) (NSP+SOC) → +U; F7_06) NSP → (SOC+U).

V_F8a	(U, J) 4f / (U,J) 3d	+U [001] (con) (eV)	MAE (100)	MAE (210)	MAG [μ B/fu]
v_f8_01	(6.8; 0.7) / none	-46.53242653	648.2	-39.3	2.1 + 2.0
v_f8_02	(6.8; 0.75) / none	-46.39882182	-107.0	-106.5	2.0 + 1.2
v_f8_03	(6.1; 0.0) / none	-46.53241653	-38.4		2.1 + 2.0
v_f8_04	(4.45; 0.0) / none	-46.39881910	-107.6	-109.4	2.0 + 1.2
v_f8_05	none / 3d (1.5; 0.8)	-44.40034668	-17.8	-18.0	2.2 + 2.0
v_f8_06	none / 3d (0.7; 0.0)	-44.40034668	-17.8	-18.0	2.2 + 2.0
v_f8_07	(6.8; 0.7) / (1.5; 0.8)	-43.20552226	-36.0	-35.0	2.3 + 2.2
v_f8_08	(5.2; 0.75) / (1.5; 0.8)	-43.08848411		-115.8	2.3 + 1.4
v_f8_09	(6.1; 0.0) / (0.7; 0.0)	-43.20552225	-35.9	-35.1	2.3 + 2.2
v_f8_10	(4.45; 0.0) / (0.7; 0.0)	-43.08849918	-115.5	-115.9	2.3 + 1.4
v_f8_18	(6.4; 0.7) / none	-46.18204623	-42.4		2.0 + 1.1
v_f8_19	(6.0; 0.7) / none	-46.24588048	-40.9		2.0 + 1.1
v_f8_20	(5.2; 0.7) / none	-46.31527058		-108.1	2.0 + 1.0
V_F8b	(U, J) 4f / (U,J) 3d	+U [001] (con) (eV)	MAE (100)	MAE (210)	MAG [μ B/fu]
v_f8_14	(6.8; 0.7) / none	-46.51842427	1451.9	446.7	1.4 + 1.8
v_f8_17	(5.2; 0.75) / (1.5; 0.8)	-42.86211441	-18.8	17.2	1.6 + 1.1
v_f8_22	(6.1; 0.0) / none	-43.75605859	-5176.3	-4619.0	2.1 + 0.4
v_f8_24	(6.1; 0.0) / (0.7; 0.0)	-45.72394855	-1537.4		5.0 – 1.6
v_f8_26	(6.6; 0.7) / none	-46.54574424		13.2	2.1 + 2.0
v_f8_27	(6.4; 0.7) / none	-46.33526598		-434.7	1.9 + 1.8

v_f8_29	(6.0; 0.7) / none	-46.58676476	41.7		1.4 + 2.1
v_f8_30	(5.8; 0.7) / none	-45.80004821	129.4	3617.3	2.8 – 0.9
v_f8_32	(5.4; 0.7) / none	-46.65776032	-12.0		2.0 + 2.6
V_F9a	(U, J)_4f / (U,J)_3d	+U [001] (con) (eV)		MAE (100)	MAG [μ B/fu]
v_f9a_01	(6.8; 0.7) / none	-46.50457125		437.2	2.2 + 2.9
v_f9a_02	(6.4; 0.7) / none	-46.52876341			2.1 + 2.9
v_f9a_03	(6.0; 0.7) / none	-46.56118537		559.1	2.1 + 2.9
v_f9a_05	(5.2; 0.7) / none	-46.64595101		320.8	2.0 + 2.8
v_f9a_08	(6.0; 0.7) / (1.5; 0.8)	-43.23252011		-120.2	2.4 + 3.1
v_f9a_09	(5.6; 0.7) / (1.5; 0.8)	-43.27436519			2.3 + 3.2
v_f9a_10	(5.4; 0.7) / (1.5; 0.8)	-43.32239941			2.3 + 3.1
V_F9b	(U, J)_4f / (U,J)_3d	+U [001] (con) (eV)		MAE (100)	MAG [μ B/fu]
v_f9b_01	(6.8; 0.7) / none	-46.52867014		-52.1	2.2 + 2.0
v_f9b_02	(6.4; 0.7) / none	-46.55098662		-51.2	2.2 + 2.0
v_f9b_03	(6.0; 0.7) / none	-46.57766892			2.2 + 2.0
v_f9b_04	(5.6; 0.7) / none	-46.61073927		-45.4	2.2 + 2.1
v_f9b_05	(5.2; 0.7) / none	-46.65229456			2.1 + 2.4
v_f9b_06	(6.8; 0.7) / (1.5; 0.8)	-43.19933757		-46.2	2.5 + 2.2
v_f9b_07	(6.4; 0.7) / (1.5; 0.8)	-43.22206885		-45.4	2.4 + 2.2
v_f9b_08	(6.0; 0.7) / (1.5; 0.8)	-43.24980529		-42.0	2.4 + 2.2
v_f9b_09	(5.6; 0.7) / (1.5; 0.8)	-43.28434722		-37.2	2.4 + 2.3
v_f9b_10	(5.4; 0.7) / (1.5; 0.8)	-43.32771742		-26.9	2.4 + 2.3

22) $SmCo_5$ “v_F8, F9” – (a;c)=(0.5002;0.3961); G-7x7x8 k-pts.; GGA; +U=conv.; LREAL; GGA_COMPAT; ISMEAR=-5; LASPH; LMAXMIX=6; ISYM=-1; EC= 10^{-6} ; ADDGRID. F8a) NSP → SRC → (SOC+U) ; F8b) SOC+U; F9a) NSP → SOC → (SOC+U); F9b) NSP → (SOC+U).

V_G1_a	(U, J)_4f	+U [001] (con) (eV)		MAE (MJ/m ³)	MAG [μ B/fu]
v_g1_a_01	(6.8; 0.7)	-46.54708864		654.9	2.1 + 2.0
v_g1_a_02	(6.4; 0.7)	-46.57892629			2.1 + 2.0
v_g1_a_03	(6.0; 0.7)	-46.61622382		631.4	2.0 + 1.9
v_g1_a_04	(5.6; 0.7)	-46.66018833		514.5	2.0 + 1.9
v_g1_a_05	(5.2; 0.7)	-46.70922116		465.8	2.0 + 1.9
V_G1_b	(U, J)_4f	+U [001] (con) (eV)		MAE (MJ/m ³)	MAG [μ B/fu]
v_g1_b_01	(6.8; 0.7)	-46.31667487			1.9 + 3.2
v_g1_b_02	(6.4; 0.7)	-46.57717318		611.8	2.1 + 1.9
v_g1_b_03	(6.0; 0.7)	-46.61589908		572.7	2.1 + 1.9
v_g1_b_04	(5.6; 0.7)	-46.66000275		595.5	2.1 + 1.9
v_g1_b_05	(5.2; 0.7)	-46.70931231		472.4	2.1 + 1.9
V_G1_c	(U, J)_4f	+U [001] (con) (eV)		MAE (MJ/m ³)	MAG [μ B/fu]
v_g1_c_01	(6.8; 0.7)	-46.54708713		-42.0	2.1 + 2.0
v_g1_c_02	(6.4; 0.7)	-46.57892653		607.2	2.1 + 2.0
v_g1_c_03	(6.0; 0.7)	-46.61622343		561.0	2.0 + 1.9
v_g1_c_04	(5.6; 0.7)	-46.32525959		-110.3	1.9 + 1.2
v_g1_c_05	(5.2; 0.7)	-46.39932876		-109.8	1.9 + 1.2
V_G2_a	(U, J)_4f / (U,J)_3d	+U [001] (con) (eV)		MAE (MJ/m ³)	MAG [μ B/fu]
v_g2_01	(6.8; 0.7) / none	-43.72609812		-1959.8	7.5 + 0.2
v_g2_02	(6.0; 0.7) / none	-46.33225880		-520.9	1.9 + 1.9
v_g2_03	(6.8; 0.7) / (1.5; 0.8)	-43.23353713		5245.5	2.4 + 2.9
V_G2_b	(U, J)_4f / (U,J)_3d	+U [001] (con) (eV)		MAE (MJ/m ³)	MAG [μ B/fu]
v_g2_07	(6.8; 0.7) / none	-46.54299867		21.3	2.0 + 2.3
v_g2_08	(6.0; 0.7) / none	-46.58863903		-23.2	2.1 + 2.8
V_G2_c	(U, J)_4f / (U,J)_3d	+U [001] (con) (eV)		MAE (MJ/m ³)	MAG [μ B/fu]
v_g2_19	(5.2; 0.7) / none	-44.92036929		72.4	4.1 + 1.3
v_g2_18*	(6.0; 0.7) / 7x7x8	-46.57253568		25.8	2.4 + 1.5

23) $SmCo_5$ “v_G1, G2” – (a;c)=(0.5002;0.3961); G-5x5x7 k-pts.; +U=conv.; LREAL; GGA_COMPAT; ISMEAR=-5; LASPH; LMAXMIX=6; ISYM=-1; EC= 10^{-6} ; ADDGRID. G1a) NSP→SRC→SOC→+U; G1b) NSP→SOC → +U; G1c) NSP→SRC→SOC+U; G2a) NSP+U→SRC+U→SOC+U; G2b) NSP+U→SOC+U; G2c) SOC+U.

V_G3a	(U, J)_4f / (U,J)_3d	+U [001] (con) (eV)	MAE (MJ/m ³)	MAG [μ B/fu]
v_g3_01	(6.8; 0.7) / none	-46.50572486	3158.1	2.2 + 2.4
v_g3_02	(6.0; 0.7) / none	-46.60555047	-7.2	2.0 + 2.1
v_g3_03	(6.8; 0.7) / (1.5; 0.8)	-43.21009634	3442.1	2.4 + 2.5
v_g3_04	(6.0; 0.7) / (1.5; 0.8)	-43.28384770	-10.2	2.3 + 2.6
v_g3_06	(6.8; 0.7) / none / 7x7x8-k	-46.58547416	-27.8	2.1 + 2.3
V_G3b	(U, J)_4f / k-mesh	+U [001] (con) (eV)	MAE (MJ/m ³)	MAG [μ B/fu]
v_g3_07	(6.8; 0.7) / 5x5x7	-46.20941969	-598.3	1.9 + 1.8
v_g3_08	(6.0; 0.7) / 5x5x7	-46.61109035	52.9	2.2 + 2.6
v_g3_10	(6.0; 0.7) / 7x7x8	-46.56157918	-107.5	2.1 + 2.5
V_G3c	(U, J)_4f / k-mesh	+U [001] (con) (eV)	MAE (MJ/m ³)	MAG [μ B/fu]
v_g3_11	(6.8; 0.7) / 5x5x7	-46.54057280	-41.6	2.1 + 2.1
v_g3_12	(6.0; 0.7) / 5x5x7	-46.61240584	-34.6	2.0 + 2.6
V_G3d	(U, J)_4f / k-mesh	+U [001] (con) (eV)	MAE (MJ/m ³)	MAG [μ B/fu]
v_g3_18	(6.0; 0.7) / 7x7x8	-46.60217214	563.5	0.7 + 0.7

24) $SmCo_5$ “v_G3” – (a;c)=(0.5002;0.3961); G-5x5x7; ISMEAR=1; +U=conv.; LREAL; LASPH; GGA_COMPAT; LMAXMIX=6; ISYM=-1; EC=10⁻⁶; ADDGRID; (U;J) from start. G3a) NSP+U → SRC+U → SOC+U; G3b) NSP+U → SOC+U; G3c) SRC+U → SOC+U; G3d) SOC+U.

V_G4, G5	(U, J)_4f / (U,J)_3d	+U [001] (con) (eV)	MAE (MJ/m ³)	MAG [μ B/fu]
v_g4_01	(6.8; 0.7) / none	-46.54299867	21.3	2.0 + 2.3
v_g4_03	(6.0; 0.7) / none	-46.58863903	-23.2	2.1 + 2.8
v_g4_04	(5.6; 0.7) / none	-46.45265860	-267.6	1.9 + 1.8
v_g4_17	(5.4; 0.7) / none	-46.66861447	4.1	2.0 + 2.6
v_g4_05	(5.2; 0.7) / none	-46.68885339	25.8	2.1 + 2.6
v_g4_07	(6.4; 0.7) / (1.4; 0.8)	-43.68406436	329.3	2.4 + 2.5
v_g4_08	(6.0; 0.7) / (1.4; 0.8)	-43.75338189	54.2	2.4 + 2.9
v_g4_09	(5.6; 0.7) / (1.4; 0.8)	-43.78820365	-2.5	2.3 + 2.6
v_g4_11	(6.8; 0.7) / (1.2; 0.8)	-44.65001502		2.4 + 2.8
v_g4_12	(6.4; 0.7) / (1.2; 0.8)	* -44.67863747		* 7.5 + 0.5
v_g4_13	(6.0; 0.7) / (1.2; 0.8)	-44.69882108	-40.4	2.4 + 2.8
v_g4_14	(5.6; 0.7) / (1.2; 0.8)	-44.73673897	49.6	2.4 + 2.9
v_g4_15	(5.2; 0.7) / (1.2; 0.8)	-44.74857404	-19.3	2.1 + 2.2
v_g5_16	(5.2; 0.5) / 7x7x8-k	-44.74284863	-22.4	2.3 + 2.3

25) $SmCo_5$ “v_G4, G5” – (a;c)=(0.5002;0.3961); G-5x5x7; ISMEAR=1; GGA; +U=conv.; LREAL; GGA_COMPAT; LASPH; LMAXMIX=6; ISYM=-1; EC=10⁻⁶; ADDGRID. (NSP+U) → (SOC+U). * in [100].

V_G6 @FX	(U, J)_4f	+U [001] (con) (eV)	MAE (MJ/m ³)	MAG [μ B/fu]
v_g6_01	(5.2; 0.4)	-46.64820787	15.7	2.1 + 2.4
v_g6_02	(5.2; 0.5)	-43.82500092	-5234.4	7.5 + 0.5
v_g6_03	(5.2; 0.6)	-46.66693053	0.9	1.7 + 2.1
v_g6_04	(5.2; 0.7)	-46.68885339	25.8	2.1 + 2.6
v_g6_05	(5.2; 0.8)	-46.70781119	48.1	2.1 + 2.7
v_g6_06	(5.2; 0.9)	-46.56021422	-1.0	1.9 + 1.8
v_g6_07	(5.2; 1.0)	-46.56427808	-358.9	1.9 + 1.9

26) $SmCo_5$ “v_G6” (a;c)=(0.5002;0.3961); G-5x5x7; ISMEAR=1; GGA; +U=conv.; LREAL; GGA_COMPAT; LASPH; LMAXMIX=6; ISYM=-1; EC=10⁻⁶; ADDGRID; @VSC2. (NSP+U) → (SOC+U).

V_G9	(U, J)_4f	+U [001] (con) (eV)	MAE (MJ/m ³)	MAG [μ B/fu]
v_g9_01	(5.4; 1.0)	-46.69720194	-9.9	2.1 + 2.7
v_g9_02	(5.4; 0.9)	-46.66571948	-5.5	2.1 + 2.3
v_g9_03	(5.4; 0.8)	-43.88258522	-512.3	7.1 + 0.4
v_g9_04	(5.4; 0.7)	-46.63451710	33.8	2.1 + 2.1
v_g9_05	(5.4; 0.6)	-46.64035554	-3.1	2.1 + 2.6
v_g9_06	(5.4; 0.5)	-46.61497780	-34.7	2.2 + 2.1
v_g9_07	(5.4; 0.4)	-46.60410260	41.2	2.1 + 2.2

27) $SmCo_5$ “v_G9” – (a;c)=(0.5002;0.3961); G-5x5x7; ISMEAR=1; +U=conv.; LREAL; GGA_COMPAT; LASPH; LMAXMIX=6; ISYM=-1; EC=10⁻⁶; ADDGRID; @VSC3. (NSP+U) → (SOC+U).

V_H1	REL	+U [001] (con) (eV)	MAE (MJ/m ³)	MAG [μ B/fu]
v_h1_01	ISIF = 3	-46.52115982	7.3	1.8 + 1.7
v_h1_02	ISIF = 4	-46.52104021	10.3	1.8 + 1.7
v_h1_03	ISIF = 0	-46.52026151	7.8	1.8 + 1.7

28) $SmCo_5$ “v_H1” – (a;c)=(0.5002;0.3961); G-5x5x7; ISMEAR=1; +U=conv.; LREAL; LASPH; GGA_COMPAT; LMAXMIX=6; ISYM=-1; EC=10⁻⁶; ADDGRID; PBE-“Sm”+ “Co_sv”+“Fe_sv”; (U;J)=(5.2;0.7) from start; OPT: ISIF=7. (NSP+U) → (SOC+U) → (SOC+U-OPT) → (SOC+U-REL).

V_H5 @VSC2	Change in c	+U [001] (con) (eV)	MAE (MJ/m ³)	MAG [μ B/fu]
v_h5_01	-2.0 %	-46.67786120	24.4	2.1 + 2.5
v_h5_02	-1.5 %	-46.67691740	-75.6	2.1 + 2.4
v_h5_03	-1.0 %	-46.69433481	-59.0	2.1 + 2.7
v_h5_05	0.0 %	-46.54299867	21.3	2.0 + 2.3
v_h5_06	+0.5 %	-46.69041322	-37.5	2.1 + 2.7
v_h5_07	+1.0 %	-46.68374337		
v_h5_09	+2.0 %	-46.64296604	-11.9	2.1 + 2.5
V_H6 @FX	Change in c	+U [001] (con) (eV)	MAE (MJ/m ³)	MAG [μ B/fu]
v_h6_01	-2.0 %	-46.65448717	471.2	2.1 + 2.1
v_h6_02	-1.5 %	-46.69443686	40.7	2.1 + 2.8
v_h6_03	-1.0 %	-43.90329181	-5227.4	7.0 + 0.5
v_h6_04	-0.5 %	-46.64279420	-88.0	2.1 + 2.5
v_h6_05	0.0 %	-46.68885339	25.8	2.1 + 2.6
v_h6_06	+0.5 %	-46.61132751	-118.6	2.1 + 1.8
v_h6_07	+1.0 %	-46.67977451	33.0	2.1 + 2.7
v_h6_08	+1.5 %	-46.65902869	20.8	2.8 + 2.1
v_h6_09	+2.0 %	-46.63121863	283.7	2.0 + 2.6

30) $SmCo_5$ “v_H5 & v_H6” – (a;c)=(0.5002;0.3961); G-5x5x7; ISMEAR=1; d(a)=0; d(c)≠0; +U=conv.; LREAL; GGA_COMPAT; LASPH; LMAXMIX=6; ISYM=-1; EC=10⁻⁶; ADDGRID; (U;J)=(5.2; .7). NSP+U → SOC+U.

V_H7_a	Fe or Cu site	+U [001] (con) (eV)	MAE (MJ/m ³)	MAG [μ B/fu]
v_h7_a_01&2	No Fe or Cu	-46.63424785	33.3	2.2 + 2.1
v_h7_a_03	Fe (2c – TM 1)	-47.96523544	11.2	3.1 + 2.8
v_h7_a_04	Fe (3g – TM 4)	-47.87535770	19.3	3.0 + 2.4
v_h7_a_05	Cu (2c – TM 1)	-43.22827261	79.2	0.3 + 2.2
v_h7_a_06	Cu (3g – TM 4)	-43.18074313	93.6	0.4 + 2.3

31) $SmCo_5$ & $SmCo_4Fe$ & $SmCo_4Cu$ “v_H7” – (a;c)=(0.5002;0.3961); G-5x5x7., ISMEAR=1; +U=conv.; LREAL; LASPH; GGA_COMPAT; LMAXMIX=6; EC=10⁻⁶; ADDGRID; Sm-4f-(U;J)=(5.2;0.7). NSP+U → SOC+U.

V_H8a	Fe or Cu site	+U-REL [001] (con) (eV)	MAE (MJ/m ³)	MAG [μ B/fu]
v_h8_01	Fe (2c – TM 1)	-48.01579761	133.3	3.0 + 2.3
v_h8_02	Fe (3g – TM 4)	-47.89396133	-16.4	2.6 + 3.0
v_h8_03	Cu (2c – TM 1)			
v_h8_04	Cu (3g – TM 4)	-43.28897467	0.6	0.3 + 2.4

32) $SmCo_4Fe$ & $SmCo_4Cu$ “v_H8” – (a;c)=(0.5002;0.3961); G-5x5x7; ISMEAR=1; +U= conv.; LREAL; GGA_COMPAT; LASPH; LMAXMIX=6; ISYM=-1; EC=10⁻⁶; ADDGRID; Sm-4f-(U;J)=(5.4;0.7). NSP+U → SOC+U → SOC+U-OPT → SOC+U-REL.